

Aus dem Zentrum für Tumor- und Immunbiologie
Geschäftsführender Direktor: Prof. Dr. Rolf Müller
des Fachbereichs Medizin der Philipps-Universität Marburg

**The intercellular signaling network
in the tumor microenvironment of
ovarian high-grade serous carcinoma**

Inaugural-Dissertation

zur Erlangung des Doktorgrades
der Naturwissenschaften
(Dr. rer. nat.)

dem Fachbereich Medizin
der Philipps-Universität Marburg
vorgelegt von

Leah Sommerfeld

geboren in Chiangrai

Marburg, 2023

Angenommen vom Fachbereich Medizin der Philipps-Universität Marburg am:
21.03.2023

Gedruckt mit Genehmigung des Fachbereichs Medizin.

Dekanin: Frau Prof. Dr. Denise Hilfiker-Kleiner

Referent: Herr Prof. Dr. Rolf Müller

Korreferent: Herr Prof. Dr. Matthias Lauth

TABLE OF CONTENTS

List of abbreviations..... III

1. Abstract 1

2. Introduction..... 5

 2.1 Ovarian carcinoma..... 5

 2.2 The tumor microenvironment in high-grade serous ovarian cancer..... 6

 2.2.1 Immune cells in the TME 7

 2.2.2 Stromal host cells in the TME 9

 2.3 WNT4..... 11

 2.4 Prostacyclin..... 12

 2.5 Aims of this dissertation 13

3. Publication summaries 14

 3.1 The multicellular signalling network of ovarian cancer metastases 14

 3.1.1 Results..... 14

 3.1.2 Description of own contribution..... 18

 3.2 Tumor-associated macrophages promote ovarian cancer cell migration by secreting transforming growth factor beta induced (TGFB1) and tenascin C..... 18

 3.2.1 Results..... 18

 3.2.2 Description of own contribution..... 19

 3.3 Prostacyclin released by cancer-associated fibroblasts promotes immunosuppressive and pro-metastatic macrophage polarization in the ovarian cancer microenvironment..... 19

 3.3.1 Results..... 19

 3.3.2 Description of own contribution..... 23

4. Discussion..... 24

 4.1 The intercellular network of tumor and host cells in HGSC metastases 24

4.2 Comparison of omental TU and TAM to their counterparts derived from ascites	25
4.3 Pro-metastatic function of WNT4 in the crosstalk of CAF and tumor cells....	26
4.4 TGFBI and TNC secreted by ascTAM promote tumor migration	27
4.5 PGI ₂ mediated crosstalk between CAF and ascTAM.....	28
4.6 Conclusion	30
5. References	32
6. Publications	45
7. Appendicies	148
7.1 All publications of the author	149
7.2 Curriculum vitae	150
7.3 Directory of academic teachers.....	150
7.4 Ehrenwörtliche Erklärung	151

List of abbreviations

6-keto PGF1a	6-keto-prostaglandin F1 α
AA	Arachidonic acid
ADI	omental adipocytes
asc-MDM	ascites-differentiated monocyte-derived macrophages
ascTAM	ascites derived tumor-associated macrophages
ascTU	ascites derived tumor cells
CAF	cancer-associated fibroblast
CAM	cell adhesion molecule
CM	conditioned media
COX1/2	cyclooxygenase 1/2
ECM	Extracellular matrix
EMT	epithelial to mesenchymal transition
FACS	Fluorescent activated cell sorting
FN1	fibronectin 1
FZD	frizzled class receptor
GM-CSF	granulocyte-macrophage colony-stimulating factor
GO	gene ontology
HGSC	ovarian high-grade serous carcinoma
HSP70	heat shock protein family A
LC-MS/MS	liquid chromatography mass spectrometry mass spectrometry
LPA	lysophosphatidic acid
LRP	LDL receptor related protein
m0-MDM	m0-differentiated monocyte-derived macrophages
m1-MDM	m1-differentiated monocyte-derived macrophages
m2-MDM	m2-differentiated monocyte-derived macrophages
MACS	magnetic activated cell sorting
MDM	monocyte-derived macrophage
MESO	mesothelial cells
MFI	mean fluorescence intensity

LIST OF ABBREVIATIONS

MMT	mesothelial-to-mesenchymal transition
mRNA	messenger RNA
MS	mass spectrometry
NF- κ B	Nuclear factor kappa-light-chain-enhancer of activated B cells
OC	ovarian cancer
omTAM	omental tumor-associated macrophages
omTU	omental tumor cells
PGE ₂	Prostaglandin E ₂
PGI ₂	Prostaglandin I ₂ , Prostacyclin
PPAR β/δ	peroxisome proliferator-activated receptor β/δ
PTGIR	Prostaglandin I ₂ Receptor
PTGIS	Prostaglandin I ₂ synthase
RFS	relapse free survival
RNA	ribonucleic acid
RNA-Seq	RNA sequencing
RT-qPCR	reverse transcription quantitative polymerase chain reaction
scRNA-Seq	single cell RNA sequencing
SMA	smooth muscle actin
TAM	tumor-associated macrophages
TAT	tumor-associated T-cells
TGFBI	transforming growth factor beta-induced
TGF β	Tumor growth factor β family
TME	tumor microenvironment
TNC	tenascin C
TPM	transcripts per million
VEGFA	Vascular endothelial growth factor A
WB	Western Blot
WNT	Wingless and Int-related protein
WNT 4	Wnt Family Member 4

1. Abstract

Ovarian cancer, especially ovarian high-grade serous carcinoma (HGSC), is one of the most fatal malignancies in women. For this reason, it is of great importance to discover new potential targets for therapeutic intervention. Transcoelomic spread of tumor cells via malignant ascites, particularly to the omentum, is the major route of HGSC metastasis. HGSC is characterized by its unique tumor microenvironment, consisting of two different anatomic compartments, i.e., ascites and solid tumor lesions, which are both composed of tumor and host cells. Although there are several published studies on signaling networks between ascites cells, the pathways of host-tumor interactions in omental metastases, as well as across different tumor microenvironment compartments, are largely unexplored.

Therefore, the primary aim of this work was to establish a comprehensive network of cytokines, growth factors, lipid-mediators and extracellular matrix components, secreted by tumor and host cells, and their corresponding receptors in the HGSC tumor microenvironment. For this purpose, we performed transcriptomic analysis of tumor cells, adipocytes, mesothelial cells, cancer-associated fibroblasts (CAF) and tumor-associated macrophages (TAM) from omental metastases, as well as tumor cells, TAM and tumor-associated T cells from ascites. This study uncovered an unexpected major function of tumor-associated stroma and immune cells within this network, being the predicted key source of most cytokines, growth factors and extracellular matrix proteins. While 176 cytokines and growth factors were selectively expressed by stroma and tumor-associated immune cells, only 13 were tumor-cell-selective. Many of these mediators are significantly associated with a poor clinical outcome and are linked to metastasis. We also found cell-type-selective pathways within the HGSC tumor microenvironment, some of which were further analyzed in functional studies.

Functional studies demonstrated that CAF stimulate tumor cell migration and adhesion to a mesothelial monolayer via the highly cell-type-selective secretion of the ligand WNT4. Additionally, both TNC and TGFB1 secreted by ascites-derived TAM (ascTAM) were found to play a potentially pivotal role in HGSC progression by enhancing tumor cell migration.

Apart from cytokines and growth factors, we also investigated the role for tumor-associated host cells in lipid-mediated signaling. We detected a cell-type-selective production of prostacyclin (PGI₂) by omental CAF and mesothelial cells. Due to high expression and ligand-induced activation of the corresponding PGI₂ receptor, TAM were identified as a potential target cell population. Using a PGI₂ analog, we observed a shift of the differentiation state and transcriptional profile of ascTAM towards a mixed-polarization phenotype with immunosuppressive characteristics. Furthermore, PGI₂ analogs reduced the phagocytic capability of TAM-like macrophages that were derived from monocytes differentiated in the presence of ascites. Moreover, a potential role for the PGI₂-regulated secretome in metastatic growth was revealed by experiments showing an increase in tumor cell migration and adhesion to mesothelial cells by conditioned medium from PGI₂-treated TAM.

Finally, we compared the transcriptional profile of omental versus ascites-derived tumor cells and TAM. This analysis, in conjunction with subsequent functional studies, demonstrated that the omental tumor microenvironment triggers pro-inflammatory NFκB signaling in ascTAM via extracellular HSP70 derived from omental tumor cells and TAM.

Taken together, these findings indicate that omental immune and stromal cells - in particular CAF and TAM - play an essential role in biological process linked to HGSC progression, hence lending support to the hypothesis that targeting tumor-host-interactions might be an attractive option to improve ovarian cancer treatment.

Zusammenfassung

Das Ovarialkarzinom, insbesondere der hochgradig seröse Subtyp (HGSC), ist eine der tödlichsten bösartigen Erkrankungen bei Frauen. Aus diesem Grund ist es von großer Bedeutung, neue potenzielle Angriffspunkte für therapeutische Maßnahmen zu entdecken. Die transcoelomische Ausbreitung von Tumorzellen über malignen Aszites, insbesondere in das Omentum, ist der Hauptweg der HGSC Metastasierung. HGSC zeichnet sich durch eine einzigartige Tumormikroumgebung aus, die aus zwei verschiedenen anatomischen Kompartimenten besteht, nämlich dem Aszites und den soliden Tumorkläsionen, die beide aus Tumor- und Wirtszellen zusammengesetzt sind. Obwohl es mehrere veröffentlichte Studien über Signalnetzwerke zwischen Asziteszellen gibt, sind die Wege der Wirt-Tumor-Interaktionen in der Omentum-Metastase sowie zwischen den verschiedenen Kompartimenten der Tumormikroumgebung weitgehend unerforscht.

Das primäre Ziel dieser Arbeit war es daher, ein umfassendes Netzwerk von Zytokinen, Wachstumsfaktoren, Lipiden und Bestandteilen der extrazellulären Matrix, die von Tumor- und Wirtszellen sezerniert werden, sowie ihren entsprechenden Rezeptoren in der HGSC-Tumormikroumgebung zu erstellen. Zu diesem Zweck haben wir eine Transkriptomanalyse von Tumorzellen, Adipozyten, Mesothelzellen, Tumor-assoziierten Fibroblasten (CAF) und Tumor-assoziierten Makrophagen (TAM) aus omentalen Metastasen sowie von Tumorzellen, TAM und Tumor-assoziierten T-Zellen aus Aszites durchgeführt. Diese Studie deckte eine unerwartete Hauptfunktion des Tumor-assoziierten Stromas und der Immunzellen innerhalb dieses Netzwerks auf, da sie die prognostizierte Hauptquelle der meisten Zytokine, Wachstumsfaktoren und extrazellulären Matrixproteine sind. Während 176 Zytokine und Wachstumsfaktoren selektiv von Stroma- und Tumor-assoziierten Immunzellen exprimiert wurden, waren nur 13 selektiv für Tumorzellen. Viele dieser Mediatoren stehen in signifikantem Zusammenhang mit einem schlechten klinischen Ergebnis und sind mit der Metastasierung verbunden. Wir fanden auch Zelltyp-spezifische Signalwege in der Mikroumgebung des HGSC-Tumors, von denen einige funktionell weiter analysiert wurden.

Funktionelle Studien zeigten, dass CAF die Migration und Adhäsion von Tumorzellen an einer Mesothelschicht durch die hochgradig Zelltyp-spezifische Sekretion des Liganden WNT4 stimulieren. Darüber hinaus wurde festgestellt, dass sowohl TNC als auch TGFBI, die von aus Aszites isolierten TAM (ascTAM) sezerniert werden, eine potenziell entscheidende Rolle bei der HGSC-Progression spielen, indem sie die Migration von Tumorzellen fördern.

Neben den Zytokinen und Wachstumsfaktoren untersuchten wir auch die Rolle der Tumor-assoziierten Wirtszellen bei der Lipid-vermittelten Signalübertragung. Wir wiesen eine Zelltyp-selektive Produktion von Prostazyklin (PGI_2) durch CAF und Mesothelzellen nach. Aufgrund der hohen Expression und der ligandeninduzierten Aktivierung des entsprechenden PGI_2 -Rezeptors wurden die TAM als potenzielle Zielzellpopulation identifiziert. Unter Verwendung eines PGI_2 -Analoga beobachteten wir eine Verschiebung des Differenzierungszustands und des Transkriptionsprofils von ascTAM hin zu einem gemischt-polarisierten Phänotyp mit immunsuppressiven Eigenschaften. Darüber hinaus verringerten die PGI_2 -Analoge die phagozytische Fähigkeit von TAM-ähnlichen Makrophagen, die aus Monozyten in Gegenwart von Aszites differenziert wurden. Ferner wurde eine mögliche Rolle des PGI_2 -regulierten Sekretoms beim Metastasenwachstum durch Experimente aufgedeckt, die eine Zunahme der Migration von Tumorzellen und der Adhäsion an Mesothelzellen durch konditioniertes Medium aus PGI_2 -behandelten TAM zeigten.

Schließlich verglichen wir das Transkriptionsprofil von Tumorzellen und TAM aus dem Omentum mit dem von Aszites. Diese Analyse zeigte, zusammen mit anschließenden funktionellen Studien, dass die Mikroumgebung der Omentum-Metastase über extrazelluläres HSP70, das aus Tumorzellen und TAM stammt, pro-inflammatorische NF κ B-Signale in ascTAM auslöst.

Zusammengefasst deuten diese Ergebnisse darauf hin, dass Immun- und Stromazellen des Omentums - insbesondere CAF und TAM - eine wesentliche Rolle bei biologischen Prozessen spielen, die mit dem Fortschreiten von HGSC verbunden sind. Dies unterstützt die Hypothese, dass die gezielte Beeinflussung von Tumor-Wirt-Interaktionen eine attraktive Option für eine verbesserte Therapie des Ovarialkarzinoms sein könnte.

2. Introduction

2.1 Ovarian carcinoma

Despite advances in treatment regimens in recent years, ovarian cancer (OC) remains one of the most frequent and aggressive cancers in women (Kurnit et al., 2021). Five substantially distinct main epithelial OC types are classified on the basis of histological features and molecular genetics. High-grade serous ovarian cancer (HGSC), accounting for 70% of cases, is the most deadly OC type (Prat et al., 2012; Pogge von Strandmann et al., 2017). The high lethality is mainly due to late diagnosis of three quarters of patients at stage III and IV, leading to an overall 5-year-survival rate of less than 50%. The main cause for diagnosis at advanced stages is the lack of specific symptoms and scarcity of clinically effective screening strategies (Lheureux et al., 2019; Liberto et al., 2022). Thus, new research findings on biomarkers and novel targets for therapeutic interventions, are of particular importance. To date, standard therapy is based on debulking surgery combined with chemotherapy (carboplatin/ paclitaxel). New options for OC treatment are poly (ADPribose) polymerase inhibitors, which hamper the DNA damage repair capacity of tumor cells (Kurnit et al., 2021) and Bevacizumab, a monoclonal antibody against VEGF-A (Haunschild & Tewari, 2020). Although initially therapy results in high responsiveness, most patients exhibit relapses in the following years, due to different mechanisms of chemoresistance including inherent, acquired and conditional resistance (Pogge von Strandmann et al., 2017).

A special hallmark of HGSC is its transcoelomic spread via the peritoneal fluid, which at advanced stages occurs as malignant ascites, as the major route of metastasis (Lengyel, 2010). The omentum, a visceral adipose tissue with immunological functions, represents the major metastatic site of this peritoneal dissemination (Meza-Perez & Randall, 2017; Ma, 2020). The two different anatomic compartments (ascites and solid tumor lesions), containing tumor, immune and stroma cells contribute to a unique tumor microenvironment (TME) in HGSC (illustrated in Figure 1; Worzfeld et al., 2017).

2.2 The tumor microenvironment in high-grade serous ovarian cancer

HGSC is characterized by genetic heterogeneity as well as an intertumoral and intratumoral heterogeneous composition of the TME (Yang et al., 2020; Rickard et al., 2021). During peritoneal dissemination of single tumor cells and multicellular spheroids to the peritoneal mesothelium, malignant ascites accumulates due to increased vascular permeability (Lengyel, 2010). Ascites, which is associated to poor clinical outcome (Ayantunde & Parsons, 2007), not only serves as a carrier for cancer cells in HGSC, but comprises cancer-associated host cells, extracellular vesicles and tumor-promoting soluble factors (Peng et al., 2011; Worzfeld et al., 2017; Finkernagel et al., 2019; Bortot et al., 2021). These secreted mediators and the cellular components form a complex network and have been the subject of intense investigations in the last decade (e.g., Kulbe et al., 2012; Finkernagel et al., 2016; Reinartz et al. 2016). Microvesicles are major components of the TME and also play a significant role in intercellular communication by transporting proteins, lipids and nucleic acids (Pogge von Strandmann et al., 2017).

Various soluble factors present in OC ascites are associated with a poor clinical outcomes and play important roles in tumor progression, including metastatic spread, regulation of angiogenesis and immune suppression. Among them are TGF- β , MUC16, LIF, IL-6, IL-10, chemokines and VEGF (Lane et al., 2011; Thériault et al., 2011; Matte et al., 2012; Reinartz et al. 2016; Worzfeld et al., 2018). Apart from cytokines and growth factors, bioactive lipids, including arachidonic acid (AA) and prostanoids, exhibit pro-tumorigenic functions in HGSC (Reinartz et al., 2019; Dietze et al., 2021). As of now, studies on the signaling network of HGSC have mainly focused on ascites derived cells. The routes of host-tumor interactions in the metastatic omentum and potential links to soluble and cellular compounds of the ascites are largely unknown. The omentum, composed mainly of adipocytes, is separated from the peritoneal cavity by a mesothelial monolayer, which is discontinuous at "milky spots" consisting primarily of lymphocytes and macrophages (Figure 1). The immune cells of the milky spots participate in peritoneal immunomodulatory functions, but

also play a role in tumor progression of OC (Platell et al., 2000; Meza-Perez & Randall, 2017).

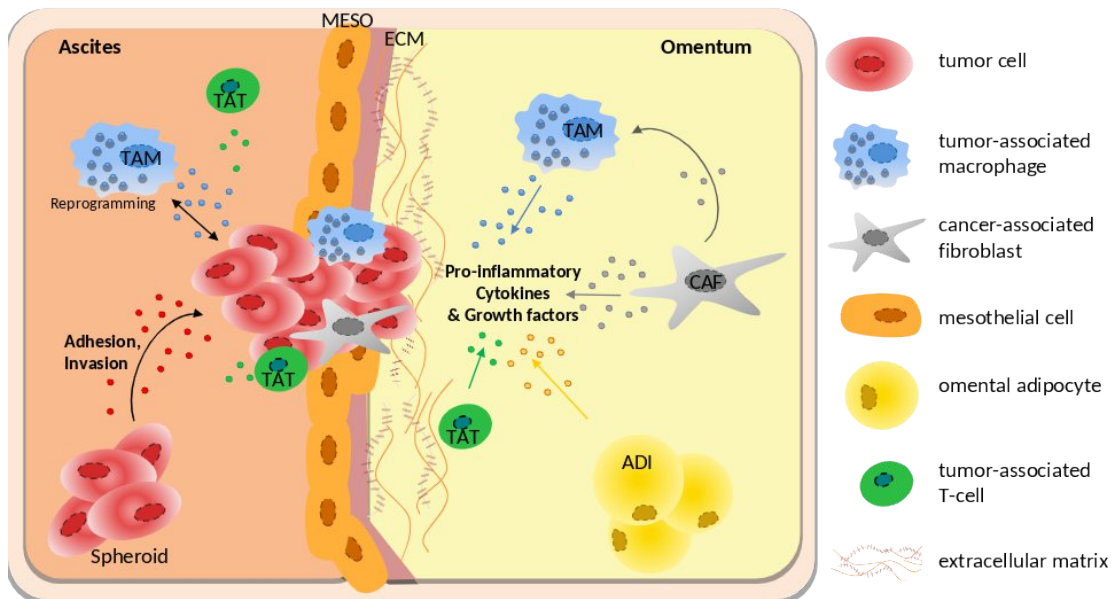


Figure 1. The tumor microenvironment of HGSC. Simplified illustration of the two anatomic sites of HGSC, ascites fluid and solid omental metastasis. The main cell types, as well as ECM and soluble factors in this tumor microenvironment are delineated.

In the following, the different immune and stromal host cells within this TME will be described into more detail.

2.2.1 Immune cells in the TME

The main types of immune cells in the ovarian TME are macrophages, representing one arm of the innate immune response, and T lymphocytes, the major components of the adaptive immunity. Both cell types are highly heterogeneous comprising cells with opposing effects, as they are crucial for cancer elimination, but can be reprogrammed to exert pro-tumorigenic functions in the HGSC TME. Furthermore, B lymphocytes, natural killer cells and dendritic cells are also present in the ascites of HGSC patients in small amounts and are important for cancer immunosurveillance (Worzfeld et al., 2017; Yang et al., 2020).

Tumor-associated T-cells (TAT)

Different classes of T-cells are found in ascites (collectively referred to as TAT in this work): T helper cells (CD4+ Th1 and Th2 cells), cytotoxic T-cells (CD8+) and

regulatory T-cells (Treg). They possess opposite impacts in the TME, as Th1 cells assist in cytotoxic attack by CD8⁺ T-cells on TU, while Th2 and Treg support an immunosuppressive microenvironment (Yang et al., 2020; Rakina et al., 2022).

Ascites in HGSC is known to inhibit clinically favorable (Hamanishi et al., 2007) cytotoxic T cells activation (Lieber et al., 2018) and to promote Treg infiltration, which is associated with shorter survival (Curiel et al., 2004). Moreover, transcriptomic analysis, published by our group, revealed that TAT derived from HGSC ascites strongly express the checkpoint regulators PD-L1 and CTLA4 and supply multiple immunosuppressive mediators (Worzfeld et al., 2018).

Tumor-associated macrophages (TAM)

The macrophages in ascites and metastatic lesions evolve from monocytes and resident peritoneal macrophages (Noy & Pollard, 2014). TAM are altered to adopt an immunosuppressive and tumor-promoting activation state (Takaishi et al., 2010; Reinartz et al., 2014; Yin et al., 2016; Finkernagel et al., 2016). A special characteristic of these phagocytes is their plasticity (Noy & Pollard, 2014). Thus, TAM display both intra- and inter-patient heterogeneity and are characterized by mixed polarization states and functions (Reinartz et al., 2014; Izar et al., 2020). Intriguingly, the fraction of TAM with high expression of CD163 correlates with an early relapse in HGSC (Reinartz et al., 2014), whereas an upregulation of genes linked to interferon signaling in TAM is associated with a favorable clinical outcome (Adhikary et al., 2017).

A variety of soluble factors are secreted by TAM in HGSC and thereby contribute to tumor progression. For example, VEGF, MMPs and CCL18 promote angiogenesis, and the checkpoint regulator PD-L1 supports cancer immune evasion (Worzfeld et al., 2018). Furthermore, ascites derived TAM in HGSC secrete IL-6 and IL-10, which promote tumor cell proliferation by inducing STAT3 signaling (Takaishi et al., 2010; Reinartz et al., 2016). A cooperation of TAM and tumor cells in HGSC was also observed in extracellular matrix (ECM) remodeling, a necessary step in tumor metastasis (Finkernagel et al., 2016; Worzfeld et al., 2018), pointing to a role of TAM in cell migration and invasion in HGSC. This supports the notion that milky spots, containing macrophages for peritoneal

immunosurveillance, facilitate metastatic colonization in early phases (Clark et al., 2013; Krishnan et al., 2020). Further evidence for the importance of tissue-resident macrophages is provided by the *in vivo* paracrine effects of omental TAM, in particular the CD163+Tim4+ subset, on the metastatic spread of tumor cells (Etzerodt et al., 2020). Despite recent advances, the interactions and signaling networks between tissue-derived immune cells and tumor cells remain largely unknown, representing a major obstacle to the discovery of new therapeutic targets.

2.2.2 Stromal host cells in the TME

Apart from immune cells, different stromal cell types are present in the peritoneum and omentum. In OC, they can be reeducated to cancer-associated stroma cells with features supporting the attraction of tumor cells to the omentum and subsequent metastasis. Through paracrine signaling networks and direct interactions, an active reciprocal crosstalk between cancer and stromal cells takes place (Motohara et al., 2019).

Omental adipocytes (ADI)

Adipocytes are the most abundant cell type in the omentum (Meza-Perez & Randall, 2017). Omental adipocytes (ADI) and visceral adipocytes differ from subcutaneous adipocytes in both origin and properties (Cha & Koo, 2019). For instance, the expression of genes coding for enzymes involved in the biosynthesis of lipid mediators, is higher in ADI than in subcutaneous adipocytes (Michaud et al., 2014). Cancer-associated ADI promote tumor invasion into the omentum via secretion of adipokines, e.g. IL-6 and IL-8, as well as through the transfer of fatty acids supporting tumor cell metabolism (Nieman et al., 2011; Ladanyi et al., 2018; Motohara et al., 2019). In addition, ADI in OC induce resistance to chemotherapy by secretion of ANGPTL4 and release of AA (Zhou et al., 2020; Yang et al., 2019).

Mesothelial cells (MESO)

Another major cell type of the omentum are MESO. They cover the peritoneum as a monolayer, which functions as a protective anatomical barrier. Apart from that, MESO also play an important role in the regulation of fluid and solute

transport, as well as in inflammation via antigen presentation and in tissue repair. (Mutsaers, 2004).

Little is known about the role of MESO in OC. In a 3D model intact mesothelial lining inhibited invasion of OC cells (Kenny et al., 2007), while other studies showed that the altered tumor-associated MESO enhance the adhesion of tumor cells (reviewed in Mogi et al., 2021). The promotion of tumor cell attachment to the mesothelial layer and subsequent metastasis is probably linked to the expression of proteins with functions in ECM reorganization, cell adhesion and chemotaxis by MESO (Mogi et al., 2021). Furthermore, it has been reported that malignant ascites can stimulate the proliferation (Matte et al., 2014) of MESO but also trigger their senescence (Mikuła-Pietrasik et al., 2016). Intriguingly, there is evidence that senescent MESO support tumor cell adhesion (Ksiazek et al., 2009) and angiogenesis (Ksiazek et al., 2008), and may thereby enhance tumor progression. Mikuła-Pietrasik et al. postulate that the high senescence rate of MESO might be connected to enhanced proliferation of MESO due to accelerated exhaustion (Mikuła-Pietrasik et al., 2016). Because of these protective versus tumor-promoting functions, as well as their plasticity and adaption of fibroblast-like features (Sandoval et al., 2013), MESO are a potentially highly relevant cell type within the HGSC TME.

Cancer-associated fibroblasts (CAF)

Fibroblasts play a crucial role in connective tissues, as they secrete ECM components and are activated during wound healing response (Kalluri, 2016). They are able to adapt their cellular phenotype dependent on the microenvironment. Tumor cells are known to reprogram fibroblasts to cancer-associated fibroblasts (CAF). Compared to normal fibroblasts CAF exhibit distinct expression markers, e.g. α -smooth muscle actin (SMA), FAP and PDGFR (Motohara et al., 2019). In OC, CAF have been linked to poor prognosis and are involved in most stages of tumor progression (Givel et al., 2018; Zhang et al., 2011). CAF in OC are derived from different origins. For example, tumor cells are able to convert resident fibroblasts to CAF via TGF- β 1 signaling (Cai et al., 2012) and to induce transcriptional reprogramming in omental fibroblasts (Mitra et al., 2012). Furthermore, lysophosphatidic acid (LPA) secreted by ovarian tumor cells stimulates the differentiation of mesenchymal stem cells (MSC) to myofibroblast-

like cells (Jeon et al., 2008). Another source for CAF are MESO undergoing mesothelial-to-mesenchymal transition (MMT) (Sandoval et al., 2013). Furthermore, CAF might derive from endothelial cells through endothelial-to-mesenchymal transition (Potenta et al., 2008) and trans-differentiation of adipocytes (Bochet et al., 2013).

Four CAF subpopulations were found in OC based on differential marker expression. Among these, the subtype CAF-S1 (FAP, CD29, SMA), considered as activated immunosuppressive fibroblasts, is of particular interest (Givel et al., 2018). The diversity of CAF within patients was also verified on the basis of single cell RNA-Seq (scRNA-Seq) (Izar et al., 2020; Olbrecht et al., 2021).

In OC, CAF are known to promote tumor progression via various mechanisms and by secretion of numerous factors, including cytokines, growth factors and lipids. CAF contribute to the pre-metastatic niche and thus colonization. They enhance cancer growth, migration and invasion, as well as angiogenesis. Moreover, CAF play a pivotal role in ECM remodeling and immune suppression (reviewed in Motohara et al., 2019; Thuwajit et al., 2018). Taken together, CAF are of central interest in this context, because their influence in HGSC TME points to novel treatment strategies.

2.3 WNT4

Wingless and Int-related protein (WNT) ligands are the tumor-promoting signaling molecules of interest in the TME of OC. WNT signaling pathways are associated with tumor development and progression of OC and play a crucial role in differentiation, proliferation and stemness (McMellen et al., 2020). WNT ligands are evolutionary conserved glycoproteins with important functions during embryonic development and tissue repair. The human WNT family consists of 19 members. WNT family member 4 (WNT4), expressed in fibroblast, is known to play a role in wound healing and fibrosis (Labus et al., 1998; Surendran et al., 2002). Secreted WNT ligands bind to various transmembrane-receptors of the frizzled (FZD) family together with co-receptors, e.g. ROR2 and LDL receptor related protein (LRP) 5 or 6, triggering three distinct downstream signaling cascades: Canonical WNT/ β -dependent pathway, non-canonical planar cell polarity pathway and non-canonical WNT/ Ca^{2+} pathway (Komiya & Habas, 2008).

WNT4, which triggers all three pathways, mainly signals via FZD8 and the co-receptors LRP5/6 (Dijksterhuis et al., 2015).

WNT signaling is strongly associated with different tumor entities, among them OC (Chehover et al., 2020; Kotrbová et al., 2020; Teeuwssen & Fodde, 2019). WNT4 has been reported to promote tumor progression in breast cancer, laryngeal carcinoma and colorectal cancer, and has been linked to multiple pro-tumorigenic functions, including proliferation, migration, invasion, EMT and angiogenesis (Huang & Feng, 2017; Vouyovitch et al., 2016; Wang et al., 2020; Yang et al., 2020). These pro-metastatic functions highlight the significance of WNT4, even though its role in the TME of HGSC has not been addressed.

2.4 Prostacyclin

Besides growth factors and cytokines, lipid mediators play a role in tumor progression of HGSC and have been linked to poor clinical outcome, e.g. AA, prostaglandins and LPA (Dietze et al., 2021; Hammoud et al., 2022; Reinartz et al., 2016, 2019). Prostacyclin (prostaglandin I₂; PGI₂), a bioactive lipid mediator of the eicosanoid superfamily, is mainly known as a potent vasodilator and platelet aggregation inhibitor with protective functions in the cardiovascular system. Prostaglandins, including prostaglandin D₂, prostaglandin E₂ (PGE₂) and PGI₂, are synthesized in several steps from AA by cyclooxygenases-1 or -2 (COX1/2) followed by specific prostaglandin synthases (Moncada & Vane, 1979; Mitchell & Kirkby, 2019). Prostaglandin I₂ synthase (PTGIS), a member of cytochrome P450 superfamily (DeWitt & Smith, 1983), is expressed in a variety of cell types, including smooth muscle, endothelial and dendritic cells as well as fibroblasts (Moncada et al., 1976; Lee et al., 2005; Stratton & Shiwen, 2010; Mitchell et al., 2022). PGI₂ has a short half-life *in vivo*, and is rapidly degraded to the inactive derivate 6-keto-prostaglandin F1α (6-keto PGF1a) (Lewis & Dollery, 1983). PGI₂ can trigger two main signaling pathways. Binding to the PGI₂ membrane receptor (PTGIR) leads to cAMP production via adenylate cyclase (Shaul et al., 1991; Midgett et al., 2011). PGI₂ can also signal through activation of the nuclear peroxisome proliferator-activated receptor β/δ (PPARβ/δ) (Hertz et al., 1996; Gupta et al., 2000).

In the past decades regulatory functions of the innate and adaptive immune response was assigned to PGI₂, but their conclusions are partly contradictory. While several studies have demonstrated anti-inflammatory and anti-fibrotic effects of PGI₂, pro-inflammatory signaling has also been reported (Aronoff et al., 2007; Dorris & Peebles, 2012; Stitham et al., 2011). In the context of the OC TME it may be of particular interest that PGI₂ analogs suppressed phagocytosis, inhibited bacterial killing and enhanced IL-6 production in peritoneal macrophages in a rat model (Aronoff et al., 2007).

Contradictory data have also been published with respect to the role of PGI₂ in cancer growth and progression. In lung cancer, PGI₂ suppressed tumor growth and metastasis (Keith & Geraci, 2006; Li et al., 2018). Moreover, the PGI₂ analog Iloprost inhibited invasion of OC cells via downregulation of metalloproteinases (MMP) 2 (Ahn et al., 2018). In contrast, several studies reported a correlation of high PTGIS expression with reduced survival of breast cancer, OC and colorectal cancer patients (Klein et al., 2015; Reinartz et al., 2019; Dai et al., 2020).

2.5 Aims of this dissertation

The goal of this work was to establish a comprehensive network of cytokines, growth factors, lipids and ECM components secreted by tumor and host cells, and their corresponding receptors in the HGSC TME. This was achieved by establishing purification protocols for different cell types of the HGSC, followed by transcriptomic and secretome analysis. Unlike previous studies, which focused on malignant ascites, this global analysis of host-tumor interactions integrated all major cell types cell types of omental metastases, i.e., ADI, MESO and CAF. Additionally, this study aimed to identify commonalities and differences in the gene expression profiles of tumor cells and TAM from different TME compartments of HGSC, i.e. ascites and omental metastases. To elucidate the clinical relevance of ligand-receptor interactions predicted by this analysis, associations with with relapse-free survival of HGSC patients were investigated. Finally, functional studies of selected cell-type-selective pathways were performed, showing their impact on biological processes impacting metastatic spread, e.g. tumor cell migration, adhesion and immune suppression.

3. Publication summaries

3.1 The multicellular signalling network of ovarian cancer metastases

Sommerfeld, L., Finkernagel, F., Jansen, J. M., Wagner, U., Nist, A., Stiewe, T., Müller-Brüsselbach, S., Sokol, A. M., Graumann, J., Reinartz, S., & Müller, R. (2021). The multicellular signalling network of ovarian cancer metastases. *Clinical and Translational Medicine*, 11(11), e633. <https://doi.org/10.1002/ctm2.633>

3.1.1 Results

The transcriptome and secretome of tumor and tumor-associated host cells in HGSC

In this work we isolated and analyzed all major cell types from metastatic omental tissue (omTU, CAF, MESO, ADI, omTAM) and from ascites (ascTU, ascTAM, ascTAT) (study conception shown in Fig. 1). The RNA sequencing (RNA-Seq) data was adjusted for contaminating cells, indicated in Fig. 2A and S1, using a bioinformatic approach on the basis of our previously published method (Reinartz et al., 2016). A coherent correlation between cytokines and growth factors detected in the transcriptome and in the mass-spectrometry based proteome of conditioned media (CM) from CAF (Fig. 2C and D) indicated that RNA-Seq data can be used for the prediction of secreted proteins.

Normalized RNA-Seq data may underestimate the contribution of tumor cells to the HGSC secretome because they contain more RNA per cell than the host cell types. We prepared RNA from equal numbers of tumor cells and host cells to address this issue and performed RT-qPCR without normalization of two selected genes (*NDUFS2* and *NFSL1C*) which displayed the lowest variability of expression across all samples and cell types. Therefore, differences in PCR signals directly corresponded to differences in the amount of mRNA per cell. Only a restricted dissimilarity of cell-type-selective mRNA content (maximally 2-fold) was observed (Fig. 2E and F), indicating that the mRNA content has no significant impact on the interpretation of the RNA-Seq data.

To unravel the signaling network of the HGSC TME, we first analyzed which growth factors and cytokines (n=284 detected) are expressed by the different cell types (Fig. 3). This analysis revealed an unexpected major function of host cells

in this network, being the key source of secreted mediators. While 176 growth factor and cytokine genes were selectively expressed by stroma and tumor-associated immune cells, only 13 were tumor-cell-selective. Especially the stromal cells (CAF, MESO and ADI) seem to play a substantial role in the TME of HGSC (with n=99 selective genes). In addition, 31 of stroma-selective genes were significantly associated with a poor clinical outcome, including *BMP2*, *TGFB3*, *VEGFC* and *ADIPOQ*, whereas only one gene (*BNDF*) was associated with a longer survival was identified (Table 1).

To obtain a global picture of the HGSC network, the potential target cells of the identified cell-type selective soluble factors were determined utilizing the transcriptomic data. Fig. 4 shows a simplified illustration of the relative expression of all receptors that bind to the indicated ligands, illustrating a clear target cell-type selectivity with the signaling network.

The clinical importance of these findings is underscored by the observation that 200 of the growth factor and cytokine genes of this network have previously been linked to metastasis (in the genecards.org database), and a number of these are associated with a short survival. Interestingly, corresponding receptors of 122 of these pro-metastatic genes were found on omTU (illustrated in Fig. 5).

Moreover, the RNA-Seq data revealed an essential contribution by omental host cells to ECM-mediated signaling and ECM reorganization (Fig. 7), as well as in lipid-mediated signaling, thereby contributing to a pro-metastatic HGSC niche. As expected, stromal cells are the main source of collagens, while interacting integrins are expressed in a cell-type specific manner. We also found hitherto unknown cell-type selective expression patterns of proteases and cell adhesion molecules (CAM) within the ECM-associated signaling. For instance, *MMP9* is only expressed by TAM and *BCAM* shows a selectivity for tumor cells and MESO. Altogether, the sequencing data indicate that the omental TME of HGSC is substantially dependent on factors secreted by stroma and immune cells.

WNT4 as a highly cell-type-selective ligand in the omental TME

Our RNA-Seq data revealed WNT4 as a highly cell-type-selective ligand from CAF in the HGSC TME (>10-fold higher expression than all other cell types; Fig 6A). This is remarkable, because WNT-signaling plays a crucial role in the

progression of OC (Teeuwssen & Fodde, 2019). Therefore, WNT4 was selected as an example to verify the functional significance of host cells in the cross-talk and progression of HGSC. FZD8 is the primary receptor of WNT4, and its main co-receptors are LRP5 and 6. Expression of these receptors (shown in Fig. 6A) identified tumor cells as the major target cell type for WNT4 in the HGSC TME. Hence, we hypothesized that WNT4 is implicated in pro-metastatic signaling in HGSC.

Using OVCAR4 as a model cell line, we observed reduced migration towards CM from CAF transfected with siRNAs against WNT4 compared to siCtrl and untransfected controls (Fig 6 B and S8, knockdown verification in Fig. S6). This finding was confirmed by further assays with transiently overexpressed WNT4 in LP9 cells (human MESO line with low WNT4 level). Using CM from these cells, a higher migratory potential (Fig. 6C and S9), an induced motility in a wound healing assay (Fig. 6E and S10) as well as an increased adhesion to a confluent mesothelial monolayer (Fig. 6F and S11) were observed.

Migration and adhesion assays with primary HGSC tumor cells from ascites (Fig. 6D and G; microscopic representative pictures in S9 and 11) confirmed WNT4-mediated induction of tumor cell migration and adhesion. In summary, our findings provide strong evidence for a pro-metastatic function of WNT4 in the cross-talk between CAF and tumor cells in HGSC.

Comparative analysis of TU and TAM from ascites vs omentum

This work presents the first study of a transcriptomic comparison of matched pairs of ascites-derived TU or TAM and their cellular omental counterparts. Although we found a high correlation between the two TU subsets (Spearman's $r = 0.98$, Fig. S12) as well as between ascTAM and omTAM (Spearman's $r = 0.95$, Fig. S14), we could identify numerous differentially expressed genes (fold change >3 , TPM >3). Whereas the expression of 83 genes was increased and the expression of 38 genes decreased in omTU versus ascTU (Fig. 8A), a larger number of 674 regulated genes (nominal $p < 0.05$) was detected in TAM (Fig. 9A).

To analyze these gene expression patterns into more detail, functional annotation analyses were performed, which showed that 31 genes upregulated in omTU

versus ascTU are linked to both 'epithelial differentiation' and 'pro-inflammatory', indicating a coherency. In both TU and TAM, genes targeted by MAPK-mediated or pro-inflammatory signaling were more strongly expressed in the TME of the omentum compared to ascites (Fig 8B and 9E). Intriguingly, only two cytokines or growth factor genes showed an increased expression in omTU compared to ascTU (*CXCL2*, *EDN1*), whereas numerous genes were upregulated in omTAM in comparison to their counterparts in ascites. Among these were genes coding for ECM proteins and pro-inflammatory cytokines, e.g. *MMP2* and *IL-1A* (Fig. 9F).

The RNA-Seq data also revealed an upregulation of genes linked to cell cycle progression in omTAM, suggesting enhanced proliferation (Fig. 9A and S15). This conclusion was validated by flow cytometry staining of Ki67, a marker of proliferation (Fig. 9C).

Additionally, the comparative analysis showed an upregulated expression of heat shock protein family A (*HSP1A/HSP70*) on both TU and TAM from the omentum (Fig. 8C and 9F). This finding is of particular interest, as HSP70 levels in ascites are strongly associated with a poor relapse-free survival (RFS) (Finkernagel et al., 2019).

The role of extracellular HSP70 signaling in TAM from HGSC

HSP70 is predominantly found intracellularly and known for its cytoprotective functions, but is also released as an extracellular mediator. Binding of extracellular HSP70 to toll-like-receptors 2 and 4 (TLR2/4) and the CD14 coreceptor leads to activation of pro-inflammatory NFκB-signaling (Asea et al., 2002; Juhasz et al., 2013). In view the observed enrichment of genes linked to pro-inflammatory signaling upregulated in omTAM and omTU, which include *HSPA1A*, and the association of HSP70 in ascites with a poor survival, a role for HSP70 in pro-tumorigenic intercellular signaling in the HGSC TME was postulated. This was exemplarily demonstrated in ascTAM, which strongly express the HSP70 receptors CD14 and TLR2/4. Our findings revealed an activation of the NFκB-signaling in ascTAM after treatment with low-endotoxin rhHSP70 (Fig. 10), as shown by nuclear translocation of the NFκB subunit p65

and enhanced levels of I κ B kinase IKK α / β , concomitant with an upregulation of IL-6 secretion in rhHSP70 stimulated TAM.

3.1.2 Description of own contribution

My personal contributions to the preparation of this publication included, the establishment of all methods required for the isolation and characterization of tumor and host cells from omental metastases, the isolation of the samples for the RNA-Seq and proteomics (used for Fig. 1-5, Fig. 6, Fig. 7-9 and Fig. S1, S2, S4, S5, S12-S16). Moreover, I conducted the experimental setup, execution and data analysis of all functional assays (illustrated in Fig. 2E+F, Fig. 6B-G, Fig. 9C, Fig. 10A-E, Fig. S3 and Fig. S6-S11). I also assisted in writing the manuscript.

3.2 Tumor-associated macrophages promote ovarian cancer cell migration by secreting transforming growth factor beta induced (TGFB1) and tenascin C

Steitz, A. M., Steffes, A., Finkernagel, F., Unger, A., **Sommerfeld, L.**, Jansen, J. M., Wagner, U., Graumann, J., Müller, R., & Reinartz, S. (2020). Tumor-associated macrophages promote ovarian cancer cell migration by secreting transforming growth factor beta induced (TGFB1) and tenascin C. *Cell Death & Disease*, 11(4), 249. <https://doi.org/10.1038/s41419-020-2438-8>

3.2.1 Results

An alternative approach to decipher the TAM secretome and its contribution to metastasis was published in the study by Steitz et al. *In vitro* assays showed that CM from ascTAM induced the migration of patient-derived cultured ascTU (Fig. 1A+B) similar to CM from ascites-differentiated (asc-MDM) and M2-differentiated (m2-MDM) monocyte-derived macrophages (MDM), but not from m1-MDMs (Fig. 1C-E). LC-MS/MS secretome analysis revealed nine proteins selectively secreted by asc-MDM and m2-MDM compared to m1-MDM. Among them were tenascin C (TNC), transforming growth factor beta-induced (TGFB1) and fibronectin 1 (FN1), all of which stimulated tumor cell migration (Fig. 2). In addition, all three proteins were abundant in ascites (SOMAscan, Fig. 3A) and their levels were significantly associated with a shorter RFS (Fig. 4A-C). Our secretome and transcriptome data suggest that ascTAM are a major source of these three migration-promoting factors. As the role of FN1 in tumor cell migration

had already been reported, we focused our further studies on TGFBI and TNC. Using neutralizing antibodies against TGFBI or TNC (Fig. 6), as well as siRNA-mediated silencing of TGFBI expression (Fig. 7), we observed decreased migration of cultured ascTU towards CM from asc-MDM and m2-MDM. These findings confirmed that TNC and TGFBI are promigratory factors secreted by ascites-polarized TAM, which further strengthens the pivotal role of the TAM-TU crosstalk in HGSC progression.

3.2.2 Description of own contribution

My personal contribution to the establishment of this publication included the participation in isolation of patient derived samples.

3.3 Prostacyclin released by cancer-associated fibroblasts promotes immunosuppressive and pro-metastatic macrophage polarization in the ovarian cancer microenvironment

Sommerfeld, L., Knuth, I., Finkernagel, F., Pesek, J., Nockher, W. A., Jansen, J. M., Wagner, U., Nist, A., Stiewe, T., Müller-Brüsselbach, S., Müller, R., & Reinartz, S. (2022). Prostacyclin Released by Cancer-Associated Fibroblasts Promotes Immunosuppressive and Pro-Metastatic Macrophage Polarization in the Ovarian Cancer Microenvironment. *Cancers* 14, no. 24: 6154. <https://doi.org/10.3390/cancers14246154>

3.3.1 Results

The role of tumor-associated host cells in lipid-mediated signaling

In this study, we used the RNA-Seq data described in section 3.1 (Sommerfeld et al., 2021) to extend the network between tumor and host cells to lipid-mediated signaling. Analysis of this dataset revealed a pivotal role of stromal and immune cells in the generation of, and signaling by, lipid mediators (supplementary table S3 and S4). The results were summarized in Fig. 1. Several lipid-metabolizing enzymes were found in various cell-types, but some pathways were clearly cell-type-selective, e.g., expression of *LIPE* in ADI or *ALOX5* in TAM. Additionally, some target receptors were also expressed in a cell-type-selective manner. Among these, the selectivity of prostacyclin (PGI₂) production and signaling was particularly striking, as PGI₂ synthase (PTGIS) is expressed strongly by CAF (and MESO), while the highest mRNA level of the corresponding membrane

receptor, PGI₂ receptor (PTGIR), was detected in ascTAM (Fig. 1 and supplementary table S5). Furthermore, in contrast to other tumor entities, high PTGIS expression was linked to poor clinical outcomes in OC (Fig. 2A and S3). These observations provided the rationale for investigating the function of PGI₂ signaling between CAF and TAM in the TME of HGSC.

PGI₂-mediated crosstalk between CAF and ascTAM

The expression of PGIS and PTGIR by cells of the HGSC TME was validated by RT-qPCR (Fig. 2B and Fig. 3A). Both, enzyme and receptor mRNA levels, were in line with the RNA-Seq data. A CAF-selective protein expression of PTGIS was confirmed using immunoblot (Fig. 2C). To analyze whether the high PTGIS expression in CAF corresponds to a high PGI₂ production, lipid LC-MS/MS was performed. We detected an increased level of 6k-PGF1a (stable degradation product of PGI₂) in CM from CAF (Fig. 2D), which was blocked in part by inhibitors of COX1/2 (Fig. 2E), which are upstream enzymes in the biosynthetic pathway of PGI₂ and expressed in CAF (Fig. 1D). These results indicate that high levels of PGI₂ in ascites versus other prostanoids (e.g. PGE₂; Fig. 1A and S5) majorly originate from CAF (maybe also from MESO, see Fig. 1).

PTGIR expression was low in all cell types analyzed (Fig. 1A). The highest expression of PTGIR was detected in ascTAM and CAF by RT-qPCR (Fig. 3A), while cell-surface staining (FACS) revealed the highest PTGIR protein expression for ascTAM relative to both tumor cells and CAF (Fig. 3B, C). This points to ascTAM as the primary target cell type for CAF-derived PGI₂ in HGSC, and suggests that an autocrine PGI₂ activity in CAF is unlikely.

To verify PGI₂ signaling via the G_s-coupled receptor PTGIR, activation of adenylate cyclase was measured. Consistent with the PTGIR expression data described above, treatment with the PGI₂ analog MRE-269 induced intracellular cAMP accumulation in ascTAM, but only weakly, if at all, in CAF and ascTU (Fig. 3D). This PTGIR dependency was confirmed by using asc-MDM as a model system (Steitz et al., 2020). Equivalent to ascTAM, asc-MDM exhibited a low PTGIS expression (Fig. S4), a strong cell-surface expression of PTGIR (Fig. S7) as well as a MRE-269-induced cAMP accumulation (Fig. 3E), which was partially prevented by the PTGIR antagonist CAY10449.

These observations point to a crosstalk between PGI₂-producing CAF and PTGIR-expressing ascTAM with a potential role in HGSC progression. We, therefore, investigated the impact of PGI₂ on TAM polarization and function.

PGI₂ analogs affect the transcriptome and polarization of macrophages

First, we analyzed the effect of PGI₂ on the transcriptomic profile and differentiation of ascTAM. For this purpose, ascTAM treated ± MRE-269 were analyzed by RNA-Seq. The effect of PGI₂ on polarization of ascTAM is illustrated in Figure 4B, which shows regulation of M1- and M2-related genes but no direction of polarization. For example, *CCR7*, *CD86*, *ITGAX* (M1 marker genes) and *VEGFA* (M2 marker gene) are upregulated, while *CD80*, *FCGRs*, *TNF* (M1 marker genes) and *CD163*, *MRC1/CD206*, *MSR* (M2 marker genes) are downregulated due to MRE-269 treatment. Surface marker expression measured by FACS on asc-MDM was consistent with the RNA-Seq data from ascTAM, as M2-associated mannose receptor CD206 (Fig. 4E) was decreased and the M1-linked receptor CD86 (Fig. 4F) increased. In addition, the induction of VEGF secretion by PGI₂ analogs was confirmed by ELISA in ascTAM as well as in asc-MDM (Fig. 4D). These observations point to the induction of a mixed-polarization phenotype by PTGI₂, consistent with previous data on ascTAM (Reinartz et al., 2014).

Further analysis of the RNA-Seq dataset identified 34 cytokine genes linked to metastasis (genecards.org database) to be induced by PGI₂ analogs, e.g. *ANGPTL4*, *BMP6*, *TGFB3*, *VEGFA*, *WNT5B* (Fig. 5B and Supplementary Table S7). PGI₂ also seems to play a role in ECM remodeling, as different matrix proteins were upregulated by PGI₂, e.g. *ADAM8*, *LAMA1* and *MMP19* (Fig. 5C). Moreover, cytokine genes relevant for immune cell infiltration, e.g. *CCL8*, *CXCL10* and *IL12A* were downregulated, while genes involved in PGE₂ synthesis were upregulated, suggesting that PGI₂ skews TAM towards an immunosuppressed and immunosuppressive phenotype (Fig. 5D, E and Supplementary Table S8).

In summary, PGI₂ treatment shifts the differentiation, transcriptional profile and secretome of macrophages towards a pro-tumorigenic and immunosuppressive phenotype. As *PDK4*, a PPARβ/δ target gene, was not elevated by

(Supplementary Table S6) PGI₂ analogs, we conclude that the observed effects of PGI₂ are mediated via its membrane receptor PTGIR and not via PPARβ/δ signaling.

The phagocytic capability of macrophages decreases with PGI₂ treatment

Finally, we asked whether the observed phenotype switch in PGI₂-induced asc-MDM may influence on the phagocytic activity of macrophages. To this end, macropinocytosis assays using FITC dextran were performed with asc-MDM. As expected, PGI₂ analog treatment of asc-MDM resulted in significantly reduced macropinocytosis (Fig 6A). This was partially impaired by the PTGIR antagonists CAY10449 and CAY10441, while the PPARβ/δ agonist L165041 did not affect the phagocytic capacity of asc-MDM (Fig. 6B) in contrast to m0-MDM (Fig. S9C). Previous work has shown that ascites leads to accumulation of endogenous PPARβ/δ ligands in TAM, which renders them largely unresponsive to exogenous synthetic PPARβ/δ agonists (Adhikary et al., 2015). These findings point to a signaling via PTGIR rather than PPARβ/δ in the phagocytosis of ascTAM in HGSC.

Next, we sought to verify the impact of PGI₂ secreted by primary CAF on the macropinocytotic activity of asc-MDM. To this end, CAF were co-cultured with asc-MDM and supplemented with AA as substrate for PGI₂ synthesis (Fig. S10A). In this experimental setup, we observed reduced macropinocytosis by asc-MDM when co-cultured with CAF in comparison to asc-MDM alone (Fig. S10B). Blocking COX1/2 could partially reverse this effect in 4 out of 6 donors. This findings support the conclusion that PGI₂ released by CAF inhibits the phagocytotic potential of macrophages.

Pro-tumorigenic function of the PGI₂-induced TAM secretome

Our RNA-Seq data of PGI₂-treated ascTAM revealed changes in the expression of genes linked to motility, metastasis and ECM remodeling (Fig. 5B, C and Supplementary Table S7). We therefore asked whether PGI₂ may alter the TAM secretome to promote a pro-tumorigenic TME.

This hypothesis was confirmed by the finding that primary tumor cells showed an increased migration when pre-cultured with CM of MRE-269-treated ascTAM in

a transwell assay (Fig. 7A, B). Similar results were obtained for the adhesion of tumor cells on a MESO monolayer (Fig. 7C, D, integrity of MESO monolayer is shown in Fig. S1). As in the experiments described in preceding sections, PTGIR rather than PPAR β/δ appeared to be the target receptor for PGI₂ in this scenario, as the MRE-269-induced migration and adhesion of tumor cells were inhibited by the selective PTGIR antagonist CAY10449, and in contrast to MRE-269 no effect was observed for the PPAR β/δ agonist L165041. Taken together our data point to a pro-tumorigenic function of the PGI₂-induced TAM secretome via PTGIR activation.

3.3.2 Description of own contribution

My contributions to this publication included the conceptual and experimental setup, execution and analysis of the functional assays shown in Fig. 2C-E, Fig. 3B-E, Fig. 4D, Fig. 6B, Fig. 7 and Supplementary Fig. S1, S4-S6, S7B, C, S9C, S1. The transcriptomic data depicted in Figure 1 is based on the samples which I isolated for the study described in section 3.1. In addition, I performed the culture and treatment of ascTAM as well as RNA isolation for the analysis shown in Figure 4A-C and 5. The contributing author Isabel Knuth worked as an undergraduate student under my supervision.

4. Discussion

4.1 The intercellular network of tumor and host cells in HGSC metastases

Our study, published in 2021 (Sommerfeld et al., 2021), was the first to define a comprehensive model of intercellular signaling pathways between tumor cells and host cells in different compartments of the HGSC TME. To this end, we isolated all major cell types (omTU, CAF, MESO, ADI, omTAM) from the omentum, which represents the major metastatic site of the peritoneal dissemination of HGSC (Meza-Perez & Randall). Subsequently, bulk RNA-Seq was performed for these cell types as well as for ascites-derived ascTAM, ascTAT and ascTU. The transcriptomic data unraveled an unexpected major function of host cells in this network, being the key source of cytokines and growth factors in the HGSC TME. Especially the stromal cells (CAF, MESO and ADI) seem to play a substantial role, as they produce more than half of the selectively expressed genes and 31 of these are associated with a poor clinical outcome (Table 1). Recently published scRNA-Seq data supports this conclusion (Olbrecht et al., 2021). Besides this cell-type-selective synthesis of growth factors and cytokines, our transcriptome data revealed a clear cell-type-selective expression of their cognate receptors.

The essential contribution by omental host cells to ECM-mediated signaling and ECM reorganization discovered in this study extends former findings on ascites-derived cells in HGSC (Finkernagel et al., 2016; Worzfeld et al., 2018). Intriguingly, 200 of the identified genes were previously associated with different aspects of tumor progression and metastasis. Apart from the known essential role of stroma cells in the expression of collagens (Kalluri, 2016), we detected novel cell-type selective expression patterns, for example BCAM expression in tumor cells and MESO. This is of particular interest, because a study recently published by our group suggests that BCAM promotes metastasis in HGSC via enhancing the spread of cancer cell spheroids (Sivakumar et al., 2023).

Apart from cytokines and growth factors bioactive lipids, such as LPA, AA and prostanoids, have been linked to pro-tumorigenic functions and to a poor clinical outcome in previous studies (Dietze et al., 2021; Kobayashi et al., 2018; Reinartz

et al., 2019). Our transcriptomic data offered new insights into the role of tumor-associated host cells in the lipid-mediated intercellular crosstalk in the HGSC TME. Aside from ubiquitously expressed lipid-metabolizing enzymes, we identified cell-type-selective pathways. For example, PTGIS expressed in CAF seems to play a critical role in this network (Sommerfeld et al., 2022).

The early peritoneal metastasis via transcoelomic dissemination of tumor cells and spheroids is a substantial clinical problem in HGSC. Invasion of these detached tumor cells and spheroids into metastatic sites is strongly influenced by their interaction with host cells. Likewise, tumor-host-cell interactions play a pivotal role in the conditional resistance of tumor cells during chemotherapy (Pogge von Strandmann et al., 2017). The development of a global picture of the signaling network in HGSC, as presented within this work, is therefore of great importance to overcome therapy resistance, with tumor-host-interactions as new potential targets. Moreover, as many of the detected soluble factors, ECM and lipid mediators are associated with survival and tumor progression, their potential utility as biomarkers is evident.

Individual mediators and signaling pathways of particular interest will be discussed in more detail below.

4.2 Comparison of omental TU and TAM to their counterparts derived from ascites

This work also presents the first study of a transcriptomic comparison of matched pairs of ascites-derived tumor cells or TAM with their omental counterparts. One important finding was a very high similarity between the two TU subsets as well as between the two TAM subsets, indicating their utility (easily accessible) of ascTAM and ascTU for research projects aiming at defining their function in the HGSC TME. Nonetheless, we identified differentially expressed genes, e.g., upregulated genes linked to cell cycle progression in omTAM. An enhanced proliferation of omTAM was validated via FACS staining, which is likely due to stromal expression of CSF-1, known as the main growth factor of survival and proliferation of monocytes and macrophages (Pollard, 2004). This observation indicates that replication of resident macrophages, apart from blood-derived monocytes, might be the source of ascTAM in HGSC.

Another crucial discovery of the comparative analysis is the higher expression of pro-inflammatory signaling in omental tumor cells and TAM. Both omTU and omTAM showed an induced expression of HSP70 genes in the metastasis-derived cell types. This is of special significance as extracellular HSP70 has been linked to tumor progression (Seclì et al., 2021), and HSP70 in HGSC ascites is significantly associated with a poor RFS (Finkernagel et al., 2019). Apart from its cytoprotective functions, HSP70 can be released as an extracellular mediator and activate pro-inflammatory NF κ B- and MAPK-signaling (Asea et al., 2002; Juhasz et al., 2013). Consistent with these published findings, we detected enhanced nuclear translocation of p65 and increased levels of IKK α/β in rHSP70-treated ascTAM, pointing to an activation of NF κ B-signaling in ascTAM by extracellular HSP70, associated with increased IL-6 secretion. Pro-inflammatory IL-6 signaling is linked to the promotion of metastasis in OC by supporting EMT, migration, proliferation and other pro-tumorigenic functions (Browning et al., 2018). Interestingly, the CD163+Tim4+ subset of tissue-resident macrophages, which are characterized by upregulation of the IL6-responsive JAK-STAT pathway, has been reported to play an essential role in the metastatic spread of OC cells (Etzerodt et al., 2020).

Taken together, our data provide evidence for a high similarity of ascTU versus omTU and ascTAM versus omTAM, respectively, but also show that the omental HGSC TME represents an inflammation-promoting environment. Thus, selective pathways within this TME can be of interest for further studies to elucidate their role in the establishment of pre-metastatic niches in HGSC.

4.3 Pro-metastatic function of WNT4 in the crosstalk of CAF and tumor cells

In view of the central role of WNT signaling in cancer (Teeuwssen & Fodde, 2019), WNT4 was selected as an example to verify the significance of host cells in the network of HGSC metastases. Our RNA-Seq data revealed WNT4 as a highly cell-type-selective ligand from CAF (Sommerfeld et al., 2021; Fig. 6A), which is consistent with its known high expression in fibroblasts as well as its role in wound healing and fibrosis (Labus et al., 1998; Surendran et al., 2002). Furthermore, a recent study detected upregulation of WNT4 in the activated CAF-

subtype CAF-S1 compared to CAF-S4 in HGSC, which is enriched for genes involved in ECM-remodeling and adhesion (Givel et al., 2018).

The observed expression pattern of FZD8, the primary receptor of WNT4 and its main co-receptors LRP5/6 (Dijksterhuis et al., 2015), indicated tumor cells as major target cells for WNT4. Consistent with this notion, functional assays with OVCAR4 as well as primary HGSC OC cells pointed to a role of WNT4 secreted by CAF in the induction of tumor cell motility, migration and adhesion to a MESO monolayer (Sommerfeld et al., 2021, Fig. 6), providing evidence for a pro-metastatic function of WNT4 in the cross-talk between CAF and tumor cells in HGSC. This is in accordance with published pro-tumorigenic functions of WNT4 in breast cancer, laryngeal carcinoma and colorectal cancer (Huang & Feng, 2017; Vouyovitch et al., 2016; Wang et al., 2020; Yang et al., 2020).

4.4 TGFBI and TNC secreted by ascTAM promote tumor migration

Our study (Steitz et al., 2020) revealed that TNC, TGFBI and FN1 secreted by TAM promote OC cell migration. This is in line with previous publications reporting pro-tumorigenic functions of FN1 in OC (Lou et al., 2013; Yousif, 2014). All three proteins are known as TGF- β inducible ECM constituents (Lowy & Oskarsson, 2015; Noble et al., 1992; Ween et al., 2012) and have been reported to promote tumor progression (Paron et al., 2011; Suzuki et al., 2018; Yousif, 2014). Furthermore, TGFBI, TNC and FN1 were associated with a poor clinical outcome in various cancer entities (Gocheva et al., 2017; Gopal et al., 2017; Suzuki et al., 2018). In OC, Ween and colleagues described TGFBI as both a tumor suppressor and oncogene, which may be dependent on features determined by the TME (Ween et al., 2012). Within our HGSC patient cohort, increased ascites levels of TGFBI, TNC and FN1 were significantly associated with a shorter RFS. Our secretome and transcriptome data point to ascTAM and stroma cells in omental metastasis (especially CAF) as the major sources of these three factors (Sommerfeld et al., 2021). This is consistent with published data for other cancer types, where a promigratory function of CAF-derived TNC, TGFBI and FN1 has been described (Gopal et al., 2017; Lowy & Oskarsson, 2015; Suzuki et al., 2018). Functional assays with MDMs using neutralizing antibodies against TGFBI or TNC and siRNA-mediated silencing of TGFBI expression showed decreased

migration of ascTU towards CM of asc-MDMs, indicating a pro-tumorigenic impact of these mediators (Steitz et al., 2020, Fig. 6 and 7).

Taken together, our study links TGFBI and TNC secreted from ascTAM to tumor cell migration. Since these ECM proteins are also produced by stromal cells, especially by CAF, investigating a cooperative function of TAM and CAF in modulating ECM interactions during metastatic processes would be of interest for further research.

4.5 PGI₂ mediated crosstalk between CAF and ascTAM

Based on bioinformatic analysis of the transcriptome of tumor and different host cell types from ascites and omental metastases, we predicted several potentially relevant lipid-mediated intercellular pathways in the HGSC TME. In this context, a particularly interesting finding was the cell-type-selective expression of PTGIS in CAF and MESO in conjunction with COX1 and 2. The multistep synthesis of PGI₂ from AA is catalyzed by COX1/2 followed by prostaglandin-specific synthase PTGIS (Moncada et al., 1976; Mitchell & Kirkby, 2019). The role of COX2 in tumor progression was investigated intensively in the past and elevated expression was linked to a poor survival of multiple solid tumors (Hashemi Goradel et al., 2019), including OC (Lee et al., 2013). Even though far less attention has been paid to COX1 in tumor promotion, COX1 was proposed as marker for OC already in 1995 (Lee & Ng, 1995). Moreover, differing from most malignancies, various studies reported a higher expression of COX1 than COX2 in HGSC (Beeghly-Fadiel et al., 2018; Daikoku et al., 2005; Wilson et al., 2015). This is consistent with our data showing higher PTGS1/COX1 mRNA levels in tumor cells and CAF (Sommerfeld et al., 2022, Fig. 1). These observations may be relevant in view of the fact that reported association of a reduced incidence of OC with the intake of COX inhibitors, especially the non-steroidal anti-inflammatory drug (NSAID) aspirin (Barnard et al., 2018; Trabert et al., 2014).

Our study provides strong evidence for a novel PGI₂-mediated crosstalk between CAF and TAM leading to altered TAM phenotypes with pro-tumorigenic functions in HGSC. Due to elevated PTGIS mRNA and protein expression, CAF were identified as the major producers of PGI₂ in this TME, which was validated by lipid LC-MS/MS. Consistent with this finding, CAF-selective PTGIS expression has

previously been described for pancreatic ductal adenocarcinoma (Gubbala et al., 2022). Our RNA-Seq data also indicate high PTGIS expression in MESO, which may thus contribute to the high PGI₂ level in HGSC ascites. This may be linked to the plasticity of MESO, which can undergo MMT to assume a CAF-like phenotype (Sandoval et al., 2013).

Pro- as well as anti-tumorigenic effects have been attributed to PTGIS and its product PGI₂ (Ahn et al., 2018; Dai et al., 2020; Li et al., 2018). Based on the PRECOG database, high intra-tumoral PTGIS expression is linked to a decreased overall survival of HGSC patients, contrary to other cancer entities. We identified ascTAM as a main target of CAF-secreted PGI₂ based on PTGIR expression and activation. Autocrine functions of PGI₂ on CAF, as published for fibroblasts (Kamio et al., 2007), may also play a role in HGSC. Since PTGIR-signaling in CAF seems to be negligible due to low PTGIR expression levels and low intracellular cAMP accumulation in response to PGI₂, we focused on the crosstalk of CAF with ascTAM.

Based on transcriptional and phenotypical analyses, we conclude that upon PGI₂ analog stimulation TAM acquire an immunosuppressing and mixed-polarization phenotype, including both M1- and M2-like characteristics (Sommerfeld et al., Fig. 4). This is in line with a previous publication by our group (Reinartz et al., 2014) as well as recent studies based on scRNA-Seq data (Izar et al., 2020; Olbrecht et al., 2021), providing evidence for intra-tumoral heterogeneity of TAM in HGSC.

In the past decades, immunoregulating functions have been assigned to PGI₂. Besides pro-inflammatory signaling, anti-inflammatory and anti-fibrotic effects of PGI₂ have been reported (Aronoff et al., 2007; Dorris & Peebles, 2012). For instance, PGI₂ analogs suppressed phagocytotic capacity, inhibited bacterial killing and enhanced IL-6 production in peritoneal rat macrophages, which had differential effects on macrophages from distinct anatomic sites, which correlated with PTGIR expression (Aronoff et al., 2007). This anatomic difference is compatible with our own observations that ascTAM exhibit higher PTGIR expression than omTAM, and that the phagocytotic capability and phagocytosis-related markers were downregulated by PGI₂ analogs in asc-MDM.

PTGIR can also signal through activation of the nuclear receptor PPAR β/δ (Hertz et al., 1996). In the present study, the effect of PGIS analogs on macropinocytosis was partially prevented by PTGIR antagonists, while the PPAR β/δ activation had no detectable effect, indicating a minor role for PPAR β/δ , if any. This conclusion is supported by a previous study showing that PPAR β/δ target genes are constitutively upregulated in TAMs by endogenous fatty acid ligands and therefore largely refractory to synthetic agonists (Schumann et al., 2015).

Finally, we identified a previously unknown PGI₂-mediated, PTGIR-dependent reprogramming of TAM enhancing primary tumor cell migration and adhesion to a MESO monolayer (Sommerfeld et al., Fig. 7). Thus, our RNA-Seq data of PGI₂-treated ascTAM revealed upregulation of multiple genes linked to motility, metastasis and ECM remodeling, including *EGF*, *FN1*, *TNC* and *TGFBI*, which are secreted by macrophages and are known to support tumor cell migration (Steitz et al., 2020; Zeng et al., 2019). Additional mediators, found within the upregulated cytokines in MRE-269 treated ascTAM, could be EREG and AREG, which both are EGFR ligands and promote cancer migration and invasion (Cheng et al., 2021; So et al., 2014).

Collectively, our results indicate that PGI₂ released by CAF promotes immunosuppressive and pro-metastatic macrophage polarization. Thus, inhibiting PGI₂ synthesis might be a promising option for improving HGSC treatment.

4.6 Conclusion

Our studies on patient-derived tumor and host cells - TAM, TAT, ADI, MESO, CAF - provide new insights into the intercellular network signaling in the TME of HGSC and led to the establishment of a comprehensive model of intercellular signaling pathways. A key aspect of this network is an unexpected dominant role of factors secreted by stroma and host cells. These cytokines and growth factors create an inflammation-promoting environment, which is enhanced in omental TAM and tumor cells as compared to their ascites-derived counterparts.

On the basis of our transcriptomic data, we analyzed the functional relevance of novel cell-type-selective signaling pathways supporting HGSC progression. Exemplarily, we could show a direct pro-metastatic function of the highly cell-selective mediator WNT4 produced by CAF. In addition, we identified TGFBI and

TNC in the secretome of ascTAM as essential factors promoting tumor cell migration. Our results also point to a potentially important role of CAF in modulating the phenotype and function of TAM in the HGSC TME. By releasing high amounts of PGI₂, CAF promote an immunosuppressive and pro-metastatic polarization of macrophages with indirect effects on tumor cell migration.

Our data may serve as a basis for the potential application of stroma-selective cytokines, growth factors, ECM proteins and lipid-mediators as biomarkers, since many of these factors are associated with a poor clinical outcome. Furthermore, our datasets will provide relevant information for future research projects aiming at an improved understanding of the molecular mechanisms of HGSC metastasis. Finally, a global picture of the signaling network gained by this work may pave the way for the identification of new potential drug targets to interfere with HGSC progression and overcome therapy resistance.

5. References

- Adhikary, T., Wortmann, A., Finkernagel, F., Lieber, S., Nist, A., Stiewe, T., Wagner, U., Müller-Brüsselbach, S., Reinartz, S., & Müller, R. (2017). Interferon signaling in ascites-associated macrophages is linked to a favorable clinical outcome in a subgroup of ovarian carcinoma patients. *BMC Genomics*, 18(1), 243. <https://doi.org/10.1186/s12864-017-3630-9>
- Adhikary, T., Wortmann, A., Schumann, T., Finkernagel, F., Lieber, S., Roth, K., Toth, P. M., Diederich, W. E., Nist, A., Stiewe, T., Kleinesudeik, L., Reinartz, S., Müller-Brüsselbach, S., & Müller, R. (2015). The transcriptional PPAR β/δ network in human macrophages defines a unique agonist-induced activation state. *Nucleic Acids Research*, 43(10), 5033–5051. <https://doi.org/10.1093/nar/gkv331>
- Ahn, J.-H., Lee, K.-T., Choi, Y. S., & Choi, J.-H. (2018). Iloprost, a prostacyclin analog, inhibits the invasion of ovarian cancer cells by downregulating matrix metalloproteinase-2 (MMP-2) through the IP-dependent pathway. *Prostaglandins & Other Lipid Mediators*, 134, 47–56. <https://doi.org/10.1016/j.prostaglandins.2017.12.002>
- Aronoff, D. M., Peres, C. M., Serezani, C. H., Ballinger, M. N., Carstens, J. K., Coleman, N., Moore, B. B., Peebles, R. S., Faccioli, L. H., & Peters-Golden, M. (2007). Synthetic Prostacyclin Analogs Differentially Regulate Macrophage Function via Distinct Analog-Receptor Binding Specificities. *The Journal of Immunology*, 178(3), 1628–1634. <https://doi.org/10.4049/jimmunol.178.3.1628>
- Asea, A., Rehli, M., Kabingu, E., Boch, J. A., Baré, O., Auron, P. E., Stevenson, M. A., & Calderwood, S. K. (2002). Novel Signal Transduction Pathway Utilized by Extracellular HSP70. *Journal of Biological Chemistry*, 277(17), 15028–15034. <https://doi.org/10.1074/jbc.M200497200>
- Ayantunde, A. A., & Parsons, S. L. (2007). Pattern and prognostic factors in patients with malignant ascites: A retrospective study. *Annals of Oncology: Official Journal of the European Society for Medical Oncology*, 18(5), 945–949. <https://doi.org/10.1093/annonc/mdl499>
- Barnard, M. E., Poole, E. M., Curhan, G. C., Eliassen, A. H., Rosner, B. A., Terry, K. L., & Tworoger, S. S. (2018). Association of Analgesic Use With Risk of Ovarian Cancer in the Nurses' Health Studies. *JAMA Oncology*, 4(12), 1675. <https://doi.org/10.1001/jamaoncol.2018.4149>
- Bochet, L., Lehuédé, C., Dauvillier, S., Wang, Y. Y., Dirat, B., Laurent, V., Dray, C., Guiet, R., Maridonneau-Parini, I., Le Gonidec, S., Couderc, B., Escourrou, G., Valet, P., & Muller, C. (2013). Adipocyte-derived fibroblasts promote tumor progression and contribute to the desmoplastic reaction in breast cancer. *Cancer Research*, 73(18), 5657–5668. <https://doi.org/10.1158/0008-5472.CAN-13-0530>
- Bortot, B., Apollonio, M., Rampazzo, E., Valle, F., Brucale, M., Ridolfi, A., Ura, B., Addobbati, R., Di Lorenzo, G., Romano, F., Buonomo, F., Ripepi, C., Ricci, G., & Biffi, S. (2021). Small extracellular vesicles from malignant ascites of patients with advanced ovarian

- cancer provide insights into the dynamics of the extracellular matrix. *Molecular Oncology*, 15(12), 3596–3614. <https://doi.org/10.1002/1878-0261.13110>
- Browning, L., Patel, M., Bring Horvath, E., Tawara, K., & Jorcyk, C. L. (2018). IL-6 and ovarian cancer: Inflammatory cytokines in promotion of metastasis. *Cancer Management and Research*, Volume 10, 6685–6693. <https://doi.org/10.2147/CMAR.S179189>
- Cai, J., Tang, H., Xu, L., Wang, X., Yang, C., Ruan, S., Guo, J., Hu, S., & Wang, Z. (2012). Fibroblasts in omentum activated by tumor cells promote ovarian cancer growth, adhesion and invasiveness. *Carcinogenesis*, 33(1), 20–29. <https://doi.org/10.1093/carcin/bgr230>
- Cha, Y. J., & Koo, J. S. (2019). Roles of omental and bone marrow adipocytes in tumor biology. *Adipocyte*, 8(1), 304–317. <https://doi.org/10.1080/21623945.2019.1643189>
- Chehover, M., Reich, R., & Davidson, B. (2020). Expression of Wnt pathway molecules is associated with disease outcome in metastatic high-grade serous carcinoma. *Virchows Archiv*, 477(2), 249–258. <https://doi.org/10.1007/s00428-019-02737-z>
- Cheng, W.-L., Feng, P.-H., Lee, K.-Y., Chen, K.-Y., Sun, W.-L., Van Hiep, N., Luo, C.-S., & Wu, S.-M. (2021). The Role of EREG/EGFR Pathway in Tumor Progression. *International Journal of Molecular Sciences*, 22(23), 12828. <https://doi.org/10.3390/ijms222312828>
- Clark, R., Krishnan, V., Schoof, M., Rodriguez, I., Theriault, B., Chekmareva, M., & Rinker-Schaeffer, C. (2013). Milky spots promote ovarian cancer metastatic colonization of peritoneal adipose in experimental models. *The American Journal of Pathology*, 183(2), 576–591. <https://doi.org/10.1016/j.ajpath.2013.04.023>
- Curiel, T. J., Coukos, G., Zou, L., Alvarez, X., Cheng, P., Mottram, P., Evdemon-Hogan, M., Conejo-Garcia, J. R., Zhang, L., Burow, M., Zhu, Y., Wei, S., Kryczek, I., Daniel, B., Gordon, A., Myers, L., Lackner, A., Disis, M. L., Knutson, K. L., ... Zou, W. (2004). Specific recruitment of regulatory T cells in ovarian carcinoma fosters immune privilege and predicts reduced survival. *Nature Medicine*, 10(9), 942–949. <https://doi.org/10.1038/nm1093>
- Dai, D., Chen, B., Feng, Y., Wang, W., Jiang, Y., Huang, H., & Liu, J. (2020). Prognostic value of prostaglandin I2 synthase and its correlation with tumor-infiltrating immune cells in lung cancer, ovarian cancer, and gastric cancer. *Aging*, 12(10), 9658–9685. <https://doi.org/10.18632/aging.103235>
- Daikoku, T., Wang, D., Tranguch, S., Morrow, J. D., Orsulic, S., DuBois, R. N., & Dey, S. K. (2005). Cyclooxygenase-1 Is a Potential Target for Prevention and Treatment of Ovarian Epithelial Cancer. *Cancer Research*, 65(9), 3735–3744. <https://doi.org/10.1158/0008-5472.CAN-04-3814>
- DeWitt, D. L., & Smith, W. L. (1983). Purification of prostacyclin synthase from bovine aorta by immunoaffinity chromatography. Evidence that the enzyme is a hemoprotein. *Journal*

- of *Biological Chemistry*, 258(5), 3285–3293. [https://doi.org/10.1016/S0021-9258\(18\)32859-X](https://doi.org/10.1016/S0021-9258(18)32859-X)
- Dietze, R., Hammoud, M. K., Gómez-Serrano, M., Unger, A., Bieringer, T., Finkernagel, F., Sokol, A. M., Nist, A., Stiewe, T., Reinartz, S., Ponath, V., Preußner, C., von Strandmann, E. P., Müller-Brüsselbach, S., Graumann, J., & Müller, R. (2021). Phosphoproteomics identify arachidonic-acid-regulated signal transduction pathways modulating macrophage functions with implications for ovarian cancer. *Theranostics*, 11(3), 1377–1395. <https://doi.org/10.7150/thno.52442>
- Dijksterhuis, J. P., Baljinnyam, B., Stanger, K., Sercan, H. O., Ji, Y., Andres, O., Rubin, J. S., Hannoush, R. N., & Schulte, G. (2015). Systematic mapping of WNT-FZD protein interactions reveals functional selectivity by distinct WNT-FZD pairs. *The Journal of Biological Chemistry*, 290(11), 6789–6798. <https://doi.org/10.1074/jbc.M114.612648>
- Dorris, S. L., & Peebles, R. S. (2012). PGI₂ as a regulator of inflammatory diseases. *Mediators of Inflammation*, 2012, 926968. <https://doi.org/10.1155/2012/926968>
- Etzerodt, A., Moulin, M., Doktor, T. K., Delfini, M., Mossadegh-Keller, N., Bajenoff, M., Sieweke, M. H., Moestrup, S. K., Auphan-Anezin, N., & Lawrence, T. (2020). Tissue-resident macrophages in omentum promote metastatic spread of ovarian cancer. *Journal of Experimental Medicine*, 217(4), e20191869. <https://doi.org/10.1084/jem.20191869>
- Finkernagel, F., Reinartz, S., Lieber, S., Adhikary, T., Wortmann, A., Hoffmann, N., Bieringer, T., Nist, A., Stiewe, T., Jansen, J. M., Wagner, U., Müller-Brüsselbach, S., & Müller, R. (2016). The transcriptional signature of human ovarian carcinoma macrophages is associated with extracellular matrix reorganization. *Oncotarget*, 7(46), 75339–75352. <https://doi.org/10.18632/oncotarget.12180>
- Finkernagel, F., Reinartz, S., Schuldner, M., Malz, A., Jansen, J. M., Wagner, U., Worzfeld, T., Graumann, J., von Strandmann, E. P., & Müller, R. (2019). Dual-platform affinity proteomics identifies links between the recurrence of ovarian carcinoma and proteins released into the tumor microenvironment. *Theranostics*, 9(22), 6601–6617. <https://doi.org/10.7150/thno.37549>
- Givel, A.-M., Kieffer, Y., Scholer-Dahirel, A., Sirven, P., Cardon, M., Pelon, F., Magagna, I., Gentric, G., Costa, A., Bonneau, C., Mieulet, V., Vincent-Salomon, A., & Mehta-Grigoriou, F. (2018). MiR200-regulated CXCL12 β promotes fibroblast heterogeneity and immunosuppression in ovarian cancers. *Nature Communications*, 9(1), 1056. <https://doi.org/10.1038/s41467-018-03348-z>
- Gocheva, V., Naba, A., Bhutkar, A., Guardia, T., Miller, K. M., Li, C. M.-C., Dayton, T. L., Sanchez-Rivera, F. J., Kim-Kiselak, C., Jaiikhani, N., Winslow, M. M., Del Rosario, A., Hynes, R. O., & Jacks, T. (2017). Quantitative proteomics identify Tenascin-C as a promoter of lung cancer progression and contributor to a signature prognostic of patient survival. *Proceedings of the National Academy of Sciences*, 114(28). <https://doi.org/10.1073/pnas.1707054114>

- Gopal, S., Veracini, L., Grall, D., Butori, C., Schaub, S., Audebert, S., Camoin, L., Baudelet, E., Radwanska, A., Beghelli-de la Forest Divonne, S., Violette, S. M., Weinreb, P. H., Rekima, S., Ilie, M., Sudaka, A., Hofman, P., & Van Obberghen-Schilling, E. (2017). Fibronectin-guided migration of carcinoma collectives. *Nature Communications*, 8(1), 14105. <https://doi.org/10.1038/ncomms14105>
- Gubbala, V. B., Jytosana, N., Trinh, V. Q., Maurer, H. C., Naeem, R. F., Lytle, N. K., Ma, Z., Zhao, S., Lin, W., Han, H., Shi, Y., Hunter, T., Singh, P. K., Olive, K. P., Tan, M. C. B., Kaech, S. M., Wahl, G. M., & DelGiorno, K. E. (2022). Eicosanoids in the Pancreatic Tumor Microenvironment—A Multicellular, Multifaceted Progression. *Gastro Hep Advances*, 1(4), 682–697. <https://doi.org/10.1016/j.gastha.2022.02.007>
- Gupta, R. A., Tan, J., Krause, W. F., Geraci, M. W., Willson, T. M., Dey, S. K., & DuBois, R. N. (2000). Prostacyclin-mediated activation of peroxisome proliferator-activated receptor delta in colorectal cancer. *Proceedings of the National Academy of Sciences of the United States of America*, 97(24), 13275–13280. <https://doi.org/10.1073/pnas.97.24.13275>
- Hamanishi, J., Mandai, M., Iwasaki, M., Okazaki, T., Tanaka, Y., Yamaguchi, K., Higuchi, T., Yagi, H., Takakura, K., Minato, N., Honjo, T., & Fujii, S. (2007). Programmed cell death 1 ligand 1 and tumor-infiltrating CD8+ T lymphocytes are prognostic factors of human ovarian cancer. *Proceedings of the National Academy of Sciences of the United States of America*, 104(9), 3360–3365. <https://doi.org/10.1073/pnas.0611533104>
- Hashemi Goradel, N., Najafi, M., Salehi, E., Farhood, B., & Mortezaee, K. (2019). Cyclooxygenase-2 in cancer: A review. *Journal of Cellular Physiology*, 234(5), 5683–5699. <https://doi.org/10.1002/jcp.27411>
- Haunschild, C. E., & Tewari, K. S. (2020). Bevacizumab use in the frontline, maintenance and recurrent settings for ovarian cancer. *Future Oncology (London, England)*, 16(7), 225–246. <https://doi.org/10.2217/fon-2019-0042>
- Hertz, R., Berman, I., Keppler, D., & Bar-Tana, J. (1996). Activation of gene transcription by prostacyclin analogues is mediated by the peroxisome-proliferators-activated receptor (PPAR). *European Journal of Biochemistry*, 235(1–2), 242–247. <https://doi.org/10.1111/j.1432-1033.1996.00242.x>
- Huang, Z., & Feng, Y. (2017). Exosomes Derived From Hypoxic Colorectal Cancer Cells Promote Angiogenesis Through Wnt4-Induced β -Catenin Signaling in Endothelial Cells. *Oncology Research*, 25(5), 651–661. <https://doi.org/10.3727/096504016X14752792816791>
- Izar, B., Tirosh, I., Stover, E. H., Wakiro, I., Cuoco, M. S., Alter, I., Rodman, C., Leeson, R., Su, M.-J., Shah, P., Iwanicki, M., Walker, S. R., Kanodia, A., Melms, J. C., Mei, S., Lin, J.-R., Porter, C. B. M., Slyper, M., Waldman, J., ... Regev, A. (2020). A single-cell landscape of high-grade serous ovarian cancer. *Nature Medicine*, 26(8), 1271–1279. <https://doi.org/10.1038/s41591-020-0926-0>

- Jeon, E. S., Moon, H. J., Lee, M. J., Song, H. Y., Kim, Y. M., Cho, M., Suh, D.-S., Yoon, M.-S., Chang, C. L., Jung, J. S., & Kim, J. H. (2008). Cancer-Derived Lysophosphatidic Acid Stimulates Differentiation of Human Mesenchymal Stem Cells to Myofibroblast-Like Cells. *Stem Cells*, 26(3), 789–797. <https://doi.org/10.1634/stemcells.2007-0742>
- Juhász, K., Lipp, A.-M., Nimmervoll, B., Sonnleitner, A., Hesse, J., Haselgruebler, T., & Balogi, Z. (2013). The complex function of hsp70 in metastatic cancer. *Cancers*, 6(1), 42–66. <https://doi.org/10.3390/cancers6010042>
- Kalluri, R. (2016). The biology and function of fibroblasts in cancer. *Nature Reviews. Cancer*, 16(9), 582–598. <https://doi.org/10.1038/nrc.2016.73>
- Kamio, K., Liu, X., Sugiura, H., Togo, S., Kobayashi, T., Kawasaki, S., Wang, X., Mao, L., Ahn, Y., Hogaboam, C., Toews, M. L., & Rennard, S. I. (2007). Prostacyclin Analogs Inhibit Fibroblast Contraction of Collagen Gels through the cAMP-PKA Pathway. *American Journal of Respiratory Cell and Molecular Biology*, 37(1), 113–120. <https://doi.org/10.1165/rcmb.2007-0009OC>
- Keith, R. L., & Geraci, M. W. (2006). Prostacyclin in lung cancer. *Journal of Thoracic Oncology: Official Publication of the International Association for the Study of Lung Cancer*, 1(6), 503–505.
- Klein, T., Benders, J., Roth, F., Baudler, M., Siegle, I., & Kömhoff, M. (2015). Expression of Prostacyclin-Synthase in Human Breast Cancer: Negative Prognostic Factor and Protection against Cell Death In Vitro. *Mediators of Inflammation*, 2015, 1–9. <https://doi.org/10.1155/2015/864136>
- Kenny, H. A., Krausz, T., Yamada, S. D., & Lengyel, E. (2007). Use of a novel 3D culture model to elucidate the role of mesothelial cells, fibroblasts and extra-cellular matrices on adhesion and invasion of ovarian cancer cells to the omentum. *International Journal of Cancer*, 121(7), 1463–1472. <https://doi.org/10.1002/ijc.22874>
- Komiya, Y., & Habas, R. (2008). Wnt signal transduction pathways. *Organogenesis*, 4(2), 68–75. <https://doi.org/10.4161/org.4.2.5851>
- Kobayashi, K., Omori, K., & Murata, T. (2018). Role of prostaglandins in tumor microenvironment. *Cancer Metastasis Reviews*, 37(2–3), 347–354. <https://doi.org/10.1007/s10555-018-9740-2>
- Kotrbová, A., Ovesná, P., Gybel', T., Radaszkiewicz, T., Bednaříková, M., Hausnerová, J., Jandáková, E., Minář, L., Crha, I., Weinberger, V., Závěský, L., Bryja, V., & Pospíchalová, V. (2020). WNT signaling inducing activity in ascites predicts poor outcome in ovarian cancer. *Theranostics*, 10(2), 537–552. <https://doi.org/10.7150/thno.37423>
- Krishnan, V., Tallapragada, S., Schaar, B., Kamat, K., Chanana, A. M., Zhang, Y., Patel, S., Parkash, V., Rinker-Schaeffer, C., Folkins, A. K., Rankin, E. B., & Dorigo, O. (2020). Omental macrophages secrete chemokine ligands that promote ovarian cancer

- colonization of the omentum via CCR1. *Communications Biology*, 3(1), 524. <https://doi.org/10.1038/s42003-020-01246-z>
- Ksiazek, K., Jörres, A., & Witowski, J. (2008). Senescence Induces a Proangiogenic Switch in Human Peritoneal Mesothelial Cells. *Rejuvenation Research*, 11(3), 681–683. <https://doi.org/10.1089/rej.2008.0736>
- Ksiazek, K., Mikula-Pietrasik, J., Korybalska, K., Dworacki, G., Jörres, A., & Witowski, J. (2009). Senescent peritoneal mesothelial cells promote ovarian cancer cell adhesion: The role of oxidative stress-induced fibronectin. *The American Journal of Pathology*, 174(4), 1230–1240. <https://doi.org/10.2353/ajpath.2009.080613>
- Kulbe, H., Chakravarty, P., Leinster, D. A., Charles, K. A., Kwong, J., Thompson, R. G., Coward, J. I., Schioppa, T., Robinson, S. C., Gallagher, W. M., Galletta, L., Australian Ovarian Cancer Study Group, Salako, M. A., Smyth, J. F., Hagemann, T., Brennan, D. J., Bowtell, D. D., & Balkwill, F. R. (2012). A dynamic inflammatory cytokine network in the human ovarian cancer microenvironment. *Cancer Research*, 72(1), 66–75. <https://doi.org/10.1158/0008-5472.CAN-11-2178>
- Kurnit, Katherine C., Gini F. Fleming, und Ernst Lengyel. „Updates and New Options in Advanced Epithelial Ovarian Cancer Treatment“. *Obstetrics & Gynecology* 137, Nr. 1 (Januar 2021): 108–21. <https://doi.org/10.1097/AOG.0000000000004173>.
- Lane, D., Matte, I., Rancourt, C., & Piché, A. (2011). Prognostic significance of IL-6 and IL-8 ascites levels in ovarian cancer patients. *BMC Cancer*, 11(1), 210. <https://doi.org/10.1186/1471-2407-11-210>
- Ladanyi, A., Mukherjee, A., Kenny, H. A., Johnson, A., Mitra, A. K., Sundaresan, S., Nieman, K. M., Pascual, G., Benitah, S. A., Montag, A., Yamada, S. D., Abumrad, N. A., & Lengyel, E. (2018). Adipocyte-induced CD36 expression drives ovarian cancer progression and metastasis. *Oncogene*, 37(17), 2285–2301. <https://doi.org/10.1038/s41388-017-0093-z>
- Lee, G., & Ng, H. T. (1995). Clinical evaluations of a new ovarian cancer marker, COX-1. *International Journal of Gynaecology and Obstetrics: The Official Organ of the International Federation of Gynaecology and Obstetrics*, 49 Suppl, S27-32. [https://doi.org/10.1016/0020-7292\(95\)02406-3](https://doi.org/10.1016/0020-7292(95)02406-3)
- Lee, I. Y., Ko, E.-M., Kim, S.-H., Jeoung, D.-I., & Choe, J. (2005). Human Follicular Dendritic Cells Express Prostacyclin Synthase: A Novel Mechanism to Control T Cell Numbers in the Germinal Center. *The Journal of Immunology*, 175(3), 1658–1664. <https://doi.org/10.4049/jimmunol.175.3.1658>
- Lee, J.-Y., Myung, S.-K., & Song, Y.-S. (2013). Prognostic role of cyclooxygenase-2 in epithelial ovarian cancer: A meta-analysis of observational studies. *Gynecologic Oncology*, 129(3), 613–619. <https://doi.org/10.1016/j.ygyno.2013.02.011>

- Lengyel, E. (2010). Ovarian cancer development and metastasis. *The American Journal of Pathology*, 177(3), 1053–1064. <https://doi.org/10.2353/ajpath.2010.100105>
- Lewis, P. J., & Dollery, C. T. (1983). Clinical pharmacology and potential of prostacyclin. *British Medical Bulletin*, 39(3), 281–284. <https://doi.org/10.1093/oxfordjournals.bmb.a071834>
- Lheureux, S., Braunstein, M., & Oza, A. M. (2019). Epithelial ovarian cancer: Evolution of management in the era of precision medicine. *CA: A Cancer Journal for Clinicians*, caac.21559. <https://doi.org/10.3322/caac.21559>
- Li, H. Y., McSharry, M., Walker, D., Johnson, A., Kwak, J., Bullock, B., Neuwelt, A., Poczobutt, J. M., Sippel, T. R., Keith, R. L., Weiser-Evans, M. C. M., Clambey, E., & Nemenoff, R. A. (2018). Targeted overexpression of prostacyclin synthase inhibits lung tumor progression by recruiting CD4+ T lymphocytes in tumors that express MHC class II. *Oncolmmunology*, 7(5), e1423182. <https://doi.org/10.1080/2162402X.2017.1423182>
- Liberto, J. M., Chen, S.-Y., Shih, I.-M., Wang, T.-H., Wang, T.-L., & Pisanic, T. R. (2022). Current and Emerging Methods for Ovarian Cancer Screening and Diagnostics: A Comprehensive Review. *Cancers*, 14(12), 2885. <https://doi.org/10.3390/cancers14122885>
- Lieber, S., Reinartz, S., Raifer, H., Finkernagel, F., Dreyer, T., Bronger, H., Jansen, J. M., Wagner, U., Worzfeld, T., Müller, R., & Huber, M. (2018). Prognosis of ovarian cancer is associated with effector memory CD8 + T cell accumulation in ascites, CXCL9 levels and activation-triggered signal transduction in T cells. *Oncolmmunology*, 7(5), e1424672. <https://doi.org/10.1080/2162402X.2018.1424672>
- Lou, X., Han, X., Jin, C., Tian, W., Yu, W., Ding, D., Cheng, L., Huang, B., Jiang, H., & Lin, B. (2013). SOX2 targets fibronectin 1 to promote cell migration and invasion in ovarian cancer: New molecular leads for therapeutic intervention. *Omics: A Journal of Integrative Biology*, 17(10), 510–518. <https://doi.org/10.1089/omi.2013.0058>
- Lowy, C. M., & Oskarsson, T. (2015). Tenascin C in metastasis: A view from the invasive front. *Cell Adhesion & Migration*, 9(1–2), 112–124. <https://doi.org/10.1080/19336918.2015.1008331>
- Ma, X. (2020). The omentum, a niche for premetastatic ovarian cancer. *The Journal of Experimental Medicine*, 217(4), e20192312. <https://doi.org/10.1084/jem.20192312>
- Matte, I., Lane, D., Bachvarov, D., Rancourt, C., & Piché, A. (2014). Role of malignant ascites on human mesothelial cells and their gene expression profiles. *BMC Cancer*, 14, 288. <https://doi.org/10.1186/1471-2407-14-288>
- Matte, I., Lane, D., Laplante, C., Rancourt, C., & Piché, A. (2012). Profiling of cytokines in human epithelial ovarian cancer ascites. *American Journal of Cancer Research*, 2(5), 566–580.

- McMellen, A., Woodruff, E. R., Corr, B. R., Bitler, B. G., & Moroney, M. R. (2020). Wnt Signaling in Gynecologic Malignancies. *International Journal of Molecular Sciences*, 21(12), 4272. <https://doi.org/10.3390/ijms21124272>
- Meza-Perez, S., & Randall, T. D. (2017). Immunological Functions of the Omentum. *Trends in Immunology*, 38(7), 526–536. <https://doi.org/10.1016/j.it.2017.03.002>
- Michaud, A., Lacroix-Pépin, N., Pelletier, M., Daris, M., Biertho, L., Fortier, M. A., & Tchernof, A. (2014). Expression of genes related to prostaglandin synthesis or signaling in human subcutaneous and omental adipose tissue: Depot differences and modulation by adipogenesis. *Mediators of Inflammation*, 2014, 451620. <https://doi.org/10.1155/2014/451620>
- Midgett, C., Stitham, J., Martin, K. A., & Hwa, J. (2011). Prostacyclin receptor regulation—From transcription to trafficking. *Current Molecular Medicine*, 11(7), 517–528. <https://doi.org/10.2174/156652411800615144>
- Mikuła-Pietrasik, J., Uruski, P., Matuszkiewicz, K., Szubert, S., Moszyński, R., Szpurek, D., Sajdak, S., Tykarski, A., & Książek, K. (2016). Ovarian cancer-derived ascitic fluids induce a senescence-dependent pro-cancerogenic phenotype in normal peritoneal mesothelial cells. *Cellular Oncology (Dordrecht)*, 39(5), 473–481. <https://doi.org/10.1007/s13402-016-0289-1>
- Mitchell, J. A., & Kirkby, N. S. (2019). Eicosanoids, prostacyclin and cyclooxygenase in the cardiovascular system. *British Journal of Pharmacology*, 176(8), 1038–1050. <https://doi.org/10.1111/bph.14167>
- Mitchell, J. A., Vinokurova, M., Lopes-Pires, M. E., Shala, F., Armstrong, P. C., Ahmetaj-Shala, B., Elghazouli, Y., Liu, B., Zhou, Y., Hao, C., Herschman, H. R., & Kirkby, N. S. (2022). Tissue fibroblasts are a critical source of prostacyclin and anti-thrombotic protection [Preprint]. *Pharmacology and Toxicology*. <https://doi.org/10.1101/2022.01.11.475814>
- Mitra, A. K., Zillhardt, M., Hua, Y., Tiwari, P., Murmann, A. E., Peter, M. E., & Lengyel, E. (2012). MicroRNAs Reprogram Normal Fibroblasts into Cancer-Associated Fibroblasts in Ovarian Cancer. *Cancer Discovery*, 2(12), 1100–1108. <https://doi.org/10.1158/2159-8290.CD-12-0206>
- Moncada, S., Gryglewski, R., Bunting, S., & Vane, J. R. (1976). An enzyme isolated from arteries transforms prostaglandin endoperoxides to an unstable substance that inhibits platelet aggregation. *Nature*, 263(5579), 663–665. <https://doi.org/10.1038/263663a0>
- Moncada, S., & Vane, J. R. (1979). The role of prostacyclin in vascular tissue. *Federation Proceedings*, 38(1), 66–71.
- Mogi, K., Yoshihara, M., Iyoshi, S., Kitami, K., Uno, K., Tano, S., Koya, Y., Sugiyama, M., Yamakita, Y., Nawa, A., Tomita, H., & Kajiyama, H. (2021). Ovarian Cancer-Associated Mesothelial Cells: Transdifferentiation to Minions of Cancer and Orchestrate Developing

- Peritoneal Dissemination. *Cancers*, 13(6), 1352. <https://doi.org/10.3390/cancers13061352>
- Motohara, T., Masuda, K., Morotti, M., Zheng, Y., El-Sahhar, S., Chong, K. Y., Wietek, N., Alsaadi, A., Carrami, E. M., Hu, Z., Artibani, M., Gonzalez, L. S., Katabuchi, H., Saya, H., & Ahmed, A. A. (2019). An evolving story of the metastatic voyage of ovarian cancer cells: Cellular and molecular orchestration of the adipose-rich metastatic microenvironment. *Oncogene*, 38(16), 2885–2898. <https://doi.org/10.1038/s41388-018-0637-x>
- Mutsaers, S. E. (2004). The mesothelial cell. *The International Journal of Biochemistry & Cell Biology*, 36(1), 9–16. [https://doi.org/10.1016/S1357-2725\(03\)00242-5](https://doi.org/10.1016/S1357-2725(03)00242-5)
- Nieman, K. M., Kenny, H. A., Penicka, C. V., Ladanyi, A., Buell-Gutbrod, R., Zillhardt, M. R., Romero, I. L., Carey, M. S., Mills, G. B., Hotamisligil, G. S., Yamada, S. D., Peter, M. E., Gwin, K., & Lengyel, E. (2011). Adipocytes promote ovarian cancer metastasis and provide energy for rapid tumor growth. *Nature Medicine*, 17(11), 1498–1503. <https://doi.org/10.1038/nm.2492>
- Noble, N. A., Harper, J. R., & Border, W. A. (1992). In vivo interactions of TGF-beta and extracellular matrix. *Progress in Growth Factor Research*, 4(4), 369–382. [https://doi.org/10.1016/0955-2235\(92\)90017-c](https://doi.org/10.1016/0955-2235(92)90017-c)
- Noy, R., & Pollard, J. W. (2014). Tumor-Associated Macrophages: From Mechanisms to Therapy. *Immunity*, 41(1), 49–61. <https://doi.org/10.1016/j.immuni.2014.06.010>
- Olbrecht, S., Busschaert, P., Qian, J., Vanderstichele, A., Loverix, L., Van Gorp, T., Van Nieuwenhuysen, E., Han, S., Van den Broeck, A., Coosemans, A., Van Rompuy, A.-S., Lambrechts, D., & Vergote, I. (2021). High-grade serous tubo-ovarian cancer refined with single-cell RNA sequencing: Specific cell subtypes influence survival and determine molecular subtype classification. *Genome Medicine*, 13(1), 111. <https://doi.org/10.1186/s13073-021-00922-x>
- Paron, I., Berchtold, S., Vörös, J., Shamarla, M., Erkan, M., Höfler, H., & Esposito, I. (2011). Tenascin-C Enhances Pancreatic Cancer Cell Growth and Motility and Affects Cell Adhesion through Activation of the Integrin Pathway. *PLoS ONE*, 6(6), e21684. <https://doi.org/10.1371/journal.pone.0021684>
- Peng, P., Yan, Y., & Keng, S. (2011). Exosomes in the ascites of ovarian cancer patients: Origin and effects on anti-tumor immunity. *Oncology Reports*, 25(3), 749–762. <https://doi.org/10.3892/or.2010.1119>
- Platell, C., Cooper, D., Papadimitriou, J. M., & Hall, J. C. (2000). The omentum. *World Journal of Gastroenterology*, 6(2), 169–176. <https://doi.org/10.3748/wjg.v6.i2.169>
- Pogge von Strandmann, E., Reinartz, S., Wager, U., & Müller, R. (2017). Tumor-Host Cell Interactions in Ovarian Cancer: Pathways to Therapy Failure. *Trends in Cancer*, 3(2), 137–148. <https://doi.org/10.1016/j.trecan.2016.12.005>

- Pollard, J. W. (2004). Tumour-educated macrophages promote tumour progression and metastasis. *Nature Reviews Cancer*, 4(1), 71–78. <https://doi.org/10.1038/nrc1256>
- Potenta, S., Zeisberg, E., & Kalluri, R. (2008). The role of endothelial-to-mesenchymal transition in cancer progression. *British Journal of Cancer*, 99(9), 1375–1379. <https://doi.org/10.1038/sj.bjc.6604662>
- Prat, J. (2012). Ovarian carcinomas: Five distinct diseases with different origins, genetic alterations, and clinicopathological features. *Virchows Archiv*, 460(3), 237–249. <https://doi.org/10.1007/s00428-012-1203-5>
- Rakina, M., Kazakova, A., Villert, A., Kolomiets, L., & Larionova, I. (2022). Spheroid Formation and Peritoneal Metastasis in Ovarian Cancer: The Role of Stromal and Immune Components. *International Journal of Molecular Sciences*, 23(11), 6215. <https://doi.org/10.3390/ijms23116215>
- Reinartz, S., Finkernagel, F., Adhikary, T., Rohnalter, V., Schumann, T., Schober, Y., Nockher, W. A., Nist, A., Stiewe, T., Jansen, J. M., Wagner, U., Müller-Brüsselbach, S., & Müller, R. (2016). A transcriptome-based global map of signaling pathways in the ovarian cancer microenvironment associated with clinical outcome. *Genome Biology*, 17(1), 108. <https://doi.org/10.1186/s13059-016-0956-6>
- Reinartz, S., Lieber, S., Pesek, J., Brandt, D. T., Asafova, A., Finkernagel, F., Watzer, B., Nockher, W. A., Nist, A., Stiewe, T., Jansen, J. M., Wagner, U., Konzer, A., Graumann, J., Grosse, R., Worzfeld, T., Müller-Brüsselbach, S., & Müller, R. (2019). Cell type-selective pathways and clinical associations of lysophosphatidic acid biosynthesis and signaling in the ovarian cancer microenvironment. *Molecular Oncology*, 13(2), 185–201. <https://doi.org/10.1002/1878-0261.12396>
- Rickard, B. P., Conrad, C., Sorrin, A. J., Ruhi, M. K., Reader, J. C., Huang, S. A., Franco, W., Scarcelli, G., Polacheck, W. J., Roque, D. M., Del Carmen, M. G., Huang, H.-C., Demirci, U., & Rizvi, I. (2021). Malignant Ascites in Ovarian Cancer: Cellular, Acellular, and Biophysical Determinants of Molecular Characteristics and Therapy Response. *Cancers*, 13(17), 4318. <https://doi.org/10.3390/cancers13174318>
- Sandoval, P., Jiménez-Heffernan, J. A., Rynne-Vidal, Á., Pérez-Lozano, M. L., Gilsanz, Á., Ruiz-Carpio, V., Reyes, R., García-Bordas, J., Stamatakis, K., Dotor, J., Majano, P. L., Fresno, M., Cabañas, C., & López-Cabrera, M. (2013). Carcinoma-associated fibroblasts derive from mesothelial cells via mesothelial-to-mesenchymal transition in peritoneal metastasis. *The Journal of Pathology*, 231(4), 517–531. <https://doi.org/10.1002/path.4281>
- Schumann, T., Adhikary, T., Wortmann, A., Finkernagel, F., Lieber, S., Schnitzer, E., Legrand, N., Schober, Y., Nockher, W. A., Toth, P. M., Diederich, W. E., Nist, A., Stiewe, T., Wagner, U., Reinartz, S., Müller-Brüsselbach, S., & Müller, R. (2015). Dereglulation of PPAR β/δ target genes in tumor-associated macrophages by fatty acid ligands in the ovarian cancer microenvironment. *Oncotarget*, 6(15), 13416–13433. <https://doi.org/10.18632/oncotarget.3826>

- Seclì, L., Fusella, F., Avalle, L., & Brancaccio, M. (2021). The dark-side of the outside: How extracellular heat shock proteins promote cancer. *Cellular and Molecular Life Sciences: CMLS*, 78(9), 4069–4083. <https://doi.org/10.1007/s00018-021-03764-3>
- Shaul, P. W., Kinane, B., Farrar, M. A., Buja, L. M., & Magness, R. R. (1991). Prostacyclin production and mediation of adenylate cyclase activity in the pulmonary artery. Alterations after prolonged hypoxia in the rat. *The Journal of Clinical Investigation*, 88(2), 447–455. <https://doi.org/10.1172/JC1115324>
- Sivakumar, S., Lieber, S., Librizzi, D., Keber, C., Sommerfeld, L., Finkernagel, F., Roth, K., Reinartz, S., Bartsch, J. W., Graumann, J., Müller-Brüsselbach, S., Müller, R. (2023). Basal cell adhesion molecule promotes metastasis-associated processes in ovarian cancer. *Clin Transl Med*. 2023; 13:e1176. <https://doi.org/10.1002/ctm2.1176>
- So, W.-K., Fan, Q., Lau, M.-T., Qiu, X., Cheng, J.-C., & Leung, P. C. K. (2014). Amphiregulin induces human ovarian cancer cell invasion by down-regulating E-cadherin expression. *FEBS Letters*, 588(21), 3998–4007. <https://doi.org/10.1016/j.febslet.2014.09.017>
- Sommerfeld, L., Finkernagel, F., Jansen, J. M., Wagner, U., Nist, A., Stiewe, T., Müller-Brüsselbach, S., Sokol, A. M., Graumann, J., Reinartz, S., & Müller, R. (2021). The multicellular signalling network of ovarian cancer metastases. *Clinical and Translational Medicine*, 11(11), e633. <https://doi.org/10.1002/ctm2.633>
- Sommerfeld, L., Knuth, I., Finkernagel, F., Pesek, J., Nockher, W. A., Jansen, J. M., Wagner, U., Nist, A., Stiewe, T., Müller-Brüsselbach, S., Müller, R., & Reinartz, S. (2022). Prostacyclin Released by Cancer-Associated Fibroblasts Promotes Immunosuppressive and Pro-Metastatic Macrophage Polarization in the Ovarian Cancer Microenvironment. *Cancers*, 14(24), 6154. <https://doi.org/10.3390/cancers14246154>
- Steitz, A. M., Steffes, A., Finkernagel, F., Unger, A., Sommerfeld, L., Jansen, J. M., Wagner, U., Graumann, J., Müller, R., & Reinartz, S. (2020). Tumor-associated macrophages promote ovarian cancer cell migration by secreting transforming growth factor beta induced (TGFB1) and tenascin C. *Cell Death & Disease*, 11(4), 249. <https://doi.org/10.1038/s41419-020-2438-8>
- Stitham, J., Midgett, C., Martin, K. A., & Hwa, J. (2011). Prostacyclin: An inflammatory paradox. *Frontiers in Pharmacology*, 2, 24. <https://doi.org/10.3389/fphar.2011.00024>
- Stratton, R., & Shiwen, X. (2010). Role of prostaglandins in fibroblast activation and fibrosis. *Journal of Cell Communication and Signaling*, 4(2), 75–77. <https://doi.org/10.1007/s12079-010-0089-8>
- Surendran, K., McCaul, S. P., & Simon, T. C. (2002). A role for Wnt-4 in renal fibrosis. *American Journal of Physiology-Renal Physiology*, 282(3), F431–F441. <https://doi.org/10.1152/ajprenal.0009.2001>
- Suzuki, M., Yokobori, T., Gombodorj, N., Yashiro, M., Turtoi, A., Handa, T., Ogata, K., Oyama, T., Shirabe, K., & Kuwano, H. (2018). High stromal transforming growth factor β -induced expression is a novel marker of progression and poor prognosis in gastric cancer:

- SUZUKI et al. *Journal of Surgical Oncology*, 118(6), 966–974. <https://doi.org/10.1002/jso.25217>
- Takaishi, K., Komohara, Y., Tashiro, H., Ohtake, H., Nakagawa, T., Katabuchi, H., & Takeya, M. (2010). Involvement of M2-polarized macrophages in the ascites from advanced epithelial ovarian carcinoma in tumor progression via Stat3 activation. *Cancer Science*, 101(10), 2128–2136. <https://doi.org/10.1111/j.1349-7006.2010.01652.x>
- Teeuwssen, M., & Fodde, R. (2019). Wnt Signaling in Ovarian Cancer Stemness, EMT, and Therapy Resistance. *Journal of Clinical Medicine*, 8(10), 1658. <https://doi.org/10.3390/jcm8101658>
- Thériault, C., Pinard, M., Comamala, M., Migneault, M., Beaudin, J., Matte, I., Boivin, M., Piché, A., & Rancourt, C. (2011). MUC16 (CA125) regulates epithelial ovarian cancer cell growth, tumorigenesis and metastasis. *Gynecologic Oncology*, 121(3), 434–443. <https://doi.org/10.1016/j.ygyno.2011.02.020>
- Thuwajit, C., Ferraresi, A., Titone, R., Thuwajit, P., & Isidoro, C. (2018). The metabolic cross-talk between epithelial cancer cells and stromal fibroblasts in ovarian cancer progression: Autophagy plays a role. *Medicinal Research Reviews*, 38(4), 1235–1254. <https://doi.org/10.1002/med.21473>
- Trabert, B., Ness, R. B., Lo-Ciganic, W.-H., Murphy, M. A., Goode, E. L., Poole, E. M., Brinton, L. A., Webb, P. M., Nagle, C. M., Jordan, S. J., Australian Ovarian Cancer Study Group, the Australian Cancer Study (Ovarian Cancer), Risch, H. A., Rossing, M. A., Doherty, J. A., Goodman, M. T., Lurie, G., Kjaer, S. K., Hogdall, E., Jensen, A., ... on behalf of the Ovarian Cancer Association Consortium. (2014). Aspirin, Nonaspirin Nonsteroidal Anti-inflammatory Drug, and Acetaminophen Use and Risk of Invasive Epithelial Ovarian Cancer: A Pooled Analysis in the Ovarian Cancer Association Consortium. *JNCI Journal of the National Cancer Institute*, 106(2), djt431–djt431. <https://doi.org/10.1093/jnci/djt431>
- Vouyovitch, C. M., Perry, J. K., Liu, D. X., Bezin, L., Vilain, E., Diaz, J.-J., Lobie, P. E., & Mertani, H. C. (2016). WNT4 mediates the autocrine effects of growth hormone in mammary carcinoma cells. *Endocrine-Related Cancer*, 23(7), 571–585. <https://doi.org/10.1530/ERC-15-0528>
- Wang, N., Yan, H., Wu, D., Zhao, Z., Chen, X., Long, Q., Zhang, C., Wang, X., Deng, W., & Liu, X. (2020). PRMT5/Wnt4 axis promotes lymph-node metastasis and proliferation of laryngeal carcinoma. *Cell Death & Disease*, 11(10), 864. <https://doi.org/10.1038/s41419-020-03064-x>
- Ween, M. P., Oehler, M. K., & Ricciardelli, C. (2012). Transforming growth Factor-Beta-Induced Protein (TGFB1)/(βig-H3): A matrix protein with dual functions in ovarian cancer. *International Journal of Molecular Sciences*, 13(8), 10461–10477. <https://doi.org/10.3390/ijms130810461>
- Wilson, A. J., Fadare, O., Beeghly-Fadiel, A., Son, D.-S., Liu, Q., Zhao, S., Saskowski, J., Uddin, Md. J., Daniel, C., Crews, B., Lehmann, B. D., Pietenpol, J. A., Crispens, M. A.,

- Marnett, L. J., & Khabele, D. (2015). Aberrant over-expression of COX-1 intersects multiple pro-tumorigenic pathways in high-grade serous ovarian cancer. *Oncotarget*, 6(25), 21353–21368. <https://doi.org/10.18632/oncotarget.3860>
- Worzfeld, T., Finkernagel, F., Reinartz, S., Konzer, A., Adhikary, T., Nist, A., Stiewe, T., Wagner, U., Looso, M., Graumann, J., & Müller, R. (2018). Proteotranscriptomics Reveal Signaling Networks in the Ovarian Cancer Microenvironment. *Molecular & Cellular Proteomics: MCP*, 17(2), 270–289. <https://doi.org/10.1074/mcp.RA117.000400>
- Worzfeld, T., Pogge von Strandmann, E., Huber, M., Adhikary, T., Wagner, U., Reinartz, S., & Müller, R. (2017). The Unique Molecular and Cellular Microenvironment of Ovarian Cancer. *Frontiers in Oncology*, 7, 24. <https://doi.org/10.3389/fonc.2017.00024>
- Yang, D., Li, Q., Shang, R., Yao, L., Wu, L., Zhang, M., Zhang, L., Xu, M., Lu, Z., Zhou, J., Huang, L., Huang, X., Cheng, D., Yang, Y., & Yu, H. (2020). WNT4 secreted by tumor tissues promotes tumor progression in colorectal cancer by activation of the Wnt/ β -catenin signalling pathway. *Journal of Experimental & Clinical Cancer Research*, 39(1), 251. <https://doi.org/10.1186/s13046-020-01774-w>
- Yang, J., Zaman, M. M., Vlasakov, I., Roy, R., Huang, L., Martin, C. R., Freedman, S. D., Serhan, C. N., & Moses, M. A. (2019). Adipocytes promote ovarian cancer chemoresistance. *Scientific Reports*, 9(1), 13316. <https://doi.org/10.1038/s41598-019-49649-1>
- Yang, Y., Yang, Y., Yang, J., Zhao, X., & Wei, X. (2020). Tumor Microenvironment in Ovarian Cancer: Function and Therapeutic Strategy. *Frontiers in Cell and Developmental Biology*, 8, 758. <https://doi.org/10.3389/fcell.2020.00758>
- Yin, M., Li, X., Tan, S., Zhou, H. J., Ji, W., Bellone, S., Xu, X., Zhang, H., Santin, A. D., Lou, G., & Min, W. (2016). Tumor-associated macrophages drive spheroid formation during early transcoelomic metastasis of ovarian cancer. *Journal of Clinical Investigation*, 126(11), 4157–4173. <https://doi.org/10.1172/JCI87252>
- Yousif, N. G. (2014). Fibronectin promotes migration and invasion of ovarian cancer cells through up-regulation of FAK-PI3K/Akt pathway. *Cell Biology International*, 38(1), 85–91. <https://doi.org/10.1002/cbin.10184>
- Zhang, Y., Tang, H., Cai, J., Zhang, T., Guo, J., Feng, D., & Wang, Z. (2011). Ovarian cancer-associated fibroblasts contribute to epithelial ovarian carcinoma metastasis by promoting angiogenesis, lymphangiogenesis and tumor cell invasion. *Cancer Letters*, 303(1), 47–55. <https://doi.org/10.1016/j.canlet.2011.01.011>
- Zhou, S., Wang, R., & Xiao, H. (2020). Adipocytes induce the resistance of ovarian cancer to carboplatin through ANGPTL4. *Oncology Reports*, 44(3), 927–938. <https://doi.org/10.3892/or.2020.7647>

6. Publications

ARTICLE

Open Access

Tumor-associated macrophages promote ovarian cancer cell migration by secreting transforming growth factor beta induced (TGFB1) and tenascin C

Anna Mary Steitz¹, Alina Steffes², Florian Finkernagel¹, Annika Unger¹, Leah Sommerfeld¹, Julia M. Jansen³, Uwe Wagner³, Johannes Graumann^{4,5}, Rolf Müller¹ and Silke Reinartz²

Abstract

A central and unique aspect of high-grade serous ovarian carcinoma (HGSC) is the extensive transcoelomic spreading of tumor cell via the peritoneal fluid or malignant ascites. We and others identified tumor-associated macrophages (TAM) in the ascites as promoters of metastasis-associated processes like extracellular matrix (ECM) remodeling, tumor cell migration, adhesion, and invasion. The precise mechanisms and mediators involved in these functions of TAM are, however, largely unknown. We observed that HGSC migration is promoted by soluble mediators from ascites-derived TAM, which can be emulated by conditioned medium from monocyte-derived macrophages (MDM) differentiated in ascites to TAM-like asc-MDM. A similar effect was observed with IL-10-induced alternatively activated m2c-MDM but not with LPS/IFN γ -induced inflammatory m1-MDM. These observations provided the basis for deconvolution of the complex TAM secretome by performing comparative secretome analysis of matched triplets of different MDM phenotypes with different pro-migratory properties (asc-MDM, m2c-MDM, m1-MDM). Mass spectrometric analysis identified an overlapping set of nine proteins secreted by both asc-MDM and m2c-MDM, but not by m1-MDM. Of these, three proteins, i.e., transforming growth factor beta-induced (TGFB1) protein, tenascin C (TNC), and fibronectin (FN1), have been associated with migration-related functions. Intriguingly, increased ascites concentrations of TGFB1, TNC, and fibronectin were associated with short progression-free survival. Furthermore, transcriptome and secretome analyses point to TAM as major producers of these proteins, further supporting an essential role for TAM in promoting HGSC progression. Consistent with this hypothesis, we were able to demonstrate that the migration-inducing potential of asc-MDM and m2c-MDM secretomes is inhibited, at least partially, by neutralizing antibodies against TGFB1 and TNC or siRNA-mediated silencing of TGFB1 expression. In conclusion, the present study provides the first experimental evidence that TAM-derived TGFB1 and TNC in ascites promote HGSC progression.

Introduction

Ovarian carcinoma is the most lethal gynecological cancer with an overall 12-year survival rate of <20%, and represents the fifth leading cause of cancer-associated deaths in females¹. A hallmark of high-grade serous

carcinoma (HGSC), the most common and aggressive subtype, is its extensive peritoneal metastasis, which occurs at a very early stage of disease and contributes to its fatal clinical outcome². Metastatic spreads occurs predominantly to the omentum and serous membranes lining the peritoneal organs through transcoelomic dissemination of tumor cells via the peritoneal fluid^{3–5}. The peritoneal tumor microenvironment (TME), which consists of tumor-infiltrated host tissues and peritoneal fluid (or ascites at advanced stages), is an essential determinant of metastatic disease progression. Ascites contains large

Correspondence: Rolf Müller (rolf.mueller@uni-marburg.de)

¹Institute of Molecular Biology and Tumor Research (IMT), Center for Tumor Biology and Immunology, Philipps University, Marburg, Germany

²Clinic for Gynecology, Gynecologic Oncology and Endocrinology, Center for Tumor Biology and Immunology, Philipps University, Marburg, Germany

Full list of author information is available at the end of the article
Edited by H.-U. Simon

© The Author(s) 2020



Open Access This article is licensed under a Creative Commons Attribution 4.0 International License, which permits use, sharing, adaptation, distribution and reproduction in any medium or format, as long as you give appropriate credit to the original author(s) and the source, provide a link to the Creative Commons license, and indicate if changes were made. The images or other third party material in this article are included in the article's Creative Commons license, unless indicated otherwise in a credit line to the material. If material is not included in the article's Creative Commons license and your intended use is not permitted by statutory regulation or exceeds the permitted use, you will need to obtain permission directly from the copyright holder. To view a copy of this license, visit <http://creativecommons.org/licenses/by/4.0/>.

numbers of cells including tumor spheroids and immune cells, such as tumor-associated macrophages and T cells (TAMs and TATs, respectively)^{6–8}, as well as soluble factors and extracellular vesicles released by tumor and host cells^{2,9,10}, collectively referred to as the tumor secretome and recognized as a key player in the communication network of the TME^{11–13}. A detailed understanding of the secretome composition, the origin of single compounds, and their role in tumor–host crosstalk remains, however, elusive.

TAMs constitute a prominent cell population in ascites known to promote tumor growth, metastasis, and immunosuppression^{14–16}. TAMs are reprogrammed by factors of the TME to adopt a pro-tumorigenic and immunosuppressive phenotype, which is linked to a poor clinical outcome^{8,13,17,18}. TAMs contribute to the tumor secretome by releasing a plethora of soluble mediators, such as interleukin (IL)-6, IL-10, C-C chemokine motif ligand 18 (CCL18), CCL22, tumor necrosis factor α , and transforming growth factor beta (TGF β), that trigger pro-tumorigenic signaling pathways in both tumor and host cells of the TME^{19–21}. For example, it is suggested that TAM and tumor cells cooperate in extracellular matrix (ECM) remodeling, which is a prerequisite for tumor cell adhesion and invasion^{7,13,14}. Consistent with this model, it has been reported that TAM secrete migration-promoting factors like insulin-like growth factor 1 (IGF1), epidermal growth factor (EGF), and CHI3L1 pointing to a presumably central role of TAM in cancer cell migration, adhesion, and invasion^{22–24}.

The TAM-derived mediators that promote cancer migration in the context of the HGSC microenvironment remain largely unknown. This is largely due to the fact that macrophages secrete a plethora of soluble factors, thus complicating the identification of relevant mediators. To address this issue, we designed an experimental setting that compares the secretomes of macrophages with different migration-stimulating properties. This was achieved by comparing matched pairs of monocyte-derived macrophages (MDM) from healthy donors that were differentiated into TAM-like MDM by ascites (asc-MDM), alternatively activated M2 by IL-10 (m2c-MDM)²⁵ as well as MDM classically activated by lipopolysaccharide (LPS) and interferon- γ (IFN γ) (m1-MDM). While asc-MDM and m2c-MDM share the potential to stimulate HGSC cell migration similarly to patient-derived TAMs, m1-MDM has no migration-promoting potential.

By combining mass spectrometry (MS)-based proteomics, bioinformatic analyses, and tumor migration assays, we found three candidates with migration-promoting properties released by both asc-MDM and m2c-MDM, but not by m1-MDM. These secreted proteins were transforming growth factor beta induced

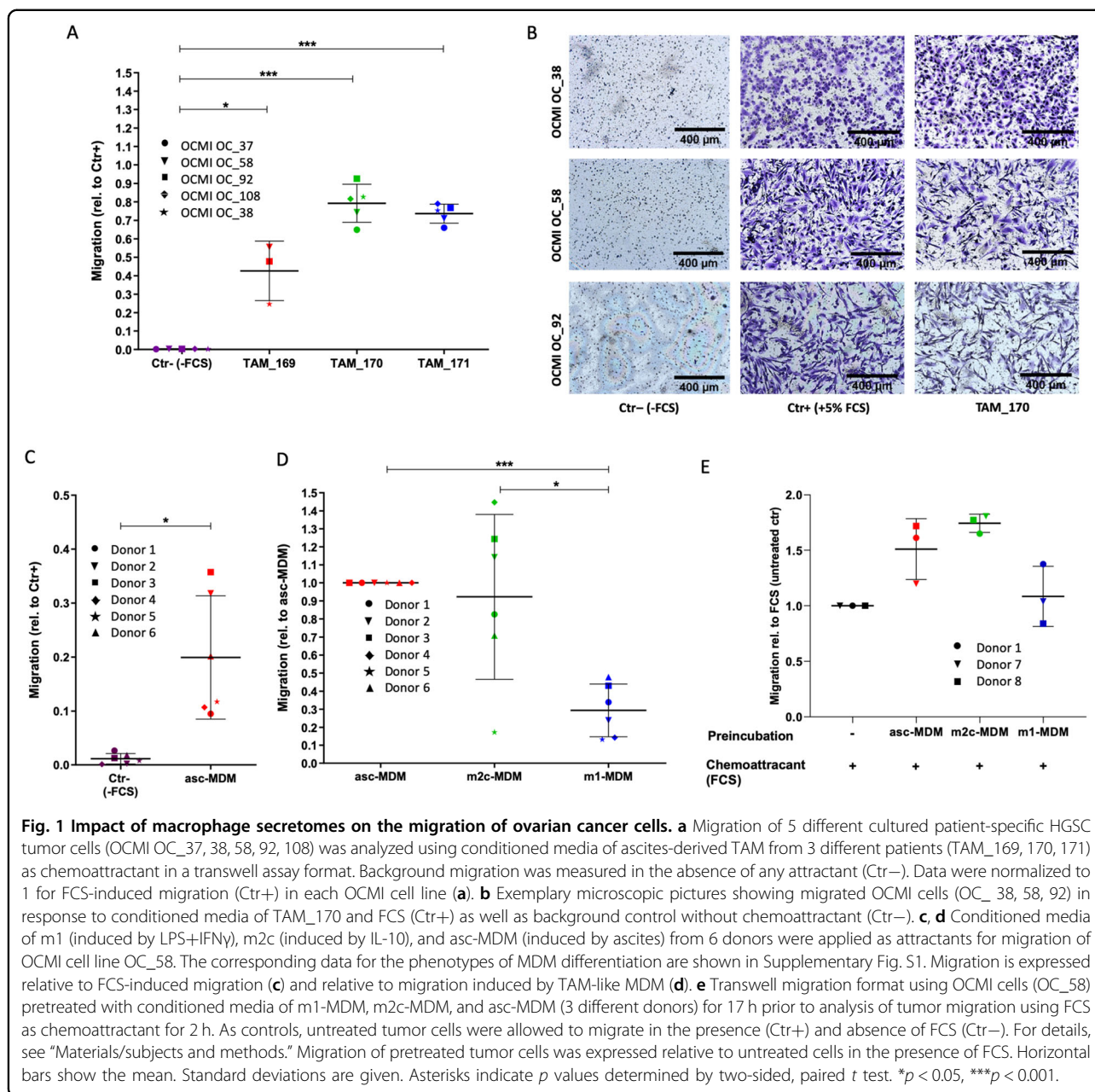
(TGFBI), tenascin C (TNC), and fibronectin (FN1), which have in common that they are ECM proteins and as such may provide support for tumor cell adhesion and migration. In general, excessive synthesis and deposition of ECM proteins is a hallmark of the tumor stroma, which is especially mediated not only by carcinoma-associated fibroblasts (CAFs)²⁶ but also by TAM^{13,27}. So far, TNC and TGFBI secretion by TAM has not been linked to tumor cell migration. In the present study, we identified TGFBI, TNC, and FN1 in ascites and found correlations with HGSC progression, supporting a potential clinical relevance of these mediators in the TME. For TGFBI and TNC in particular, we provide evidence for enhanced secretion into the TME as a novel mechanism by which TAM promote HGSC migration.

Results

Ascites-derived TAM secrete soluble mediators promoting HGSC migration

As shown in Fig. 1, the secretome of ascites-derived TAM induced strong migration of cultured patient-derived HGSC cells (termed OCMI cells) when applied as chemoattractant in a transwell assay. These findings were validated using conditioned media of TAM from three patients and tumor cells from five patients, indicating that ascites-derived TAM secrete migration-promoting mediators acting on different OCMI tumor cells (Fig. 1a, b).

The highly complex composition of the TAM secretome, which consists of several hundred proteins, complicates the identification of the pro-migratory mediators that are relevant within the HGSC microenvironment. We therefore designed an experimental approach suitable to selectively identify the TAM-derived mediators able to promote HGSC cell migration (see also “Introduction”). This approach is based on our observation that MDM differentiated in vitro with malignant ascites into TAM-like MDM (asc-MDM) emulated the pro-migratory potential of the patients’ TAM secretomes. This was demonstrated in a transwell migration assays, where conditioned medium from asc-MDM significantly induced tumor cell migration when used as chemoattractant (Fig. 1c and Supplementary Fig. S1). A similar impact on migration was observed by conditioned medium from MDM alternatively activated by IL-10 (m2c-MDM), whereas migration was not significantly affected by conditioned medium MDM skewed to a pro-inflammatory phenotype by LPS and IFN γ (m1-MDM) (Fig. 1d and Supplementary Fig. S1). These observations were confirmed in a second migration assay format, where conditioned media was used for pre-incubating tumor cells (prior to the migration assay) rather than as chemoattractant. As shown in Fig. 1e, tumor cells that were pre-incubated with conditioned media of asc-MDM and



m2c-MDM, but not of m1-MDM, exhibited increased migratory potential (Fig. 1e).

The MDM differentiation phenotypes were also verified by flow cytometry (see Supplementary Fig. S2). TAM-like asc-MDM were characterized by an increased expression of CD14, CD16, and the m2c markers CD163 and CD206, as well as downregulated expression of the M1 markers CD86 and CCR7 in all tested donors (relative to m1-MDM; Fig. S2).

The differential effects of asc-MDM and m2c-MDM on the one hand and m1-MDM on the other hand paved the way for a detailed comparative analysis of the

corresponding secretomes aiming at the identification of candidate proteins with a pro-migratory function secreted by asc-MDM and m2c-MDM (and by TAM in malignant ascites) but not by m1-MDM.

Comparative secretome analysis of MDM subtypes identifies candidates related to tumor migration

Comparative analysis of conditioned media from functionally different MDM subtypes was performed by MS-based proteomics. In total, we identified 700 proteins annotated as "predicted secreted" in the Human Protein Atlas in the supernatant of at least one asc-MDM sample

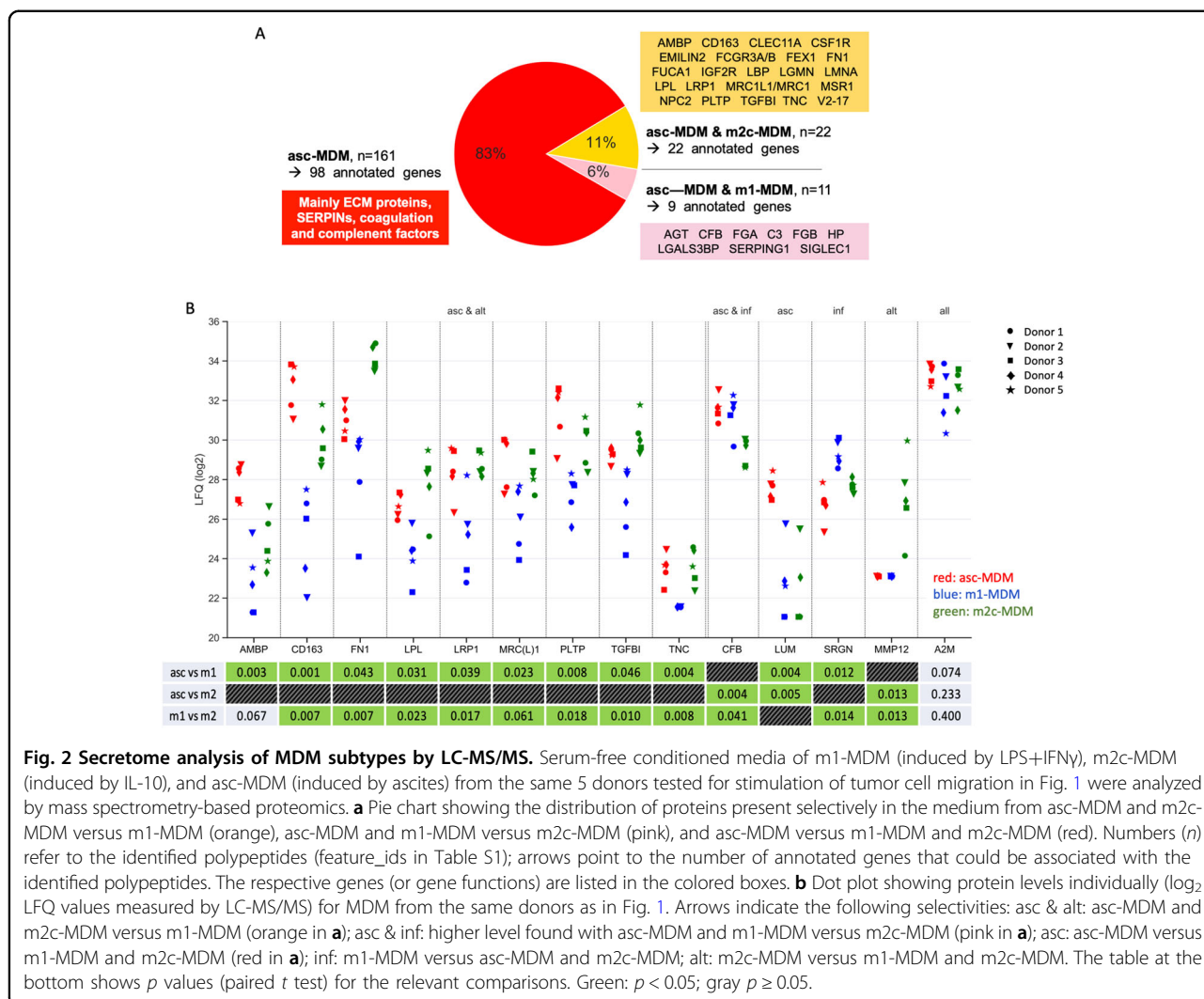


(Table S1). Of these, the 22 proteins were present at higher levels in conditioned media from asc-MDM and m2c-MDM compared to m1-MDM in at least four out of five triplets (Fig. 2a; Tables 1 and S2). Nine of these proteins (AMB, CD163, FN1, LPL, LRP1, MRC1L1/MRC1, PLTP, TGFBI, TNC) perfectly fit this distribution in all five triplets (Fig. 2b). Among these, three proteins are migration-promoting candidates as suggested by literature data^{28–30}, i.e., TGFBI, TNC, and FN1 (Table 1). A similar observation was made for macrophage mannose receptor 1 (MRC1, CD206) and scavenger receptor cysteine-rich type 1 protein (CD163), which are known to be commonly upregulated in TAM and alternatively activated macrophages^{8,17,25}, and thus serve as plausibility controls.

We also identified proteins selective for other MDM subtypes, including 9 proteins with annotated genes for asc-MDM and m1-MDM versus m2c-MDM (Table S3; Fig. 2a), as well as 98 proteins for asc-MDM versus both

m1-MDM and m2c-MDM (Table S4; Fig. 2a). This is exemplified in Fig. 2b by lumican (LUM), serglycin (SRGN), and metalloproteinase 12 (MMP12), which are secreted proteins selective for asc-MDM, m1-MDM, or m2c-MDM. In contrast, alpha-2-macroglobulin (A2M) is a protein present at similar levels in conditioned media from all macrophage subtypes (Fig. 2b).

Intriguingly, the proteins secreted selectively by asc-MDM are mainly composed of ECM-associated polypeptides (such as collagens, BCAM, LUM, SERPIN protease inhibitors) as well as complement factors (Table S4; Fig. 2a). This is consistent with previous reports describing these proteins as a hallmark of TAM in HGSC ascites^{7,13}, further validating the experimental approach.

TGFBI, TNC, and FN1 are secreted by ascites TAM in vivo and are associated with a short relapse-free survival (RFS)

To assess the clinical significance of TGFBI, TNC, and FN1, we analyzed their levels in ascites from 70 HGSC

Table 1 Top 22 secreted proteins overexpressed in the secretomes of asc-MDM and m2c-MDM compared to m1-MDM.

Gene name	Protein name	Match (n) ^a
AMBP	Alpha-1 microglobulin	5
CD163	Scavenger receptor CD163	5
FN1	Fibronectin	5
LPL	Lipoprotein lipase	5
LRP1	LDL receptor-related protein 1	5
MRC(L)1	Macrophage mannose receptor 1	5
PLTP	Phospholipid transfer protein	5
TGFBI	Transforming growth factor beta induced	5
TNC	Tenascin	5
IGF2R	Cation-independent mannose-6-phosphate receptor	4
CLEC11A	C-type lectin domain family 11 member A	4
CSF1R	Macrophage colony-stimulating factor 1 receptor	4
EMILIN2	Elastin Microfibril Interfacer 1	4
FCGR3A	Fc fragment of IgG receptor IIIA	4
FUCA1	Alpha-1 fucosidase	4
LBP	Lipopolysaccharide-binding protein	4
LGMN	Legumain	4
LMNA	Lamin A/C	4
MSR1	Macrophage scavenger receptor 1	4
NPC2	Epididymal secretory protein E1	4
STAB1 (FEX1)	Stabilin	4
V2-17	Ig lambda chain V-IV region Hil	4

^aMatch (n) = number of donors matching the classification of selectivity (n out of 5).

patients and 30 blood plasma samples in our recently published dataset³¹ obtained by the aptamer-based SOMAscan technology³². All three proteins were present at significantly higher levels in ascites compared to plasma from patients of the same cohort ($n = 20$) as well as plasma from patients with benign gynecological diseases ($n = 10$) ($p < 0.0001$, Fig. 3a). To elucidate the origin of TGFBI, TNC, and FN1 in HGSC ascites, we made use of our transcriptome, proteome, and secretome datasets for tumor cells, TAMs, and TATs^{7,33}. As shown in Fig. 3 for both TGFBI and FN1, RNA expression, intracellular protein levels, as well as secretion were consistently strongest in TAMs compared to tumor cells and TATs (Fig. 3b–d). These findings are consistent with the data reported in the present study showing that asc-MDM secrete TGFBI and FN1. TNC, on the other hand, is also

secreted by TAMs at a level comparable to TGFBI (Fig. 3d), but in the corresponding omics datasets TNC mRNA was very low in TAM (Fig. 3b) and intracellular TNC protein was not detectable (Fig. 3c). This apparent discrepancy was confirmed with in vitro differentiated asc-TAM by quantitative reverse transcription polymerase chain reaction (qRT-PCR) and western blotting (see below and Fig. 5d–g), which may be explained by an unusual instability of TNC mRNA in macrophages combined with rapid protein secretion.

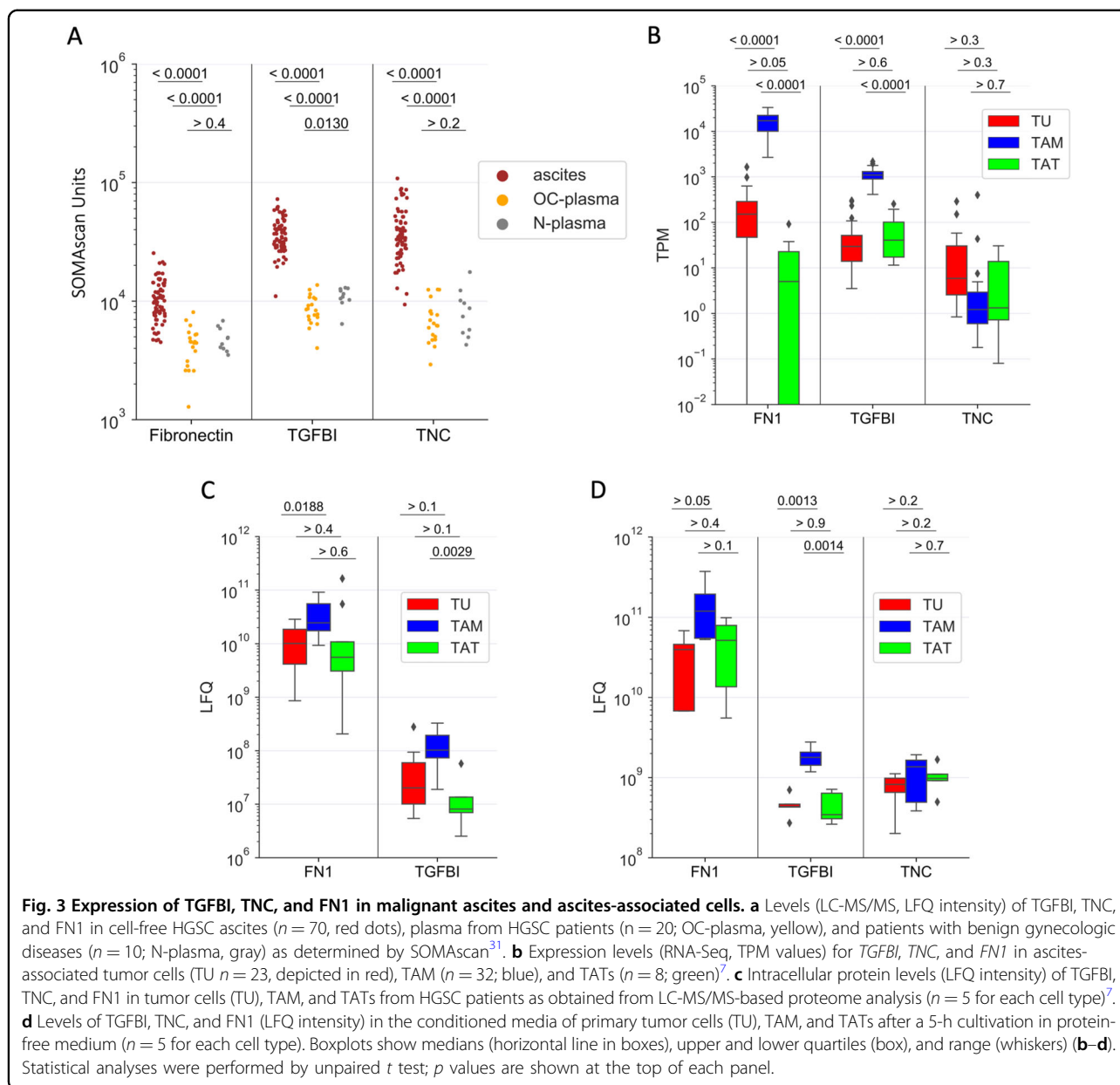
Next, we evaluated the potential clinical significance of TGFBI, TNC, and FN1 by associating their ascites levels (SOMAscan data as above) and RFS in a set of 66 HGSC patients. As illustrated in Fig. 4, Kaplan–Meier plots revealed a significant association with high ascites concentrations of TGFBI (Fig. 4a; logrank $p = 0.010$; hazard ratio (HR) = 2.35), TNC (Fig. 4b; $p = 0.005$; HR = 2.99), or FN1 (Fig. 4c; $p = 0.016$; HR = 2.10). These findings are consistent with public datasets (Fig. 4d) showing that the expression of TGFBI, TNC, and FN1 mRNA expression in tumor tissue is inversely associated with overall survival (OS) in both database queried, i.e., The Cancer Genome Atlas (TCGA)³⁴ and Kaplan–Meier Plotter (KMP)³⁵. Both FN1 and TGFBI also showed an association with a short OS in the PRECOG database³⁶.

Validation of TGFBI and TNC secretion by asc-MDM and m2c-MDM

In agreement with our data, TAM isolated from human tumors have been reported to express a matrix-related signature including FN1 affecting tumor cell motility²⁷, whereas a role of TGFBI and TNC in the crosstalk between macrophages and tumor cells has not been addressed in previous studies. We therefore focused our work on these two mediators. To validate and extend the proteomics data in Fig. 2b, which showed increased TGFBI and TNC secretion by asc-MDM and m2c-MDM versus m1-MDM, we applied qRT-PCR, western blot, and enzyme-linked immunosorbent assay (ELISA).

As illustrated in Fig. 5, TGFBI mRNA (Fig. 5a) was significantly higher in m2c-MDM compared to both asc-MDM and m1-MDM but was similar among the latter two MDM subtypes. At the intracellular protein level, TGFBI was weak or even undetectable in m1-MDM and m2c-MDM but higher in asc-MDM in single donors (Fig. 5b). TGFBI secretion was strongest in m2c-MDM but was also elevated in asc-MDM versus m1-MDM (Fig. 5c), which is consistent with the MS data (Fig. 2b). It thus appears that the differences in TGFBI secretion observed among the three MDM subtypes do not solely result from differential regulation of mRNA expression but also from subtype-specific effects on secretion itself.

TNC mRNA expression (Fig. 5d) were similar in asc-MDM and m1-MDM but elevated in m2c-MDM (though



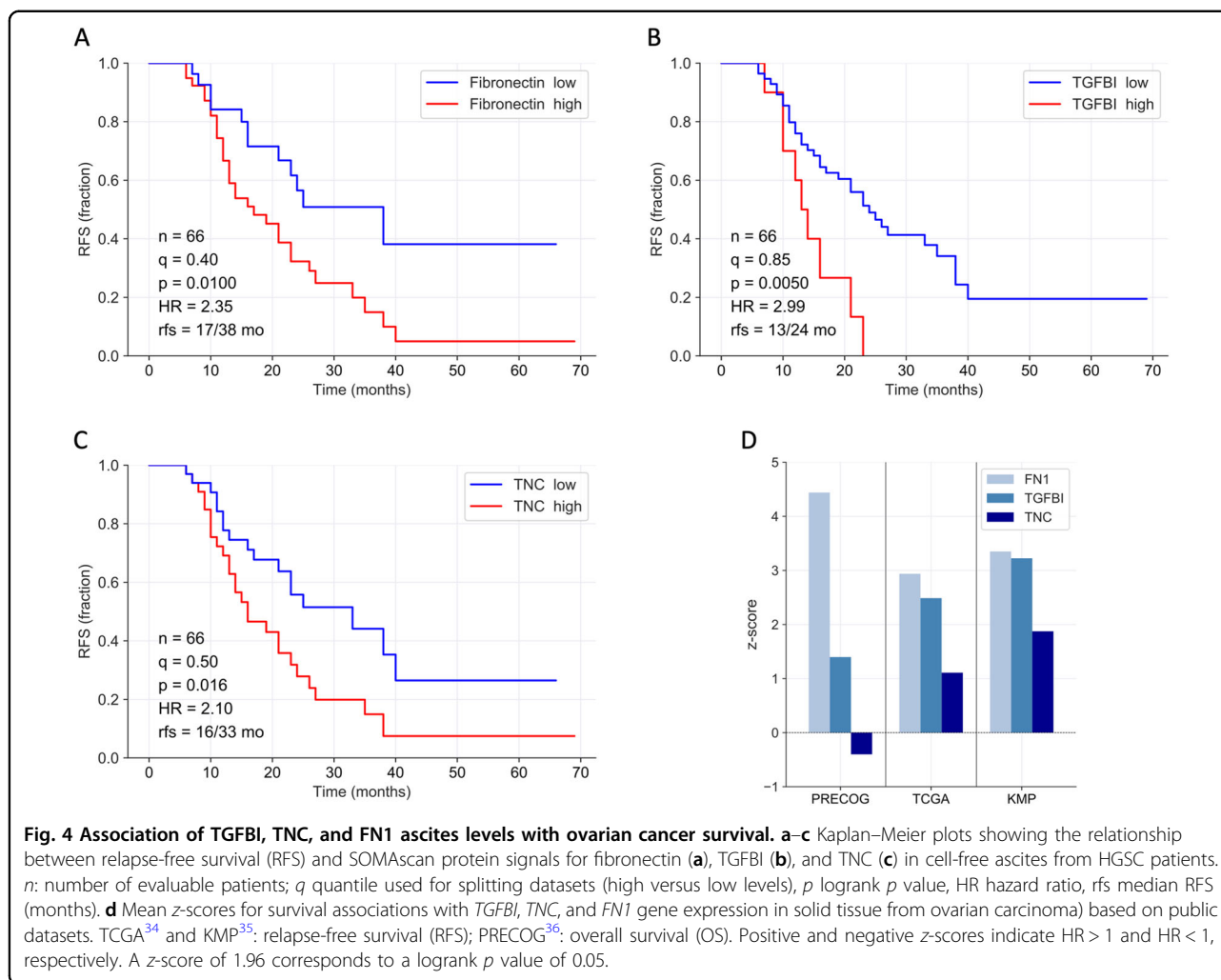
$p > 0.05$ due to the very low expression), whereas intracellular TNC was only detectable in asc-MDM (Fig. 5e). As for TGFBI, TNC secretion was also higher in asc-MDM and m2c-MDM versus m1-MDM (Fig. 5f, g), pointing to a similar subtype-dependent regulation of the secretory pathway.

In summary, these analyses fully confirm the MS data and suggest that differential regulation of both gene expression and secretion are responsible for the differences in TGFBI and TNC secretion by MDM subtypes.

Pro-migratory effects are impaired by neutralizing TGFBI and TNC in the MDM secretome

We next addressed the impact of TGFBI and TNC secreted by macrophages on tumor migration. TGFBI and

TNC both bind to integrins and, in case of TNC, additionally to EGF receptors present on the surface of tumor cells, thereby activating migration-inducing pathways^{28,29,37–39}. We could demonstrate that patient-derived tumor cells selectively bind to rTGFBI or rTNC (full-length protein) but not to rTNC-EGFL, which is a smaller fragment harboring EGFL repeats but lacking integrin-binding domains (Fig. 6a). As illustrated in Fig. 6b, rTGFBI as well as both rTNC forms enhanced migration of OCMI cells, which was accomplished by pre-incubating OCMI cells with the recombinant proteins prior to setting up the transwell assay with fetal calf serum (FCS) as chemoattractant. Our findings thus indicate that, in the case of TNC, integrin interaction is required for adhesion but dispensable for migration.

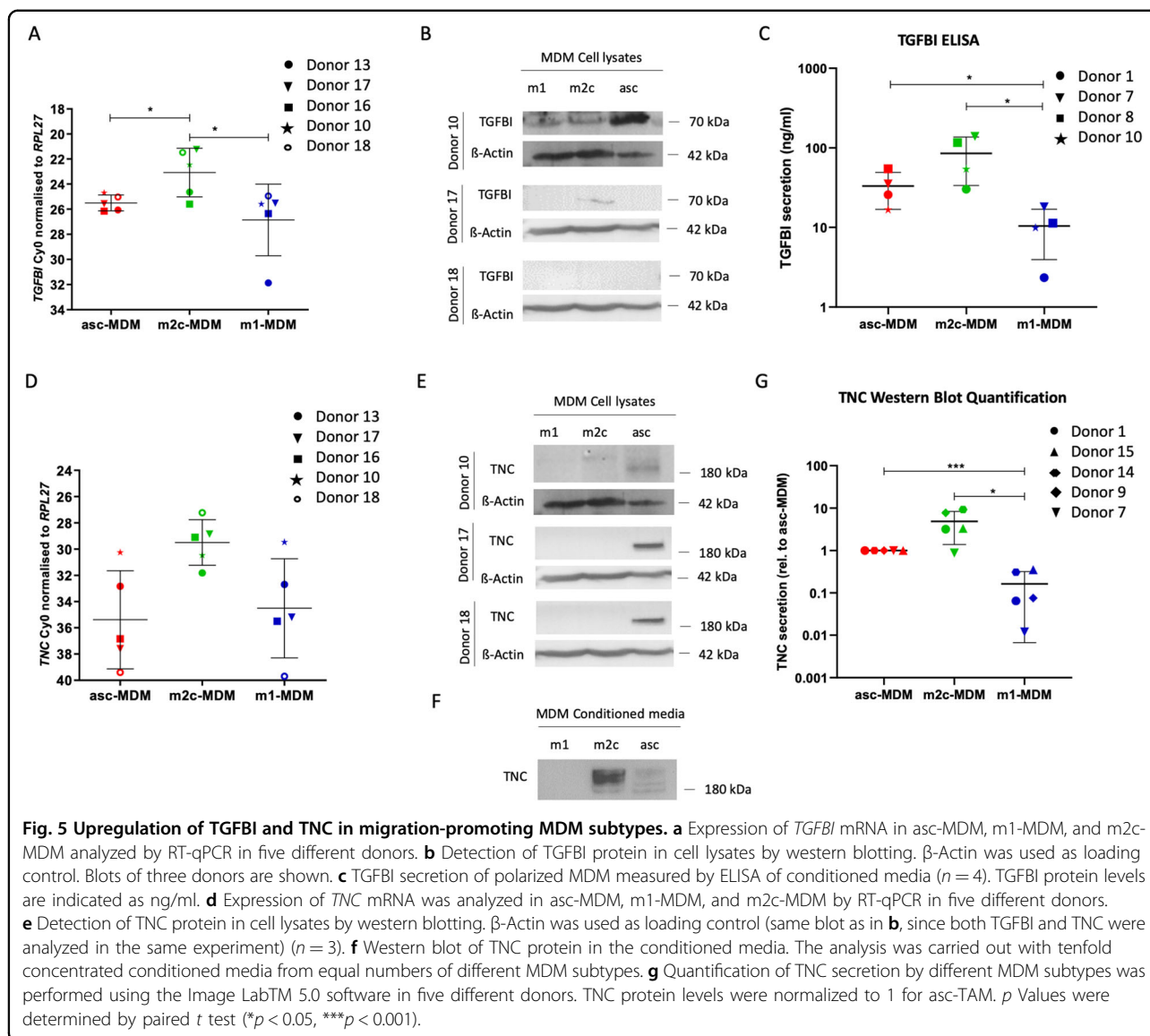


To assess the relevance of TGFBI and TNC in the context of the TAM secretome, we analyzed the effect of neutralizing antibodies directed against these proteins. As a proof of principle, we found that tumor migration induced by rTGFBI and rTNC was blocked by neutralizing anti-TGFBI (Supplementary Fig. S3A, B) and anti-TNC antibodies (Supplementary Fig. S3C, D). More importantly, similar results were obtained when conditioned media from asc-MDM or m2c-MDM were pre-incubated with the neutralizing antibodies against TGFBI (Fig. 6c, d) and TNC (Fig. 6e, f). In both cases, a significant reduction of cellular migration compared to untreated or IgG control-treated conditioned media was found for five different donors. In conclusion, these data indicate that TNC and TGFBI as constituents of the TAM secretome promote tumor cell migration.

Small interfering RNA (siRNA)-mediated TGFBI silencing in m2c-MDM/asc-MDM blocks tumor migration

To validate our findings by an independent experimental approach, we made use of siRNA-mediated interference. We

focused on TGFBI because of the low expression of TNC mRNA and TNC protein (Fig. 5d, e), which makes it difficult to reliably monitor silencing efficacy. TGFBI silencing was performed in asc-MDM and m2c-MDM and achieved reduction of TGFBI RNA and intracellular TGFBI protein expression by TGFBI siRNA transfection relative to control siRNA (Supplementary Fig. S4A, B). Importantly, TGFBI secretion by asc-MDM and m2c-MDM was also inhibited by TGFBI siRNA compared to untransfected ($p < 0.05$) and control siRNA-transfected MDM ($p < 0.01$) (Fig. 7a). To investigate the functional impact of TGFBI knockdown on the migration-inducing capacity of asc-MDM and m2c-MDM, transwell assays were performed analogous to the neutralizing experiments above. As shown in Fig. 7b, c, the conditioned media from untransfected or control siRNA-transfected asc-MDM and m2c-MDM induced OCMI cell migration to a very similar extent, whereas transfection with TGFBI siRNA resulted in a reduced effect. Taken together, these results establish an essential role for TGFBI as a migration-promoting factor in the TAM secretome.

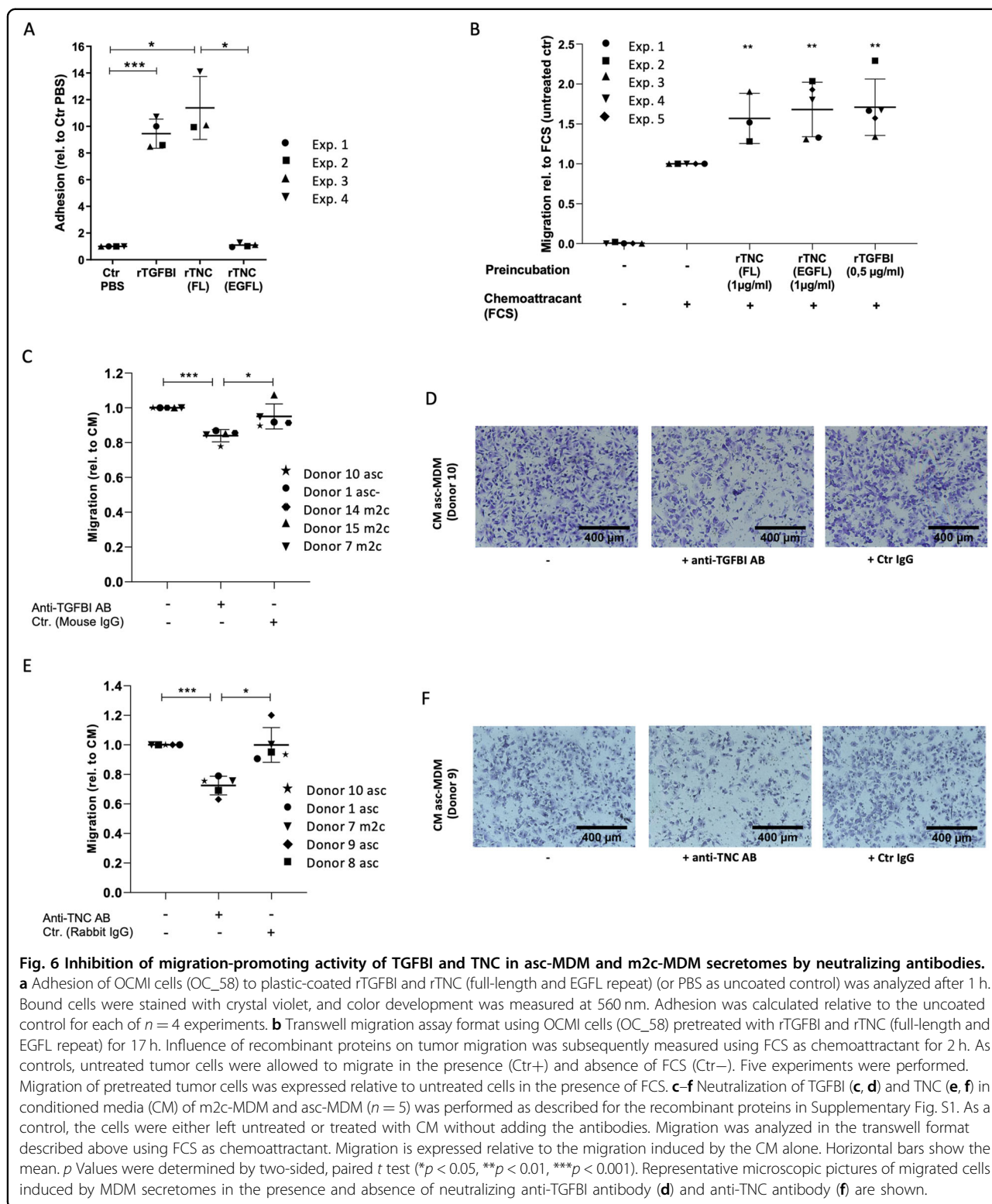


Discussion

In the present study we identified TGFBI, TNC, and FN1 as potential mediators of TAM-induced ovarian cancer migration, underscoring the known role of ECM proteins in tumor progression. A clinical importance of all three proteins is supported by our finding that increased ascites level is associated with a short RFS (Fig. 4a–c). Consistent with this observation, we found a similar association of FN1, TGFBI, and TNC gene expression in solid tumor tissue with a poor clinical outcome (Fig. 4d). These findings are in line with studies on colorectal cancer and esophageal squamous cell carcinoma where a poor prognosis correlates with TGFBI expression in tumor stroma^{40,41}. For TNC, similar clinical associations have been reported for different tumor entities^{42–45}. Furthermore, FN1, TNC, and TGFBI have been reported

to promote tumor migration, invasion, and adhesion, which are functions facilitating metastatic spread^{28–30}. In this context, FN1 has been proposed as a promoter of ovarian cancer released by CAFs⁴⁵ and TAMs²⁷, a hypothesis our results confirm. On the other hand, a mechanistic link of TAM-secreted TNC and TGFBI with tumor migration, as identified in our study, has not been described as of yet.

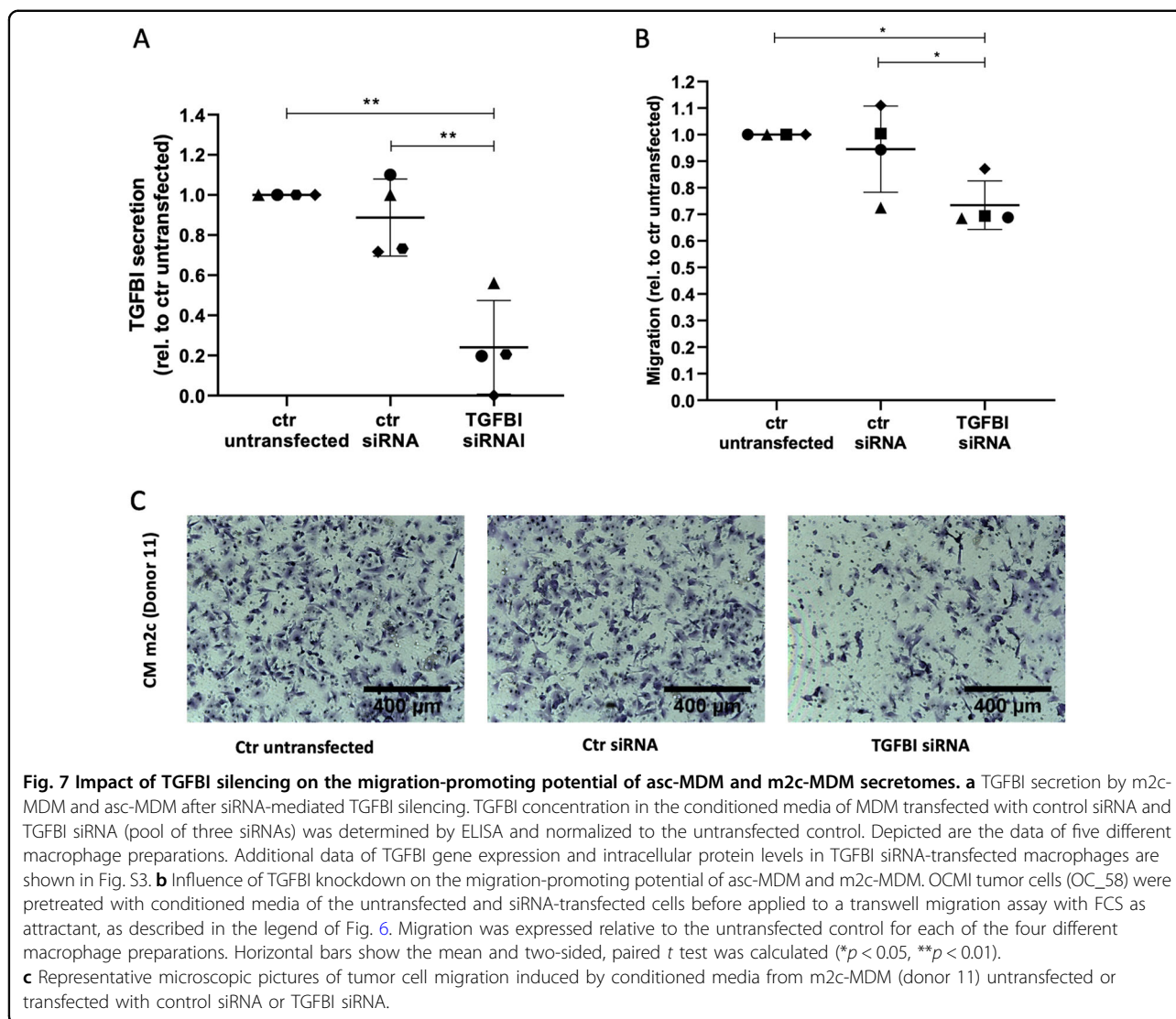
TGFBI often functions as a linker protein to interconnect ECM molecules and induces cell interactions through integrins^{37,46–49}. Different physiological functions including migration and adhesion have been attributed to TGFBI^{37,50–52}. Previous work has shown that TGFBI is expressed by stromal fibroblasts and cancer cells⁵³. TGFBI upregulation in M2 macrophages has also been linked to acute inflammation processes and ECM remodeling⁵¹, but



TAMs have not been identified as producers of TGFBI to date.

In ovarian cancer and esophageal squamous cell carcinoma, a dual function of TGFBI depending on its cellular

origin has been discussed^{38,41,54}. Here TGFBI has been proposed to act as tumor suppressor as it is down-regulated in tumor cells and as tumor promoter when expressed by peritoneal stroma cells. In accordance with



these reports, we demonstrated that TAM secrete higher amounts of TGFBI compared to other cell populations in the ascites, e.g., tumor cells or TATs (Fig. 3), and that TGFBI in the TAM secretome enhances tumor migration proven by neutralizing antibodies (Fig. 6) and RNA silencing (Fig. 7).

Both anti- and pro-adhesive features have been attributed to TGFBI affecting cell motility and invasion. In the case of melanoma, TGFBI exhibits anti-adhesive properties concomitant with anti-migratory activity^{55,56}, whereas TGFBI mediates adhesion and migration in renal cell carcinoma⁵⁷. Judging from our data, TGFBI seems to have a pro-adhesive effect in HGSC, since primary OCMI cells adhere strongly to rTGFBI, which is accompanied by enhanced tumor motility (Fig. 6).

Similar to TGFBI, TNC also functions as a modulator of cell adhesion and migration, but a broad range of functions linked to different TNC isoforms (180–330 kDa) have been reported beyond these^{58,59}. TNC is

downregulated in healthy tissue but transiently re-expressed under pathological conditions like inflammation, wound healing, and cancer^{58,60}. Moreover, TNC was found at the invasive front of different tumors with CAFs being the main producers^{61–63}. For macrophages, TNC secretion has so far only been shown in atherosclerotic plaques⁶⁴. In the present study, we identify TAM as a cellular origin of TNC in the ovarian TME supporting tumor migration. As shown by western blot, migration-promoting macrophages predominantly secrete large TNC variants of about 200–250 kDa (Fig. 5f), which have been proposed to promote a tumor-supporting TME⁵⁹. Interestingly, a number of studies point to an association between cancer progression and the occurrence of large TNC isoforms harboring alternatively spliced FNIII repeats^{59,65}. Alternatively spliced FNIII repeats as well as the RGD-containing FNIII 3 repeat present in TNC isoforms mediate cell adhesion via interaction with different

integrins expressed on the surface of tumor cells^{58,66–68}. Our data showing that only a full-length rTNC promoted cellular attachment, whereas a smaller fragment lacking integrin-binding sites exhibited anti-adhesive properties (Fig. 6a) may be considered to generally support that assumption. By contrast, both rTNC equally induced tumor migration indicating that the EGFL repeats present in both TNC forms might be involved in tumor migration through activation of EGF receptor signaling.

TGFBI and TNC are both induced by TGF β signaling and share common binding partners like fibronectin, collagen, and proteoglycans^{37,69}. Moreover, both proteins bind to integrins expressed on tumor cells and mediate their function via the integrin signaling pathway⁶⁷. These similarities may contribute to a functional cooperation of TGFBI and TNC in mediating tumor migration, when secreted by TAMs and other cells in the TME.

Other factors, including EGF, IGF1, and CHI3L1, have been proposed to be involved in the migration-promoting function of macrophages^{22–24}, but these mediators are not among the proteins upregulated in the pro-migratory MDM secretomes identified by our approach. Several reasons are likely to contribute to these differences.

- (i) Our strategy was to identify proteins that are selectively secreted by migration-promoting asc-MDM and m2c-MDM relative to m1-MDM, which do not impact tumor migration. CHI3L1 is actually present in the secretomes from all three MDM subtypes, albeit with elevated levels for m1-MDM (Table S2), which, however, does not preclude a contribution of CHI3L1 to tumor cell migration as seen in other studies²⁴.
- (ii) The published studies differ from ours in that they use either the THP1 macrophage cell line or MDM differentiated to M2a cells by IL-4, which are likely to secrete different factors.
- (iii) We consider only proteins to be relevant that are produced by TAM in vivo. EGF and IGF1 are both not expressed by TAM from HGSC ascites (median transcripts per kilobase million (TPM) < 0.1) or at very low levels (median TPM = 1), respectively (<https://www.ovara.net/resources>)⁷. Both proteins were neither detectable in the intracellular proteome of TAM nor in their secretome⁷ and were not found in the conditioned medium from asc-TAM (and this study, Table S2). It therefore appears unlikely that EGF and IGF1 play a role in the HGSC TME as proteins secreted by TAMs. However, both proteins are present in the ascites proteome of HGSC patients³¹, pointing to other cell types as producers of EGF and IGF1. Therefore, a role of these proteins in tumor migration and HGSC metastasis cannot be ruled out.

In conclusion, TGFBI, TNC, and FN1, predicted by our experimental model as migration-promoting proteins secreted by TAMs were validated to be (i) present in the HGSC ascites, (ii) secreted by TAMs derived from ascites, (iii) associated with a poor clinical outcome, and (iv) promote tumor migration as part of the TAM secretome. These findings provide further evidence for the essential role of TAMs and the ECM in HGSC metastasis.

Materials/subjects and methods

Ascites and cells isolated from ovarian cancer patients

Ascites was collected from untreated patients with HGSC prior to surgery at Marburg University Hospital. The collection and analysis of human material were approved by the ethics committee at Philipps University (reference number 205/10). Donors provided written consent in accordance with the Declaration of Helsinki. TAMs, TATs, and tumor cells were isolated from ascites as previously described^{7,33}. Briefly, mononuclear cells were separated by Lymphocyte Separation Medium 1077 (PromoCell, Heidelberg, Germany) density gradient centrifugation followed by MACS separation of CD14+ TAMs and CD3+ TATs and purification of tumor spheroids by size exclusion. Cell-free ascites was cryopreserved at -80°C . Permanent primary tumor cell cultures (termed OCMI tumor cells) were established from ascites tumor spheroids according to Ince et al.⁷⁰ with modifications, as previously reported⁷¹. This culture system allows for the propagation of ovarian cancer cells over long periods of time in the absence of culture-induced crisis or genetic alterations as compared to the original tumor. Cultured HGSC patient-derived OCMI cell lines (OCMI OC_37, OC_38, OC_58, OC_92, and OC_108) were tested for mycoplasma contamination before use for functional analysis.

Isolation and culture of MDMs from healthy donors

Buffy coats from healthy adult volunteers were kindly provided by the Center for Transfusion Medicine and Hemotherapy at the University Hospital Gießen and Marburg, and mononuclear cells were isolated by Ficoll density gradient centrifugation. CD14+ monocytes were purified by adherence selection and used for subsequent differentiation at a concentration of approximately 2.5×10^6 cells per 6-well plate. For differentiation into TAMs like asc-MDM, monocytes were cultured in cell-free ascites pool derived from 5 patients for 7 days. m1-MDM and m2c-MDM were generated by culturing monocytes in RPMI1640 (Life Technologies, Darmstadt, Germany) supplemented with 5% human AB serum (Sigma), 1% sodium pyruvate (Sigma Aldrich, Taufkirchen, Germany), and 100 ng/ml granulocyte macrophage colony-stimulating factor (CSF) (Peprotech, Hamburg, Germany) for m1-MDM or 20 ng/ml macrophage CSF (M-CSF; Biolegend, San Diego, CA, USA) for m2c-MDM²⁵.

After 5 days, 100 ng/ml LPS (Sigma Aldrich, Taufkirchen, Germany) and 20 ng/ml IFN γ (Biozol, Echingen, Germany) was added for m1-MDM and 20 ng/ml IL-10 (Biozol, Echingen, Germany) for m2c-MDM activation for 2 days.

Flow cytometry

The differentiation phenotype of MDM was characterized by flow cytometry (FACSCanto II BD Biosciences) as described previously⁸ using the following antibodies for surface staining: anti-human CD14-FITC (5170518160, Miltenyi Biotec, Bergisch Gladbach, Germany), CD86-FITC (5170620163, Miltenyi Biotec), CD16-PE-Cy7 (4273442, eBioscience, Frankfurt, Germany), CD163-PE (4303842, eBioscience), HLA-DR-APC (4330406, eBioscience), CCR7-PE (5247917, BD Biosciences, Heidelberg, Germany), and CD206-APC (B202691, Biolegend). Corresponding isotype-matched controls were purchased from Miltenyi Biotec (5161221581; 5161017246) and BD Biosciences (6286946; 25471442). The gating for macrophages was performed based on the surface expression of CD14 marker. Results were calculated as the percentage of positive cells and mean fluorescence intensities.

Generation of conditioned media

For the proteomic analysis in Fig. 3, conditioned media from ascites-derived tumor spheroids, TAMs, and TATs were generated as described by Worzfeld et al.⁷ Conditioned media of TAMs were also used for tumor migration assays (Fig. 1). Therefore, freshly prepared TAMs were cultured in autologous cell-free ascites (or ascites pool of five patients) at a density of 2.5×10^6 cells per 6-well plate for 16 h at 37 °C and 5% CO₂. Thereafter, the ascites was aspirated, and the cells were washed three times in phosphate-buffered saline (PBS) and twice in serum-free media M199 (Gibco, Thermo Fisher Scientific, Schwerte, Germany) mixed 1:2 with Dulbecco's Modified Eagle's Medium/Ham's F-12 (1:1 Biochrom, Berlin, Germany). TAMs were cultured in medium (750 μ l per 6-well) without ascites or serum for another 5 h at 37 °C and 5% CO₂ before collecting the conditioned media for secretome analysis and functional testing. This time point was chosen as prolonged incubation of TAMs resulted in increased cell death as shown by lactate dehydrogenase release. Conditioned media from differentiated MDM were obtained analogously, except that MDM were cultured for 18 h in serum-free medium. For immunoblotting, conditioned media were concentrated tenfold using a vacuum concentrator.

Proteomic and transcriptomic analyses

Cell culture supernatants from MDM cultures was obtained as described above. Up to 40 μ g of proteins were loaded on a gradient gel (NuPAGE 4–12% Bis-Tris gel, Invitrogen, Carlsbad, CA, USA), separated by sodium dodecyl sulfate-polyacrylamide gel electrophoresis prior

to in-gel digestion⁷² and analyzed by liquid chromatography tandem MS/MS as previously reported⁷. The proteomics data have been deposited to the ProteomeXchange Consortium via the PRIDE partner repository⁷³ at www.ebi.ac.uk/pride/archive (dataset identifier PXD016555). Data were processed as described⁷ using the human UniProt database (canonical and isoforms, downloaded on 02/09/2018, 183579 entries). Relevant parameters for instrumentation extracted using MARMoSET⁷⁴ and are, along with MaxQuant^{75–77} (v. 1.6.1.0) parameters, included in Supplementary Materials. Transcriptomic and proteomic data for TAMs, TATs and tumor cells from ascites were derived from our published datasets^{7,33}.

Identification of secreted proteins selective for MDM subtypes

MS data were filtered to include only proteins detected in at least 1 of the 5 asc-MDM samples with a minimum log₂ LFQ of 22 (corresponding to the median of the entire dataset with missing values replaced by imputation). Differences between asc-MDM, m1-MDM, and m2c-MDM were determined for each protein and triplet. Proteins were considered subtype-selective if they were present in the medium from one MDM subtype at a higher level than in the culture supernatant from another subtype in at least four out of the five triplets.

Tumor cell migration

Transwell migration assays were performed using two different formats. In a first approach, the migration of primary OCMI tumor cells was determined in the presence of conditioned media of macrophages or recombinant human rTGFBI (R&D Systems, Wiesbaden, Germany) and rTNC (fragment containing the EGFL repeats: R&D Systems; full-length protein: Merck, Darmstadt, Germany) as chemoattractant. 50,000 tumor cells were seeded in 300 μ l serum-free OCMI medium per transwell insert (8.0 μ m pore size; BD Biosciences). Conditioned media of macrophages (1:3 diluted in serum-free OCMI) and rTGFBI (0.5–5 μ g/ml) and rTNC (1–10 μ g/ml) (or 5% FBS as positive control) in serum-free OCMI medium were added as chemoattractants to the lower chamber. The cells were allowed to migrate through the filter for 17 h at 37 °C in a 5% CO₂ incubator. Filters were stained with crystal violet solution (0.2% in 20% methanol, 1:5 dilution) for 10 min and evaluated under a Leica DMI3000B microscope (Leica, Wetzlar, Germany). Migrated cells were counted in seven visual fields per filter using the ImageJ software. In a second setting, OCMI tumor cells were pre-incubated with conditioned media of macrophages (1:3 diluted in OCMI medium) and recombinant proteins for 17 h at 37 °C and 5% CO₂ prior to performing transwell migration assays with 5% FCS as chemoattractant. Where indicated, neutralizing antibodies (10 μ g/ml) directed against

TGFBI (3054632, Proteintech, Manchester, UK) and TNC (10000035, Merck)—or equivalent amounts of species-matched rabbit (I5006-10MG, Sigma Aldrich) and mouse IgG (131515, Jackson Immuno Research, Cambridgeshire, UK) as controls—were added to conditioned macrophage medium or recombinant proteins for 1 h before applying to the tumor cells. In each case, the pretreated tumor cells were allowed to migrate for 2 h and analyzed as described above.

Tumor cell adhesion to TNC and TGFBI

Ninety-six-well plates were coated in triplicates with 10 µg/ml rTGFBI and rTNC in PBS (or PBS alone as negative control) overnight at 4°C. Wells were blocked with 1% bovine serum albumin in PBS for 1 h at 37°C and washed three times with PBS. Fifty thousand tumor cells in OCMI media were added per well and allowed to adhere for 2 h at 37°C. The wells were washed with PBS twice to remove any unbound cells. Adherent cells were fixed with glutaraldehyde and stained with 0.1% crystal violet as described⁷⁸. The photometric measurement was performed at 560 nm, and cell adhesion was expressed relative to the negative control.

TGFBI quantification by ELISA

TGFBI concentrations in conditioned media of macrophages were quantified by commercial ELISA (human βIG-H3 ELISA duo set, R&D Systems, Wiesbaden, Germany) according to the instructions of the manufacturer.

Immunoblotting and protein quantification

Immunoblots were performed according to standard western blotting protocols using the following antibodies: α-TGFBI (5601, Cell Signaling, Danvers, MA, USA), α-TNC (10000035, Merck), α-β-Actin (A5441, Sigma Aldrich), α-rabbit IgG horseradish peroxidase (HRP)-linked AB (27, Cell Signaling), and α-mouse IgG HRP-linked AB (32, Cell Signaling). Imaging and quantification was done using the ChemiDoc MP system and Image Lab software version 5 (Bio-Rad, Hercules, CA, USA).

RNA isolation and RT-qPCR

cDNA isolation and qPCR analyses were performed as described previously⁷⁹. L27 was used for normalization. RT-qPCR was carried out using the following primers: RPL27, AAAGCTGTCATCGTGAAGAAC and GCTGTCACTTTGCGGGGGTAG; TGFBI, AAAGACATCCTA GCCACCAACG and AGCTGGCCTCTAAGTATCTG TACC; and TNC, GCCTCCACAGCCAAAGAACC and TCTGGTGCTGAACGAACTGC. Raw data were evaluated with the Cy0 method⁸⁰.

siRNA transfection of macrophages for transient TGFBI knockdown

siRNA transfection was performed in m2c-MDM and TAM-like differentiated asc-MDM as well as ascites-

derived TAMs according to the manufacturer's protocol using the TransIT-X2 reagent from Mirus (Madison, WI, USA). The following equimolar mixtures of three siRNA oligonucleotides each from Sigma Aldrich (Taufkirchen, Germany) were used for transfection: siRNA TGFBI #1 (HA12627314; HA12627315), siRNA TGFBI #2 (HA12627318; HA12627319), and siRNA TGFBI #3 (HA12627316; HA12627317). MISSION siRNA Universal Negative Control # 2 from Sigma Aldrich was used as a control siRNA (si-ctrl). For m2c-MDM, transfection was performed in RPMI/5% AB-media containing M-CSF and IL-10. Since ascites interferes with siRNA transfection, ascites-containing culture medium in asc-MDM or TAM was replaced by RPMI/5% AB-media during transfection. In this case, after 6 h transfection medium was changed and ascites was added again to maintain the TAM-like phenotype. Cells were harvested 48 h after transfection for analysis of RNA/protein expression and generation of conditioned media for functional assays.

Statistical analysis

Comparative data were statistically analyzed by unpaired (Fig. 3) or paired Student's *t* test (Figs. 1, 2, 5–7) (two-sided, equal variance). Significance levels are indicated as four (****), three (***), double (**) and single (*) asterisks for $p < 0.0001$, $p < 0.001$, $p < 0.01$, and $p < 0.05$, respectively. Box plots in Fig. 3 depicting medians (line), upper and lower quartiles (box), range (whiskers), and outliers/fliers (diamonds) were constructed using the Seaborn boxplot function with Python. Associations with RFS (logrank test), HR, and median survival times were analyzed using the Python Lifelines KaplanMeierFitter and CoxPHFitter functions. All logrank test results are presented as nominal *p* values. The data in Fig. 4d were obtained from the PRECOG and KMP meta-analysis databases^{35,36} and TCGA³⁴.

Acknowledgements

We are grateful to Traute Plaum-Allmeroth, Achim Allmeroth, and Sylvia Jeratsch for expert technical assistance. This work was supported by a grant from the German Cancer Aid (Deutsche Krebshilfe) to R.M. and S.R.

Author details

¹Institute of Molecular Biology and Tumor Research (IMT), Center for Tumor Biology and Immunology, Philipps University, Marburg, Germany. ²Clinic for Gynecology, Gynecologic Oncology and Endocrinology, Center for Tumor Biology and Immunology, Philipps University, Marburg, Germany. ³Clinic for Gynecology, Gynecological Oncology and Gynecological Endocrinology, University Hospital Giessen and Marburg (UKGM), Marburg, Germany. ⁴Biomolecular Mass Spectrometry, Max-Planck-Institute for Heart and Lung Research, Bad Nauheim, Germany. ⁵The German Centre for Cardiovascular Research (DZHK), Partner Site Rhine-Main, Max Planck Institute for Heart and Lung Research, Bad Nauheim, Germany

Conflict of interest

The authors declare that they have no conflict of interest.

Publisher's note

Springer Nature remains neutral with regard to jurisdictional claims in published maps and institutional affiliations.

Supplementary Information accompanies this paper at (<https://doi.org/10.1038/s41419-020-2438-8>).

Received: 2 December 2019 Revised: 10 March 2020 Accepted: 10 March 2020

Published online: 20 April 2020

References

- Narod, S. Can advanced-stage ovarian cancer be cured? *Nat. Rev. Clin. Oncol.* **13**, 255–261 (2016).
- Pogge von Strandmann, E., Reinartz, S., Wager, U. & Müller, R. Tumor–host cell interactions in ovarian cancer: pathways to therapy failure. *Trends Cancer* **3**, 137–148 (2017).
- Lengyel, E. Ovarian cancer development and metastasis. *Am. J. Pathol.* **177**, 1053–1064 (2010).
- Pradeep, S. et al. Hematogenous metastasis of ovarian cancer: rethinking mode of spread. *Cancer Cell* **26**, 77–91 (2014).
- Sehoul, J. et al. Intra-abdominal tumor dissemination pattern and surgical outcome in 214 patients with primary ovarian cancer. *J. Surg. Oncol.* **99**, 424–427 (2009).
- Latifi, A. et al. Isolation and characterization of tumor cells from the ascites of ovarian cancer patients: molecular phenotype of chemoresistant ovarian tumors. *PLoS ONE* **7**, e46858 (2012).
- Worzfeld, T. et al. Proteotranscriptomics reveal signaling networks in the ovarian cancer microenvironment. *Mol. Cell. Proteomics* **17**, 270–289 (2018).
- Reinartz, S. et al. Mixed-polarization phenotype of ascites-associated macrophages in human ovarian carcinoma: Correlation of CD163 expression, cytokine levels and early relapse. *Int. J. Cancer* **134**, 32–42 (2014).
- Kulbe, H. et al. A dynamic inflammatory cytokine network in the human ovarian cancer microenvironment. *Cancer Res.* **72**, 66–75 (2012).
- Peng, P., Yan, Y. & Keng, S. Exosomes in the ascites of ovarian cancer patients: origin and effects on anti-tumor immunity. *Oncol. Rep.* **25**, 749–762 (2011).
- Reiners, K. S. et al. Soluble ligands for NK cell receptors promote evasion of chronic lymphocytic leukemia cells from NK cell anti-tumor activity. *Blood* **121**, 3658–3665 (2013).
- Sever, R. & Brugge, J. S. Signal transduction in cancer. *Cold Spring Harb. Perspect. Med.* **5**, a006098 (2015).
- Finkernagel, F. et al. The transcriptional signature of human ovarian carcinoma macrophages is associated with extracellular matrix reorganization. *Oncotarget* **7**, 75339–75352 (2016).
- Condeelis, J. & Pollard, J. W. Macrophages: obligate partners for tumor cell migration, invasion, and metastasis. *Cell* **124**, 263–266 (2006).
- Sica, A. & Bronte, V. Altered macrophage differentiation and immune dysfunction in tumor development. *J. Clin. Invest.* **117**, 1155–1166 (2007).
- Qian, B.-Z. & Pollard, J. W. Macrophage diversity enhances tumor progression and metastasis. *Cell* **141**, 39–51 (2010).
- Adhikary, T. et al. Interferon signaling in ascites-associated macrophages is linked to a favorable clinical outcome in a subgroup of ovarian carcinoma patients. *BMC Genomics* **18**, 1053 (2017).
- Quatromoni, J. G. & Eruslanov, E. Tumor-associated macrophages: function, phenotype, and link to prognosis in human lung cancer. *Am. J. Transl. Res.* **4**, 376–389 (2012).
- Rodriguez, G. C. et al. Regulation of invasion of epithelial ovarian cancer by transforming growth factor- β . *Gynecol. Oncol.* **80**, 245–253 (2001).
- Worzfeld, T. et al. The unique molecular and cellular microenvironment of ovarian cancer. *Front. Oncol.* **7**, v23 (2017).
- Lewis, C. E. & Pollard, J. W. Distinct role of macrophages in different tumor microenvironments. *Cancer Res.* **66**, 605–612 (2006).
- Liu, L. et al. Upregulation of IGF1 by tumor-associated macrophages promotes the proliferation and migration of epithelial ovarian cancer cells. *Oncol. Rep.* **39**, 818–826 (2018).
- Zeng, X.-Y. et al. M2-like tumor-associated macrophages-secreted EGF promotes epithelial ovarian cancer metastasis via activating EGFR-ERK signaling and suppressing lncRNA LIMT expression. *Cancer Biol. Ther.* **20**, 956–966 (2019).
- Chen, Y., Zhang, S., Wang, Q. & Zhang, X. Tumor-recruited M2 macrophages promote gastric and breast cancer metastasis via M2 macrophage-secreted CHI3L1 protein. *J. Hematol. Oncol.* **10**, 78 (2017).
- Mantovani, A. et al. The chemokine system in diverse forms of macrophage activation and polarization. *Trends Immunol.* **25**, 677–686 (2004).
- Kalluri, R. & Zeisberg, M. Fibroblasts in cancer. *Nat. Rev. Cancer* **6**, 392–401 (2006).
- Liguori, M., Solinas, G., Germano, G., Mantovani, A. & Allavena, P. Tumor-associated macrophages as incessant builders and destroyers of the cancer stroma. *Cancers* **3**, 3740–3761 (2011).
- Paron, I. et al. Tenascin-C enhances pancreatic cancer cell growth and motility and affects cell adhesion through activation of the integrin pathway. *PLoS ONE* **6**, e21684 (2011).
- Ween, M. P. et al. Transforming growth factor-beta-induced protein secreted by peritoneal cells increases the metastatic potential of ovarian cancer cells. *Int. J. Cancer* **128**, 1570–1584 (2011).
- Yousif, N. G. Fibronectin promotes migration and invasion of ovarian cancer cells through up-regulation of FAK-P13K/Akt pathway. *Cell Biol. Int.* **38**, 85–91 (2014).
- Finkernagel, F. et al. Dual-platform affinity proteomics identifies links between the recurrence of ovarian carcinoma and proteins released into the tumor microenvironment. *Theranostics* **9**, 6601–6617 (2019).
- Lollo, B., Steele, F. & Gold, L. Beyond antibodies: new affinity reagents to unlock the proteome. *Proteomics* **14**, 638–644 (2014).
- Reinartz, S. et al. A transcriptome-based global map of signaling pathways in the ovarian cancer microenvironment associated with clinical outcome. *Genome Biol.* **17**, 1053 (2016).
- The Cancer Genome Atlas Research Network. Integrated genomic analyses of ovarian carcinoma. *Nature* **474**, 609–615 (2011).
- Gyorffy, B., Lanczky, A. & Szallasi, Z. Implementing an online tool for genome-wide validation of survival-associated biomarkers in ovarian-cancer using microarray data from 1287 patients. *Endocr. Relat. Cancer* **19**, 197–208 (2012).
- Gentles, A. J. et al. The prognostic landscape of genes and infiltrating immune cells across human cancers. *Nat. Med.* **21**, 938–945 (2015).
- Thapa, N., Lee, B.-H. & Kim, I.-S. TGFBIp/ β ig-h3 protein: a versatile matrix molecule induced by TGF- β . *Int. J. Biochem. Cell Biol.* **39**, 2183–2194 (2007).
- Tumbarello, D. A., Andrews, M. R., Brenton, J. D. & Cukierman, E. SPARC regulates transforming growth factor beta induced (TGFB1) extracellular matrix deposition and paclitaxel response in ovarian cancer cells. *PLoS ONE* **11**, e0162698 (2016).
- Swindle, C. S. et al. Epidermal growth factor (EGF)-like repeats of human tenascin-C as ligands for EGF receptor. *J. Cell Biol.* **154**, 459–468 (2001).
- Zhu, J., Chen, X., Liao, Z., He, C. & Hu, X. TGFB1 protein high expression predicts poor prognosis in colorectal cancer patients. *Int. J. Clin. Exp. Pathol.* **8**, 702–710 (2015).
- Ozawa, D. et al. TGFB1 expression in cancer stromal cells is associated with poor prognosis and hematogenous recurrence in esophageal squamous cell carcinoma. *Ann. Surg. Oncol.* **23**, 282–289 (2016).
- Gocheva, V. et al. Quantitative proteomics identify Tenascin-C as a promoter of lung cancer progression and contributor to a signature prognostic of patient survival. *Proc. Natl Acad. Sci. USA* **114**, E5625 (2017).
- Yang, Z. et al. Tenascin-C as a prognostic determinant of colorectal cancer through induction of epithelial-to-mesenchymal transition and proliferation. *Exp. Mol. Pathol.* **105**, 216–222 (2018).
- Ma, L.-J. et al. Fibronectin overexpression is associated with latent membrane protein 1 expression and has independent prognostic value for nasopharyngeal carcinoma. *Tumor Biol.* **35**, 1703–1712 (2014).
- Gopal, S. et al. Fibronectin-guided migration of carcinoma collectives. *Nat. Commun.* **8**, 14105 (2017).
- Billings, P. C. et al. The transforming growth factor- β -inducible matrix protein β ig-h3 interacts with fibronectin. *J. Biol. Chem.* **277**, 28003–28009 (2002).
- Hanssen, E., Reinboth, B. & Gibson, M. A. Covalent and non-covalent interactions of β ig-h3 with collagen VI. *J. Biol. Chem.* **278**, 24334–24341 (2003).
- Kim, J.-E. et al. Identification of motifs for cell adhesion within the repeated domains of transforming growth factor- β -induced gene, β ig-h3. *J. Biol. Chem.* **275**, 30907–30915 (2000).
- Son, H.-N., Nam, J.-O., Kim, S. & Kim, I.-S. Multiple FAS1 domains and the RGD motif of TGFB1 act cooperatively to bind α v β 3 integrin, leading to anti-angiogenic and anti-tumor effects. *Biochim. Biophys. Acta Mol. Cell Res.* **1833**, 2378–2388 (2013).

50. LeBaron, R. G. et al. β IG-H3, a novel secretory protein inducible by transforming growth factor- β , is present in normal skin and promotes the adhesion and spreading of dermal fibroblasts in vitro. *J. Invest. Dermatol.* **104**, 844–849 (1995).
51. Gratchev, A. et al. Alternatively activated macrophages differentially express fibronectin and its splice variants and the extracellular matrix protein beta1G-H3. *Scand. J. Immunol.* **53**, 386–392 (2001).
52. Nam, J.-O. et al. Identification of the α v β 3 integrin-interacting motif of Big-h3 and its anti-angiogenic effect. *J. Biol. Chem.* **278**, 25902–25909 (2003).
53. Suzuki, M. et al. High stromal transforming growth factor β -induced expression is a novel marker of progression and poor prognosis in gastric cancer. *J. Surg. Oncol.* **118**, 966–974 (2018).
54. Ween, M. P., Oehler, M. K. & Ricciardelli, C. Transforming growth factor-beta-induced protein (TGFB1)/(β IG-H3): a matrix protein with dual functions in ovarian cancer. *Int. J. Mol. Sci.* **13**, 10461–10477 (2012).
55. Nummela, P. et al. Transforming growth factor beta-induced (TGFB1) is an anti-adhesive protein regulating the invasive growth of melanoma cells. *Am. J. Pathol.* **180**, 1663–1674 (2012).
56. Lauden, L. et al. TGF- β -induced (TGFB1) protein in melanoma: a signature of high metastatic potential. *J. Investigative Dermatol.* **134**, 1675–1685 (2014).
57. Shang, D., Liu, Y., Yang, P., Chen, Y. & Tian, Y. TGFB1-promoted adhesion, migration and invasion of human renal cell carcinoma depends on inactivation of von Hippel-Lindau tumor suppressor. *Urology* **79**, 966.e1 (2012).
58. Midwood, K. S., Chiquet, M., Tucker, R. P. & Orend, G. Tenascin-C at a glance. *J. Cell Sci.* **129**, 4321–4327 (2016).
59. Giblin, S. P. & Midwood, K. S. Tenascin-C: form versus function. *Cell Adh. Migr.* **9**, 48–82 (2015).
60. Midwood, K. S., Hussenet, T., Langlois, B. & Orend, G. Advances in tenascin-C biology. *Cell. Mol. Life Sci.* **68**, 3175–3199 (2011).
61. Lowy, C. M. & Oskarsson, T. Tenascin C in metastasis: a view from the invasive front. *Cell Adh. Migr.* **9**, 112–124 (2015).
62. Boeck, A. et al. Differential secretome analysis of cancer-associated fibroblasts and bone marrow-derived precursors to identify microenvironmental regulators of colon cancer progression. *Proteomics* **13**, 379–388 (2013).
63. Santi, A., Kugeratski, F. G. & Zanivan, S. Cancer associated fibroblasts: the architects of stroma remodeling. *Proteomics* **18**, 1700167 (2018).
64. Wallner, K. et al. Tenascin-C is expressed in macrophage-rich human coronary atherosclerotic plaque. *Circulation* **99**, 1284–1289 (1999).
65. Borsi, L. et al. Expression of different tenascin isoforms in normal, hyperplastic and neoplastic human breast tissues. *Int. J. Cancer* **52**, 688–692 (1992).
66. Grahovac, J. & Wells, A. Matrikine and matricellular regulators of EGF receptor signaling on cancer cell migration and invasion. *Lab. Invest.* **94**, 31–40 (2014).
67. Tucker, R. P. & Chiquet-Ehrismann, R. Tenascin-C: its functions as an integrin ligand. *Int. J. Biochem. Cell Biol.* **65**, 165–168 (2015).
68. Yoshida, T., Akatsuka, T. & Imanaka-Yoshida, K. Tenascin-C and integrins in cancer. *Cell Adh. Migr.* **9**, 96–104 (2015).
69. Orend, G. & Chiquet-Ehrismann, R. Tenascin-C induced signaling in cancer. *Cancer Lett.* **244**, 143–163 (2006).
70. Ince, T. A. et al. Characterization of twenty-five ovarian tumour cell lines that phenocopy primary tumours. *Nat. Commun.* **6**, 264 (2015).
71. Reinartz, S. et al. Cell type-selective pathways and clinical associations of lysophosphatidic acid biosynthesis and signaling in the ovarian cancer microenvironment. *Mol. Oncol.* **13**, 185–201 (2019).
72. Rappsilber, J., Ishihama, Y. & Mann, M. Stop and go extraction tips for matrix-assisted laser desorption/ionization, nanoelectrospray, and LC/MS sample pretreatment in proteomics. *Anal. Chem.* **75**, 663–670 (2003).
73. Perez-Riverol, Y. et al. The PRIDE database and related tools and resources in 2019: improving support for quantification data. *Nucleic Acids Res.* **47**, D442 (2019).
74. Kiweler, M., Looso, M. & Graumann, J. MARMoSET - extracting publication-ready mass spectrometry metadata from RAW files. *Mol. Cell. Proteomics* **18**, 1700–1702 (2019).
75. Cox, J. et al. Accurate proteome-wide label-free quantification by delayed normalization and maximal peptide ratio extraction, termed MaxLFQ. *Mol. Cell. Proteomics* **13**, 2513–2526 (2014).
76. Cox, J. & Mann, M. MaxQuant enables high peptide identification rates, individualized p.p.b.-range mass accuracies and proteome-wide protein quantification. *Nat. Biotechnol.* **26**, 1367–1372 (2008).
77. Cox, J. et al. Andromeda: a peptide search engine integrated into the MaxQuant environment. *J. Proteome Res.* **10**, 1794–1805 (2011).
78. Reinartz, S., Failer, S., Schuell, T. & Wagner, U. CA125 (MUC16) gene silencing suppresses growth properties of ovarian and breast cancer cells. *Eur. J. Cancer* **48**, 1558–1569 (2012).
79. Unger, A. et al. Chromatin binding of c-REL and p65 is not limiting for macrophage IL12B transcription during immediate suppression by ovarian carcinoma ascites. *Front. Immunol.* **9**, 254 (2018).
80. Guescini, M., Sisti, D., Rocchi, M. B. L., Stocchi, L. & Stocchi, V. A new real-time PCR method to overcome significant quantitative inaccuracy due to slight amplification inhibition. *BMC Bioinformatics* **9**, 1026 (2008).

Supplementary Figure Legends

Figure S1. Representative microscopic pictures of tumor cell migration induced by MDM secretomes as chemoattractant. Conditioned media of m1-MDM, m2c-MDM and asc-MDM (donor 3) were applied as attractants for migration of OCMI tumor cell line OC_58 as described in Fig. 1D. Background migration in the absence of any attractant (Ctr-) as well as for FCS-induced migration (Ctr+) are included.

Figure S2. Phenotypic characterization of MDM differentiation. M1-MDM, m2c-MDM and asc-MDM from 6 donors were stained with antibodies to surface markers CD14 (A), CD163 (B), CD206 (C), CD16 (D), CD86 (E) and CCR7 (F) before used to study their impact on tumor migration (see Fig. 1). Expression was analyzed by flow cytometry to determine the percentage of positive cells and the mean fluorescence intensity (MFI). Depicted are expression data of donor-matched m1-MDM, m2c-MDM and asc-MDM. Horizontal lines indicate mean values. P-values were determined by two-sided, paired t-test (* $p < 0.05$, ** $p < 0.01$, *** $p < 0.001$).

Figure S3. Inhibition of tumor migration-promoting activity of recombinant TGFBI and TNC by neutralizing antibodies. Neutralization of tumor migration induced by rTGFBI (A, B) and rTNC (C, D). rTGFBI (0.5 $\mu\text{g/ml}$) and rTNC (EGFL repeat; 1 $\mu\text{g/ml}$) were pre-incubated with 10 $\mu\text{g/ml}$ neutralizing anti-TGFBI and anti-TNC antibodies or species-matched IgG as controls for 1h before adding to OCMI cells (OC_58) for 17h. As a control, the cells were either left untreated or treated with the recombinant proteins without adding the antibodies. The OCMI cells were then allowed to migrate for 2h using FCS as chemoattractant in a transwell format. Migration is expressed relative to the migration induced by rTGFBI or rTNC alone. Depicted are the data of 5 experiments. Horizontal bars show the mean. P-values were determined by two-sided, paired t-test (* $p < 0.05$, ** $p < 0.01$, *** $p < 0.001$). Representative microscopic pictures of migrated cells induced by recombinant proteins in the presence and absence of neutralizing anti-TGFBI antibody (B) and anti-TNC antibody (D) are shown.

Figure S4. Detection of TGFBI siRNA-mediated knockdown in macrophages on RNA and protein level. (A) *TGFBI* transcripts were analyzed in m2c-MDMs and asc-MDM 48h after transfection with either control siRNA or TGFBI siRNA (pool of 3 siRNAs) by RT-qPCR with *Cy0* values normalised to *L27*. The graph shows the results of 5 different experiments. Horizontal lines indicate means. Two-sided, paired t-test was calculated for each TGFBI siRNA transfection (** $p < 0.01$, *** $p < 0.001$). (B) Detection of TGFBI expression in cell lysates of m2c-MDM transfected control siRNA or TGFBI siRNA (3 individual and pooled siRNAs) by Western Blot using anti-TGFBI antibody. β -Actin was used as loading control. Untransfected m2c-MDM and CAFs known to express high levels of TGFBI were used as controls. Cell lysate from m1-MDM not secreting TGFBI was used as negative control. One representative Blot is shown for one knockdown experiment in m2c-MDM.

Figure S1

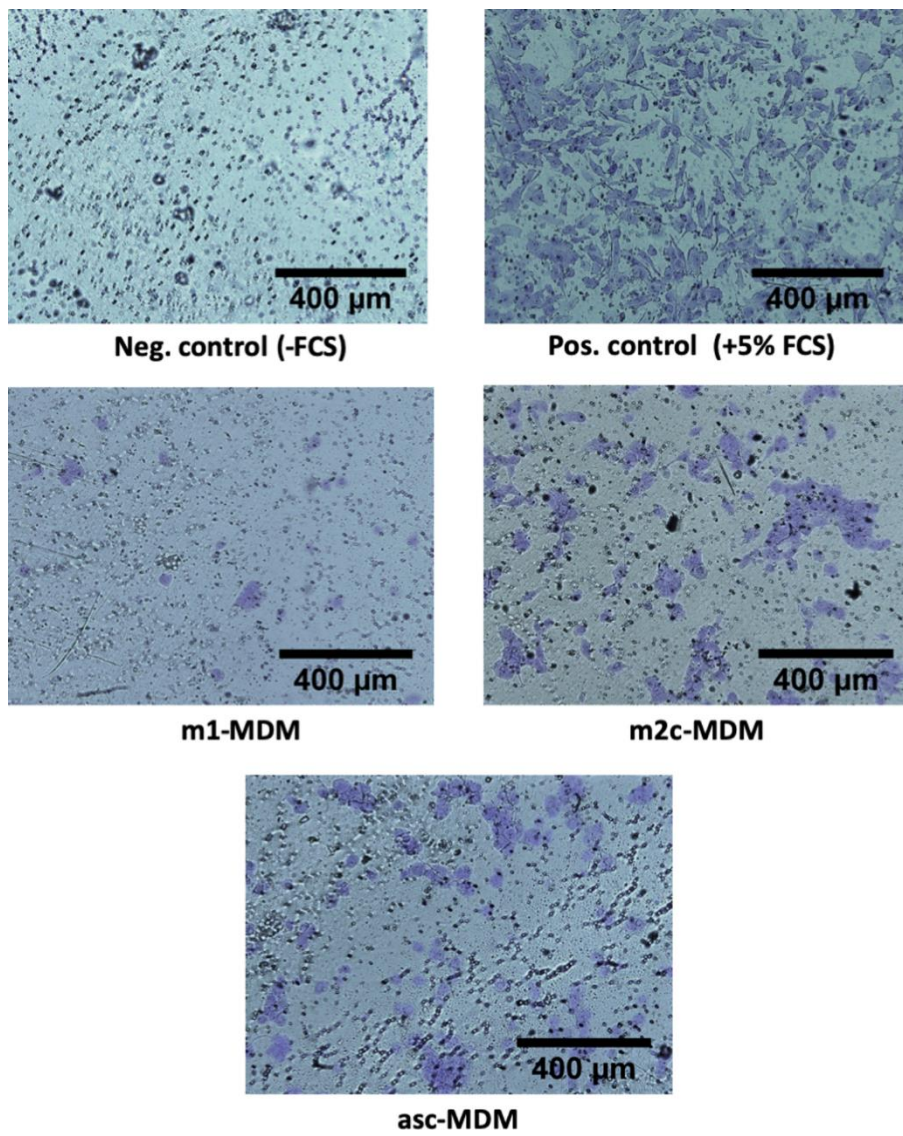


Figure S2

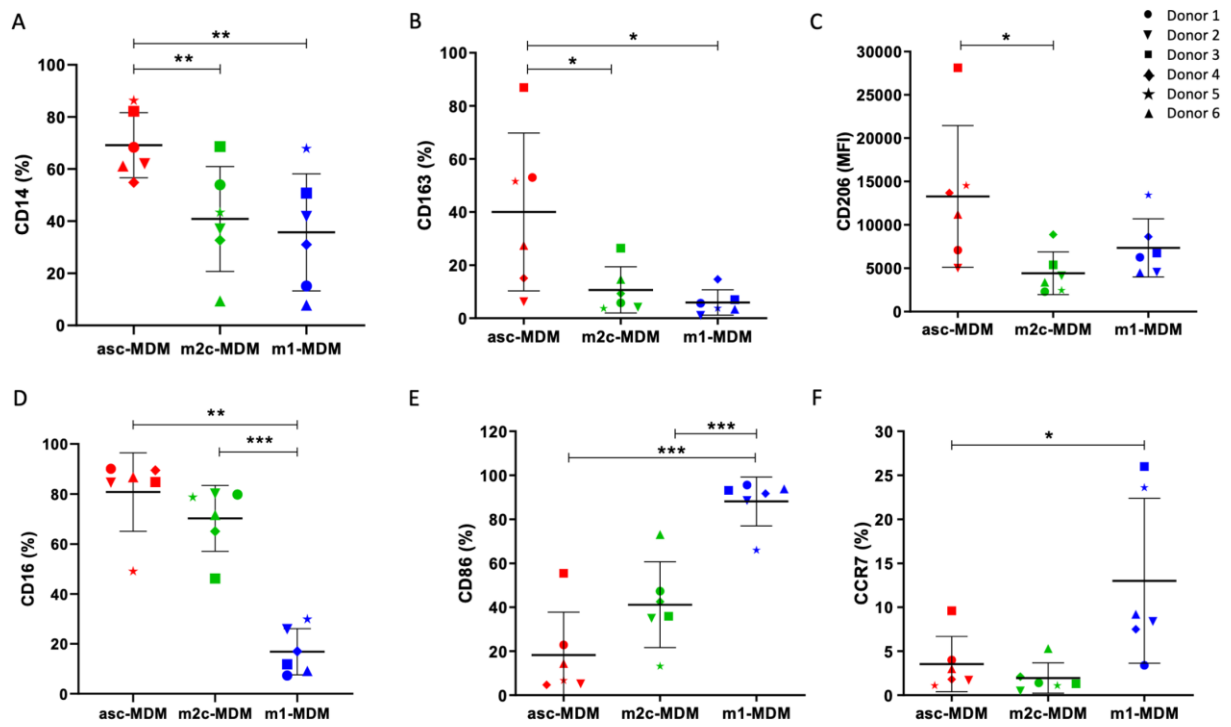


Figure S3

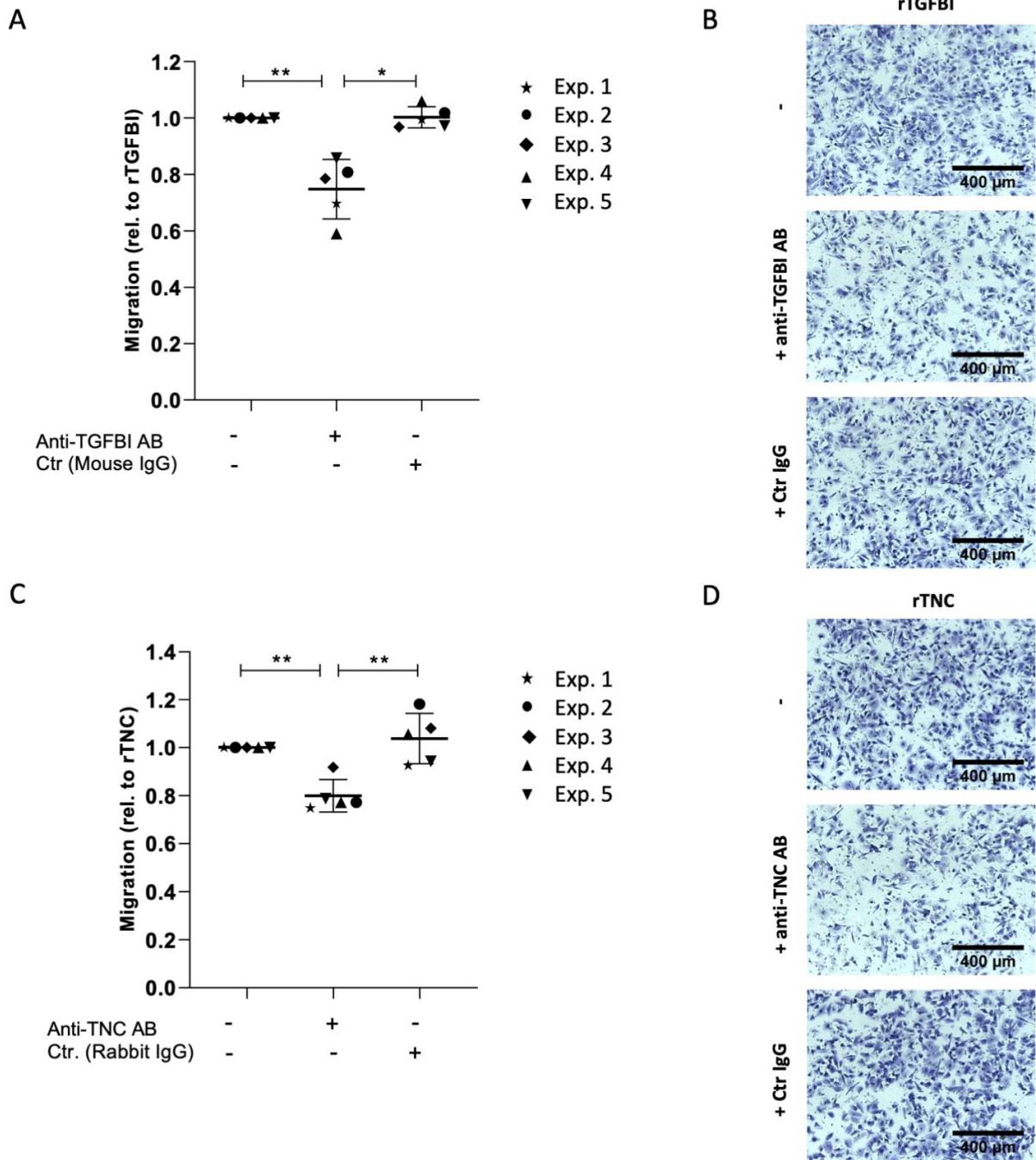
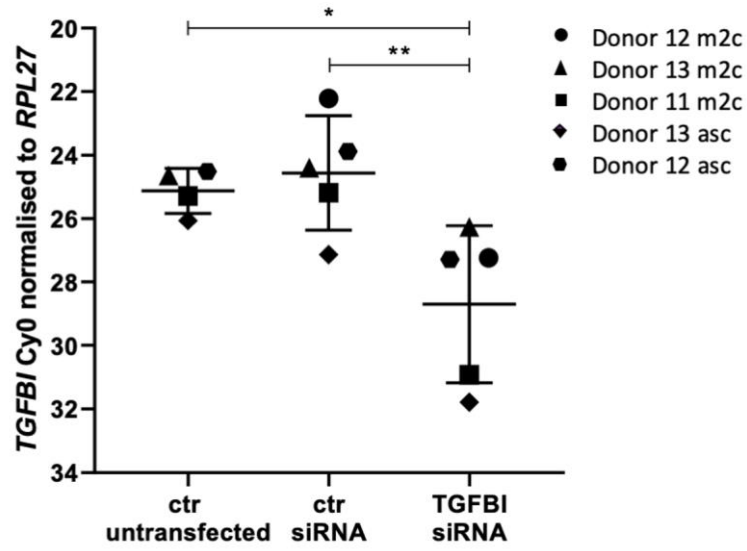
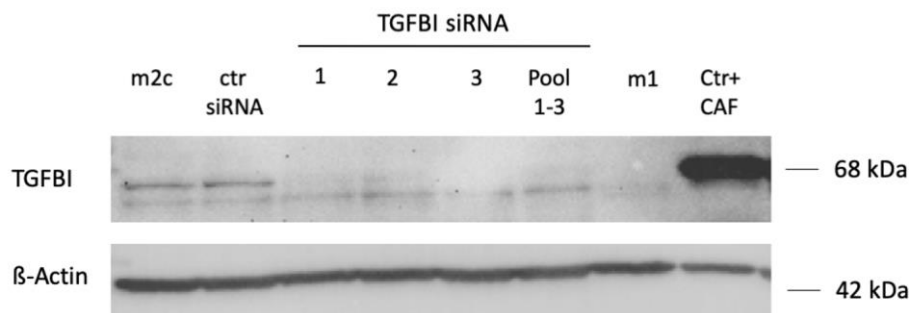


Figure S4

A





B



RESEARCH ARTICLE

The multicellular signalling network of ovarian cancer metastases

Leah Sommerfeld¹ | Florian Finkernagel¹ | Julia M. Jansen² | Uwe Wagner² |
 Andrea Nist³ | Thorsten Stiewe^{3,4} | Sabine Müller-Brüsselbach¹ | Anna M. Sokol⁵ |
 Johannes Graumann^{5,6}  | Silke Reinartz¹ | Rolf Müller¹ 

¹ Department of Translational Oncology, Center for Tumor Biology and Immunology (ZTI), Philipps University, Marburg, Germany

² Clinic for Gynecology, Gynecological Oncology and Gynecological Endocrinology, University Hospital (UKGM), Marburg, Germany

³ Genomics Core Facility, Center for Tumor Biology and Immunology (ZTI), Philipps University, Marburg, Germany

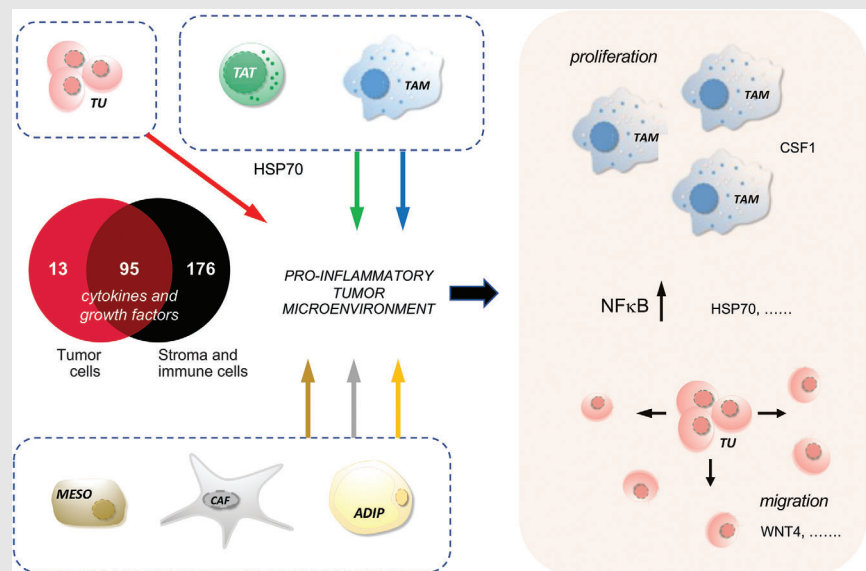
⁴ Institute of Molecular Oncology, Philipps University, Marburg, Germany

⁵ The German Centre for Cardiovascular Research (DZHK), Partner Site Rhine-Main, Max Planck Institute for Heart and Lung Research, Bad Nauheim, Germany

⁶ Institute for Translational Proteomics, Philipps University, Marburg, Germany

Correspondence



Silke Reinartz and Rolf Müller, Department of Translational Oncology, Center for Tumor Biology and Immunology (ZTI), Philipps University, Marburg, Germany. Email: silke.reinartz@uni-marburg.de; rolf.mueller@uni-marburg.de

Graphical Abstract

Besides macrophages, omental adipocytes, mesothelial cells and fibroblasts play an unexpectedly prominent role in the pro-metastatic signaling network of ovarian carcinoma, encompassing clinically relevant pathways and potential therapeutic targets. The central role of stroma-derived mediators is exemplified by (i) WNT4 stimulating tumour cell adhesion and migration, (ii) activation of pro-inflammatory signaling by extracellular HSP70 and (iii) CSF1 inducing macrophage proliferation.

RESEARCH ARTICLE

The multicellular signalling network of ovarian cancer metastases

Leah Sommerfeld¹ | Florian Finkernagel¹ | Julia M. Jansen² | Uwe Wagner² |
 Andrea Nist³ | Thorsten Stiewe^{3,4} | Sabine Müller-Brüsselbach¹ | Anna M. Sokol⁵ |
 Johannes Graumann^{5,6}  | Silke Reinartz¹ | Rolf Müller¹ 

¹ Department of Translational Oncology, Center for Tumor Biology and Immunology (ZTI), Philipps University, Marburg, Germany

² Clinic for Gynecology, Gynecological Oncology and Gynecological Endocrinology, University Hospital (UKGM), Marburg, Germany

³ Genomics Core Facility, Center for Tumor Biology and Immunology (ZTI), Philipps University, Marburg, Germany

⁴ Institute of Molecular Oncology, Philipps University, Marburg, Germany

⁵ The German Centre for Cardiovascular Research (DZHK), Partner Site Rhine-Main, Max Planck Institute for Heart and Lung Research, Bad Nauheim, Germany

⁶ Institute for Translational Proteomics, Philipps University, Marburg, Germany

Correspondence

Silke Reinartz and Rolf Müller, Department of Translational Oncology, Center for Tumor Biology and Immunology (ZTI), Philipps University, Marburg, Germany. Email: silke.reinartz@uni-marburg.de; rolf.mueller@uni-marburg.de

Funding information

Deutsche Krebshilfe (German Cancer Aid), Grant/Award Number: 70113255

Abstract

Background: Transcoelomic spread is the major route of metastasis of ovarian high-grade serous carcinoma (HGSC) with the omentum as the major metastatic site. Its unique tumour microenvironment with its large populations of adipocytes, mesothelial cells and immune cells establishes an intercellular signaling network that is instrumental for metastatic growth yet poorly understood.

Methods: Based on transcriptomic analysis of tumour cells, tumour-associated immune and stroma cells we defined intercellular signaling pathways for 284 cytokines and growth factors and their cognate receptors after bioinformatic adjustment for contaminating cell types. The significance of individual components of this network was validated by analysing clinical correlations and potentially pro-metastatic functions, including tumour cell migration, pro-inflammatory signal transduction and TAM expansion.

Results: The data show an unexpected prominent role of host cells, and in particular of omental adipocytes, mesothelial cells and fibroblasts (CAF), in sustaining this signaling network. These cells, rather than tumour cells, are the major source of most cytokines and growth factors in the omental microenvironment ($n = 176$ vs. $n = 13$). Many of these factors target tumour cells, are linked to metastasis and are associated with a short survival. Likewise, tumour stroma cells play a major role in extracellular-matrix-triggered signaling. We have verified the functional significance of our observations for three exemplary instances. We show that the omental microenvironment (i) stimulates tumour cell migration and adhesion via WNT4 which is highly expressed by CAF; (ii) induces pro-tumourigenic TAM proliferation in conjunction with high CSF1 expression by omental stroma cells and (iii) triggers pro-inflammatory signaling, at least in part via a HSP70–NF- κ B pathway.

This is an open access article under the terms of the [Creative Commons Attribution](https://creativecommons.org/licenses/by/4.0/) License, which permits use, distribution and reproduction in any medium, provided the original work is properly cited.

© 2021 The Authors. *Clinical and Translational Medicine* published by John Wiley & Sons Australia, Ltd on behalf of Shanghai Institute of Clinical Bioinformatics

Conclusions: The intercellular signaling network of omental metastases is majorly dependent on factors secreted by immune and stroma cells to provide an environment that supports ovarian HGSC progression. Clinically relevant pathways within this network represent novel options for therapeutic intervention.

KEYWORDS

adipocyte, carcinoma-associated fibroblast, HSP70, mesothelial cell, metastasis, omentum, ovarian carcinoma, signaling network, tumour microenvironment, WNT4

1 | INTRODUCTION

High-grade serous carcinoma (HGSC) is the most frequent and fatal of all gynaecologic cancers, mainly due to its early and widespread transcoelomic dissemination to peritoneal surfaces in abdominal and pelvic cavities. Transcoelomic spread is enabled by the peritoneal fluid which provides a carrier for tumour cells that are shed from solid tumour lesions.¹ At advanced stages of HGSC the peritoneal fluid increases to large volumes, referred to as malignancy-associated ascites. Ascites not only serves as a passive carrier, but also provides a tumour-promoting and immune suppressive environment mediated by soluble mediators as well as extracellular microvesicles.^{2,3} Due to its high content in bioactive compounds and its active role in peritoneal dissemination, HGSC ascites functionally differs from other human cancers, where effusions are usually reactive or represent an epiphenomenon.

The most frequent metastatic site for HGSC is the omentum,⁴ a specialised adipose tissue connected by a mesothelial layer to other intraperitoneal organs.⁵ A specific feature of the omentum are regions referred to as milky spots, which mainly consist of macrophages and lymphocytes, which contribute to peritoneal immune surveillance.⁵⁻⁷ Besides immune cells other cell types of the omentum have been reported to promote ovarian cancer growth and metastatic spread. Thus, hypoxic mesothelial cells (MESO) at milky spots secrete vascular endothelial growth factor (VEGFA), thereby potentially inducing neo-angiogenesis.⁸ Another example are omental adipocytes (ADI), which promote the homing and invasion of ovarian cancer by multiple mechanisms, including the secretion of adipokines, the promotion of tumour cell metabolism through the direct transfer of lipids to cancer cells⁹⁻¹¹ and the ADI-induced phosphorylation of salt-inducible kinase 2 (SIK2), mediating AMPK-dependent acetyl-CoA carboxylase phosphorylation and PI3K/AKT activation in tumour cells.¹² Furthermore, cancer-associated fibroblasts (CAF), derived from omental fibroblasts and mesenchymal stem cells under the influence of the tumour microenvironment,^{9,13} produce

numerous factors imping on cancer cells to promote glycolytic metabolism, proliferation, invasion, angiogenesis and metastatic colonisation.^{9,14,15}

Besides these omental cell types, tumour-associated macrophages (TAM) clearly are instrumental in metastasis, in particular the CD163⁺Tim4⁺ subset, which promotes the stemness, invasive properties and epithelial to mesenchymal transition (EMT) of tumour cells by paracrine mechanisms.¹⁶ While omentectomy or depletion of CD163⁺Tim4⁺ cells prevented metastatic dissemination in a mouse model of ovarian cancer, depletion of monocyte-derived TAM had little impact, emphasising the role of resident omental macrophages. In keeping with these findings, TAM from HGSC patients show a high degree of phenotypic, ontogenetic and tumour-promoting heterogeneity, reflected, for example, by the differential expression of CD163 and cytokines associated with tumour progression.^{17,18}

Recent progress in single-cell RNA sequencing (scRNA-Seq) confirmed the intra- and inter-patient heterogeneity of TAM in HGSC ascites.¹⁹ The authors identified four clusters characterised by genes associated with divergent phenotypes and functions, including immune stimulation (*HLA* genes, *IFNGR1*, *CDID*), complement factor components and cathepsins, and markers of M1 and M2 differentiation. Likewise, CAF from ascites were similarly heterogeneous with four clusters defined by immune-related genes, complement factors, chemokines (*CXCL1/2/10/12*) and cytokines (*IL6*, *IL10*). Previous work had identified four subtypes of HGSC, that is differentiated, proliferative, mesenchymal and immunoreactive, of which the latter two are linked to a poor or favourable outcome, respectively.^{20,21} Intriguingly, scRNA-Seq¹⁹ showed weak or no expression of mesenchymal and immunoreactive signatures by HGSC cells, but high expression by CAF and TAM clusters, respectively. This strongly suggests that the mesenchymal and immunoreactive subtypes are defined by the abundance of CAF and TAM rather than by cancer cell subpopulations, providing further evidence for the crucial role of tumour-associated host cells. Interestingly, the fraction of TAM and CAF in tumour tissue appears

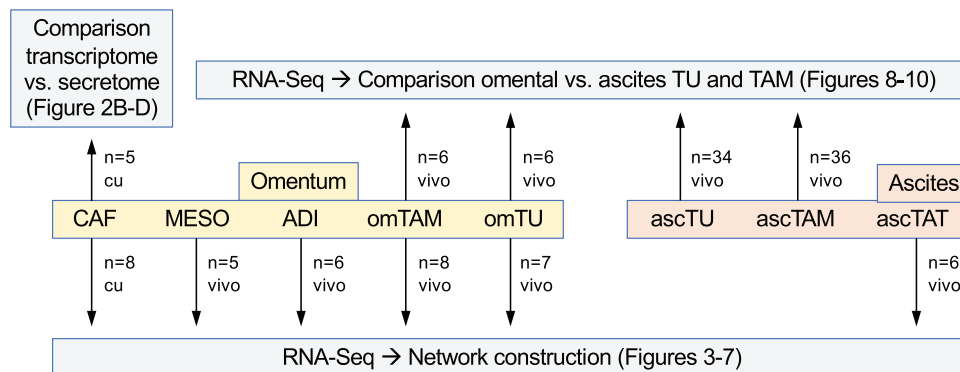


FIGURE 1 Workflow and conception of the present study. *n*: number of independent samples (different patients); vivo: samples directly used after isolation from clinical material; cu: cells cultured for xxx passages after isolation from omental metastases (CAF only). RNA-Seq samples with contaminating samples of >6% were excluded from further analyses and the remaining samples were adjusted for minor contaminations by a bioinformatic approach

to increase during progression, as suggested by a previous scRNA-Seq study.²² Other scRNA-Seq studies also confirmed a substantial heterogeneity among tumour cells^{23,24} and lead to the proposal that HGSC is defined by continuous tumour evolution with mixtures of subclones and stage-dependent infiltration of host cells rather than by discrete transcriptome subtypes.²³

Despite considerable progress over the past years, our knowledge of the intercellular signalling network operating in HGSC metastases remains fragmentary. Published systematic transcriptomic studies suitable for the development of signalling networks are limited to ascites cells,^{17,25} and were partly performed by scRNA-Seq,^{19,22,23,26} which is not informative for a subset of weakly expressed genes and possesses a limited power for differential expression studies compared to bulk analyses.^{27–32} It is also currently unclear, to which extent ascites-derived cell types resemble their counterparts in solid tumour lesions, since unbiased omics analysis have not been described for tumour-associated non-immune cells from HGSC patients.

In the present study, we have performed systematic transcriptomic bulk analyses of all major cell types from omental HGSC metastases, supported and extended by proteomic and functional studies to (i) construct a comprehensive network of cytokines, growth factors and ECM components and their cognate receptors and (ii) compare the expression of these proteins in omental versus ascites-derived TU and TAM. The workflow and general strategy of our study is schematically summarised in Figure 1. We will refer to TAM and TAT collectively as tumour-associated ‘immune cells’ and to the compartment of ADI, MESO and fibroblasts (CAF) as tumour-associated ‘stroma cells’ throughout this manuscript.

2 | METHODS

2.1 | Patient samples

Ascites and greater omentum tissue with metastatic lesions were collected from patients with ovarian HGSC undergoing primary surgery at the University Hospital in Marburg. Patient characteristics are summarised in Table S1. Clinical courses were evaluated by RECIST criteria³³ in patients with measurable disease or profiles of serum CA125 levels according to the recommendations by the Gynecologic Cancer InterGroup (GCIg). Only patients with observations periods ≥ 12 months after first-line surgery were included in the survival analysis.

2.2 | Isolation of cells from HGSC ascites

Tumour cell spheroids, TAM and TAT were isolated from ascites essentially as described.^{17,25} Briefly, mononuclear cells were isolated from ascites by density gradient centrifugation (Lymphocyte Separation Medium 1077; PromoCell). Medium size (‘M’) and large (‘L’) tumour cell spheroids were obtained by filtration using 30 and 100 μm cell strainer (Miltenyi Biotech). Smaller tumour spheroids (<30 μm ; ‘s’) and single tumour cells (sc) were further enriched by depletion of CD45⁺ leukocytes by magnetic cell sorting (MACS; Miltenyi Biotech, Bergisch Gladbach, Germany). TAM were purified by selection for CD14⁺ cells on MACS microbeads. TAT were isolated from ascites as CD3⁺ cells by MACS. All microbeads for MACS (CD3, CD14, CD45) were obtained from Miltenyi Biotech. Cell populations with a purity of > 95%, as determined by flow cytometry, were used for subsequent analysis.

2.3 | Isolation of tumour and host cells from omentum

Prior to enzymatic digestion, omentum tissue without visible metastatic lesions was dissected from omentum tumour tissue. ADI were obtained from omental tissue by digestion with 370 U/ml collagenase (Sigma Aldrich) in 10 ml adipocyte digestion buffer (5 mM D-Glucose, 1.5% BSA in PBS) per 5 g tissue for 1 h at 37°C under continuous shaking. The disaggregated cell suspension was filtered through a 400 µm filter and centrifuged (5 min, 150× g) to separate ADI by density. The supernatant containing ADI was gently washed twice with PBS. During the washing steps, contaminating cells were separated from the floating ADI layer by gravity for 5 min. This process normally yields ADI fractions with a purity of >95% which were directly used for secretome cultures or lysed in PeqGold TriFast™ (Peqlab, Erlangen, Germany) for RNA isolation. Contamination of ADI with leukocytes or omTU was determined by fluorescence microscopy using FITC-labelled anti-human CD45 and PE-labelled anti-human EpCAM (both Miltenyi) combined with Hoechst 33342 staining (Thermo Fisher Scientific, Schwerte, Germany).

For the isolation of MESO, omental tissue was washed with PBS, minced into small pieces (approx. 5 mm diameter) and subsequently digested with trypsin (20 ml 0.05% Trypsin/0.02% EDTA per 10 g tissue) for 30 min at 37°C. The digested tissue was passed through a 100 µm nylon filter and centrifuged (10 min at 300 g). This MESO-enriched fraction was cryopreserved for later purification by MACS.

To isolate tumour cells, CAF and omTAM, omental tumour tissue was treated as described for MESO, except that trypsin digestion was performed for 2 h at 37°C. The dissociated cell suspension was cryopreserved for later purification of omTU and omTAM by MACS. The residual tissue was consecutively treated with a mixture of 18.5 U/ml collagenase and 2.5 µg/ml hyaluronidase (Sigma Aldrich, Taufkirchen, Germany) in 20 ml fibroblast culture medium [DMEM/HAM'S F12 (1:1), 10% FCS, 10 ng/ml EGF, 1% Pen/Strep] overnight at 37°C, filtered through a 100 µm mesh and washed as described above to yield a cellular fraction enriched for tumour cells, omTAM and CAF for cryopreservation.

The isolation of omTU, omTAM, MESO and CAF was achieved by different MACS sorting strategies. Cryopreserved cellular fractions after enzymatic digestion were thawed and processed over a Ficoll gradient to eliminate dead cells. omTUs were purified from tumour-enriched fractions (after overnight digestion with trypsin, collagenase and hyaluronidase as described above) by MACS depletion of CD45⁺ leucocytes in combination with positive MACS selection for EpCAM⁺ cells (Miltenyi Biotech). CD14⁺ microbeads were used to isolate omTAM from the tumour fractions (after 2-h digestion with trypsin, colla-

genase and hyaluronidase as described above) by positive MACS selection. CAF were obtained from the collagenase/hyaluronidase fraction (described above) after initial preculture in fibroblast medium [DMEM/Ham's F12 (1:1) + 10% FCS + 1 ng/ml EGF + 1% penicillin/streptomycin] and subsequent MACS depletion of CD45⁺ leucocytes and EpCAM⁺ tumour cells. If necessary, a positive selection using anti-fibroblast beads (Miltenyi Biotech) was additionally applied to yield sufficiently pure CAF. The same purification strategy using CD45 and EpCAM depletion was used in parallel to isolate MESO from the 30 min trypsin digest fraction obtained from macroscopic tumour-free omentum tissue.

RNA was isolated from all cell types directly after purification (ex vivo) except for CAF, which were cultured in OCMI medium³⁴ supplemented with 50% ascites for a maximum of three passages.

2.4 | Flow cytometry analyses

Cells isolated from ascites or omentum were analysed by flow cytometry performed on a FACS Canto II instrument using Diva Software (BD Biosciences, Heidelberg, Germany) using the following staining protocol. Tumour cells were identified with Vioblue-labelled anti-human EpCAM (Miltenyi Biotech), TAM with FITC-labelled anti-human CD14 (Miltenyi Biotech) and TAT with APC-labelled anti-human CD3 (Biolegend, Koblenz, Germany). MESO and CAF were characterised by negative staining with Vioblue-labelled anti-EpCAM and further discriminated using fibroblast markers like PE-labelled anti-human CD140a (eBioscience/Thermo Fisher Scientific) and FAP (R&D Systems//Thermo Fisher Scientific) in combination with APC-labelled anti-human mesothelin (R&D Systems) and intracellular staining with APC-labelled anti-human cytokeratin and FITC-labelled anti-human vimentin (both from Miltenyi). In some cases, anti-human MUC16 antibody (clone OC125, Sigma Aldrich) combined with secondary FITC-labelled anti-mouse IgG (eBioscience) was included. Isotype control antibodies were purchased from BD Biosciences, Miltenyi Biotech and eBioscience. Results were calculated as percentage of positive cells and mean fluorescence intensities (MFI). Cell death was assessed by propidium iodide staining. Proliferation of TAM was analysed by staining with anti-human CD14 FITC (Miltenyi) and intracellular staining with anti-Ki67 APC (Biolegend).

2.5 | Protein mass spectrometry (MS) of conditioned media from CAF

For proteomic analyses of conditioned media, omental CAF or ascTU were first propagated in OCMI medium

with 50% pooled ascites. After 16 h at 37°C and 5% CO₂, the cells were washed three times in PBS and twice in serum-free medium M199 (Gibco, Thermo Fisher Scientific) mixed with an equal volume of DMEM/Ham's F-12 (Biochrom, Schaffhausen, Germany) and cultured in serum-free medium for another 0 or 20 h before harvesting the supernatants for MS-based proteomic analysis. Following acetone precipitation from supernatants, up to 40 µg of proteins were loaded on a gradient gel (NuPAGE 4–12% Bis-Tris gel, Invitrogen) and separated by SDS-PAGE prior to in-gel digestion.³¹ Analysis by liquid chromatography/tandem mass spectrometry (LC/MS2) was performed as described¹⁷ and peptide/spectrum matching as well as label free quantitation used the MaxQuant suite of algorithms^{35–37} against the human Uniprot database (canonical and isoforms; downloaded on 2020/02/05; 1888349 entries). Relevant instrument parameters were extracted and summarised using MARMoSET (see Supporting Information MS settings). Protein-specific signals were calculated by subtracting the 0-h LFQ value from the 16-h LFQ log10 value. Data in Figures 2D and 8D are represented as LFQ/10.⁷ For Figure 1C, proteins were considered 'in secretome' if there was a peptide group (identified in any sample by MaxQuant) associated to them and a higher median signal in 20-h samples compared to 0 h.

2.6 | Transient WNT4 knockdown in CAF by siRNA transfection

siRNA transfection was performed in CAF from omental metastasis cultured in OCMI plus 5% FCS using the TransIT-X2 reagent from Mirus (Madison, WI, USA) or lipofectamine 3000 (Invitrogen, Thermo Fisher Scientific), according to the manufacturer's protocol. siWNT4 ON-Target plus smartpool from Dharmacon (Horizon Discovery, Cambridge, UK) and MISSION siRNA Universal Negative Control # 2 (Sigma Aldrich) as a control siRNA were used. Untransfected CAF were included as controls. Cells were harvested 48 h after transfection for RNA and protein expression analyses and for generation of conditioned media.

2.7 | Transient WNT4 overexpression in LP9 cells

The human MESO line LP9 (AG07086, Coriell Institute, Camden, NJ) with low basal WNT4 expression level was chosen to induce WNT4 overexpression by transient transfection with WNT4_pCDNA3.1 vector (WNT4_OE) or empty pCDNA3.1 control (pCDNA3.1_Ctrl) (GenScript Biotech, Piscataway, NJ) using Lipofectamine 3000 (Invit-

rogen, Thermo Fisher Scientific) according to the manufacturer's instructions. WNT4 expression was validated 48 h after transfection by RT-qPCR (primers in Table S2). WNT4 secretion was determined in conditioned media by Western Blot analysis.

2.8 | Tumour cell migration

The impact of WNT4 secretion on tumour migration was evaluated in two Transwell assay formats using the WNT4^{low} ovarian cancer cell line OVCAR-4 (NIGMS Human Genetic Cell Repository of the NIH), which express the main WNT4 receptor FZD8 and coreceptors LRP5/6. In the first setting, tumour migration was determined in the presence of conditioned medium (CM) from LP9 cells transiently transfected with WNT4_pCDNA3.1 for overexpression of WNT4 as chemoattractant. CM from LP9 cells transfected with empty vector pCDNA3.1 and untransfected LP9 cells were included as controls. Briefly, 50 000 OVCAR-4 cells were seeded in 300 µl serum-free RPMI 1640 medium (Life Technologies, Darmstadt, Germany) per transwell insert (8.0 µm pore size; BD Biosciences). CM from LP9 cells (1:4 diluted in serum-free medium) or 10% FCS as positive control were added as chemoattractant to the lower chamber. The cells were allowed to migrate through the filter for 28 h at 37°C in a 5% CO₂ incubator. Filters were stained with crystal violet (0.2% in 20% methanol, 1:5 dilution) for 10 min and evaluated under a Leica DMI3000B microscope (Leica, Wetzlar, Germany). Migrated cells were counted in >7 visual fields per filter using the ImageJ software. In an alternative approach, OVCAR-4 cells or CellTracker green CMFAD-labelled primary ascites-derived tumour cells (ascTu OC_280, OC_261, see Section 2.10) were pre-incubated with 1:3 diluted CM of LP9 cells transiently overexpressing WNT4 or control CM (see above) for 24 h at 37°C and 5% CO₂ prior to performing transwell migration assays with 10% FCS as chemoattractant as described above.

2.9 | Wound healing assay

Forty thousand OVCAR-4 cells were grown in culture chambers with 4-well silicone inserts (Cat# 80469; IBIDI, Grärfelfing, Germany) for 24 h. After serum starvation in RPMI1680 with 1% FCS for 24 h, cells were treated with conditioned media (1:3 diluted) from transiently transfected LP9 cells (WNT4_pCDNA3.1 or empty vector pCDNA3.1) or from untransfected LP9 cells for additional 24 h. Silicon Inserts were removed and gap closure by cell migration was monitored by microscopy at time points 0, 8 and 24 h and analysed using ImageJ software.

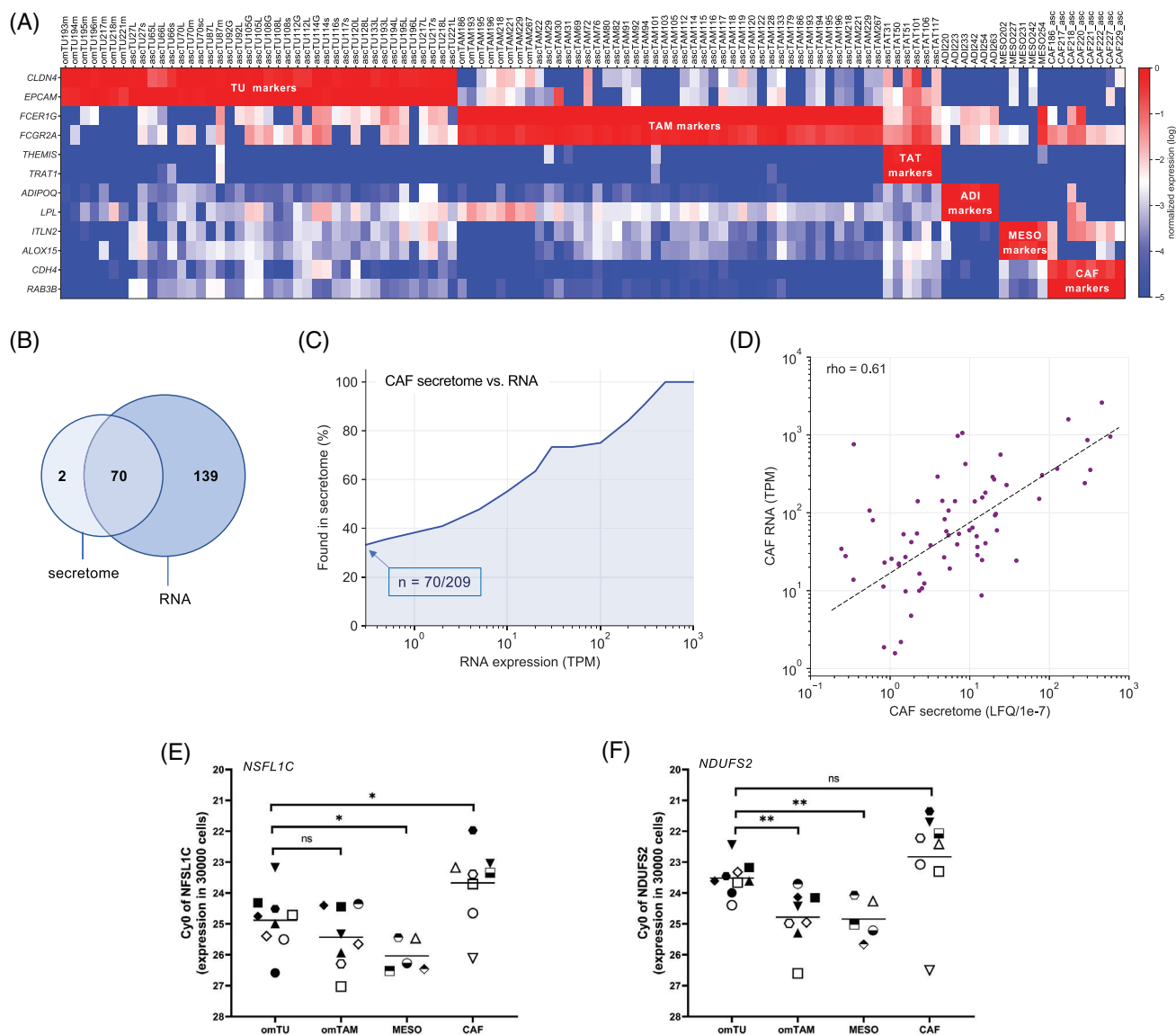


FIGURE 2 Validity of RNA-Seq data. (A) Heatmap depicting relative cell type-specific marker gene expression (TPM) in samples isolated from HGSC ascites and omentum after bioinformatic adjustment for contaminating cells. Samples with $>6\%$ of any contaminating cell type were excluded prior to adjustment. TPM values were gene-wise normalised across all samples (highest expression level = 10^0). Each datapoint represents an independent sample. The corresponding non-adjusted data is shown in Figure S1. See Figure S1 for further details. (B) Venn diagram depicting the number of cytokines and growth factors identified in the CAF secretome and transcriptome (TPM > 0.3). (C) Presence of cytokines and growth factors in the CAF secretome ($n = 5$; determined by MS-based proteomics of CM) in relation to the level of RNA expression (TPM). Details are shown in Table S9. (D) Correlation of signals obtained by RNA-Seq (median TPM) and MS-based proteomics (median LFQ) for all proteins found in the CAF secretome. (E, F) Assessment of cell-type-dependent RNA content. RNA from equal numbers of omTU, omTAM and CAF ($n = 30\,000$ cells) was analysed using primers for *NDUFS2* and *NFSL1C* mRNA without normalisation. *NDUFS2* and *NFSL1C* were chosen due to a very low variance across all samples and cell types. Each symbol indicates an individual patient. If possible, samples of different cell types were matched (i.e. from the same patient). $*p < .05$; $**p < .01$; ns, not significant by unpaired *t*-test

2.10 | Tumour cell attachment to mesothelial cells

Omentum-derived MESO (OC_140; OC_280) were plated in collagen-I-coated ($5\ \mu\text{g}/\text{cm}^2$; Gibco/Thermo Fisher Sci-

entific) 96-well plates (25 000 cells/well) and grown to confluency in OCMI/5% FCS for 3 days at 37°C , 5% CO_2 . The integrity of the MESO layer was evaluated by microscopy (Figure S11C). OVCAR-4 cells or primary ascites-derived tumour cells (ascTu OC_280) were pre-incubated with

1:3 diluted CM of LP9 cells transiently overexpressing WNT4 or control CM (see above) for 24 h. Tumour cells were harvested, labelled with 10 μ M CellTracker green CMFDA (Invitrogen/Thermo Fisher Scientific) for 30 min and washed with OCMI/5%FCS. Five thousand labelled tumour cells were added to MESO monolayers for 1 h (OVCAR4) or 2 h (ascTU), at 37°C. Plates were washed and attached tumour cells were evaluated under a Leica DMI3000B fluorescence microscope (Leica, Wetzlar, Germany). Cells were counted in 9 visual fields per preparation (3 \times 96 wells per preparation were evaluated) using the ImageJ software.

2.11 | Treatment of TAM with rhHSP70

Cryopreserved primary ascTAM derived from different ovarian cancer patients were cultured in ascites (pool of 10 different patients) for 6 days followed by overnight starvation in RPMI1680 medium supplemented with 1 mM sodium pyruvate (Sigma Aldrich). Cells were treated with 1 μ g/ml recombinant human Hsp70 protein (rhHsp70, low endotoxin; Enzo Life Sciences, Lörrach, Germany). A control (Ctrl^{low}) containing 0.005 ng/ml LPS from *E. coli* (Sigma Aldrich) corresponding to the endotoxin level of the rhHSP70 (indicated by the manufacturer) was included. To further address the potential effect of endotoxin contaminations of rhHSP70, TAM were pre-incubated with 10 μ g/ml polymyxin B (PMB, Sigma Aldrich) for 2 h prior to stimulation.

2.12 | IL-6 quantification by ELISA

IL-6 in culture supernatants of ascTAM after stimulation with rhHSP70 in the presence and absence of Polymyxin B (Sigma-Aldrich) was quantified by ELISA (Invitrogen/Thermo Fisher Scientific) according to the manufacturer's instructions.

2.13 | Immunoblotting and quantification

Immunoblots were performed according to standard western blotting protocols using the following antibodies: α -p65 monoclonal antibody (Cell Signaling Technology, Frankfurt, Germany; Cat# 8242, RRID:AB_10859369); α -GAPDH polyclonal antibody (Sigma-Aldrich; Cat# G9545, RRID:AB_796208); α -WNT4 (Clone 55025) monoclonal antibody (R&D Systems; Cat# MAB4751, RRID:AB_2215448); α -Lamin B1 polyclonal antibody (MyBioSource, San Diego, CA; Cat# MBS422963); α -

IKK α /beta (H-470) polyclonal antibody (Santa Cruz Biotechnology, Heidelberg, Germany; Cat# sc-7607, RRID:AB_675667); α -rat IgG horseradish peroxidase (HRP)-linked AB (R&D Systems; Cat# HAF005, RRID:AB_1512258), α -goat IgG HRP-linked polyclonal antibody (Jackson ImmunoResearch Labs/Dianova, Hamburg, Germany; Cat# 705-035-003, RRID:AB_2340390), α -rabbit IgG HRP-linked polyclonal antibody (Cell Signaling Technology; Cat# 7074, RRID:AB_2099233) and α -mouse IgG HRP-linked polyclonal antibody (Cell Signaling Technology; Cat# 7076, RRID:AB_330924). For validation of WNT4 secretion, conditioned media of transiently transfected LP9 cells were concentrated 10-fold using a vacuum concentrator. To determine HSP70-dependent nuclear translocation of p65, subcellular fractionation of stimulated TAM was performed as previously described.³⁸ Imaging and quantification were carried out using the ChemiDoc MP system and Image Lab software version 5 (Bio-Rad, Feldkirchen, Germany). The signals of the phosphorylated forms were normalised against the respective protein signals.

2.14 | RT-qPCR

cDNA isolation and qPCR analyses were performed as described,^{25,39} using *RPL27* for normalisation, except for *NDUFS2* and *NFSLIC* which were analysed without normalisation (Figure 1E and F). Raw data were evaluated by the Cy0 method.⁴⁰ Primer sequences are listed in Table S2.

2.15 | RNA-Seq

RNA-Seq was carried out on an Illumina NextSeq 550 as described.⁴¹ Data were aligned to the human genome retrieve from Ensembl using STAR (version STAR_2.6.1d).⁴² Gene read counts were established as read count within merged exons of protein coding transcripts (for genes with a protein gene product) or within merged exons of all transcripts (for non-coding genes) and normalised to TPM (transcripts per million) or CPM (counts per million) as appropriate for the library type (see below). TPM were calculated based on the total exon read counts and length of merged exons. All genomic sequence and gene annotation data were retrieved from Ensembl release 96, genome assembly hg38.

RNA quality was assessed using the Experion RNA Std-Sens Analysis Kit (Bio-Rad). Only samples with a RNA quality index \geq 8.0 were included in this study. RNA-Seq libraries were constructed using 'Illumina Truseq Stranded total RNA' (Illumina, Berlin, Germany) for ascites cells (previously published datasets E-MTAB-3167,

E-MTAB-4162, E-MTAB-5199, E-MTAB-5498), ‘Illumina Truseq Stranded mRNA’ for ascites and omentum cells (deposited as E-MTAB-10611 at EBI ArrayExpress) and ‘Lexogen Quantseq 3’ mRNA-seq Library Prep Kit FWD for Illumina’ (Lexogen, Vienna, Austria) in combination with the ‘Lexogen UMI Second Strand Synthesis Module for QuantSeq FWD (Illumina, Read 1)’ for CAFs (E-MTAB-10611), according to the manufacturer’s instructions. Quality of sequencing libraries was controlled on a Bioanalyzer 2100 using the Agilent High Sensitivity DNA Kit (Agilent, Waldbronn, Germany). Pooled sequencing libraries were quantified and sequenced on the Illumina NextSeq550 platform with 75 base single reads.

To test the possibility to use these datasets in comparative analyses, we determined the impact of the two Illumina methods on TPM values by direct comparison of datasets obtained for the same samples with both approaches. Apart from all histone-encoding RNAs, we found only few transcripts of annotated coding genes with significant differences among paired samples. These genes were all excluded from further analyses (*CCR2*, *CD28*, *CD84*, *MALAT1*, *PLCG2*, *RMRP*, *TERC*, *WDR74* and *ZNF460* significantly lower or missing in poly(A)-RNA based libraries; *CCNI*, *SI00A14*, *SAA1*, *SAA2-SAA4* and *SNCG* significantly lower or missing in total RNA-based libraries). We also excluded all mitochondrial genes, mitochondrial ribosomal genes, ribosomal (40S/60S) genes and non-protein-coding genes (*MIR*, *LINC*). After exclusion of these genes the data for all samples were renormalised. Comparability of Illumina full-length mRNA data in TPM and Lexogen Quantseq 3’ focused data in CPM was ascertained by quantile–quantile plot.

2.16 | Adjustment of RNA-Seq data for contaminating cells

To adjust RNA-Seq data for contaminating cells we used our previously published approach²⁵ consisting of two consecutive steps: (i) estimation of the extent of contamination and exclusion of highly contaminated samples, and (ii) based on this estimation, adjustment of the remaining RNA-Seq dataset by a linear model. To avoid ‘false-positive’ results for genes highly expressed in a particular cell type we modified the original approach by omitting the previously introduced bias towards an underestimation of contaminations.²⁵ In addition, we assumed a minimal percentage of contaminating cells as detailed further below.

In the first step, we manually identified reference samples, that is samples with the lowest levels of contaminating marker RNAs. For this purpose, we defined cell-

type-specific marker genes by applying the following criteria: (i) high expression of the marker gene in the target cell type (median TPM > 100 for TU, TAM and TAT; TPM > 1000 for ADI and MESO; TPM > 25 for CAF); (ii) maximum 10-fold difference between minimum and maximum expression (median TPM) in any sample of the target cell type; and (iii) a ratio > 10 between the minimum TPM value in the target sample set and the minimum TPM values of all other sample sets. Markers were ranked by the latter parameter and the top two marker genes from different gene families were selected (Table S3). These markers were *EPCAM* and *CLDN4* for TU, *FCER1G* and *FCGR2A* for TAM, *TRAT1* and *THEMIS* for TAT, *LPL* and *ADIPOQ* for ADI, *ITLN1* and *HAS1* for MESO and *RAB3B* and *CDH4* for CAF. Most of these are either well established cell-type-selective markers, such as *EPCAM*, *LPL* and *ADIPOQ*, or have previously been mentioned in the context of the cell-type-specific functions, e.g., *CLDN4*,⁴³ *TRAT1*,⁴⁴ *THEMIS*,⁴⁵ *ITLN1*,^{46,47} *HAS1*^{48–50} and *RAB3B*,⁵¹ while *CDH4* has not been described as a mesenchymal marker to date.

Using these markers, we defined reference samples as indicated in Table S3 and identified the following contaminating cell types to be the most relevant depending on the cell type of interest:

- ascTAM and ascTAT in samples of ascTU,
- ascTU and ascTAT in samples of ascTAM,
- ascTU and ascTAM in samples of ascTAT,
- omTAM, ascTAT, MESO and CAF in samples of omTU (ascTAT were used in place of omTAT which were not available in sufficient quantities),
- omTU, ascTAT and MESO in samples of omTAM,
- omTU, omTAM, MESO (and to lesser extent TAT) in samples of ADI,
- omTU, omTAM, ADI in samples of MESO,
- omTU, omTAM, ADI and MESO in samples of CAF.

To be able to determine the fraction of RNA from contaminating cells more precisely, we identified large marker gene sets composed of genes with (i) >50-fold median fold change between the cell type of interest and the contaminating cell type and (ii) a median expression of >10 TPM in the contaminating cell type. Fold changes were calculated with an offset of 0.001 from 0 to avoid infinite values and enable ranking. Candidate genes were ranked by fold change, and the top 25 were chosen to determine the extent of contamination. This automated procedure selected the marker gene sets listed in Table S4 for all relevant combinations (see preceding paragraph) of cell types of interest and contaminating cell types.

Contamination (%) was then assessed for each marker gene in the respective 25-marker gene set (as defined above) as

$$\frac{(TPM \text{ in target sample}) - (TPM \text{ in target reference sample})}{(TPM \text{ in reference sample of contaminating cell type})} \times 100$$

and the median of the resulting 25 values was considered the percentage of contaminating cells in the sample analysed.

The outcome of this assessment is shown in Table S5 for ascites cells and in Table S6 for cells isolated from omentum. Assumed minimum contaminations (see above) are indicated by '< ...' in both Tables S5 and S6. TU, TAM and TAT samples with $\geq 4\%$ contamination and ADI samples with $\geq 6\%$ contamination with any cell type were excluded from all subsequent analyses. None of the MESO and CAF samples were excluded. This revised set of samples was then subject to adjustment of TPM values using an algorithm based on our previously described linear model²⁵:

$$\frac{(TPM \text{ in target sample}) - (frac \times TPM \text{ in contaminating cell type})}{(1 - frac)}$$

where *frac* is the fraction of the contaminating cell type, and *TPM in contaminating cell type* is the median calculated for the sample set of the contaminating cell type, or, if patient-matched samples were available, the expression in those. Adjustments were performed iteratively for each contaminating cell type. Instances of negative corrected TPM values were set to 0. The complete adjusted and renormalised dataset is shown in Table S7.

2.17 | Functional annotations

Functional annotations were performed by PANTHER gene ontology (GO) enrichment analysis (www.geneontology.org) to reveal associations of gene sets with biological functions. In case of redundancies in the search results only the term with the highest enrichment and significance was included. For gene upregulated in omTU cells the following specific terms were significantly enriched: 'response to lipid' (GO:0033993; fold enrichment = 7.5; FDR = 2e-7), 'regulation of response to stress' (GO:0080134; fold enrichment = 4.2; FDR = 8e-5),

'apoptotic process' (GO:0006915; fold enrichment = 5.3; FDR = 2e-4) and 'regulation of cell differentiation' (GO:0045595; 3.9-fold; FDR = 2e-4). For gene upregulated

in ascTU cells 'mitotic cell cycle process' (GO:1903047; fold enrichment = 5.9; FDR = 4.6e-36) and related terms were the most significant hits by far, followed by 'cellular response to stress' (GO:0033554; fold enrichment = 2.4; FDR = 8.3e-13) on rank 29 and 'regulation of programmed cell death' (GO:0043067; fold enrichment = 2.2; FDR = 1.2e-7) on rank 109. Upstream regulators analyses were performed using the Ingenuity Pathway Analysis (IPA) database.

Lists of previously published compilations of all growth factors/cytokines and their cognate receptors⁵² were updated using the information the GeneCards database (<http://www.genecards.org>) and PubMed (Table S8). Selective ligand–receptor interaction within the EGFR, FGFR,

TGF β , SEMA and WNT families were derived from published studies and reviews.^{53–57} Based on these updated data we redefined groups of growth factor/cytokine receptors and their interacting ligands. A list of 858 proteins associated with ECM reorganisation (Table S9) was assembled by using the Ensembl database and searching for genes with the terms 'extracellular matrix', 'collagen', 'integrin' and 'adhesion' in their name or descriptions, annotated as secreted or membrane proteins in the Human Protein Atlas as previously described⁵⁷ and not overlapping with lists of growth factors, cytokines and their receptors in Table S8.

2.18 | Statistical analysis of experimental data

Comparative data were statistically analysed by paired or unpaired Student's *t*-test (two-sided, unequal variance), as indicated in the figure legends. False discovery rate (FDR) was determined by applying the Benjamini–Hochberg method to nominal *p* values determined by

t-test. Results were expressed as follows: * $p < .05$; ** $p < .01$; *** $p < .001$; **** $p < .0001$. Box plots were constructed using the Seaborn boxplot function with Python.

2.19 | Survival-associated gene expression analysis

Associations between gene expression and relapse-free survival (RFS) of ovarian cancer patients were analysed using the KM Plotter meta-analysis database⁵⁸ retrieved from <http://kmplot.com> (2015 version; serous OC; JetSet best probe), which contains the following 13 datasets: GSE14764 ($n = 80$), GSE15622 ($n = 36$), GSE18520 ($n = 63$), GSE19829 ($n = 28$), GSE23554 ($n = 28$), GSE26193 ($n = 107$), GSE26712 ($n = 195$), GSE27651 ($n = 49$), GSE30161 ($n = 58$), GSE3149 ($n = 116$), GSE51373 ($n = 28$), GSE9891 ($n = 285$) and TCGA ($n = 565$). Associations with overall survival (OS) were derived from the PRECOG database (<https://precog.stanford.edu>).⁵⁹

3 | RESULTS

3.1 | Validity of RNA-Seq data

According to our experience small fractions of contaminating cells are present even in samples with the highest enrichment, which is of particular concern where contaminating cell types have a much higher RNA content per cell, as may be the case, for instance, for tumour cells compared to host cells. Thus, a low percentage of contaminating cells could easily result in a high content of cell-type specific RNA, and thus in ‘false-positive’ results for genes highly expressed in contaminating cells. Besides excluding highly contaminated samples we adjusted the RNA-Seq data for contaminating cells by making use of our previously published method,²⁵ which uses estimated fractions of contaminating cells in linear modeling. To avoid the ‘false positives’ alluded to above, we omitted the previously introduced bias towards an underestimation of contaminations. We also assumed a minimal percentage of contaminating cells, since 100% purity cannot be achieved and minimal contaminations are extremely difficult to determine (see Section 2). By applying this adapted procedure weakly expressed genes are likely missed in cases where expression is orders of magnitude higher in another cell type. However, in view of the goal of the present study, we view such ‘false negatives’ as less concerning than the introduction of ‘false positives’, as low expressors are likely to have a limited impact within the tumour microenvironment in the presence of the high expressors.

Figures 2A and S1 illustrate the results of this approach. In the original dataset (Figure S1A), marker gene expression analysis showed no clear separation between the sample sets, indicating frequent cross-contamination, for example contamination of omTAM and ADI samples with TU, of ADI samples with TAM and MESO and of omTU samples with TAM, MESO and CAF. This problem was completely abolished (relative expression in Figure 2A; TPM values in Figure S2B) by exclusion of heavily contaminated samples (> 6% of any contaminating cell type) and adjustment for contaminating cells as described above. This adjusted dataset was used for all subsequent analyses.

We next addressed the question whether RNA expression of cytokine and growth factor genes is a suitable parameter to predict the secretion of the corresponding proteins. Towards this goal we determined the proteome of conditioned medium (CM) from CAF by mass-spectrometry-based proteomics and compared the number of cytokines and growth factors found in the proteomes with the corresponding RNA-Seq data. We chose CAF for this analysis, because CAF represent the least contaminated cell type. We detected $n = 72$ growth factors in the secretome and $n = 209$ in the transcriptome (TPM > 0.3), with an overlap of $n = 70$ (Figure 2B). The detection of these proteins in the secretome strongly correlated with the strength of RNA expression (Pearson’s $r = .77$; Figure 2C and Table S9), which increased from 33% for weakly expressed genes (0.3 TPM) to 100% for strongly expressed genes (≥ 500 TPM), reflecting the previously reported different sensitivity of both methods.¹⁷ Furthermore, we observed a good correlation (Spearman’s $\rho = .61$) between TPM values obtained by RNA-Seq and LFQ values derived from MS-based proteomics for all proteins in the CAF secretome (Figure 2D). Importantly, the observed clear correlation between RNA expression and the detection of secreted proteins provides strong evidence that RNA-Seq data are a valid source for predicting the synthesis of cytokines and growth factors, and thus for the purpose of the present study.

3.2 | Assessing the impact of cell-type-selective differences in mRNA content

Since tumour cells possibly contain higher amounts of RNA per cell than other cell types, their contribution to the HGSC secretome may be underestimated using normalised RNA-Seq data. To address this issue we took the following approach: First, we identified genes with similar normalised TPM values across all tumour and host

cell samples analysed. Among the genes with the lowest variance were *NDUFS2* and *NFSLIC* with a variability of <2-fold across all samples and cell types. We then prepared RNA from equal numbers of TU and different host cells, and analysed *NDUFS2* and *NFSLIC* mRNA levels in these samples by RT-qPCR without normalisation, so that differences in PCR signals directly reflect differences in mRNA content per cell. As shown in Figure 2E and F, mean Cy0 values for tumour cells were 1.5 higher in omTU compared to omTAM for *NDUFS2* and 0.5–1.0 for *NFSLIC*, indicating a maximally 2-fold (1.0 Cy0) higher signal for omTU. For CAF, an approximately 2-fold higher signal was observed compared to omTU. Figure S3 shows that signals increase linearly to input, thus validating the data shown in Figure 2E and F. Taken together, these findings suggest that differences in mRNA content are ≤ 2 -fold and therefore unlikely to exert a substantial influence on the interpretation of the RNA-Seq data for the purpose of the present study, which focuses on markedly higher cell-type-selective differences in expression (see below).

3.3 | The secretome of tumour and tumour-associated host cells in HGSC

As the first step to decipher the signalling network of the TME of HGSC we determined which cytokine and growth factor genes are expressed by tumour cells and the most prominent host cell types in ascites and omentum. In total, we found $n = 284$ expressed cytokine and growth factor genes (TPM > 2). Unexpectedly, the majority of these genes ($n = 176$) were selectively (FC > 5) expressed in host cells (tumour-associated immune cells and stromal cells of the omentum), whereas $n = 13$ genes were tumour-cell-selective and $n = 95$ genes were expressed in tumour and host cells with a less than 5-fold difference (Figure 3A). Among host cells, omental stromal cells expressed a greater number of cytokine and growth factor genes than immune cells ($n = 99$ vs. $n = 44$; FC > 5; Figure 3B). Among stromal cells, ADI, MESO and CAF expressed similar numbers of genes in a cell-type-selective fashion ($n = 16$, $n = 19$ and $n = 14$, respectively), but also common sets of genes (e.g., $n = 13$ genes in all three cell types; $n = 26$ genes shared by MESO and CAF; Figure 3C). Figures 3D and S4 illustrate the expression patterns of compartment- or cell-type-selective genes in cell types of the omental TME based on the values in Table S10. These observations suggest that stromal cells of the omentum make a major contribution to the HGSC TME, in particular in view of the large number of ADI and MESO in the omentum or peritoneum.

3.4 | Association of stroma-selective cytokine and growth factor genes with patient survival

To assess the potential clinical relevance of the stroma-selective cytokine and growth factor genes identified above we analysed their association with the relapse-free survival (RFS) and the overall survival (OS) of ovarian cancer patients by interrogating two meta-analysis-based databases, the Kaplan-Meier-Plotter (KMP) database⁵⁸ for RFS and the PRECOG database⁵⁹ for OS. As shown in Table 1, 32 stroma-selective genes showed a significant association with both RFS and OS [$|z$ -score| > 1.96]. Intriguingly, 31 of these genes were associated with a short RFS and OS. Only *BDNF* showed a significant association with a longer survival (HR < 1, z -score \leftarrow 1.96). This result clearly points to a strong tumour-promoting role for cytokines and growth factors produced by the stromal compartment of the omentum.

3.5 | Target cells of the HGSC secretome

We next sought to define the targets of cell-type-selective ligands of the omental TME. As many ligands bind to more than one receptor, the signalling network of the HGSC TME is extremely complex (Figure S5). To visualise the network for the ligands identified in Figure 3D in a comprehensible way we reduced its complexity by determining a normalised value for each ligand reflecting the relative expression of all receptor genes among different cell types (see legend to Figure 4 for details; complete dataset in Table S11). The heat maps (Figure 4) constructed from this dataset illustrate that many of these cell-type-selective ligands also display considerable target cell type selectivity

3.6 | The metastasis-associated signalling network of HGSC

Next, we directed our attention to intercellular signalling pathways targeting tumour cells and potentially linked to the metastatic spread of HGSC. To this end, we first retrieved all cytokine and growth factor genes previously mentioned in the literature in the context of both metastasis and ovarian cancer from the genecards.org database. Next, we identified a subset ($n = 200$) of these genes expressed in at least one cell type of the HGSC TME. For $n = 122$ of these genes cognate receptors were expressed by omTU cells (TPM > 2; Table S12). This dataset was used to construct the signalling map in Figure 5, ordered

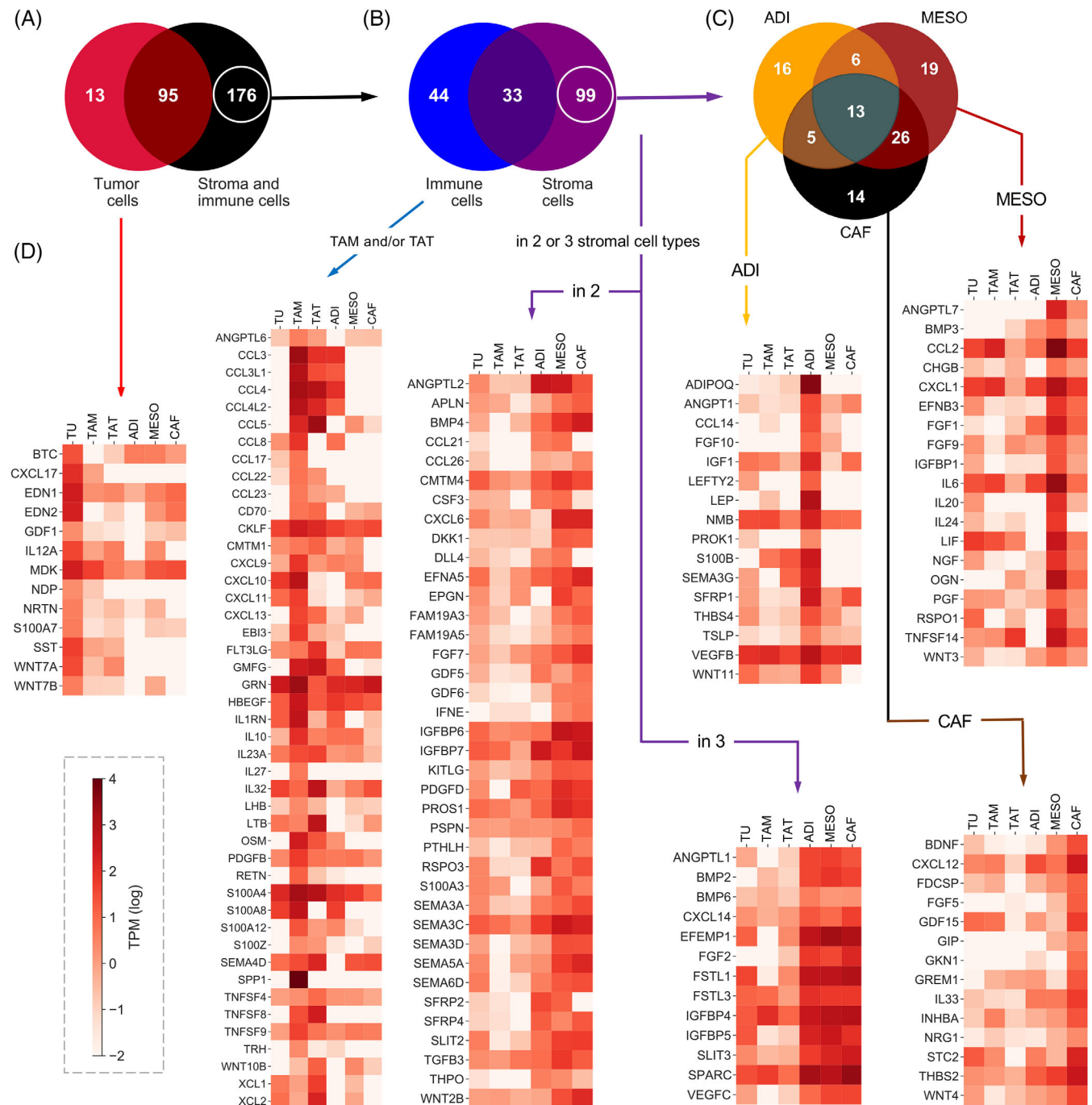


FIGURE 3 Expression of cytokine and growth factor genes in the omental TME. (A) Venn diagram showing the number of cytokine and growth factor genes expressed selectively in TU, selectively in stroma and immune cells or in all cell types ($FC > 5$). (B) Genes expressed selectively in stroma cells, selectively in immune cells or in both. (C) Genes expressed selectively in ADI, MESO, CAF or in combinations of these. (D) Expression patterns of compartment- or cell-type-selective genes in 6 different cell types of the omental TME. Expression levels are categorised (see bottom right) based on the values in Table S10

by ligands synthesised by single cell types or by groups of 2, 3, 4 or all 5 cell types. Notably, a substantial number of these gene is associated with a short survival, including *ADIPOQ*, *BMP2*, *CXCL12*, *EFEMP1*, *EFNA5*, *FGF1*, *FST*, *FSTL1*, *GREM1*, *IGF1*, *IGFBP5*, *IGFBP6*, *INHBA*, *SEMA3C*,

SFRP1, *SFRP4*, *SLIT3*, *TGFB3* and *VEGFC* (Table 1). The data clearly underscore the prominent role of the tumour-associated host cells, and in particular of omental stromal cells, in establishing a pro-metastatic cytokine- and growth-factor-driven signalling network in HGSC.

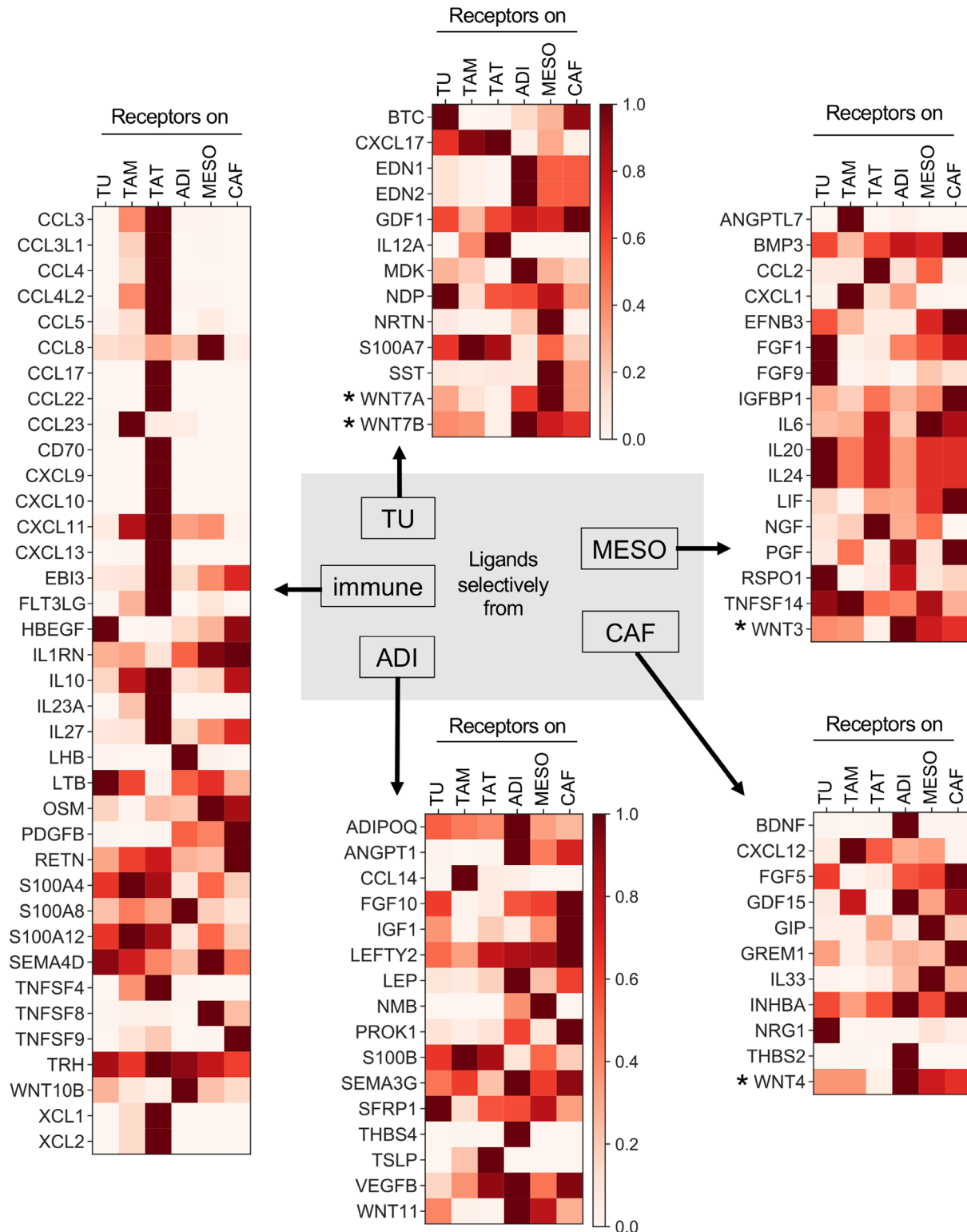


FIGURE 4 Targets of cell-type-selective ligands of the omental TME. The figure illustrates the expression of genes encoding receptors for the cell-type-selective ligands identified in Figure 2D. To take into account that numerous ligands bind to more than one receptor, we designed an algorithm that yields a normalised value for each ligand reflecting the relative expression of all receptor genes among different cell types. This was achieved by the following three consecutive steps: (i) TPM values were gene-wise normalised for each cell type, (ii) normalised TPM values for all receptors of a given ligand were added up and (iii) the resulting values were normalised to cell type (scale bar top center; Table S11). *Wnt ligands and receptors constitute a highly complex relationship which obscure a simplified representation of the data. Therefore, data shown for WNTs are presumably skewed and should be treated with caution. Some of the genes in Figure 4 do not appear in this figure because their expression falls below the cut-off of 2 TPM (e.g., *SPP1* from TAM)

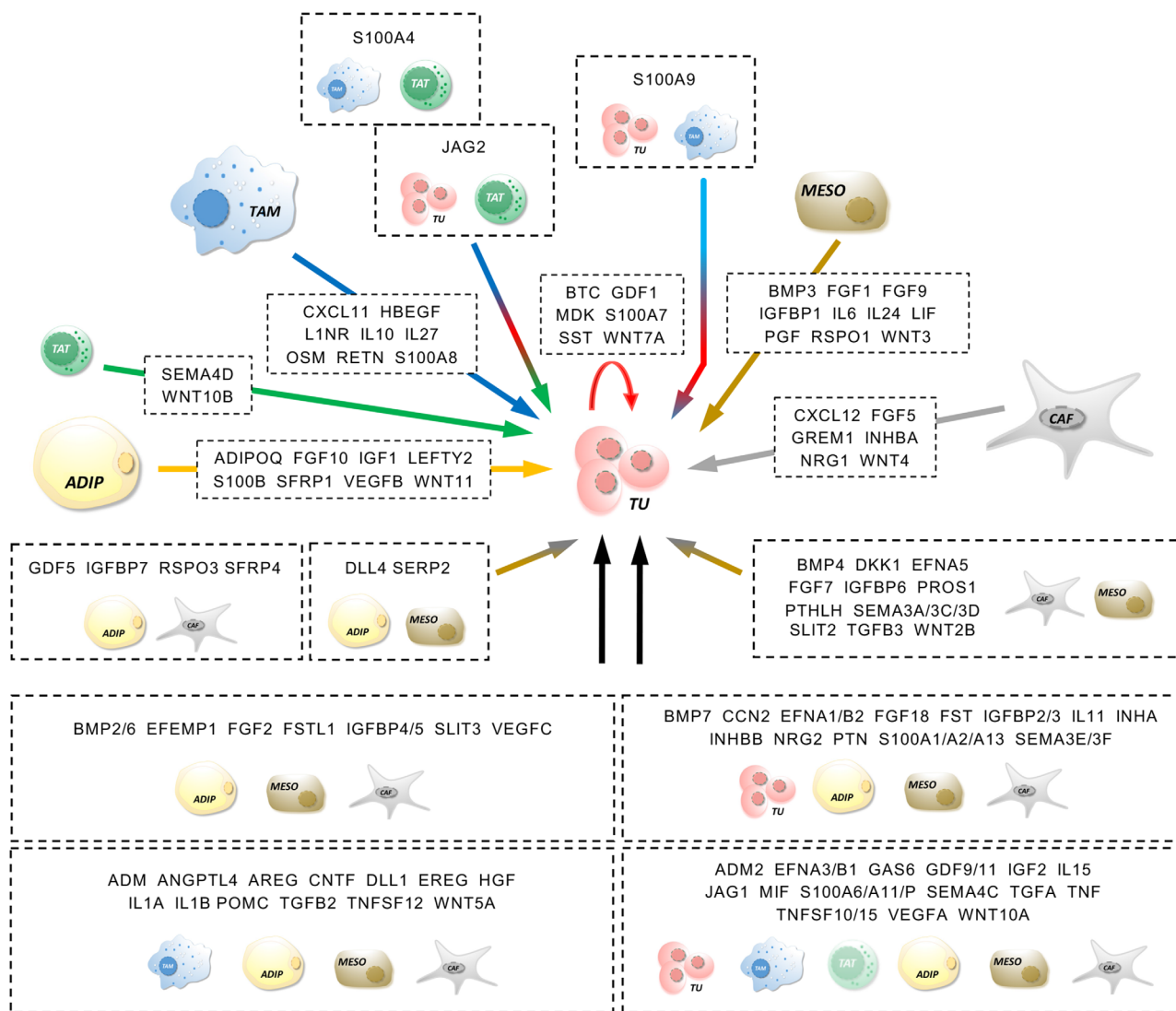


FIGURE 5 Schematic illustration of intercellular signalling pathways associated with metastasis and impinging on tumour cells. The figure incorporates all selectively expressed cytokines and growth factors previously linked to metastasis and ovarian cancer with receptors on omTU cells (TPM > 2; cell-type-selectivity threshold 5-fold; as in Figures 2 and 3; Table S12)

3.7 | WNT4-mediated cross-talk in the omental TME

We chose WNT4 as an example to study the function of a highly cell-type-selective ligand in the cellular crosstalk within the HGSC TME. WNT4 is expressed at >10-fold higher levels in CAF compared to all other cell types (see black arrow in Figure 6A). The main receptor for WNT4 is FZD8, which form trimeric ligand–receptor complexes with the coreceptors LRP5 or LRP6 to initiate signal transduction.⁶⁰ The expression pattern of these receptors (red arrows in Figure 6A) suggests that tumour cells are a prime target of WNT4, which could play a role in metastasis-associated signal transduction pathways and biological processes.

This hypothesis was confirmed by the data in Figure 6B (representative microscopic pictures in Figure S8), which shows a reduced migration-inducing potential of CM from CAF after transfection with a siRNA against WNT4 compared to control siRNA (siRNA Figure S6). To obtain direct evidence for the migration-promoting function of WNT4, we established a WNT4 overexpression model by transiently transfecting the WNT4^{low} human MESO line LP9 with a WNT4 expression vector or empty pCDNA3.1 as control. As shown in Figure S7, WNT4 expression and secretion were significantly increased 48 h after transfection in WNT4-transfected cells compared to both pCDNA3.1 and non-transfected LP9 cells. Using conditioned media (CM) from these cells, we investigated the impact of WNT4 on tumour cell motility and migration as well as tumour cell adhesion to the mesothelial layer.

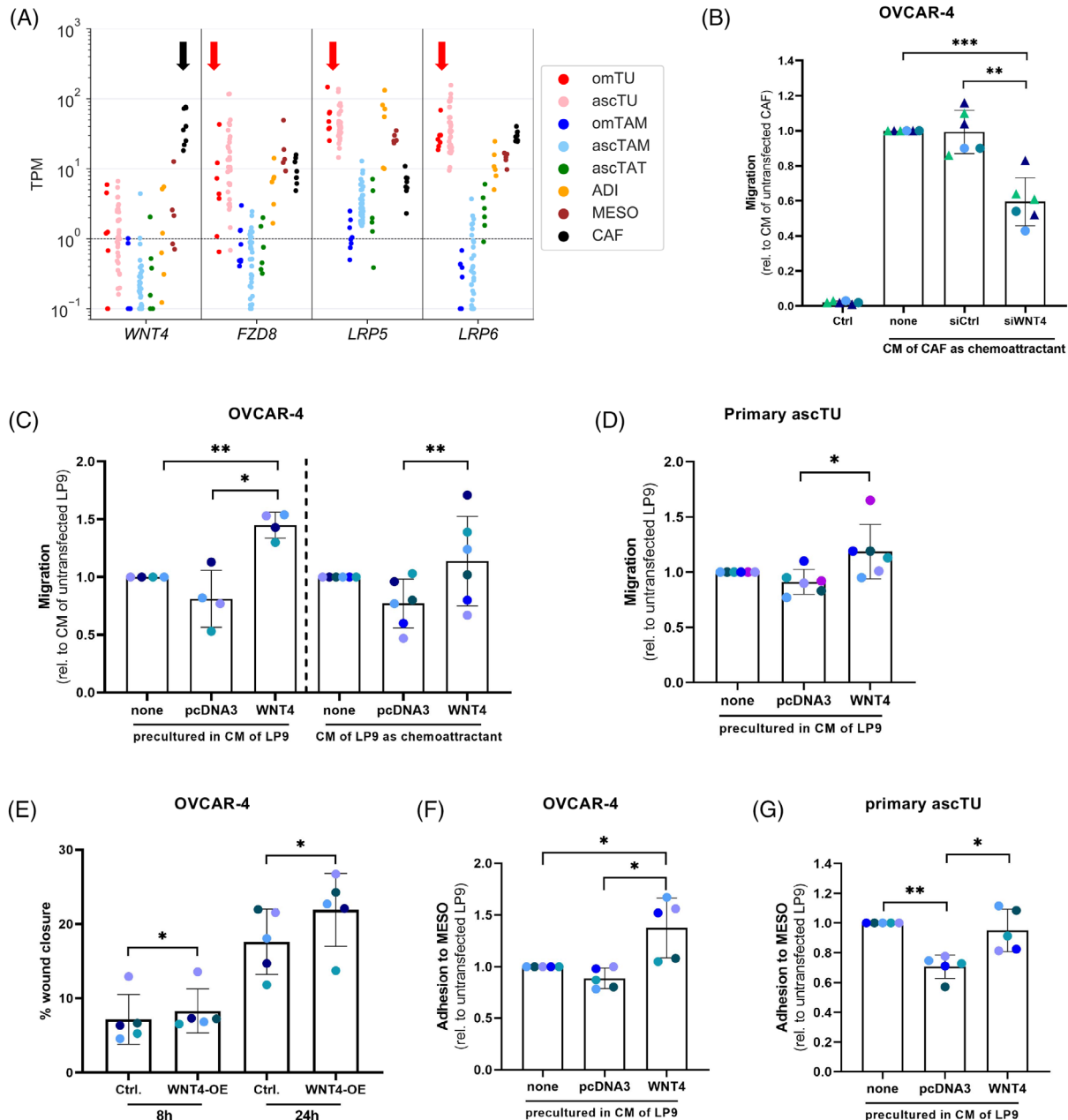


FIGURE 6 WNT4 signalling pathway and function. (A) Expression of the genes coding for WNT4, the major WNT4 receptor FZD8 and the FZD8 coreceptors LRP5 and LRP6 in different cell types from HGSC ascites and omentum. The same samples as in Figure 1A were analysed. The arrows indicate the selective expression of WNT4 in CAF and the main WNT4 receptors in tumour cells. (B) Promotion of tumour cell (OVCAR4) migration by CM from CAF and inhibition by siRNA-mediated interference with WNT4 expression by CAF. Ctrl: no conditioned medium. CM was harvested from cultured CAF isolated from four different patients used as chemoattractant for OVCAR4 cells. CAF CM of two patients (blue and green triangles) were tested in two independent experiments. (C) Migration of OVCAR4 cells in response to secreted WNT4 tested in two Transwell formats. CM from WNT4-overexpressing, control-transfected (pcDNA3) or untransfected LP9 cells were either used as chemoattractant ($n = 6$) or for pre-incubation of OVCAR4 cells prior to migration towards 10% FCS as the chemoattractant ($n = 4$). Migration was calculated relative to CM from untransfected LP9 cells. (D) Migration of primary ascites-derived HGSC cells (ascTU) pre-incubated with CM from WNT4-overexpressing, from control-transfected (pcDNA3) and from untransfected LP9 cells, respectively ($n = 6$). (E) Wound healing capacity of OVCAR4 cells after incubation with CM from WNT4-overexpressing and control-transfected (pcDNA3) LP9 cells for 8 or 24 h ($n = 5$). Results are expressed as percentage of wound closure. Adhesion of OVCAR4 cells (F) and primary ascTU cells (G) to a confluent monolayer of peritoneal mesothelial cells (MESO). Tumour cells were pre-incubated with CM from WNT4-overexpressing, from control-transfected (pcDNA3) and from untransfected LP9 cells, respectively, and labelled with CellTracker Green. Adhesion of tumour cells to the MESO layer was evaluated in comparison to CM from untransfected LP9 cells after 1 hr of coculture (OVCAR4 $n = 5$) or 2 h of coculture (ascTU $n = 5$). Columns in panels B-G represent the mean. Standard deviations are shown as error bars. Asterisks indicate p values determined by two-sided, paired t -test. * $p < .05$, ** $p < .01$, *** $p < .001$. Representative images are shown in Figures S8–S11

TABLE 1 Association of stroma-selective cytokine and growth factor gene expression with RFS (KMP data base, p -value and hazard ratio) and OS (PRECOG data; z -score)

Gene	KMP (RFS) p -value	KMP (RFS) HR	PRECOG (OS) z -score	Cell type
<i>PDGFD</i>	.000002	1.55	5.53	MESO, CAF
<i>FSTL1</i>	.036424	1.20	5.09	ADI, MESO, CAF
<i>IGFBP6</i>	.014975	1.25	4.91	MESO, CAF
<i>THBS2</i>	.000001	1.57	4.59	CAF
<i>FGF1</i>	.000002	1.51	4.43	MESO
<i>WNT11</i>	.010436	1.25	4.42	ADI
<i>CXCL12</i>	.000010	1.51	4.39	ADI, CAF
<i>ANGPTL2</i>	.001481	1.32	4.36	ADI, MESO
<i>CXCL14</i>	.000903	1.36	4.29	ADI, MESO, CAF
<i>SPARC</i>	.000069	1.45	4.19	ADI, MESO, CAF
<i>SEMA3C</i>	.001502	1.31	3.91	ADI, MESO, CAF
<i>SFRP4</i>	.020009	1.25	3.90	ADI, MESO, CAF
<i>FSTL3</i>	.001730	1.32	3.75	ADI, MESO, CAF
<i>FST</i>	.000115	1.41	3.67	ADI, MESO, CAF
<i>ADIPOQ</i>	.000028	1.43	3.62	ADI
<i>THBS1</i>	.000169	1.41	3.57	ADI, MESO
<i>VEGFC</i>	.011139	1.26	3.56	ADI, MESO, CAF
<i>ANGPT1</i>	.001125	1.36	3.28	ADI
<i>SLIT3</i>	.000265	1.41	3.23	ADI, MESO, CAF
<i>IGF1</i>	.000002	1.51	3.18	ADI
<i>EFEMP1</i>	.009509	1.27	3.07	ADI, MESO, CAF
<i>GREM1</i>	.000165	1.38	3.05	ADI, CAF
<i>BMP2</i>	.007972	1.27	3.03	ADI, MESO, CAF
<i>SEMA5A</i>	.002967	1.29	2.96	MESO, CAF
<i>OGN</i>	.004469	1.30	2.80	MESO
<i>INHBA</i>	.000117	1.43	2.54	CAF
<i>IGFBP5</i>	.020092	1.22	2.42	ADI, MESO, CAF
<i>TGFB3</i>	.002885	1.32	2.36	ADI, MESO, CAF
<i>EFNB3</i>	.049981	1.20	2.32	MESO
<i>EFNA5</i>	.010729	1.28	2.21	ADI, MESO, CAF
<i>SFRP1</i>	.021237	1.26	2.03	ADI
<i>BDNF</i>	.004150	0.75	-3.02	CAF

A positive z -score indicates a hazard ratio > 1 , a negative z -score a hazard ratio < 1 ; $|z| = 1.96$ corresponds to $p = .05$. The right-most column indicated the main expressor cell type(s) among omental stromal cells based on the data in Figure 3. The Table shows only significant instances ($p < .05$ and $|z| > 1.96$)

For these assays we used the HGSC cells line OVCAR-4, which strongly expresses the WNT4 receptor FZD8 and coreceptors LRP5/6, but low levels of the WNT4 ligand. The data in Figure 6C (representative microscopic pictures in Figure S9) show that CM from WNT4-overexpressing cells significantly enhanced the migration of OVCAR-4 compared to CM from pCDNA3.1 control cells. This effect

of WNT4-CM was observed in two different experimental setups, that is when used as chemoattractant or for pre-incubation of OVCAR-4 cells to stimulate subsequent migration towards FCS. In line with these observations, CM of WNT4-overexpressing cells increased the motility of OVCAR4 cells leading to faster gap closure in a wound healing assay (Figures 6E and S10).

As the attachment of tumour cells to a mesothelial cell layer is thought to represent an important step for transmesothelial migration and subsequent metastasis formation, we investigated whether WNT4 may play a role in this context. As demonstrated by the data in Figures 6F and S11, pre-treatment of OVCAR4 cells with WNT4 enhanced their attachment to a mesothelial cell layer. Due to the limited biological significance of results obtained with established cell lines, we additionally tested the effects of WNT4 on primary HGSC tumour cells directly obtained from ascites, which confirmed our findings with OVCAR4 cells, as CM from WNT4-overexpressing cells induced stronger tumour cell migration (Figures 6D and S9B) and adhesion to mesothelial cells (Figures 6G and S11B) compared to CM from control transfected cells. These data are consistent with a pro-metastatic function of WNT4 in HGSC via a direct communication between CAF and tumour cells.

3.8 | A major contribution by omental stroma cells to ECM-associated signalling and reorganisation

The ECM plays a pivotal role in biological and molecular events linked to HGSC metastasis, such as cancer cell adhesion, migration and ECM-mediated signalling. We therefore analysed the expression of ECM-associated genes. For this purpose, we compiled a gene list from the Ensembl and Human protein Atlas databases (see Section 2 for details) and analysed the expression of these genes in our RNA-Seq dataset (Table S13). The data for genes of particular relevance with respect to metastasis, that is ECM components, ECM-remodeling proteins, cell adhesion molecules (CAMs) and integrins as ECM signal transducers, is summarised in Figure 7A (TPM > 2). It is obvious that omental stroma cells are the main producers of most collagens and, together with tumour cells, other ECM components (fibronectin, laminins, vitronectin). A different pattern was observed for ECM-associated proteases and protease inhibitors, which are expressed by all cell types except TAT, but with clear gene-selective patterns. For example, matrix metalloprotease genes, except for *MMP7*, are expressed at higher levels by TAM and stromal cells, with a high selectivity in case of *MMP9* and *MMP24* for TAM and CAF, respectively. Similarly, several protease inhibitors are expressed by most cell types

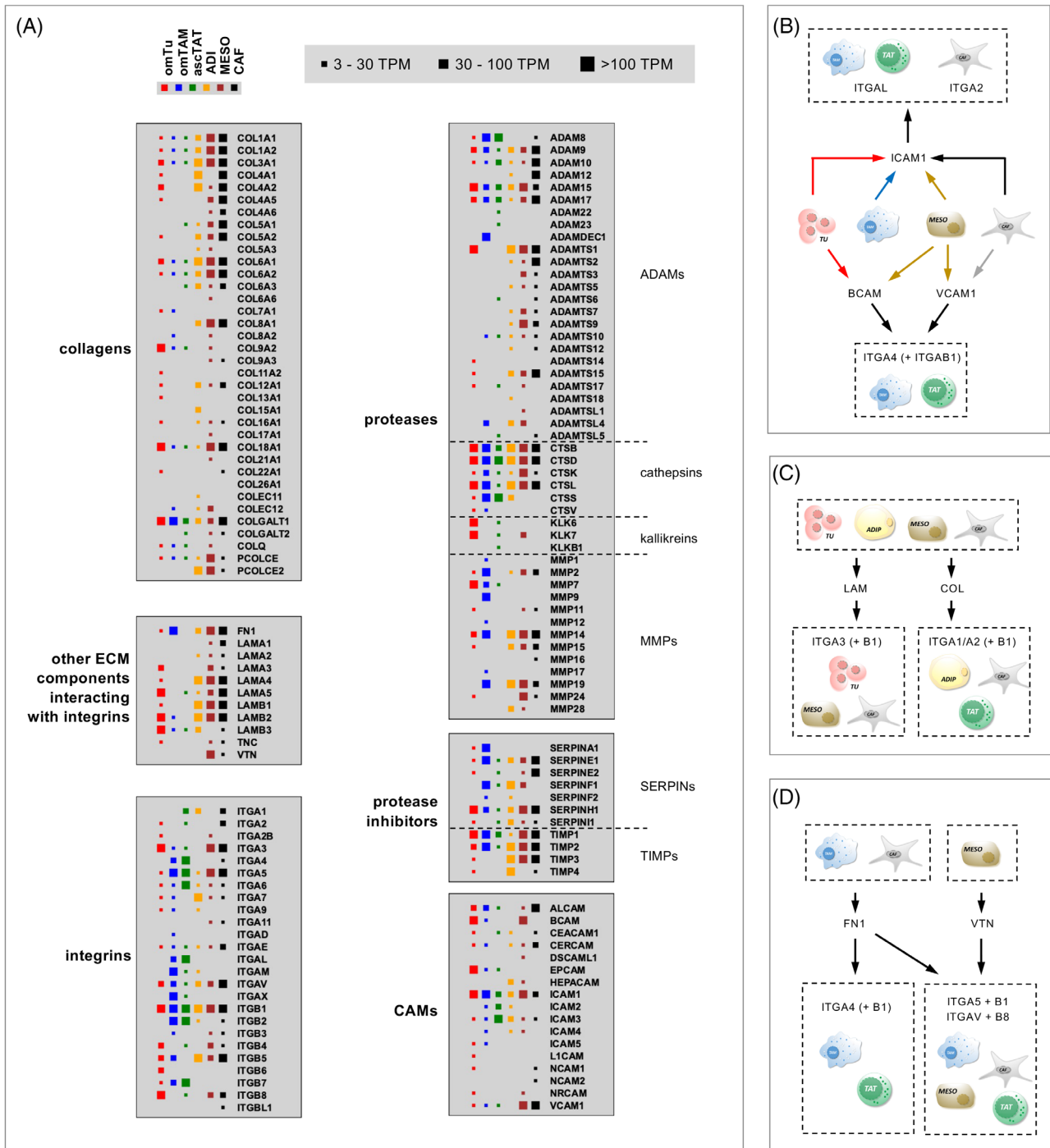


FIGURE 7 Expression of genes involved in ECM-associated signalling and reorganisation. (A) RNA expression patterns in 6 different cells types categorised as indicated at the top. The figure is based on the values in Table S13. CAMs: cell adhesion molecules. (B–D) Schematic representation of major cell-type-dependent integrin-mediated signalling pathways in the omental TME (examples) based on the data in panel A and published integrin-ligand interactions.^{99,100} The scheme depicts the cell types showing the highest expression of the respective gene or group of genes

(except TAT), such as SERPINH1 and TIMP1/2, while other are selective for TAM (*SERPINA1*), CAF (*SERPINE2*), ADI (*TIMP4*) or all stromal cells (*TIMP3*).

As expected, integrins interacting with ECM components are expressed in a cell-type-selective fashion, such as

ITGA4, *ITGAL* and *ITGB7* by immune cells, while tumour and stromal cells strongly expressed *ITGA3*, *ITGAV* and *ITGB1/4/5/6/8*. Major signalling pathways regulated by the interaction of integrins with ECM proteins or cell adhesion molecules are depicted in Figure 7B for BCAM and VCAM1

impinging mainly on TAM and TAT, for laminins interacting with tumour cells, ADI and MESO in (Figure 7C; left panel), for collagens with receptors on ADI, MESO and TAT (Figure 7C; right panel), or fibronectin interacting with TAM and TAT (Figure 7D; left panel), and for vitronectin preferentially signalling to immune cells, ADI and CAF (Figure 7D, right panel). Taken together, these observations point to an essential role of omental TAM and stromal cells in ECM-mediated signalling pathways in the HGSC microenvironment.

3.9 | Comparative analysis of tumour cells from ascites and omentum

The differential contribution by tumour cell spheroids and by tumour cells in solid metastatic lesions to the signalling network of the TME has not been analysed to date. We therefore performed a systematic transcriptomic comparison of matched omTU and ascTU samples from 6 patients. As shown in Figure S12, the two sample sets showed a remarkably high correlation of $\rho = .98$, confirming that ascTU cells are an excellent source to obtain large numbers of tumour cells to study HGSC biology. Further analyses identified $n = 121$ significantly regulated genes (FC > 3; TPM > 3; nominal p value < .05 by paired t -test), $n = 83$ genes with a higher expression in omTU versus ascTU samples and $n = 38$ genes with a lower expression in omTU (Figure 8A; Table S14).

Gene ontology (GO) term enrichment analysis of genes upregulated in omTU cells identified ‘regulation of cell differentiation’ as significantly enriched. In agreement with this finding, we found 52 out of the 60 genes upregulated in omTU cells to be associated with ‘epithelial differentiation’ in the genecards.org database (Figure S13). Examples of epithelial genes consistently upregulated in all six samples include CLDN4, GJA1 and GJB1 (components of epithelial cell junctions), ERBB4 and ERFF1 (EGF signalling), KRT16 (epithelial keratin) and the epithelial transcription factors KLF9 and KLF10. These observations point to enhanced epithelial-like traits of omTU compared to ascTU cells. No significant enrichment of GO terms was observed with genes downregulated in omTU samples. Therefore, these genes were not further analysed.

Ingenuity pathway (IPA) upstream regulator analysis identified pro-inflammatory (IRAK4, IL1) and MAPK-associated pathways as significantly enriched in the set of genes upregulated in omTU cells (Figure 8B). Consistent with this result, we found 31 of the genes upregulated in omTU cells to be associated with the term ‘pro-inflammatory’ in the genecards.org database. Remarkably all 31 genes were also present in the set of epithelial-

differentiation-linked genes (marked by dots in Figure S13), pointing to a potential connection between pro-inflammatory signalling and differentiation. Since the growth of metastases from spheroids is believed to involve transitions between epithelial and mesenchymal cancer cells phenotypes, these results could be of particular interest.

The genes upregulated in omTU cells comprised only two cytokines/growth factors (CXCL2, EDNI) and two cytokine/growth factor receptors (ERBB4, IL1RA), indicating a modest effect of different environment settings (omentum, ascites) on the contribution of TU to the signalling network of the TME (Figure 8C). Intriguingly, the upregulated ligand-encoding genes also comprised the HSP70 family members HSPA1A, HSPA1B and HSPA1L (Figure 8C), which upon their release from cells are able to act as extracellular signalling molecule.⁶¹ HSP70 proteins are of particular interest in view of the highly significant association of a short RFS with high HSPA1A levels in HGSC ascites.² In agreement with the RNA-Seq data, the secretome of tumour cells from 7 different patients contained high levels of HSPA1A after culturing in 50% ascites for 24 h, with MS signals ranking among the top 10 cytokines (Figure 8D; Table S16).

3.10 | Comparative analysis of TAM from ascites and omentum

We also compared the transcriptome of matched omTAM and ascTAM. Figure S14 shows a similarly high correlation ($\rho = .95$) as observed with tumour cells, but a larger number of differentially expressed genes ($n = 674$; TPM > 3; nominal p value < .05 by paired t -test; Table S15). Of these, $n = 516$ genes were upregulated (FC > 3) in omTAM, and $n = 158$ were downregulated in omTAM (Figure 9A).

GO term enrichment analysis of genes upregulated in omTAM cells identified ‘mitotic cell cycle process’ and >50 other terms related to the cell cycle as highly enriched and significant. Figure 9A (examples) and Figure S15 (complete set) illustrate a consistent upregulation of all these genes in five out of six patient-matched omTAM versus ascTAM samples, including numerous CDKs, cyclins, E2F and its target genes and components of the mitotic spindle checkpoint. This finding clearly suggests that enhanced proliferation is a common feature of omTAM. This conclusion was confirmed by subsequent flow-cytometric analysis of independent matched samples of omTAM and ascTAM, which revealed a clear increase in the fraction of KI67-positive cells in five out of five omTAM samples analysed (Figure 9C). The main growth factor acting on macrophages is CSF1, which is strongly expressed in omental stroma cells, in particular in ADI and MESO (Figure 9D). In view of

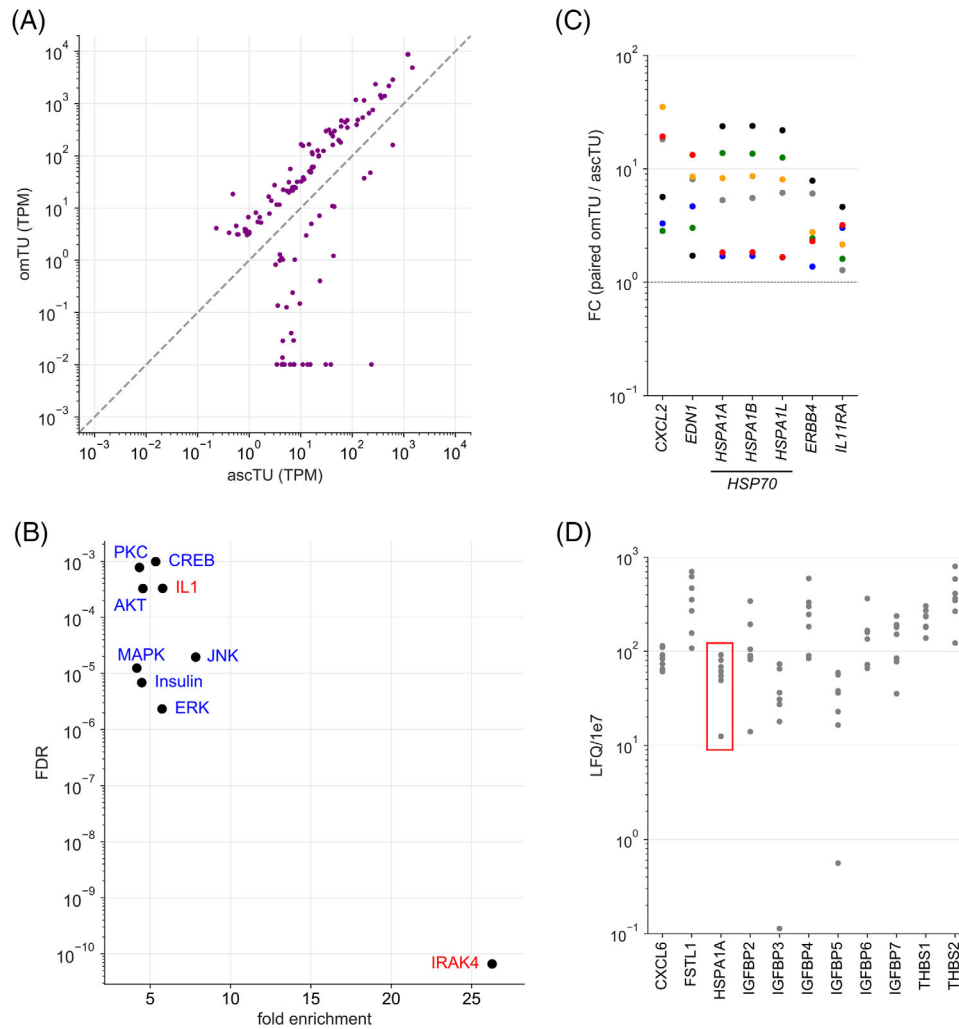


FIGURE 8 Signalling pathways of omTU compared to ascTU cells. (A) Expression of differentially expressed genes in omTU versus ascTU (FC > 3 and TPM > 3 in either cell type; nominal $p < .05$; Table S14). (B) IPA upstream regulator analysis of genes upregulated in omTU cells ($n = 60$; data points above diagonal in panel A). The plot shows the pathways with the highest significance (FDR < 0.001) and enrichment (>4-fold) and a minimum number of enriched genes ($n \geq 6$). (C) Regulation of genes coding for protein ligands in matched samples of omTU and ascTU cells (FC = TPM in omTU/TPM in ascTU). (D) MS-based proteome analysis of conditioned medium obtained after a 16-h culture of ascTU from 7 different patients. The plot shows HSPA1A (data points framed in red) and the 10 cytokines with the highest LFIQ values

their abundance in the omentum it is very likely that these cell types are responsible for inducing the proliferation of omTAM via the secretion of CSF1.

In agreement with these observations, IPA upstream regulator analysis identified pathways directly associated with cell cycle progression (CDK4, CDKN1A, E2F) as well as their upstream signalling pathways (RAS, MAPK) as highly enriched in omTAM cells (Figure 9E). Significant enrichment was also observed for pro-inflammatory pathways (IRAK4, GM-CSF; Figure 9E) similar to omTU (Figure 8B), suggesting that the omental TME represents an inflammation-promoting environment, which would be consistent with the presence of many pro-inflammatory mediators (Figure 3).

In contrast to tumour cells (see above), omTAM expressed numerous genes encoding cytokines or growth factors ($n = 18$), HSP70 family members ($n = 3$), cytokine/growth factor receptors ($n = 8$) and ECM-associated proteins ($n = 13$) at significantly higher levels as their counterparts in ascites (Figure 9F), providing further evidence for a major contribution of TAM to the omental TME. These include several genes coding for pro-inflammatory cytokines (e.g., *CCL2*, *CCL17*, *CCL22*, *IL1A*, *LIF*, *OSM*), and similar to omTU the HSP70 family genes *HSPA1A*, *HSPA1B* and *HSPAIL*.

Enrichment of GO terms was low or insignificant for genes downregulated in omTU samples. This gene set was therefore not subject to further analyses.

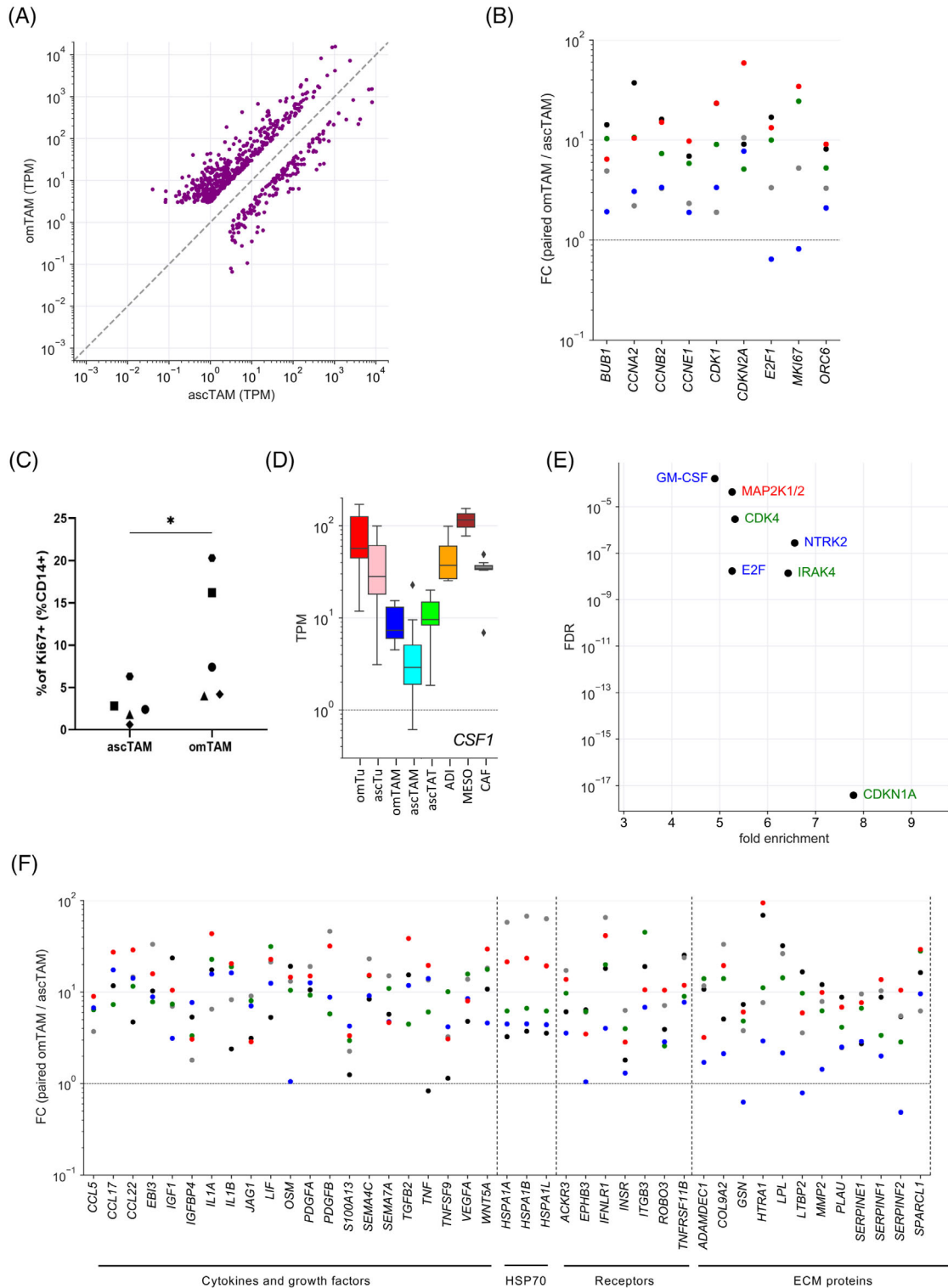


FIGURE 9 Signalling pathways of omTAM compared to ascTAM. (A) Expression of differentially expressed genes in omTAM versus ascTAM (FC > 3 and TPM > 3 in either cell type; nominal $p < .05$; Table S15). (B) Regulation of cell cycle genes in matched samples of omTU and ascTU cells (FC = TPM in omTU/TPM in ascTU). (C) Flow-cytometric analysis of KI67 expression in matched omTAM and ascTAM samples from 5 HGSC patients (* $p < .05$; paired t -test). (D) Expression of *CSF1* mRNA in different cell types from HGSC ascites and omentum. Boxplots show medians (horizontal line in boxes), upper and lower quartiles (boxes), range (whiskers) and outliers (diamonds). (E) IPA upstream regulator analysis of genes upregulated in omTAM ($n = 456$; data points above diagonal in panel A). The plot shows the pathways with the highest significance (FDR < 0.001) and enrichment (>4-fold) and a minimum number of enriched genes ($n \geq 6$). (F) Upregulation of genes coding for cytokines or growth factors, HSP70 family members, cytokine/growth factor receptors and ECM proteins in omTAM versus ascTAM (matched samples as in panel B)

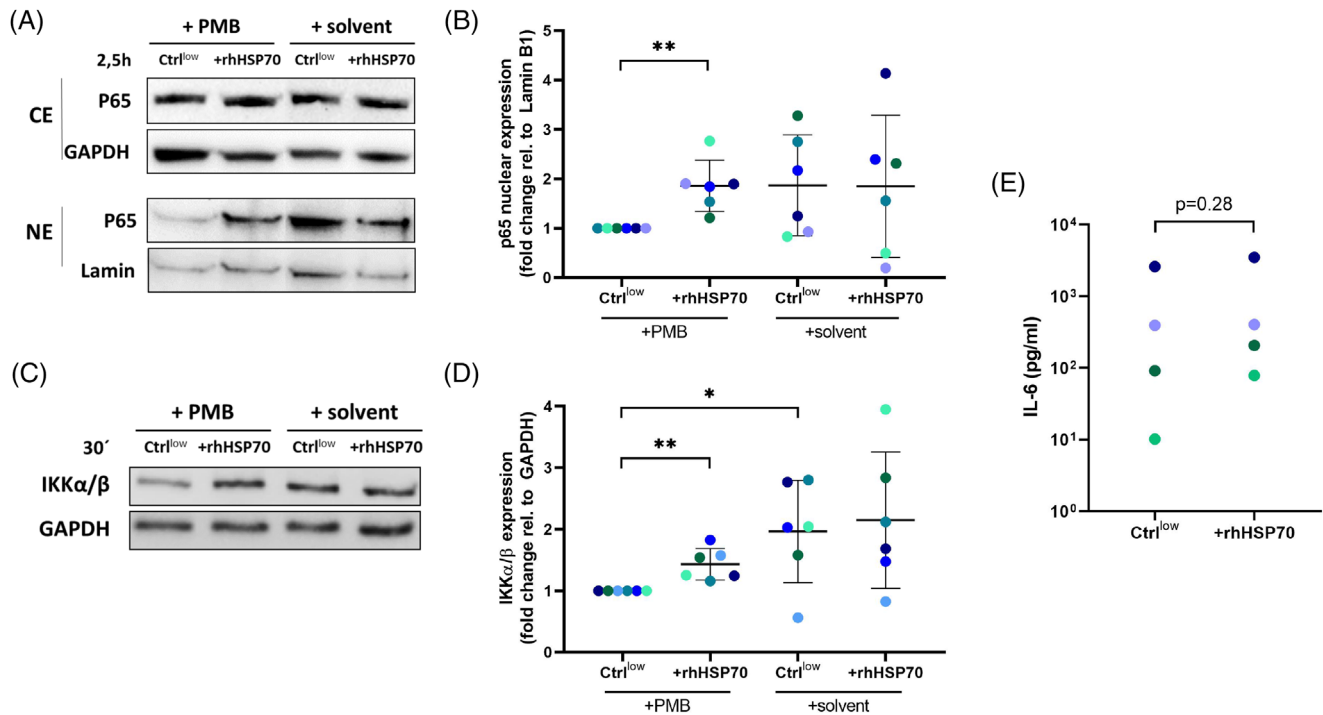


FIGURE 10 HSP70-driven signalling in TAM. (A) Representative immunoblots showing induction of nuclear translocation of p65 by rhHSP70. NE: nuclear extracts; CE: cytosolic extracts. ascTAM were pre-incubated for 2 h with 10 μ g/ml polymyxin B (PMB) before 1 μ g/ml low-endotoxin rhHSP70 was added for 2.5 h. The control (Ctrl^{low}) was spiked with the amount of LPS present in rhHSP70 as contaminant. (B) Quantification of nuclear translocation of p65 (relative to GAPDH, $n = 6$). (C) Representative immunoblot of whole cell lysates showing induction of IKK α/β (panel A) by rhHSP70. Conditions were as in panel A, except that rhHSP70 was added 30 min. (D) Quantification of IKK α/β expression (relative to GAPDH, $n = 6$). Each data point represents TAM from different patients. (E) Quantification of IL-6 secretion by TAM after 24 h of rhHSP70 stimulation. IL-6 in culture supernatants of TAM stimulated as described above were quantified by ELISA ($n = 4$ TAM). Horizontal bars indicate means. Asterisks indicate p values determined by two-sided, paired t -test. * $p < .05$, ** $p < .01$

3.11 | HSP70-driven signalling

HSP70 can function as an extracellular ligand of toll-like receptors (TLR2/4) and CD14 as coreceptor to trigger pro-inflammatory signalling transduction⁶¹ and is associated with HGSC progression.² We therefore investigated whether pro-inflammatory NF- κ B signalling is activated by extracellular HSP70 in TAM which strongly express TLR2/4 and CD14 (Table S7). As shown in Figure 10A and B, stimulation of ascTAM ($n = 6$) with rhHSP70 resulted in significantly enhanced nuclear translocation of the NF- κ B p65 (RELA) subunit compared to a control (Ctrl^{low}) containing LPS at a concentration corresponding to the contamination in low-endotoxin rhHSP70. A potential contribution of endotoxin contaminations to NF- κ B activation was further minimised by treatment with the LPS inhibitor polymyxin B.⁶² Basal cytosolic levels of p65 remained unaffected indicating that only a minor fraction of cytosolic p65 translocates in the nucleus. In accordance with these results, increased levels of the I κ B kinase IKK α/β was observed in all rhHSP70-treated ascTAM samples tested (Figure 10C and D, $n = 6$), presumably as a

consequence of decreased ubiquitin-mediated degradation of IKK α/β .⁶³ Finally, proinflammatory IL-6 secretion by HSP70 was upregulated in rhHSP70-stimulated ascTAM compared to the low-endotoxin control Ctrl^{low} in three out of the four tested patients, albeit below statistical significance (Figure 10E). Taken together, these findings support the notion that extracellular HSP70 may contribute to metastasis by triggering the NF- κ B pathway and thereby a pro-inflammatory response.

4 | DISCUSSION

In the present study, we report the first intercellular signalling map for the TME of HGSC metastases, focusing on TU, TAM, ADI, MESO and CAF from the omentum as the primary site of transcoelomic dissemination of cancer cells. We also compared the intercellular signalling map of omental TU and TAM to their counterparts in ascites to work out commonalities and differences between these compartments. In view of the limitations of single-cell sequencing for this purpose (see Section 1), we decided to

perform these investigations by bulk RNA-Seq analysis of purified cell populations obtained by protocols established and optimised as part of the present study.

4.1 | Potential caveats of using RNA-Seq data for the construction of an intercellular signalling network

A potential problem of the application of RNA-Seq data to the construction of signalling networks is the extrapolation to protein levels, in particular with respect to secreted and membrane-associated proteins, for which correlations with RNA levels are generally weak.^{64,65} We addressed this issue using CAF in short-term culture to obtain MS-based secretome and RNA-Seq data under the identical conditions (Figure 1C; Table S9). The results of this experiment showed a clear correlation ($r = .77$) between the percentage of cytokines and growth factors detected in the CM and the RNA-Seq signal, reaching 100% for highly expressed genes. This correlation suggests that a fraction of secreted proteins (those expressed from more weakly expressed genes) is missing in the secretome due to a lower sensitivity of the proteomic analysis rather than intracellular regulatory mechanisms impinging on translation and/or secretion, consistent with previous data.¹⁷ Furthermore, many of the ‘missing’ proteins are membrane-bound ligands, for example of the SEMA and TNFSF families, which is likely to result in low levels of soluble secreted protein (Table S9).

Another caveat potentially arises by using sample-normalised RNA-Seq data for the comparison of different cell types, if the latter contain highly divergent amounts of total RNA per cell. Thus, similar (normalised) TPM values could potentially obscure large differences in the absolute levels of a specific RNA (and thus of the encoded secreted protein) per cell. However, we could largely exclude this problem for the cell types analysed in the present study, since non-normalised data from RT-qPCR experiments showed a low variation across all samples and cell types for genes with a low variability (≤ 2 -fold) in the RNA-Seq dataset (*NDUFS2* and *NFSLIC*; Figure 1D). We therefore conclude that differences in mRNA content are unlikely to impact the use of RNA-Seq data for the focus of the present study.

Finally, cells isolated from omentum or ascites are invariably contaminated with other cell types. In case of highly expressed cell-type-specific genes contaminations could result in misleading data for weakly or non-expressing cell types. To eliminate such ‘false positives’, we estimated the contamination of each sample by using predefined marker gene sets and eliminated all samples with $>4\%$ of any contaminating cell type ($>6\%$ for ADI samples). RNA-Seq data for the remaining samples

were adjusted for contaminations by adapting a previously described linear model,²⁵ which solved the potential problem of cross-contaminations (Figure 1B).

Comprehensive bioinformatic analyses of this adjusted dataset revealed an unexpectedly strong contribution by host cells, in particular by stromal cells, to signalling events linked to metastatic spread and survival. To further validate the significance of these findings, we compared our results to publicly accessible scRNA-Seq data. Very recently, data for cells from seven untreated HGSC tumours were published, and for each cluster of tumour and host cells, specific transcriptomic markers were identified.²⁶ We could verify in the scRNA-Seq dataset the cell-type specificity of the majority of TU-selective (7/12), immune-cell-selective (32/43) and CAF-selective (8/13) cytokine genes identified in the present study (Figure S16), supporting the conclusions drawn from our data.

4.2 | Contribution by immune cells to the metastasis-associated intercellular signalling pathways in the omental TME

Previous studies have shown that TAM from HGSC ascites are characterised by a high degree of phenotypic and ontogenetic heterogeneity,⁵² and comprise functionally divergent subgroups.¹⁷ Of these, CD163^{high} TAM are of particular relevance, as they express metastasis-promoting genes, such as *CCL18*, *CCL23*, *KITLG* and *VEGFB*¹⁷ and are associated with rapid tumour progression and early relapse in HGSC patients.¹⁸ By contrast, CD163^{low} TAM are linked to immune surveillance and a favourable clinical course, consistent with a higher expression of T-cell-attracting CXCR3 ligands CXCL9-11.^{17,18} As indicated by the present study, a similar diversity appears to exist among omTAM: while TAM produce most of the immune-stimulatory or immune-regulatory CCL- and CXCL-type chemokines and cytokines (Figure 3D; left panel) acting on T cells (Figure 4; left panel), such as CXCR3 ligands, other TAM-derived mediators possess pro-metastatic potential and primarily address TU or stromal cells, such as HBEGF, OSM, RTN and S100A8 (Figures 3 and 4). In this context, TAM-derived CXCL11 deserves particular attention, since it seems to be able to exert either pro- and anti-tumourigenic effects dependent on its target cell. Thus, the migration of TU cells expressing CXCR3 is stimulated by CXCL11,⁶⁶ which in view of the present data may also be applicable to the omental TME of HGSC (Figures 3 and 4). Intriguingly, our data also suggest that some pro-metastatic mediators (such as SEMA4D and WNT10B) with cognate receptors on TU are selectively expressed by ascTAT (Figure 4), pointing to a potential and hitherto unrecognised role for re-educated T cells in HGSC dissemination.

4.3 | Contribution by omental ADI to metastasis-associated pathways

Numerous studies suggest that ADI within the omental TME may play an essential role in HGSC progression⁶⁷ by promoting the homing and invasion of cancer cells, angiogenesis and chemoresistance via the secretion of adipokines, including IL-6, IL-8, THF, leptin, adiponectin and resistin.^{10,68–70} Our study extends these previous data by adding additional mediators to the list of adipokines expressed by omental ADI, some of them with a high degree of selectivity compared to other cell types, for example, CCL14, IGF1, PROK1, SEMA3G and THBS4 (Figure 3). Our data also show that receptors for numerous adipokines are expressed by TU and have previously been linked to metastasis, such as ADIPOQ, FGF10, IGF1, LEFTY2, S100B, SFRP1, VEGFB and WNT11 (Figures 4 and 5), compatible with a role in promoting HGSC progression by ADI-borne mediators.

ADI have also been reported to induce CD36 on ovarian cancer cells allowing for the uptake of fatty acids and the formation of lipid droplets, thereby contributing to peritoneal metastasis.¹¹ Our data, however, are difficult to reconcile with this model, since the expression of *CD36* is invariably extremely low in omTU (0–0.14 TPM; Table S7), while *CD36* expression is readily detectable in omTAM (4–36 TPM) and very high in ADI (>964 TPM). It therefore remains to be investigated whether a CD36-mediated pathway is relevant for the stimulation of omental metastasis in HGSC patients.

4.4 | Contribution by omental MESO to metastasis-associated pathways

Another major cell type of the peritoneal TME and the omentum is the mesothelial cell. Gerber and colleagues identified hypoxic MESO at milky spots secreting vascular endothelial growth factor (VEGFA) suggesting that factors produced by MESO promote the growth of metastatic tumour cells by inducing neo-angiogenesis.⁸ Angiogenesis may also be promoted by senescent MESO, which secrete elevated levels of IL-6 and TGF β to stimulate the expression of pro-angiogenic CXCL1, CXCL8, HGF and VEGF by tumour cells.⁷¹ However, comprehensive and unbiased studies of the secretome of cancer-associated MESO have not been reported to date.

Our study clearly suggests that MESO play an important role in the intercellular signalling network of the omental TME. We have identified 19 mediators selectively expressed by MESO (Figure 3). Of these, 10 factors previously linked to metastasis directly address TU, including

BMP3, FGF1/9, IGFBP1, IL6, IL24, LIF, PGF, RSPO1 and WNT3 (Figures 4 and 5). Furthermore, MESO and CAF co-express several other potentially metastasis-promoting factors with receptors on TU, that is BMP4, EFNA5, FGF7, SEMA3A/3C/3D, SLIT2, TGFB3 and WNT2B (Figures 4 and 5). MESO also share the expression of >60 other pro-metastatic cytokine and growth factors with various other cell types of the omental TME (Figures 4 and 5). These observations clearly support the view that factors secreted by MESO partake in promoting the formation of omental lesions and presumably dissemination within the peritoneal cavity, especially considering the abundance of MESO as major constituents of all serous membranes.

4.5 | Contribution by omental CAF to metastasis-associated pathways

CAF have long been recognised as crucial components of most solid tumours, including ovarian cancer.¹⁴ CAF are derived from omental fibroblasts and mesenchymal stem cells, which is partly triggered by TGF β and LPA in the tumour microenvironment.^{9,13} CAF produce numerous factors acting on cancer cells to promote glycolytic metabolism, proliferation, invasion, angiogenesis and metastatic colonisation, including CCL5, CXCL10, IL-6, TGF α , SDF and versican.^{9,14,15} Our own data support the concept of an instrumental role for CAF in HGSC metastasis. Omental CAF are the main producers of 14 cytokines and growth factors (Figure 3C and D), of which at least 6 of these have been associated with metastasis and possess receptors on omTU, including CXCL12, FGF5 and WNT4 (Figures 4 and 5). Furthermore, CAF share many of the mediators synthesised by other stromal cell types ($n = 39$; Figure 3C), and also address other host cell types (such as TAM, MESO and ADI), providing further evidence for the relevance these stromal cell types in the pro-metastatic HGSC secretome.

To address the functional significance of the crosstalk of CAF and omTU we selected WNT4 as an example of a mediator expressed by CAF with high selectivity. Several WNT ligands have been reported to be upregulated and associated with histological grade, EMT, chemoresistance, and poor prognosis in ovarian cancer.^{72–74} Moreover, a strong inverse correlation between WNT activity and intra-tumoural T cell infiltration resembling an immunologically ‘cold’ TME, has been demonstrated.⁷⁵ WNT4 is a highly interesting ligand due to its proposed pro-metastatic functions in laryngeal and colorectal carcinoma,^{76,77} but knowledge regarding its role in the TME of other entities, including HGSC, is lacking. This problem is partly due to the diversity of FZD receptor isoforms and coreceptors and

the complexity of different canonical and non-canonical signal transduction pathways, which in turn trigger different functional outcomes.⁷⁸ For WNT4, reduced expression in ovarian tumour cells compared to normal ovarian tissue has been observed in one study,⁷⁹ which agrees with our own data showing weak expression of WNT4 in omTU (Figure 6A). Based on our observations, CAF are highly selective producers of the WNT4 ligand in the peritoneal TME. This is in line with previous publications reporting high expression of WNT4 and activation of WNT4 signalling pathways in fibroblasts in wound healing and fibrosis.^{80,81} In contrast to WNT4, FZD receptor subtypes and LRP5/6 coreceptors are widely expressed among all cell types of the omental TME (Figure 4), indicating that CAF-derived WNT4 may act on different cell types. Tumour cells present in the TME, for example, express FZD8 and LRP5/6 coreceptors (Figure 6A) known to interact with WNT4 ligand.⁶⁰ Consistently, we were able to demonstrate that WNT4 significantly enhances HGSC motility, migration and adhesion to a mesothelial layer (Figure 6), which underlines a potential role of WNT4 secreted by CAF in peritoneal metastasis.

4.6 | Invasion of tumour cells into the mesothelium

The mesothelium consists of a single layer of MESO covering a basement membrane composed of extracellular matrix (ECM) proteins. According to the prevailing opinion, the mesothelium constitutes a barrier against the adhesion of, and invasion by, cancer cells from the peritoneal fluid.⁸² The attachment of cancer cells is thought to be dependent on pre-existing lesions of the mesothelium to allow for an interaction of integrins on tumour cells with the underlying ECM proteins.^{17,83–86} Different models have been proposed to explain the occurrence of such lesions. Besides MESO senescence⁸⁷ and myosin-dependent mechanical forces exerted by tumour cells,⁸⁸ cytokine-mediated MESO activation^{89,90} has been suggested as mechanisms facilitating penetration through the mesothelial layer. The latter is compatible with our data, which indicate that a number of mediators with receptors on MESO and the potential to activate MESO are produced by TU or host cells, including IL-1A, IL-1B, IL-15, IL-23A and TGF β (Figure S4). Active MESO killing by FAS ligand⁹¹ is another mechanism proposed to enable the penetration of cancer cells through the mesothelial layer. According to our data, TAT express high levels of *FASLG* and MESO express the corresponding receptor gene (Figure S5), supporting the aforementioned hypothesis. However, other mechanisms involving death-ligand-mediated killing mechanisms are possible, as suggested

by the expression of several other death receptors of the *TNFSFR* family by MESO, for example *TNFRSF8*, *CD40* (*TNFRSF5*) and *CD27* (*TNFRSF*), which encode receptors for CD30 (TNFSF8), CD40LG and CD70 (Figure S5). Future work will address the hypotheses arising from these data.

Invasion of cancer cells is critically dependent on their interaction with collagen fibers beneath the MESO layer, consistent with the documented association of ECM modifiers with HGSC survival.⁵² As shown by our data, all cell types contribute to ECM reorganisation, but in a cell-type-selective manner and with a predominant role for TAM and stroma cells (Figure 7). This is evident from the fact that omTAM are also a major source of gene products involved of ECM reorganisation, including laminin, proteases of the ADAM, cathepsin and MMP subgroups as well as SERPIN and TIMP protease inhibitors. Stromal cells also strongly contribute to proteolysis and its regulation, but are the main producers of collagen and other ECM components. Taken together with previous findings that ECM remodeling is associated with ovarian cancer survival,^{17,52} these observations provide further strong evidence for the relevance of TAM, ADI, MESO and CAF in the TME of HGSC.

4.7 | Comparison of TU and TAM from ascites and omentum

In the present study, we also present the first comparative analysis of cell populations isolated from HGSC metastases and ascites. An important conclusion derived from this analysis is the high similarity of matched omTU/ascTU and omTAM/ascTAM samples with correlation coefficients of 0.98 and 0.95, respectively (Figures S12 and S14). Many previous studies made use of ascites cells for molecular and functional analyses, because these cells are available in large numbers and can be isolated as relatively pure fractions. Our data show that HGSC ascites cells faithfully reflect the respective cellular compartments of the TME and therefore validate their use for studying HGSC biology.

There are, however, also clear selective differences, as exemplified by the induction of cell cycle genes in omTAM (Figure 9B), which we were able to confirm by flow cytometry (Figure 9C). The induction of TAM proliferation is possibly due to their spatial proximity to omental stromal cells, which strongly express the *CSF1* gene (Figure 9D) encoding the essential macrophage-specific growth factor M-CSF.⁹² This observation also suggests that ascTAM arise from replicating resident macrophages (and blood monocytes) rather than from their proliferation in ascites.

Another marked difference between both omental and ascites cells is the upregulation of inflammatory

signalling, which was seen with both TU and TAM (Figures 8B and 9E). Among others, HSPA1A is one of the pro-inflammatory genes upregulated in both omental TU and TAM compared to their counterparts in ascites. Consistent with this observation, we found high levels of HSPA1A in conditioned medium of ascTU (Figure 8D). HSP70 can also be found at high concentrations in the ascitic fluid where its presence is linked to a poor RFS of HGSC patients.² Besides acting as an intracellular molecular chaperone, HSP70 can be released from cells in case of elevated cellular stress.⁶¹ Extracellular HSP70 (eHSP70) provides danger signals to the immune system as a damage-associated molecular pattern (DAMP) resulting in pro-inflammatory activation of macrophages, monocytes or dendritic cells by inducing secretion of cytokines such as IL-1, IL-6 and TNF- α .^{61,93} By contrast, other studies point to an inverse immunoregulatory role of eHSP70 that dampens inflammation.^{94,95} eHSP70 can exert cytokine regulatory activity by engaging TLR2 and 4 receptors, which in turn activate NF- κ B and MAPK signalling pathways,⁶¹ but the precise mechanism how eHSP70 acts on TU and TAM in the TME is unclear. Moreover, the activation of HSP70 through TLR2/4 is controversial, since contaminating LPS in the recombinant HSP70 used in one studies may account for its pro-inflammatory activity.⁹⁶ Another study reported that the stimulatory effect requires both, the presence of endotoxin and structural integrity of HSP70.⁹⁷ By using highly purified, low-endotoxin rhHSP70 in conjunction with polymyxin B treatment to suppress LPS-mediated TLR4 activation, we were able to detect activation of the NF- κ B pathway by increased nuclear p65 translocation and induction of IKK α/β in TAM of different patients (Figure 10A and B), accompanied by an upregulation of IL-6 secretion (Figure 10C). Multiple pro-tumourigenic functions have been assigned to IL-6 in ovarian cancer including invasion, migration, EMT, proliferation, over-expression of metalloproteases and chemoresistance.⁹⁸ Thus, induction of pro-inflammatory signalling (including IL-6 secretion) via upregulation of HSP70 in omTU and/or omTAM might be involved in promoting the peritoneal spread of cancer cells in HGSC patients.

4.8 | Conclusions

Factors secreted by immune and stroma cells contribute to an unexpected large extent to the intercellular signalling network of omental metastases and establish an environment that supports HGSC progression. Intriguingly, the expression of numerous genes coding for cytokines, growth factors and ECM remodeling proteins within this network are associated with tumour progression, metastasis and survival, pointing to their relevance as poten-

tial biomarkers and/or targets for therapeutic intervention. As proof of principle, we demonstrate a tumour-promoting function of the highly cell-selective mediator WNT4 produced by CAF and acting on tumour cells to induce their migration. In spite of a generally high similarity between ascites-derived cell types and their counterparts in solid tissue, a selective shift towards a pro-inflammatory gene expression pattern is activated in omTAM and omTU, probably triggered by interaction with adjacent stroma cells in the metastatic niche. Our data suggests that the omental TME represents an inflammation-promoting environment which might be linked to transitions between epithelial and mesenchymal cancer cell phenotypes as a prerequisite of metastatic growth.


ACKNOWLEDGEMENTS

We are grateful to T. Plaum, A. Allmeroth and M. Alt for expert technical assistance. This work was supported by a grant from the German Cancer Aid (Deutsche Krebshilfe; grant no. 70113255) to RM and SR.

CONFLICT OF INTEREST

The authors declare that there is no conflict of interest.

ORCID

Johannes Graumann  <https://orcid.org/0000-0002-3015-5850>

Rolf Müller  <https://orcid.org/0000-0003-3339-4248>

REFERENCES

1. Lengyel E. Ovarian cancer development and metastasis. *Am J Pathol.* 2010;177:1053-1064.
2. Finkernagel F, Reinartz S, Schuldner M, et al. Dual-platform affinity proteomics identifies links between the recurrence of ovarian carcinoma and proteins released into the tumor microenvironment. *Theranostics.* 2019;9:6601-6617.
3. Worzfeld T, Pogge Von Strandmann E, Huber M, et al. The unique molecular and cellular microenvironment of ovarian cancer. *Front Oncol.* 2017;7:24.
4. Ma X. The omentum, a niche for premetastatic ovarian cancer. *J Exp Med.* 2020;217.
5. Platell C, Cooper D, Papadimitriou JM, Hall JC. The omentum. *World J Gastroenterol.* 2000;6:169-176.
6. Meza-Perez S, Randall TD. Immunological functions of the omentum. *Trends Immunol.* 2017;38:526-536.
7. Rangel-Moreno J, Moyron-Quiroz JE, Carragher DM, et al. Omental milky spots develop in the absence of lymphoid tissue-inducer cells and support B and T cell responses to peritoneal antigens. *Immunity.* 2009;30:731-743.
8. Gerber SA, Rybalko VY, Bigelow CE, et al. Preferential attachment of peritoneal tumor metastases to omental immune aggregates and possible role of a unique vascular microenvironment in metastatic survival and growth. *Am J Pathol.* 2006;169:1739-1752.

9. Motohara T, Masuda K, Morotti M, et al. An evolving story of the metastatic voyage of ovarian cancer cells: cellular and molecular orchestration of the adipose-rich metastatic microenvironment. *Oncogene*. 2019;38:2885-2898.
10. Nieman KM, Kenny HA, Penicka CV, et al. Adipocytes promote ovarian cancer metastasis and provide energy for rapid tumor growth. *Nat Med*. 2011;17:1498-1503.
11. Ladanyi A, Mukherjee A, Kenny HA, et al. Adipocyte-induced CD36 expression drives ovarian cancer progression and metastasis. *Oncogene*. 2018;37:2285-2301.
12. Miranda F, Mannion D, Liu S, et al. Salt-inducible kinase 2 couples ovarian cancer cell metabolism with survival at the adipocyte-rich metastatic niche. *Cancer Cell*. 2016;30:273-289.
13. Cai J, Tang H, Xu L, et al. Fibroblasts in omentum activated by tumor cells promote ovarian cancer growth, adhesion and invasiveness. *Carcinogenesis*. 2012;33:20-29.
14. Yoshida GJ. Regulation of heterogeneous cancer-associated fibroblasts: the molecular pathology of activated signaling pathways. *J Exp Clin Cancer Res*. 2020;39:112.
15. Zhang Y, Tang H, Cai J, et al. Ovarian cancer-associated fibroblasts contribute to epithelial ovarian carcinoma metastasis by promoting angiogenesis, lymphangiogenesis and tumor cell invasion. *Cancer Lett*. 2011;303:47-55.
16. Etzerodt A, Moulin M, Doktor TK, et al. Tissue-resident macrophages in omentum promote metastatic spread of ovarian cancer. *J Exp Med*. 2020;217.
17. Worzfeld T, Finkernagel F, Reinartz S, et al. Proteotranscriptomics reveal signaling networks in the ovarian cancer microenvironment. *Mol Cell Proteomics*. 2018;17:270-289.
18. Reinartz S, Schumann T, Finkernagel F, et al. Mixed-polarization phenotype of ascites-associated macrophages in human ovarian carcinoma: correlation of CD163 expression, cytokine levels and early relapse. *Int J Cancer*. 2014;134:32-42.
19. Izar B, Tirosh I, Stover EH, et al. A single-cell landscape of high-grade serous ovarian cancer. *Nat Med*. 2020;26:1271-1279.
20. TheCancerGenomeAtlasResearchNetwork. Integrated genomic analyses of ovarian carcinoma. *Nature*. 2011;474:609-615.
21. Konecny GE, Wang C, Hamidi H, et al. Prognostic and therapeutic relevance of molecular subtypes in high-grade serous ovarian cancer. *J Natl Cancer Inst*. 2014;106. <https://doi.org/10.1093/jnci/dju249>. pii: dju249.
22. Shih AJ, Menzin A, Whyte J, et al. Identification of grade and origin specific cell populations in serous epithelial ovarian cancer by single cell RNA-seq. *PLoS One*. 2018;13:e0206785.
23. Geistlinger L, Oh S, Ramos M, et al. Multiomic analysis of subtype evolution and heterogeneity in high-grade serous ovarian carcinoma. *Cancer Res*. 2020;80:4335-4345.
24. Winterhoff BJ, Maile M, Mitra AK, et al. Single cell sequencing reveals heterogeneity within ovarian cancer epithelium and cancer associated stromal cells. *Gynecol Oncol*. 2017;144:598-606.
25. Reinartz S, Finkernagel F, Adhikary T, et al. A transcriptome-based global map of signaling pathways in the ovarian cancer microenvironment associated with clinical outcome. *Genome Biol*. 2016;17:108.
26. Olbrecht S, Busschaert P, Qian J, et al. High-grade serous tubo-ovarian cancer refined with single-cell RNA sequencing: specific cell subtypes influence survival and determine molecular subtype classification. *Genome Med*. 2021;13:111.
27. Zhang MJ, Ntranos V, Tse D. Determining sequencing depth in a single-cell RNA-seq experiment. *Nat Commun*. 2020;11:774.
28. Li X, Cooper NGF, O'Toole TE, Rouchka EC. Choice of library size normalization and statistical methods for differential gene expression analysis in balanced two-group comparisons for RNA-seq studies. *BMC Genomics*. 2020;21:75.
29. Sonesson C, Robinson MD. Bias, robustness and scalability in single-cell differential expression analysis. *Nat Methods*. 2018;15:255-261.
30. Svensson V, Natarajan KN, Ly L-H, et al. Power analysis of single-cell RNA-sequencing experiments. *Nat Methods*. 2017;14:381-387.
31. Haque A, Engel J, Teichmann SA, Lonnberg T. A practical guide to single-cell RNA-sequencing for biomedical research and clinical applications. *Genome Med*. 2017;9:75.
32. Trapnell C, Cacchiarelli D, Grimsby J, et al. The dynamics and regulators of cell fate decisions are revealed by pseudotemporal ordering of single cells. *Nat Biotechnol*. 2014;32:381-386.
33. Rustin GJS, Timmers P, Nelstrop A, et al. Comparison of CA-125 and standard definitions of progression of ovarian cancer in the intergroup trial of cisplatin and paclitaxel versus cisplatin and cyclophosphamide. *J Clin Oncol*. 2006;24:45-51.
34. Reinartz S, Lieber S, Pesek J, et al. Cell-type-selective pathways and clinical associations of lysophosphatidic acid biosynthesis and signaling in the ovarian cancer microenvironment. *Mol Oncol*. 2019;23:185-201.
35. Cox J, Mann M. MaxQuant enables high peptide identification rates, individualized p.p.b.-range mass accuracies and proteome-wide protein quantification. *Nat Biotechnol*. 2008;26:1367-1372.
36. Cox J, Neuhauser N, Michalski A, Scheltema RA, Olsen JV, Mann M. Andromeda: a peptide search engine integrated into the MaxQuant environment. *J Proteome Res*. 2011;10:1794-1805.
37. Cox J, Hein MY, Luber CA, Paron I, Nagaraj N, Mann M. Accurate proteome-wide label-free quantification by delayed normalization and maximal peptide ratio extraction, termed MaxLFQ. *Mol Cell Proteomics*. 2014;13:2513-2526.
38. Unger A, Finkernagel F, Hoffmann N, et al. Chromatin binding of c-REL and p65 is not limiting for macrophage IL12B transcription during immediate suppression by ovarian carcinoma ascites. *Front Immunol*. 2018;9:1425.
39. Rohhalter V, Roth K, Finkernagel F, et al. A multi-stage process including transient polyploidization and EMT precedes the emergence of chemoresistant ovarian carcinoma cells with a dedifferentiated and pro-inflammatory secretory phenotype. *Oncotarget*. 2015;6:40005-40025.
40. Guescini M, Sisti D, Rocchi MB, Stocchi L, Stocchi V. A new real-time PCR method to overcome significant quantitative inaccuracy due to slight amplification inhibition. *BMC Bioinformatics*. 2008;9:326.
41. Adhikary T, Wortmann A, Schumann T, et al. The transcriptional PPAR β/δ network in human macrophages defines a unique agonist-induced activation state. *Nucleic Acids Res*. 2015;43:5033-5051.
42. Dobin A, Davis CA, Schlesinger F, et al. STAR: ultrafast universal RNA-seq aligner. *Bioinformatics*. 2013;29:15-21.

43. Litkouhi B, Kwong J, Lot C-M, et al. Claudin-4 overexpression in epithelial ovarian cancer is associated with hypomethylation and is a potential target for modulation of tight junction barrier function using a C-terminal fragment of *Clostridium perfringens* enterotoxin. *Neoplasia*. 2007;9:304-314.
44. Schraven B, Marie-Cardine A, Hubener C, Bruyns E, Ding I. Integration of receptor-mediated signals in T cells by transmembrane adaptor proteins. *Immunol Today*. 1999;20:431-434.
45. Gascoigne NR, Acuto O. THEMIS: a critical TCR signal regulator for ligand discrimination. *Curr Opin Immunol*. 2015;33:86-92.
46. Tsuji S, Tsuura Y, Morohoshi T, et al. Secretion of intelectin-1 from malignant pleural mesothelioma into pleural effusion. *Br J Cancer*. 2010;103:517-523.
47. Au-Yeung C-L, Yeung T-L, Achreja A, et al. ITLN1 modulates invasive potential and metabolic reprogramming of ovarian cancer cells in omental microenvironment. *Nat Commun*. 2020;11:3546.
48. Koistinen V, Jokela T, Oikari S, Kärnä R, Tammi M, Rilla K. Hyaluronan-positive plasma membrane protrusions exist on mesothelial cells in vivo. *Histochem Cell Biol*. 2016;145:531-544.
49. Koistinen V, Härkönen K, Kärnä R, Arasu UT, Oikari S, Rilla K. EMT induced by EGF and wounding activates hyaluronan synthesis machinery and EV shedding in rat primary mesothelial cells. *Matrix Biol*. 2017;63:38-54.
50. Liu Z, Dobra K, Hauzenberger D, Klominek J. Expression of hyaluronan synthases and hyaluronan in malignant mesothelioma cells. *Anticancer Res*. 2004;24:599-603.
51. Song L, Webb NE, Song Y, Tuan RS. Identification and functional analysis of candidate genes regulating mesenchymal stem cell self-renewal and multipotency. *Stem Cells*. 2006;24:1707-1718.
52. Finkernagel F, Reinartz S, Lieber S, et al. The transcriptional signature of human ovarian carcinoma macrophages is associated with extracellular matrix reorganization. *Oncotarget*. 2016;17:75339-75352.
53. Singh B, Carpenter G, Coffey RJ. EGF receptor ligands: recent advances. *F1000Res*. 2016;5.
54. Garrett TPJ, Mckern NM, Lou M, et al. Crystal structure of a truncated epidermal growth factor receptor extracellular domain bound to transforming growth factor alpha. *Cell*. 2002;110:763-773.
55. Tiong KH, Mah LY, Leong CO. Functional roles of fibroblast growth factor receptors (FGFRs) signaling in human cancers. *Apoptosis*. 2013;18:1447-1468.
56. Derynck R, Budi EH. Specificity, versatility, and control of TGF-beta family signaling. *Sci Signal*. 2019;12.
57. Worzfeld T, Offermanns S. Semaphorins and plexins as therapeutic targets. *Nat Rev Drug Discov*. 2014;13:603-621.
58. Gyorffy B, Lanczky A, Szallasi Z. Implementing an online tool for genome-wide validation of survival-associated biomarkers in ovarian-cancer using microarray data from 1287 patients. *Endocr Relat Cancer*. 2012;19:197-208.
59. Gentles AJ, Newman AM, Liu CL, et al. The prognostic landscape of genes and infiltrating immune cells across human cancers. *Nat Med*. 2015;21:938-945.
60. Dijksterhuis JP, Baljinnyam B, Stanger K, et al. Systematic mapping of WNT-FZD protein interactions reveals functional selectivity by distinct WNT-FZD pairs. *J Biol Chem*. 2015;290:6789-6798.
61. Asea A, Rehli M, Kabingu E, et al. Novel signal transduction pathway utilized by extracellular HSP70: role of toll-like receptor (TLR) 2 and TLR4. *J Biol Chem*. 2002;277:15028-15034.
62. Duff GW, Atkins E. The inhibitory effect of polymyxin B on endotoxin-induced endogenous pyrogen production. *J Immunol Methods*. 1982;52:333-340.
63. Liu S, Chen ZJ. Expanding role of ubiquitination in NF-kappaB signaling. *Cell Res*. 2011;21:6-21.
64. Chevallet M, Diemer H, Van Dorssealer A, Villiers C, Rabilloud T. Toward a better analysis of secreted proteins: the example of the myeloid cells secretome. *Proteomics*. 2007;7:1757-1770.
65. Tan S, Tan HT, Chung MC. Membrane proteins and membrane proteomics. *Proteomics*. 2008;8:3924-3932.
66. Lau T-S, Chung TK-H, Cheung T-H, et al. Cancer cell-derived lymphotoxin mediates reciprocal tumour-stromal interactions in human ovarian cancer by inducing CXCL11 in fibroblasts. *J Pathol*. 2014;232:43-56.
67. Dai L, Song K, Di W. Adipocytes: active facilitators in epithelial ovarian cancer progression?. *J Ovarian Res*. 2020;13:115.
68. Quail DF, Dannenberg AJ. The obese adipose tissue microenvironment in cancer development and progression. *Nat Rev Endocrinol*. 2019;15:139-154.
69. Duong MN, Geneste A, Fallone F, Li X, Dumontet C, Muller C. The fat and the bad: mature adipocytes, key actors in tumor progression and resistance. *Oncotarget*. 2017;8:57622-57641.
70. Howe LR, Subbaramaiah K, Hudis CA, Dannenberg AJ. Molecular pathways: adipose inflammation as a mediator of obesity-associated cancer. *Clin Cancer Res*. 2013;19:6074-6083.
71. Mikuła-Pietrasik J, Sosińska P, Naumowicz E, et al. Senescent peritoneal mesothelium induces a pro-angiogenic phenotype in ovarian cancer cells in vitro and in a mouse xenograft model in vivo. *Clin Exp Metastasis*. 2016;33:15-27.
72. Chehover M, Reich R, Davidson B. Expression of Wnt pathway molecules is associated with disease outcome in metastatic high-grade serous carcinoma. *Virchows Arch*. 2020;477:249-258.
73. Kotrbova A, Ovesna P, Gybel T, et al. WNT signaling inducing activity in ascites predicts poor outcome in ovarian cancer. *Theranostics*. 2020;10:537-552.
74. Teeuwssen M, Fodde R. Wnt signaling in ovarian cancer stemness, EMT, and therapy resistance. *J Clin Med*. 2019;8.
75. Luke JJ, Bao R, Sweis RF, Spranger S, Gajewski TF. WNT/beta-catenin pathway activation correlates with immune exclusion across human cancers. *Clin Cancer Res*. 2019;25:3074-3083.
76. Wang N, Yan H, Wu D, et al. PRMT5/Wnt4 axis promotes lymph-node metastasis and proliferation of laryngeal carcinoma. *Cell Death Dis*. 2020;11:864.
77. Yang D, Li Q, Shang R, et al. WNT4 secreted by tumor tissues promotes tumor progression in colorectal cancer by activation of the Wnt/beta-catenin signalling pathway. *J Exp Clin Cancer Res*. 2020;39:251.
78. Ring L, Neth P, Weber C, Steffens S, Faussner A. beta-Catenin-dependent pathway activation by both promiscuous "canonical" WNT3a-, and specific "noncanonical" WNT4- and WNT5a-FZD receptor combinations with strong differences in LRP5 and LRP6 dependency. *Cell Signal*. 2014;26:260-267.

79. Nguyen VHL, Hough R, Bernaudo S, Peng C. Wnt/beta-catenin signalling in ovarian cancer: insights into its hyperactivation and function in tumorigenesis. *J Ovarian Res.* 2019;12:122.
80. Saitoh A, Hansen LA, Vogel JC, Udey MC. Characterization of Wnt gene expression in murine skin: possible involvement of epidermis-derived Wnt-4 in cutaneous epithelial-mesenchymal interactions. *Exp Cell Res.* 1998;243:150-160.
81. Surendran K, McCaul SP, Simon TC. A role for Wnt-4 in renal fibrosis. *Am J Physiol Renal Physiol.* 2002;282:F431-441.
82. Sodek KL, Murphy KJ, Brown TJ, Ringuette MJ. Cell-cell and cell-matrix dynamics in intraperitoneal cancer metastasis. *Cancer Metastasis Rev.* 2012;31:397-414.
83. Burleson KM, Casey RC, Skubitz KM, Pambuccian SE, Oegema TR, Skubitz APN. Ovarian carcinoma ascites spheroids adhere to extracellular matrix components and mesothelial cell monolayers. *Gynecol Oncol.* 2004;93:170-181.
84. Lessan K, Aguiar DJ, Oegema T, Siebenson L, Skubitz AP. CD44 and beta1 integrin mediate ovarian carcinoma cell adhesion to peritoneal mesothelial cells. *Am J Pathol.* 1999;154:1525-1537.
85. Strobel T, Cannistra SA. Beta1-integrins partly mediate binding of ovarian cancer cells to peritoneal mesothelium in vitro. *Gynecol Oncol.* 1999;73:362-367.
86. Birbeck MS, Wheatley DN. An electron microscopic study of the invasion of ascites tumor cells into the abdominal wall. *Cancer Res.* 1965;25:490-497.
87. Mikuła-Pietrasik J, Uruski P, Sosińska P, et al. Senescent peritoneal mesothelium creates a niche for ovarian cancer metastases. *Cell Death Dis.* 2016;7:e2565.
88. Iwanicki MP, Davidowitz RA, Ng MR, et al. Ovarian cancer spheroids use myosin-generated force to clear the mesothelium. *Cancer Discov.* 2011;1:144-157.
89. Kenny HA, Chiang C-Y, White EA, et al. Mesothelial cells promote early ovarian cancer metastasis through fibronectin secretion. *J Clin Invest.* 2014;124:4614-4628.
90. Mutsaers SE, Birnie K, Lansley S, Herrick SE, Lim C-B, Prêle CM. Mesothelial cells in tissue repair and fibrosis. *Front Pharmacol.* 2015;6:113.
91. Heath RM, Jayne DG, O'Leary R, Morrison EE, Guillou PJ. Tumour-induced apoptosis in human mesothelial cells: a mechanism of peritoneal invasion by Fas Ligand/Fas interaction. *Br J Cancer.* 2004;90:1437-1442.
92. Pollard JW. Tumour-educated macrophages promote tumour progression and metastasis. *Nat Rev Cancer.* 2004;4:71-78.
93. Johnson JD, Fleshner M. Releasing signals, secretory pathways, and immune function of endogenous extracellular heat shock protein 72. *J Leukoc Biol.* 2006;79:425-434.
94. Ferat-Osorio E, Sánchez-Anaya A, Gutiérrez-Mendoza M, et al. Heat shock protein 70 down-regulates the production of toll-like receptor-induced pro-inflammatory cytokines by a heat shock factor-1/constitutive heat shock element-binding factor-dependent mechanism. *J Inflamm (Lond).* 2014;11:19.
95. Komarova EY, Marchenko LV, Zhakhov AV, et al. Extracellular Hsp70 reduces the pro-tumor capacity of monocytes/macrophages co-cultivated with cancer cells. *Int J Mol Sci.* 2019;21:59.
96. Gao B, Tsan MF. Endotoxin contamination in recombinant human heat shock protein 70 (Hsp70) preparation is responsible for the induction of tumor necrosis factor alpha release by murine macrophages. *J Biol Chem.* 2003;278:174-179.
97. Luong M, Zhang Y, Chamberlain T, et al. Stimulation of TLR4 by recombinant HSP70 requires structural integrity of the HSP70 protein itself. *J Inflamm (Lond).* 2012;9:11.
98. Browning L, Patel MR, Horvath EB, Tawara K, Jorczyk CL. IL-6 and ovarian cancer: inflammatory cytokines in promotion of metastasis. *Cancer Manag Res.* 2018;10:6685-6693.
99. Humphries JD, Byron A, Humphries MJ. Integrin ligands at a glance. *J Cell Sci.* 2006;119:3901-3903.
100. Park EJ, Myint PK, Ito A, et al. Integrin-ligand interactions in inflammation, cancer, and metabolic disease: insights into the multifaceted roles of an emerging ligand Irisin. *Front Cell Dev Biol.* 2020;8:588066.

SUPPORTING INFORMATION

Additional supporting information may be found in the online version of the article at the publisher's website.

How to cite this article: Sommerfeld L, Finkernagel F, Jansen JM, et al. The multicellular signalling network of ovarian cancer metastases. *Clin Transl Med.* 2021;11:e633.
<https://doi.org/10.1002/ctm2.633>

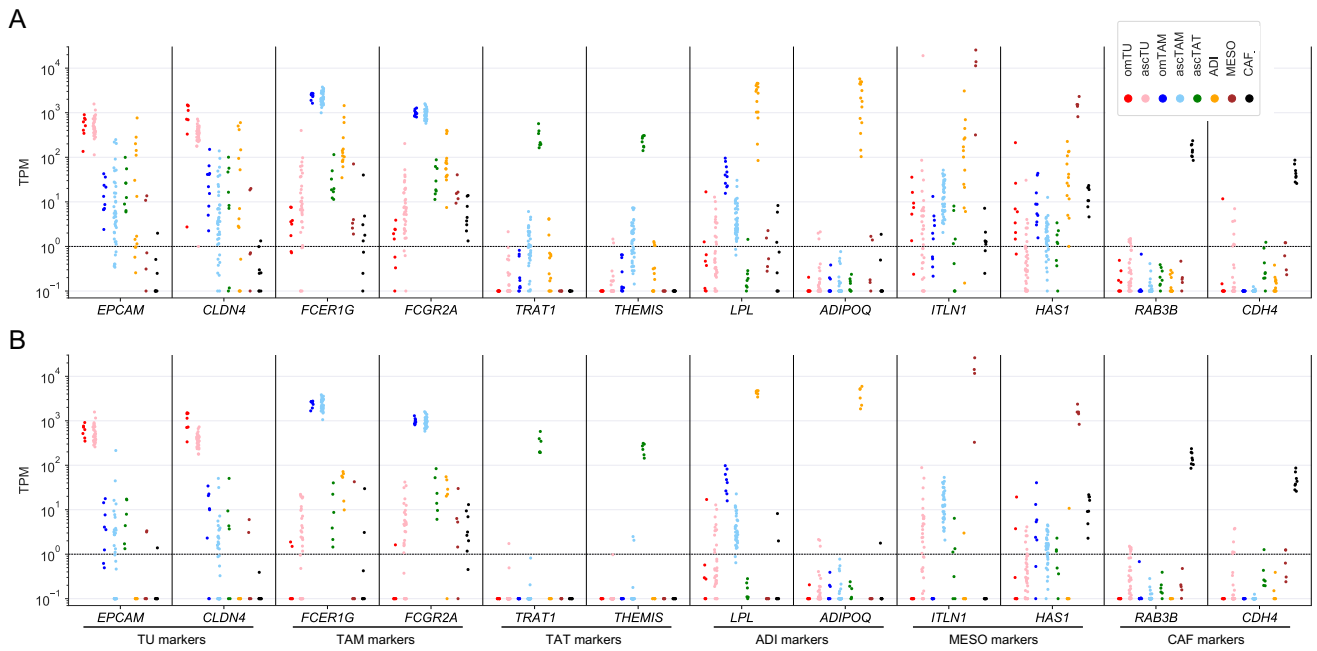


FIGURE S1

(A) Expression (TPM) of cell type-specific marker genes in all samples isolated from HGSC ascites and omentum determined by RNA-Seq. (B) Expression (TPM) of the same markers after exclusion of samples with >6% of any contaminating cell type and bioinformatic adjustment for contaminating cells. Samples with >6% of any contaminating cell type were excluded prior to adjustment. Each data point represents a different patient.

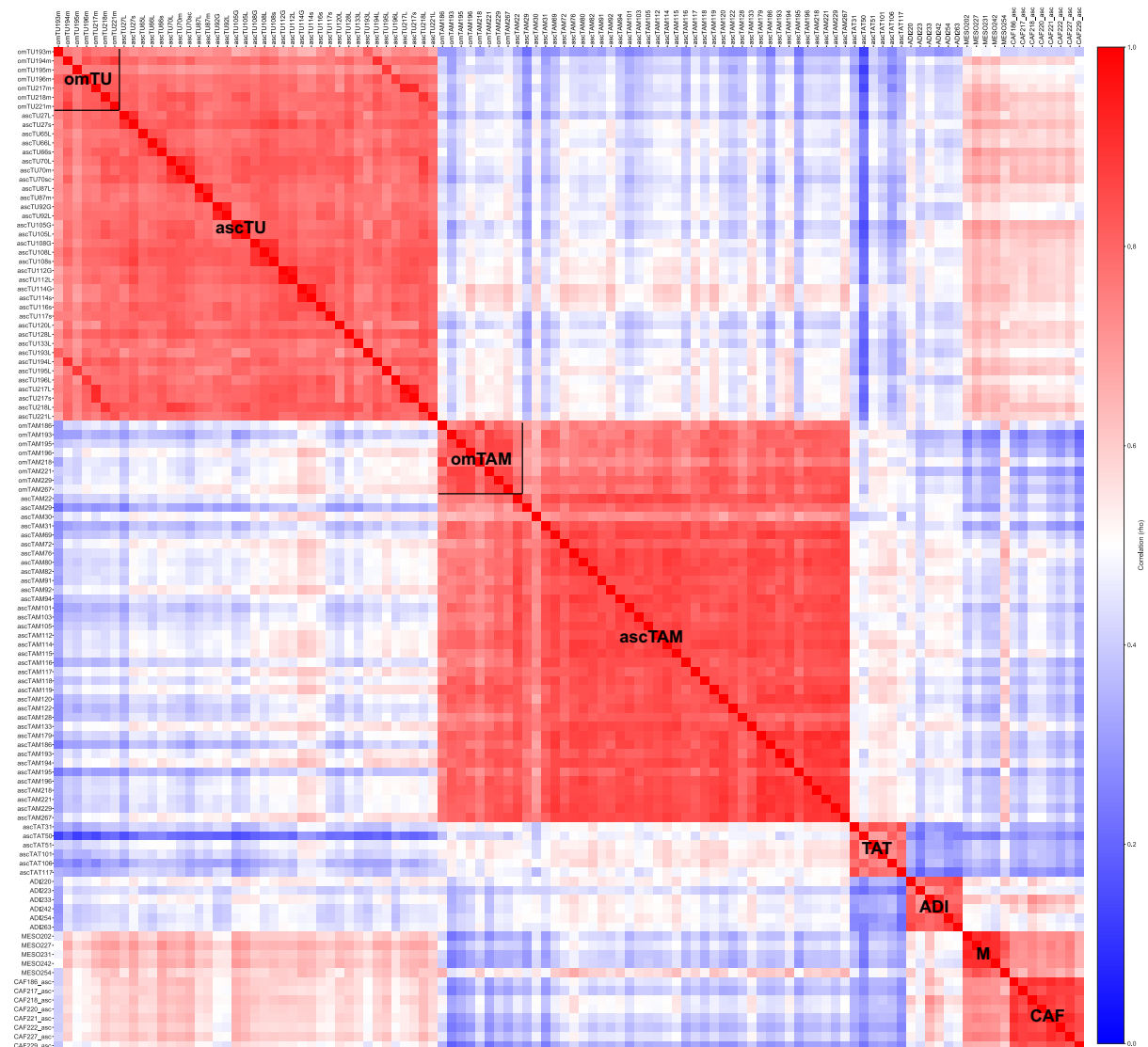


FIGURE S2

Heatmap showing the correlation (Spearman ρ) between all samples analyzed in the present study. The numbers in sample names represent the patient IDs, as listed in Table S1. Samples are ordered by cell type.

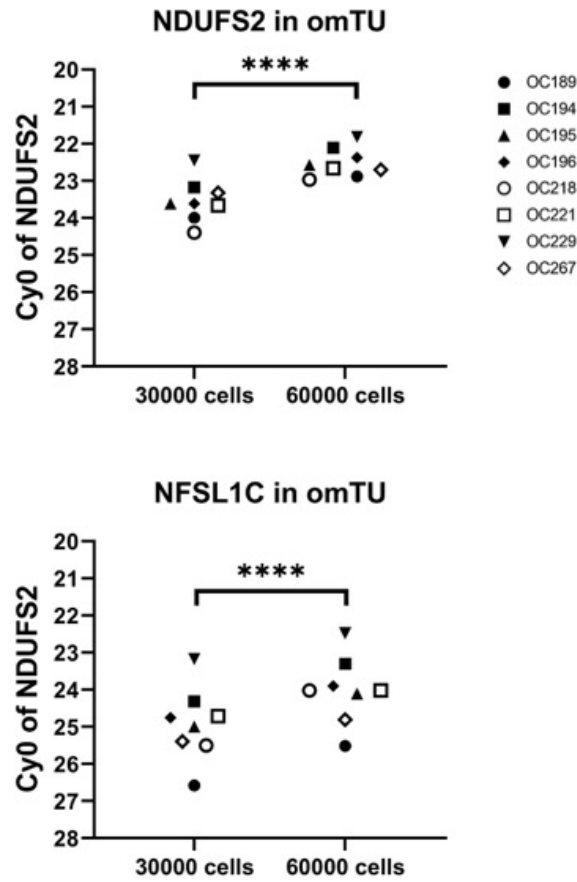


FIGURE S3

qRT-PCR data confirming a linear relationship between input and signal for the experiment in Figure 1D and E. RNA from different numbers of omTU cells was analyzed using primers for *NDUFS2* and *NFSL1C* mRNA without normalization. Each symbol indicated a different patient.

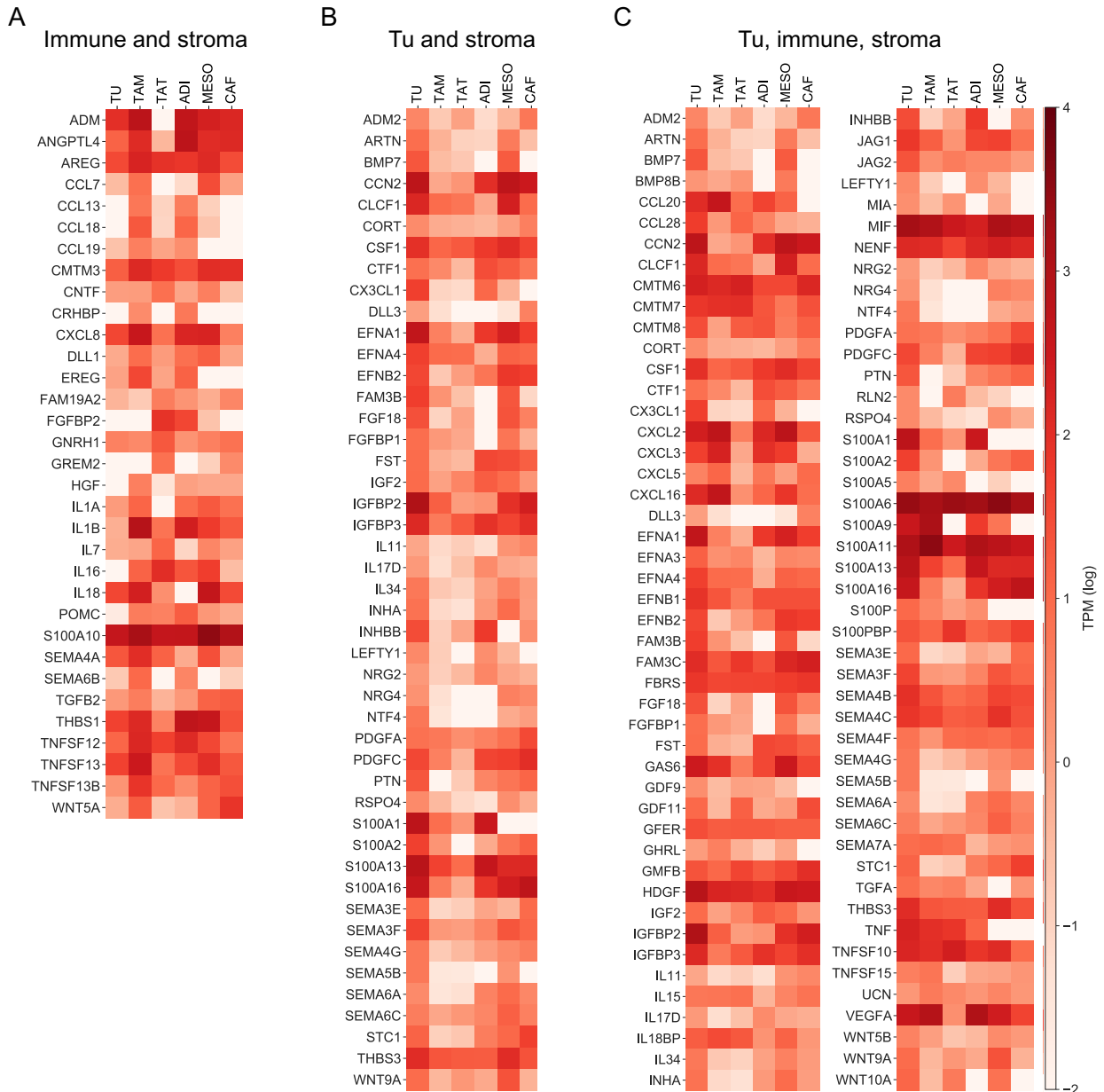


FIGURE S4

Expression patterns of genes encoding cytokines and growth factors in different compartments of the omental TME. Expression levels are categorized (see bottom left) based on the values in Table S10 (as in Figure 2C).

Supporting Information (Figures S1-S16): Sommerfeld *et al.*, The intercellular signaling network of ovarian cancer metastases



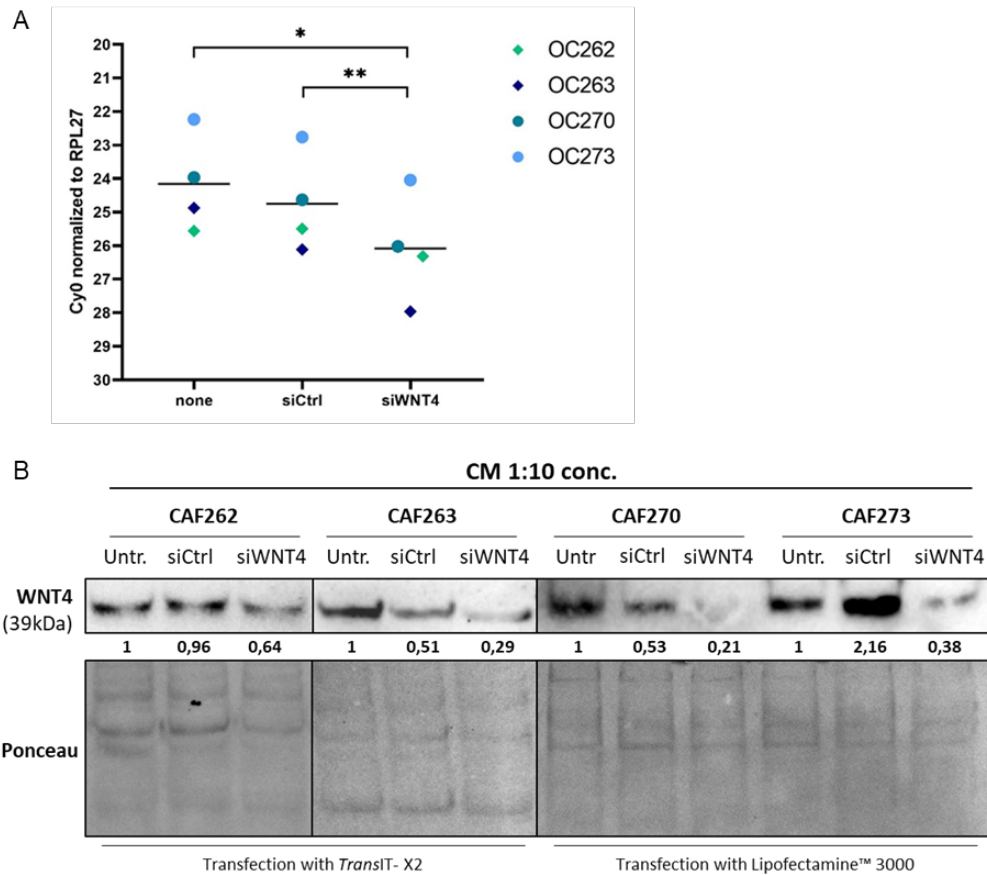


FIGURE S6

Confirmation of siRNA-mediated knockdown of WNT4 expression in CAF from four different patients using two different transfection reagents (CAF262, CAF263: TransIT-X2; CAF270, CAF273: Lipofectamine 3000). **(A)** qRT-PCR analysis of untransfected CAF and CAF transfected with control siRNA or WNT4-directed siRNA. Horizontal bars indicate means. Asterisks indicate p values determined by two-sided, paired t test. *p < 0.05, **p < 0.01. **(B)** Immunoblotting analysis of conditioned medium (CM, 1:10 concentrated) from the same samples as in panel A. Densitometry quantification of WNT4 signals are expressed relative to CM of untransfected CAF. Ponceau red staining demonstrates equal protein loading.

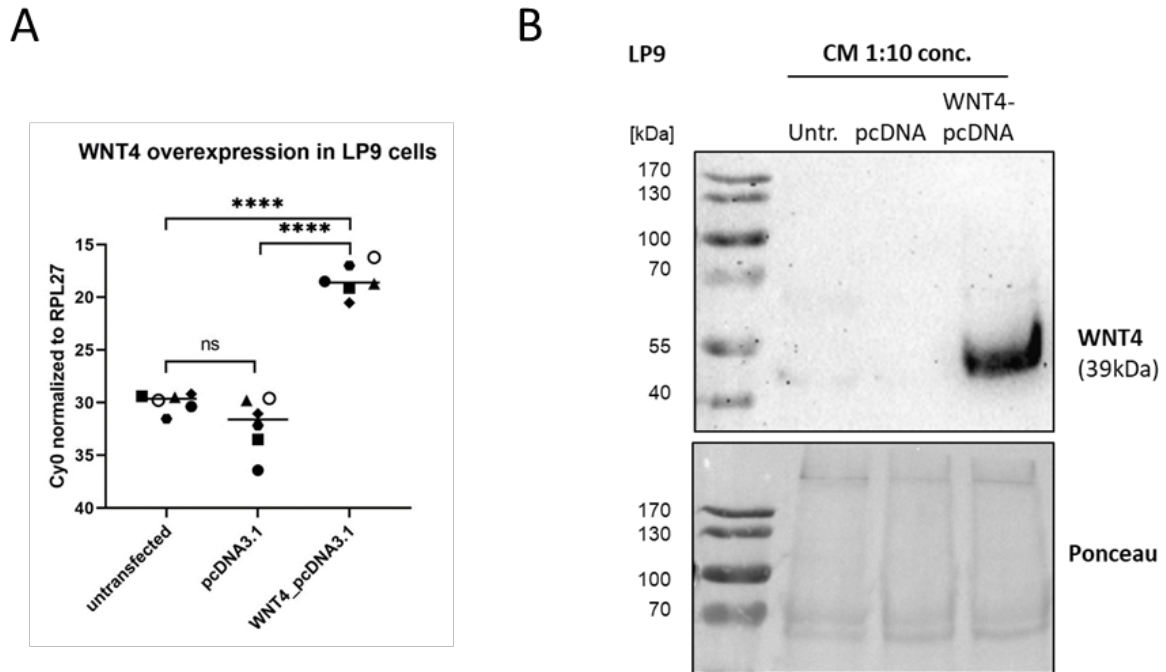


FIGURE S7

Confirmation of WNT4 overexpression in LP9 cells transiently transfected with WNT4-pcDNA. **(A)** Validation of WNT4 expression in LP9 cells by qRT-PCR. Expression was analyzed 48h after transfection with WNT4-pcDNA or pcDNA3.1 control. Untransfected cells were included as additional controls. Data were normalized to *RPL27*. Each data point represents an individual experiment and horizontal bars indicate mean. p values were determined by two-sided, paired t test (****p < 0.0001). **(B)** Representative immunoblot showing WNT4 secretion in conditioned media (CM; 10-fold concentrated) of LP9 cells transfected with WNT4-pcDNA compared to pcDNA3.1 control and untransfected cells. Loading of equal amounts of protein was verified by Ponceau red staining.

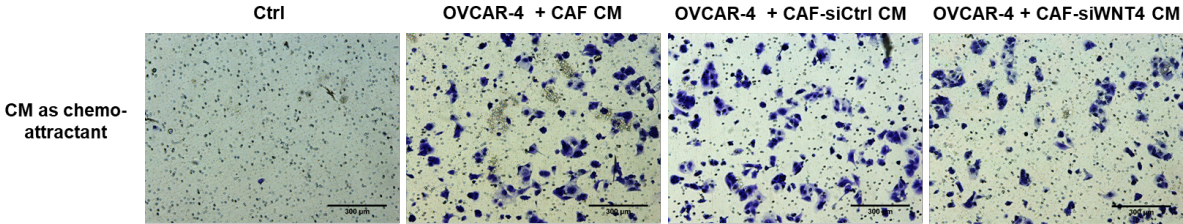


FIGURE S8
Representative microscopic images of migrated OVCAR4 cells in response to CM from untransfected CAF (CAF CM), from control transfected CAF (CAF siCtrl CM) or from siRNA-WNT4 transfected CAF (CAF siWNT4 CM) used as chemoattractant. A background control (Ctrl) of migrating tumor cells in the absence of any chemoattractant is including (left panel).

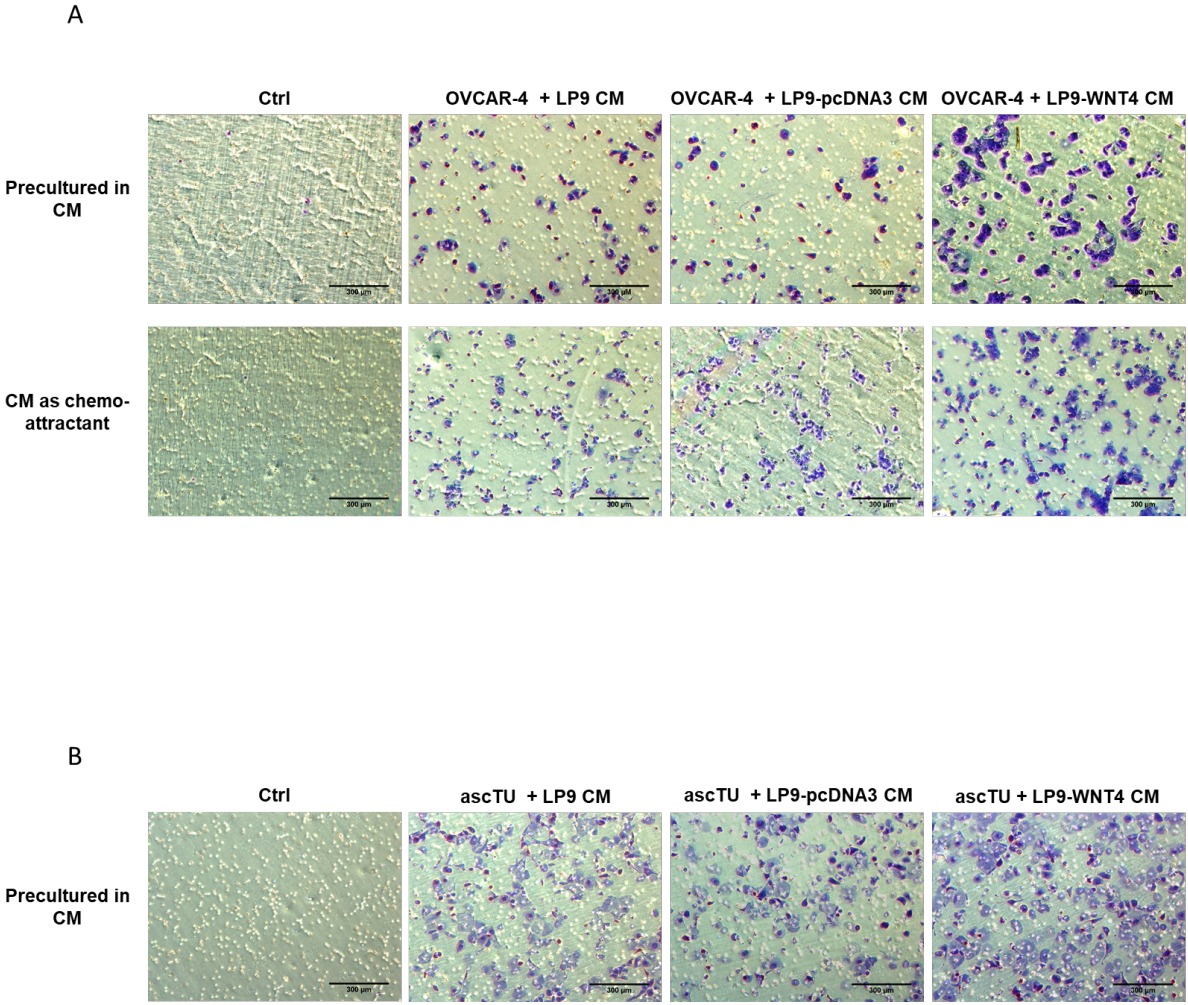


FIGURE S9
Representative microscopic images of migrated OVCAR4 cells (A) and primary ascites-derived HGSC cells (ascTU) (B) in response to WNT4. CM from WNT4-overexpressing, from control-transfected (pcDNA3) or from untransfected LP9 cells were either used as chemoattractant (A) or for preincubation of tumor cells prior to migration towards 10% FCS as the chemoattractant (A and B). A background control (Ctrl) of migrating tumor cells in the absence of any chemoattractant is including (left panel).

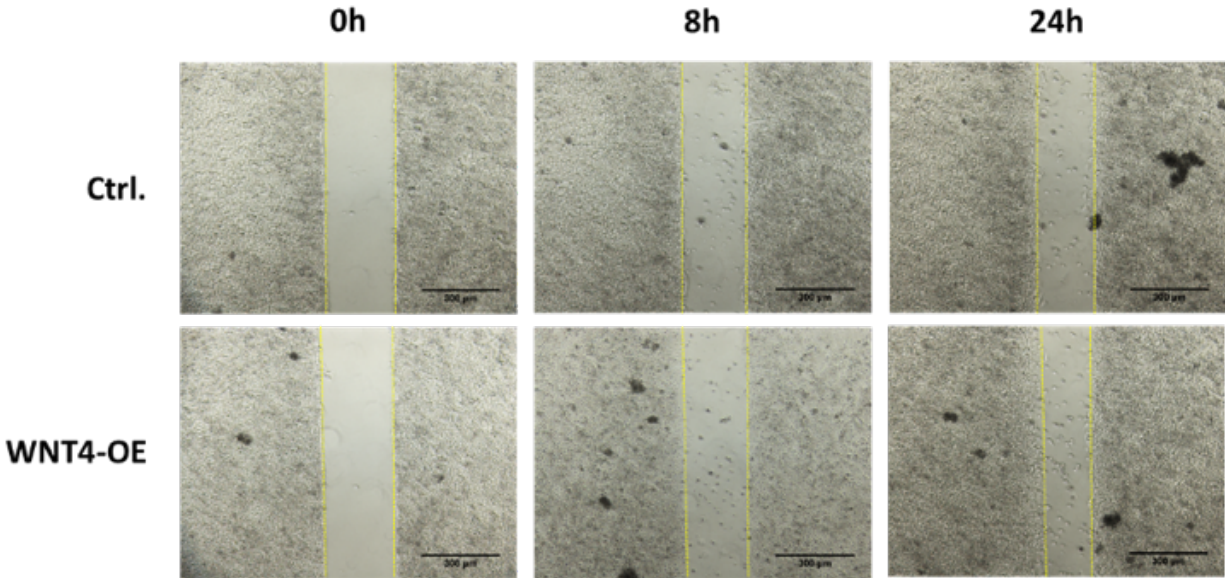


FIGURE S10
Representative microscopic images of wound closure in OVCAR4 monolayers (scratch assay) stimulated by CM of WNT4-overexpressing LP9 cells (WNT-OE) after 0, 8 and 24 hrs. Quantification of wound closure are described in Fig. 5D (n=5).

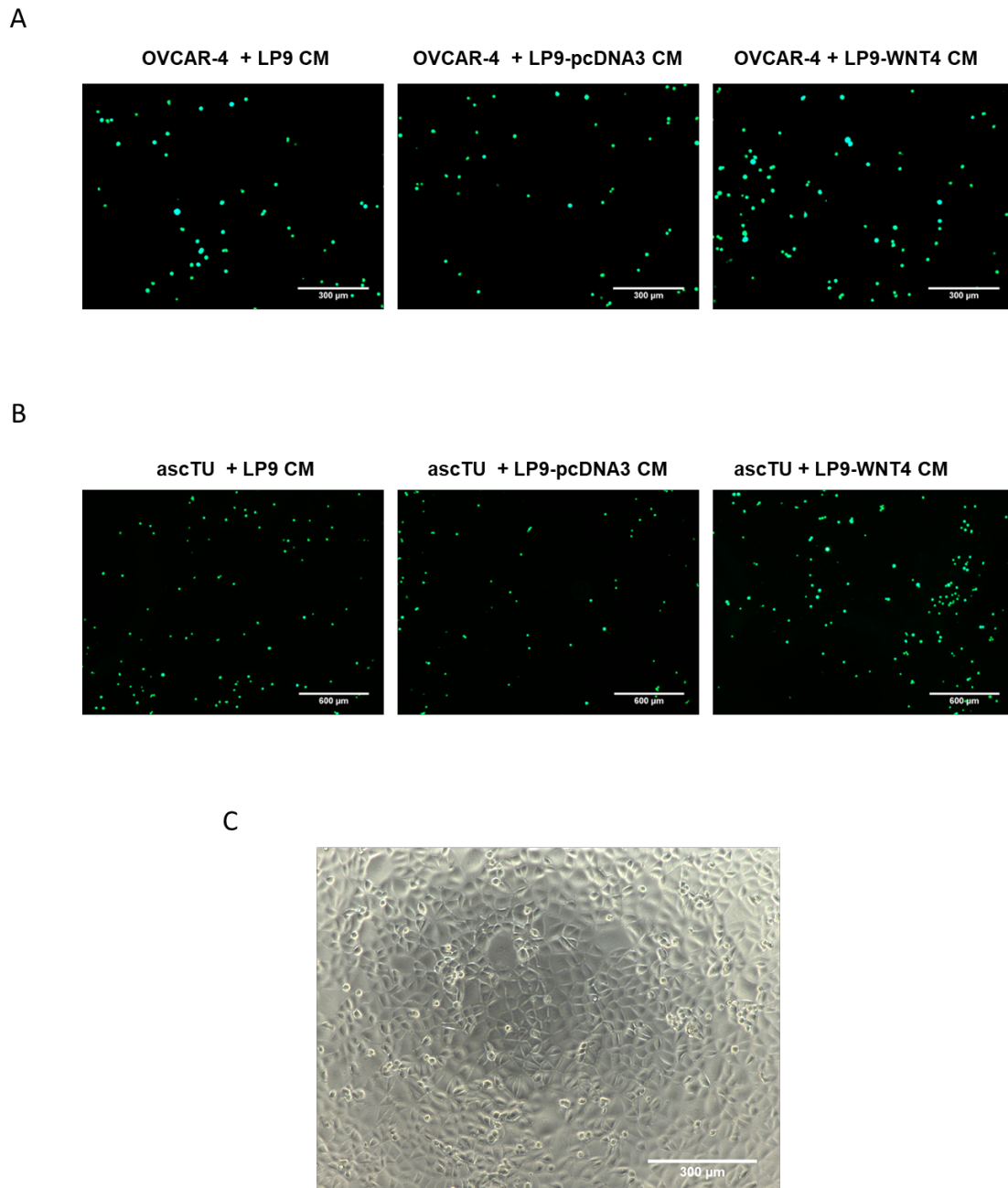


FIGURE S11

Representative images of tumor cell adhesion to a confluent monolayer of peritoneal mesothelial cells (MESO) after stimulation of tumor cells with CM of WNT4-overexpressing, control-transfected (pcDNA3) or untransfected LP9 cells. Adhesion of CellTracker green-labeled OVCAR4 cells (A) and ascites-derived primary HGSC cells (ascTU) (B) is shown after 1h (OVCAR4) or 2h (ascTU) co-culture on a MESO monolayer. (C) Microscopic evaluation of the integrity of the MESO monolayer used for adhesion assays (well of 96-well plate).

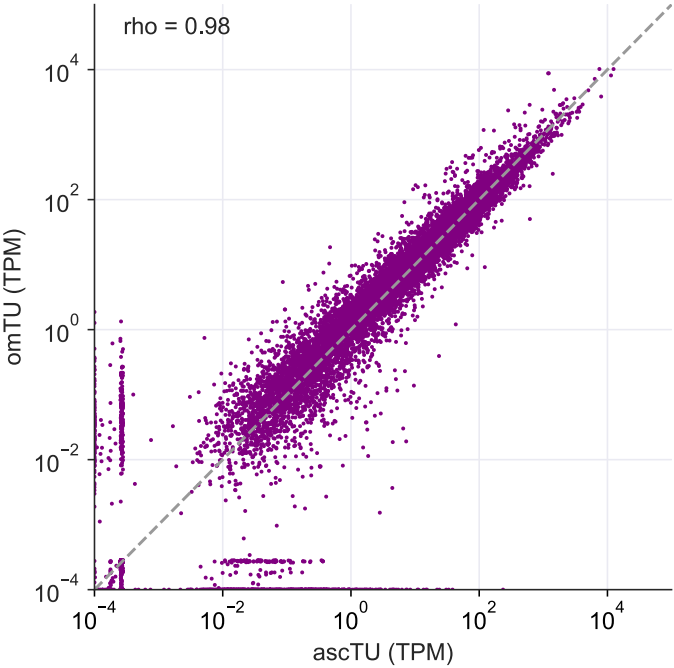


FIGURE S12
Scatter plot showing the correlation of all genes expressed in omTU versus ascTU based on the RNA-Seq data in Table S7 (medians).

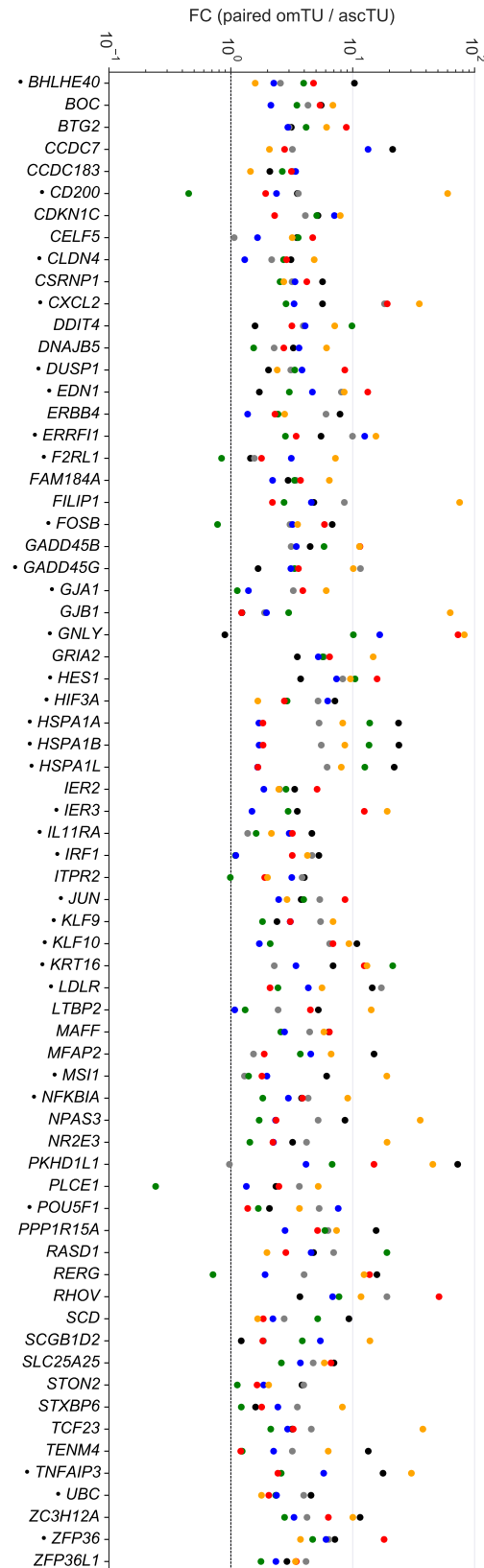


FIGURE S13

Genes upregulated in omTU versus ascTU (RNA-Seq; Table S14) and associated with the term "pro-inflammatory" in the geneCards.org database. Genes also associated with "epithelial differentiation" in the geneCards.org database are marked by dots.

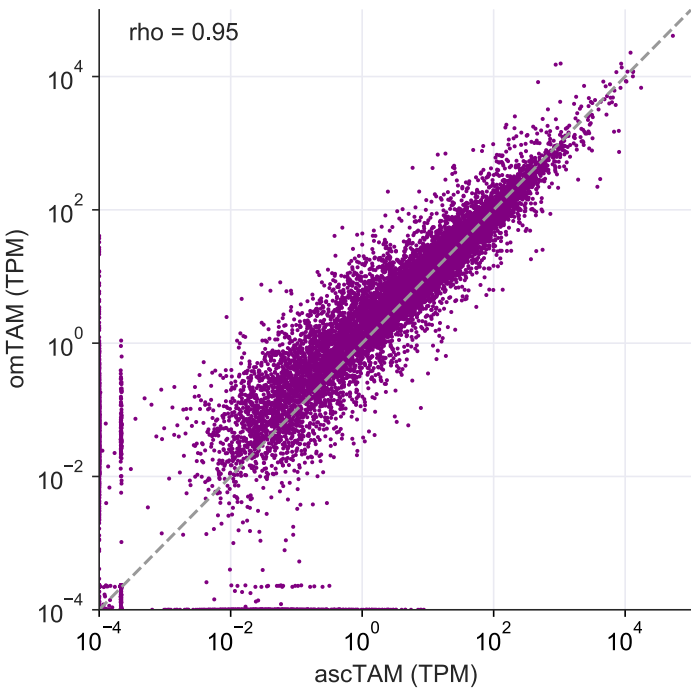


FIGURE S14
Scatter plot showing the correlation of all genes expressed in omTAM versus ascTAM based on the RNA-Seq data in Table S7 (medians).

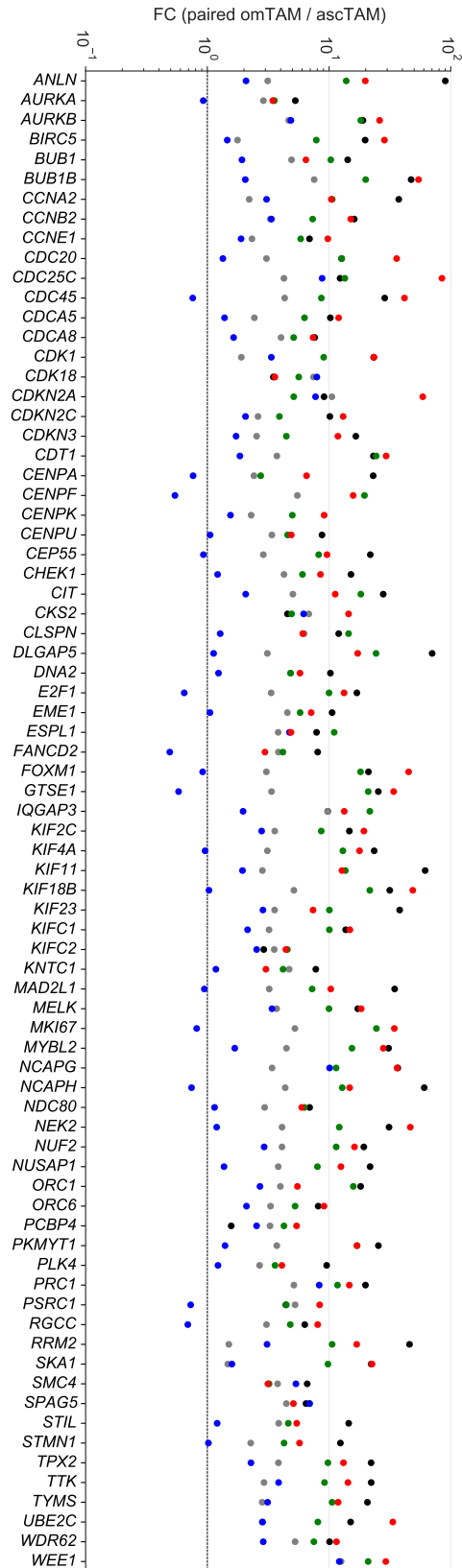


FIGURE S15
Genes upregulated in omTAM versus ascTAM (RNA-Seq; Table S15) and associated with the GO term "mitotic cell cycle process".

Supporting Information (Figures S1-S16): Sommerfeld *et al.*, The intercellular signaling network of ovarian cancer metastases

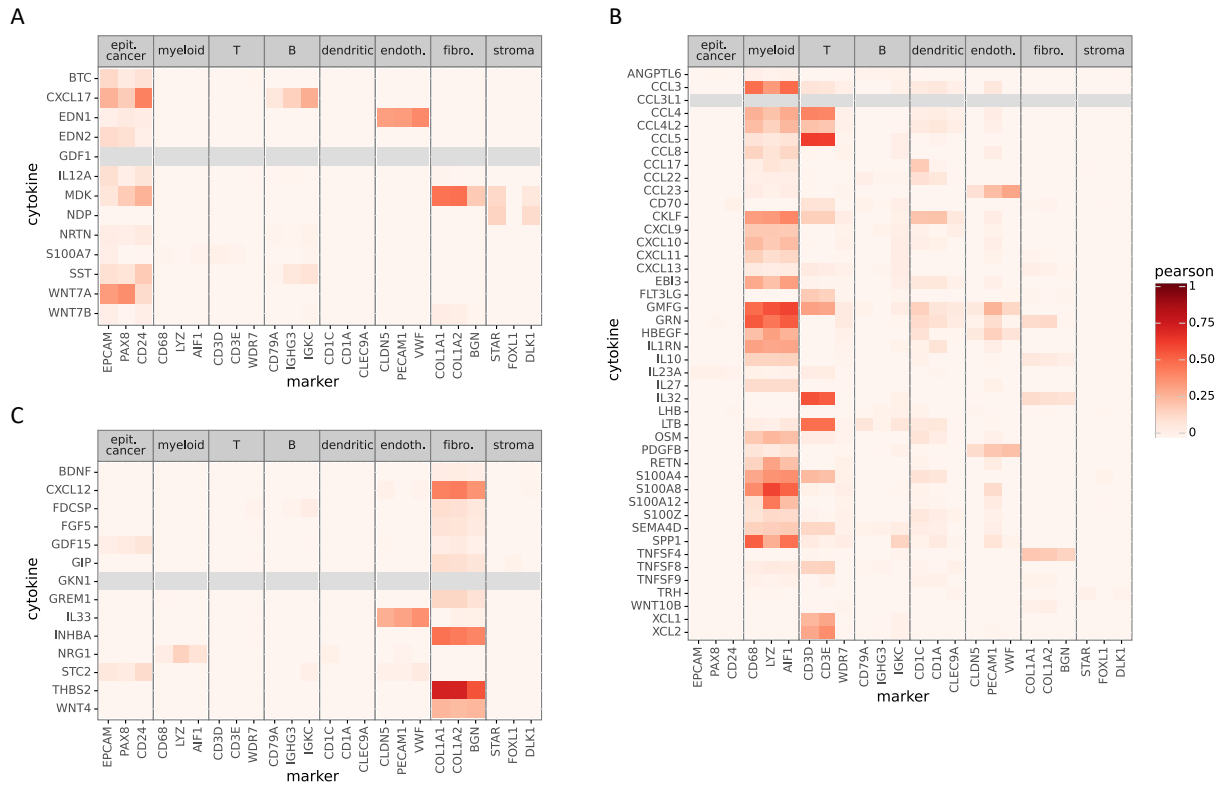


FIGURE S16

Pearson correlation analysis (on single cell gene expression) of cytokine genes expressed by omTU, immune cells or omental CAF in the present study with cell-type-selective marker genes in a published scRNA-Seq dataset for ovarian cancer.

Single cell count matrix data from Olbrecht *et al.* (2021) were processed as described by the authors, and Pearson correlation between cytokine genes identified as cell type specific (present study, Fig. 3) and cell type marker genes from Olbrecht *et al.* (2021) were calculated. Pearson correlation smaller than 0 was clipped to 0. Grey entries signify genes not present in scRNA-Seq dataset.

- (A) Tumor cell specific cytokine group.
- (B) Immune specific cytokine group.
- (C) CAF specific cytokine group.

epit. cancer: epithelial cancer; endoth: endothelial; fibro.: fibroblast; stroma: normal ovarian stroma.

Reference:
 Olbrecht, S, Busschaert, P, *et al.* High-grade serous tubo-ovarian cancer refined with single-cell RNA sequencing: specific cell subtypes influence survival and determine molecular subtype classification. *Genome Med* 2021; 13:111.

Article

Prostacyclin Released by Cancer-Associated Fibroblasts Promotes Immunosuppressive and Pro-Metastatic Macrophage Polarization in the Ovarian Cancer Microenvironment

Leah Sommerfeld ¹, Isabel Knuth ¹, Florian Finkernagel ^{1,2} , Jelena Pesek ³, Wolfgang A. Nockher ³, Julia M. Jansen ⁴, Uwe Wagner ⁴, Andrea Nist ⁵, Thorsten Stiewe ⁵, Sabine Müller-Brüsselbach ¹, Rolf Müller ^{1,*}  and Silke Reinartz ^{1,*}

¹ Translational Oncology Group, Center for Tumor Biology and Immunology (ZTI), Philipps University, 35043 Marburg, Germany

² Bioinformatics Spectrometry Core Facility, Philipps University, 35043 Marburg, Germany

³ Medical Mass Spectrometry Core Facility, Philipps University, 35043 Marburg, Germany

⁴ Clinic for Gynecology, Gynecological Oncology and Gynecological Endocrinology, University Hospital (UKGM), 35043 Marburg, Germany

⁵ Genomics Core Facility, Center for Tumor Biology and Immunology (ZTI), Philipps University, 35043 Marburg, Germany

* Correspondence: rolf.mueller@uni-marburg.de (R.M.); silke.reinartz@uni-marburg.de (S.R.)



Citation: Sommerfeld, L.; Knuth, I.; Finkernagel, F.; Pesek, J.; Nockher, W.A.; Jansen, J.M.; Wagner, U.; Nist, A.; Stiewe, T.; Müller-Brüsselbach, S.; et al. Prostacyclin Released by Cancer-Associated Fibroblasts Promotes Immunosuppressive and Pro-Metastatic Macrophage Polarization in the Ovarian Cancer Microenvironment. *Cancers* **2022**, *14*, 6154. <https://doi.org/10.3390/cancers14246154>

Academic Editor: Fabrizio Fontana

Received: 22 November 2022

Accepted: 10 December 2022

Published: 13 December 2022

Publisher's Note: MDPI stays neutral with regard to jurisdictional claims in published maps and institutional affiliations.



Copyright: © 2022 by the authors. Licensee MDPI, Basel, Switzerland. This article is an open access article distributed under the terms and conditions of the Creative Commons Attribution (CC BY) license (<https://creativecommons.org/licenses/by/4.0/>).

Simple Summary: Reciprocal interactions between tumor and host cells in the tumor microenvironment critically influence the clinical outcome in ovarian carcinoma patients. Therefore, the identification of factors triggering central communication pathways controlling tumor growth and metastasis is highly relevant. This study was conducted to uncover the contribution of lipid mediators to this signaling network by different cell types in the tumor microenvironment and subsequent functional evaluation of clinically relevant candidates. We found that prostacyclin is mainly secreted by cancer-associated fibroblast and selectively acts on prostacyclin receptor-expressing macrophages to induce pro-tumorigenic and immunosuppressive features. Our findings improve the understanding of the tumor-promoting role of prostacyclin in ovarian carcinoma and identify prostacyclin synthesis in cancer-associated fibroblast as a potential target for improved treatment approaches.

Abstract: Metastasis of high-grade ovarian carcinoma (HGSC) is orchestrated by soluble mediators of the tumor microenvironment. Here, we have used transcriptomic profiling to identify lipid-mediated signaling pathways encompassing 41 ligand-synthesizing enzymes and 23 cognate receptors in tumor, immune and stroma cells from HGSC metastases and ascites. Due to its strong association with a poor clinical outcome, prostacyclin (PGI₂) synthase (PTGIS) is of particular interest in this signaling network. PTGIS is highly expressed by cancer-associated fibroblasts (CAF), concomitant with elevated PGI₂ synthesis, whereas tumor-associated macrophages (TAM) exhibit the highest expression of its surface receptor (PTGIR). PTGIR activation by PGI₂ agonists triggered cAMP accumulation and induced a mixed-polarization macrophage phenotype with altered inflammatory gene expression, including *CXCL10* and *IL12A* repression, as well as reduced phagocytic capability. Co-culture experiments provided further evidence for the interaction of CAF with macrophages via PGI₂, as the effect of PGI₂ agonists on phagocytosis was mitigated by cyclooxygenase inhibitors. Furthermore, conditioned medium from PGI₂-agonist-treated TAM promoted tumor adhesion to mesothelial cells and migration in a PTGIR-dependent manner, and PTGIR activation induced the expression of metastasis-associated and pro-angiogenic genes. Taken together, our study identifies a PGI₂/PTGIR-driven crosstalk between CAF, TAM and tumor cells, promoting immune suppression and a pro-metastatic environment.

Keywords: high-grade serous ovarian carcinoma; prostacyclin; carcinoma-associated fibroblasts; tumor-associated macrophages; signaling network; pro-metastatic phenotype

1. Introduction

The dynamic crosstalk between host and tumor cells within the tumor microenvironment (TME) creates a milieu that is beneficial for tumor growth and metastasis. In high-grade serous ovarian carcinoma (HGSC), the transcoelomic spread of tumor cells via the peritoneal fluid (or malignant ascites in advanced stages) to visceral organs, in particular the omentum, is the primary route of peritoneal metastasis, which contributes to the fatal prognosis of this disease. A plethora of different tumor-promoting factors are released by various cell types in ascites, solid tumor and metastases. Among these, not only cytokines and growth factors but also bioactive lipids including lysophosphatidic acids (LPA), arachidonic acid (AA) and other polyunsaturated fatty acids, as well as prostanoids have been associated with pro-tumorigenic functions and clinical outcome [1–6]. Prostanoids are downstream synthesis products of the cyclooxygenase-1/-2 (COX1/2) pathway, which converts AA to prostaglandin H₂ (PGH₂) by COX1 or COX2 followed by the action of prostanoid-specific synthases.

Prostacyclin (PGI₂) is synthesized from PGH₂ by prostaglandin I₂ synthase (PTGIS)—a member of the cytochrome P450 superfamily. Two main signaling pathways have been proposed for PGI₂ which are triggered by binding to cell surface PGI₂ receptor (PTGIR) or by activation of nuclear peroxisome-proliferator-activated receptor β/δ (PPAR β/δ) [7]. PTGIR belongs to the group of G-protein-coupled transmembrane receptors that modulate second messenger systems [8]. Binding of PGI₂ to PTGIR can lead to activation of G_s protein and adenylate cyclase resulting in cAMP production and subsequent PKA activation [9]. Additionally, G_q-dependent PGI₂ signaling through the PKC pathway has been reported for PTGIR [10]. Physiologically, PGI₂ exerts important functions in vascular homeostasis by mediating vasodilative effects and inhibiting platelet aggregation [11]. Moreover, significant anti-inflammatory and anti-fibrotic effects are attributed to PGI₂, but, paradoxically, PGI₂ can also act as a pro-inflammatory mediator [12]. With respect to its role in cancer, the data from previous studies are contradictory. PGI₂ has been described to act as an anti-metastatic mediator in lung cancer mouse models [13,14] and to suppress ovarian cancer cell invasion by MMP2/MMP9 downregulation in vitro [15], whereas other studies reported an association of PTGIS expression with reduced survival of breast and ovarian cancer patients [2,16].

Macrophage polarization is an essential factor accelerating tumor aggressiveness by promoting angiogenesis, immune suppression, tumor migration and invasion [17], thereby providing a potential target for therapeutic intervention. In fact, tumor-associated macrophages (TAM) are prominent members of the HGSC TME, encompassing a broad spectrum of different polarization states with distinct clinically relevant functions [18,19]. For example, TAM exhibiting high expression of the mannose and scavenger receptors CD206 and CD163 are linked to tumor progression and poor clinical outcome [20], while TAM characterized by a transcriptional signature associated with interferon signaling correlates with a favorable clinical course [21].

PGI₂ appears to be able to regulate the innate and acquired immune response. Thus, it has been reported that forced PTGIS expression promoted an alternative activation of macrophages, which in turn alleviated the inflammatory response in alcohol-induced liver injury [22]. In another study, PGI₂ analogs inhibited bacterial killing and phagocytosis by rodent macrophages, closely resembling prostaglandin E₂ (PGE₂)-mediated effects [23].

In the present study, we performed a comparative transcriptomic analysis of different cell types of the HGSC TME, and identified cancer-associated fibroblasts (CAF) as a central cellular source of PGI₂ synthesis, while the highest expression of the cognate receptor PTGIR was found in ascites-derived TAM (ascTAM). We therefore postulated that CAF-derived PGI₂ targets PTGIR expressing TAM, thereby altering macrophage polarization and modulating their pro-tumorigenic potential. As described below we performed various biochemical, immunological and cell-based functional assays, which confirmed this hypothesis. Elucidating the contribution of PGI₂ in CAF–TAM crosstalk to promote

immune suppression, tumor growth and metastasis of HGSC, may pave the way for the development of novel therapeutic regimens.

2. Materials and Methods

2.1. Patient Samples and Isolation of Cell Types

Ascites and greater omentum tissue with metastatic lesions were collected from patients with ovarian carcinoma undergoing primary surgery at the University Hospital in Marburg. The collection and analysis of human material were approved by the ethics committee at Philipps University (reference number 205/10). Donors provided written consent in accordance with the Declaration of Helsinki. A summary of the patient characteristics is given in Supplementary Table S1. The isolation of tumor cells, TAM and tumor-associated T cells (ascTU, ascTAM, ascTAT) from ascites was performed by density gradient centrifugation followed by filtration using 30 μm and 100 μm cell strainer and magnetic cell sorting (MACS; Miltenyi Biotec, Bergisch Gladbach, Germany) as previously described [2,20]. Cell populations with a purity of >95%, as determined by flow cytometry, were either used directly for subsequent analysis or cryopreserved. Cell-free ascites was cryopreserved at $-80\text{ }^{\circ}\text{C}$. Separation of host and tumor cells from the omentum was conducted essentially according to Sommerfeld et al. [24]. Briefly, ADI were isolated from omentum tissue without macroscopic metastatic lesions by digestion with 370 U/mL collagenase (Sigma Aldrich, Taufkirchen, Germany) in adipocyte digestion buffer (5 mM D-Glucose, 1.5% BSA in PBS for 1 h at $37\text{ }^{\circ}\text{C}$). ADI were further enriched by filtration (400 μm filter) and centrifugation (5 min, $150\times g$). Contaminating cells were eliminated from the floating ADI layer by washing with PBS, which yields highly pure ADI fractions (>95%) used for secretome cultures or for preparation of lysates in PeqGold TriFastTM (Peqlab, Erlangen, Germany) for RNA isolation. Isolation of MESO was achieved from the tumor-free tissue by incubation with trypsin (0.05% Trypsin/0.02% EDTA for 30 min at $37\text{ }^{\circ}\text{C}$) followed by filtration (100 μm filter) and centrifugation (10 min at $300\times g$). Omental tumor cells (omTU), CAF and omental TAM (omTAM) were separated from omental tumor tissue by trypsin digestion (2 h at $37\text{ }^{\circ}\text{C}$). For CAF isolation, the trypsin-digested tissue was further incubated with 18.5 U/mL collagenase and 2.5 $\mu\text{g}/\text{mL}$ hyaluronidase (Sigma Aldrich) in fibroblast culture medium (DMEM/HAMs F12 (1:1), 10% FCS, 10 ng/mL EGF, 1% Pen/Strep) overnight at $37\text{ }^{\circ}\text{C}$. Different MACS sorting strategies were applied to further purify omTU, omTAM, MESO and CAF: MACS depletion of CD45⁺ leucocytes combined with EpCAM positive selection was performed to yield highly pure omTU. omTAM were purified from tumor fractions by CD14⁺ positive MACS selection. CAF enriched fractions were initially precultured in fibroblast medium before CD45⁺ leucocytes and EpCAM⁺ tumor cells were depleted by <MACS. In some cases CAF were enriched by positive selection with anti-fibroblast beads (Miltenyi Biotec). CD45 and EpCAM depletion by MACS were likewise applied to purify MESO after trypsin digestion of macroscopic tumor-free omentum tissue. RNA was obtained from all cell types without further cultivation, except for CAF which were maintained in OCMI medium supplemented with 50% ascites for maximum three passages [1].

2.2. Differentiation of Monocyte-Derived Macrophages (MDM) from Healthy Donors

Leucoreduction system chambers from healthy adult volunteers were kindly provided by the Center for Transfusion Medicine and Hemotherapy at the University Hospital Gießen and Marburg. Monocytes were isolated by Ficoll density gradient centrifugation and subsequent purification by adherence selection or using CD14⁺ MACS microbeads. Differentiation of monocytes was performed as described previously [25]. Approximately 3×10^6 monocytes per 6-well were either cultured for 7 days in cell-free ascites pool derived from 10 patients to generate TAM-like asc-MDM. For m1-MDM, monocytes were differentiated in RPMI1640 (Life Technologies, Darmstadt, Germany) supplemented with 5% human AB serum (Sigma Aldrich), 1% sodium pyruvate (Sigma Aldrich), and 100 ng/mL granulocyte macrophage colony-stimulating factor (CSF) (Peprotech, Hamburg,

Germany) for 5 days followed by activation with 100 ng/mL LPS (Sigma Aldrich) and 20 ng/mL IFN γ (Biozol, Echingen, Germany) for 2 days. M0 MDM were generated according to m1-MDM but omitting the final LPS/IFN γ stimulation step.

2.3. Primary Cell Culture and Preparation of Conditioned Media for Lipid-MS

CAF were cultured in 6-well plates in OCMI/50% ascites pool. For ex vivo ascTAM, 3×10^6 cells from frozen stocks were plated per 6-well in ascites pool for 5–7 days before used for further experiments. Primary ascTU (7.5×10^5 /6 well) were cultured for 24 h in ascites pool. In order to obtain conditioned media (CM) for lipidomics, cultures at 70–80% confluency were washed twice with PBS and twice with serum-free OCMI basal medium (M199/DMEM F12 1:1) before 760 μ L serum-free OCMI basal medium +/- 50 μ M arachidonic acid (AA) (Cayman Chemicals, Hamburg, Germany) was added. 1 μ M COX1 inhibitor SC-560 (Cayman Chemicals) and 10 μ M COX2 inhibitor celecoxib (Tocris Bioscience, Bristol, UK) were included where indicated. After 24 h, cell-free CM were harvested from each cell type for lipidomic analysis.

2.4. Treatment of Cells with PGI $_2$ Analogs

asc-MDM, ascTAM, ascTU or CAF were serum-deprived for 24 h in serum-free OCMI basal medium prior to stimulation with PGI $_2$ analog MRE-269 (selexipag-active metabolite, Cayman Chemicals), Iloprost or Treprostinil (both Sigma Aldrich) for the indicated time points and concentrations. We have chosen these analogs due to different affinities to PTGIR and prostaglandin receptors, with MRE-269 as the most specific for PTGIR [26]. In individual experiments, cells were pretreated with 1 μ M PTGIR antagonist CAY10449 or CAY10441 (both Cayman Chemicals) for 1 h before addition of PGI $_2$ analog. PPAR β/δ agonist L165041 (Biozol) was applied at 1 μ M concentrations where indicated. For generation of CM, asc-MDM or ex vivo TAM were stimulated with PGI $_2$ analog under serum-free conditions for 0 or 24 h, 37 $^{\circ}$ C, 5% CO $_2$.

2.5. Co-Cultivation of Asc-MDM and CAF

Co-culture experiments were performed to evaluate the effect of CAF-derived PGI $_2$ on biological features of asc-MDM. Therefore, asc-MDM were differentiated in ascites pool in 24 well plate and CAF were cultured separately on top of a 24 transwell insert with 4 μ m pore size (BD Biosciences, Heidelberg, Germany) in OCMI/50% ascites pool until confluency was reached. After replacing the culture medium by serum free DMEM/M199 medium supplemented with 50 μ M AA as a substrate for PGI $_2$ biosynthesis, the transwell inserts were placed inside the wells containing the asc-MDMs. Co-culture was conducted in the presence or absence of COX1 and COX2 inhibitors SC-560 (1 μ M) and celecoxib (10 μ M) for 24 h, 37 $^{\circ}$ C. Additional controls include similarly treated asc-MDM without CAF co-culture.

2.6. Quantification 6k-PGF $_{1\alpha}$ and PGE $_2$ by Lipid-MS

6k-PGF $_{1\alpha}$ and PGE $_2$ in CM of ascTAM, ascTU and CAF were quantified as described previously [27] with slight modifications. Samples (1 mL) were spiked with 100 μ L internal standard (PGE $_2$ -d4 and 6k-PGF $_{1\alpha}$ -d4, each 9.8 ng/mL) in methanol and extracted using solid reverse phase extraction columns (Bond Elut Plexa, Agilent, Santa Clara, CA, USA). After elution and lyophilization, samples were resuspended in water/acetonitrile (70:30) with 0.02% formic acid (solvent A). Analysis was performed by LC-MS/MS on an Agilent 1290 device coupled to a QTrap 5500 mass spectrometer (AB Sciex, Darmstadt, Germany). Samples were separated at a flow rate of 0.3 mL/min on a Synergi reverse-phase C18 column (2.1 \times 250 mm; Phenomenex, Aschaffenburg, Germany) using the following gradient: 1 min (0% solvent B: acetonitrile/isopropyl alcohol, 50:50, v/v), 3 min (25% B), 11 min (45% B), 13 min (60% B), 18 min (75% B), 18.5 min (90% B), 20 min (90% B), 21 min (0% B), 26 min (0% B). 6k-PGF $_{1\alpha}$ and PGE $_2$ were detected in scheduled multiple reaction monitoring mode (transitions: PGE $_2$ 351 \rightarrow 271, PGE $_2$ -d4 355 \rightarrow 275, 6k-PGF $_{1\alpha}$ 369 \rightarrow 163,

6k-PGF_{1α}-d4 373 → 167). For quantification, a 11-point calibration curve was used (0.06–60 ng/mL). Data analysis was performed using Analyst 1.7.2 and MultiQuant 2.1.1 (AB Sciex, Darmstadt, Germany).

2.7. Flow Cytometric Analysis of Cell Phenotypes

Flow cytometric phenotyping of ascites and omentum cells was performed on a FACS Canto II instrument using Diva Software (BD Biosciences, Heidelberg, Germany) and analysis by FlowJo™ v10.8 Software (BD Life Sciences, Ashland, OR, USA) as already described [24]. Briefly, tumor cells were stained with anti-human EpCAM-Vioblue (Miltenyi Biotec), TAM with anti-human CD14-FITC (Miltenyi Biotec, Bergisch Gladbach, Germany) and TAT with anti-human CD3-APC (Biolegend, Koblenz, Germany). The following antibody combinations were used to characterize MESO and CAF: anti-human CD140a-PE (eBioscience/Thermo Fisher Scientific, San Diego, CA, USA), anti-human FAP-PE (R&D Systems, Minneapolis, MN, USA), anti-human mesothelin-APC (R&D Systems, Minneapolis, MN, USA), anti-EpCAM-Vioblue for surface staining and anti-human cytokeratin-APC and anti-human vimentin-FITC (both from Miltenyi Biotec, Bergisch Gladbach, Germany) for intracellular staining.

Surface expression of CD86 and CD206 in CD14+ MDM was determined using established staining protocols [19] with anti-human CD14-FITC, CD86-FITC (both from Miltenyi Biotec), and CD206-APC (Biolegend, Koblenz, Germany). Isotype controls were derived from BD Biosciences, Miltenyi Biotec and eBioscience.

The analysis of PTGIR surface expression in different cell types was performed using anti-PTGIR antibody (ab196653; Abcam, Cambridge, UK) for 1 h, 4 °C, followed by detection with anti-rabbit-FITC secondary antibody (eBioscience, San Diego, CA, USA) for 30 min at 4 °C. Results were calculated as percentage of positive cells and mean fluorescence intensity (MFI).

2.8. Macropinocytosis Assay

To determine the phagocytic capacity of MDM and ascTAM pretreated with or without PGI₂ analogs (30 min, 37 °C) or derived from CAF co-culture experiments, 0.5 mg/mL FITC-Dextran (70 kDa, Sigma Aldrich, Taufkirchen, Germany) was added to macrophages under standard culture conditions for 1 h at 37 °C. Incubation of cells for 1 h at 4 °C was included as negative control for detection of FITC dextran binding. Cells were then washed three times and analyzed by flow cytometry. The MFI of each sample was calculated and the value of the corresponding FITC dextran binding control was subtracted. To verify PTGIR signaling, macrophages were treated with PTGIR antagonist CAY10449 prior to stimulation with PGI₂ analog in additional experiments or with PPARβ/δ agonist L165 alone.

2.9. cAMP Assay

The intracellular accumulation of cAMP upon stimulation by PGI₂ analogs was measured in different cell types using a commercial competitive cAMP parameter assay kit (R&D Systems, Minneapolis, MN, USA). Therefore, m1-MDM, asc-MDM, ascTAM, ascTU and CAF cultured on a 6 well plate were serum-starved for 24 h before adding 0.1 mM phosphodiesterase (PDE) inhibitor isobutylmethylxanthine (IBMX) for 15 min to block inactivation of cAMP. The cells were then stimulated with MRE-269, Iloprost or Treprostinil for 15 min. A pre-incubation with PTGIR antagonist CAY10449 (1 μM) for 1 h was included where indicated. After treatment, cells were washed in cold PBS and lysed in 250 μL lysis buffer. The assay was performed with frozen cell lysates in duplicates according to the manufacturer's instructions.

2.10. Tumor Cell Migration Assay

The effect of soluble mediators secreted by ascTAM after stimulation with PGI₂ analog MRE-269 on tumor migration was evaluated in a Transwell assay format using primary ascTU cells, which lacks PTGIR surface expression [24]. Briefly, CellTracker green CMFAD-

labelled ascTU were preincubated with 1:3 diluted CM of MRE-269-stimulated ascTAM for 24 h at 37 °C and 5% CO₂ before tumor cell migration was measured in a Transwell system using 10% FCS as chemoattractant for 24 h. CM derived from untreated or PPAR β/δ agonist L165 treated ascTAM as well as from ascTAM stimulated with MRE-269 in the presence of PTGIR antagonist CAY10449 (1 μ M) were used as additional controls. Migrated cells were stained with crystal violet (0.2% in 20% methanol, 1:5 dilution) for 10 min and evaluated under a Leica DMI3000B microscope (Leica, Wetzlar, Germany). Migrating tumor cells were counted in >7 visual fields per filter using the ImageJ software (version 1.52n/1.8.0_201, Bethesda, MD, USA).

2.11. Tumor Cell Attachment to Mesothelial Cells

To determine the influence of the secretome of PGI₂ analog-treated ascTAM on tumor cell adherence to mesothelial layer, we conducted an attachment assay as previously described [24]. Briefly, a confluent monolayer of omentum-derived MESO was generated on collagen-I-coated (5 μ g/cm²; Gibco/Thermo Fisher Scientific, Waltham, MA, USA) 96-well plates by culturing in OCMI/5% FCS. MESO confluency was evaluated by microscopic imaging (Supplementary Figure S1). After preincubation of primary ascTU with 1:3 diluted CM of stimulated ascTAM for 24 h and labeling with CellTracker green CMFDA (Invitrogen/Thermo Fisher Scientific, Carlsbad, CA, USA), ascTU were applied to the MESO monolayer (2 h at 37 °C). Controls were included as described for the tumor migration assays. Tumor cell adhesion was detected by microscopic evaluation of 9 visual fields per preparation (DMI3000B fluorescence microscope; Leica, Wetzlar, Germany) and subsequent counting using the ImageJ software.

2.12. VEGF-A Quantification by ELISA

VEGF-A levels in CM of ascTAM or asc-MDM stimulated with PGI₂ analog or solvent control (DMSO) were quantified by ELISA (Human VEGF DuoSet ELISA, R&D Systems) according to the manufacturer's instructions.

2.13. Transient PTGIR Knockdown in ascTAM and Asc-MDM by RNA Interference

To verify the specificity of PTGIR surface staining, siRNA transfection was performed in ascTAM or MDM differentiated in ascites (asc-MDM) with lipofectamine 3000 (Invitrogen, Thermo Fisher Scientific, Carlsbad, CA, USA) as described by the manufacturer. siPTGIR ONTarget plus smartpool from Dharmacon (Horizon Discovery, Cambridge, UK) and MISSION siRNA Universal Negative Control # 2 (Sigma Aldrich) were included as control siRNA. Additional controls were untransfected ascTAM or asc-MDM. RNA and protein expression was analyzed in cells 48 h after transfection.

2.14. Immunoblotting

The following antibodies were used for staining of immunoblots according to established protocols: α -GAPDH polyclonal antibody (Sigma-Aldrich, Cat# G9545), α - β -actin monoclonal antibody (Sigma-Aldrich, Cat# A5441), α -hPTGIR (Abcam, Cat# ab196653), α -hPTGIS (R&D Systems, Cat# MAB7788), α -rabbit IgG HRP-linked polyclonal antibody (Cell Signaling Technology, Cat# 7074), and α -mouse IgG HRP-linked polyclonal antibody (Cell Signaling Technology, Cat# 7076). Blots were imaged and quantified using the ChemiDoc MP system and Image Lab software version 5 (Bio-Rad, Feldkirchen, Germany).

2.15. RT-qPCR

cDNA isolation and RT-qPCR analyses were performed as described [2,28] using RPL27 for normalization. Raw data were evaluated by the Cy0 method [29]. Primer sequences are listed in Supplementary Table S2.

2.16. RNA Sequencing

RNA-Seq datasets for ascites cells (ascTAM, ascTU, ascTAT) and omental cells (omTAM, omTU, CAF, MESO, ADI) were retrieved from Sommerfeld et al. [24] and used for Figure 1, Supplementary Figure S2 and Supplementary Tables S3–S5 (accession numbers E-MTAB-3167, E-MTAB-4162, E-MTAB-10611). MDM, ascTAM and CAF were treated with 1 μM MRE-269 or solvent control (DMSO) for 5 h and total RNA was isolated using the NucleoSpin RNA II kit (Macherey-Nagel, Düren, Germany). RNA-Seq was carried out on by Novogene (Cambridge, UK; full-length ligation based protocol on mRNA enriched using poly-T oligo magnetic beads; datasets used for Supplementary Tables S6–S9), or on an Illumina NextSeq 550 using “QuantSeq 3’ mRNA-Seq Library Prep Kit FWD for Illumina” (Lexogen, Vienna, Austria) for library preparation (datasets used for Supplementary Table S10). RNA-Seq data were deposited at EBI ArrayExpress (accession numbers E-MTAB-12437 and E-MTAB-12441) and processed as described previously [2,20] using Ensembl 96 [30]. Only protein-coding genes were considered for further analyses.

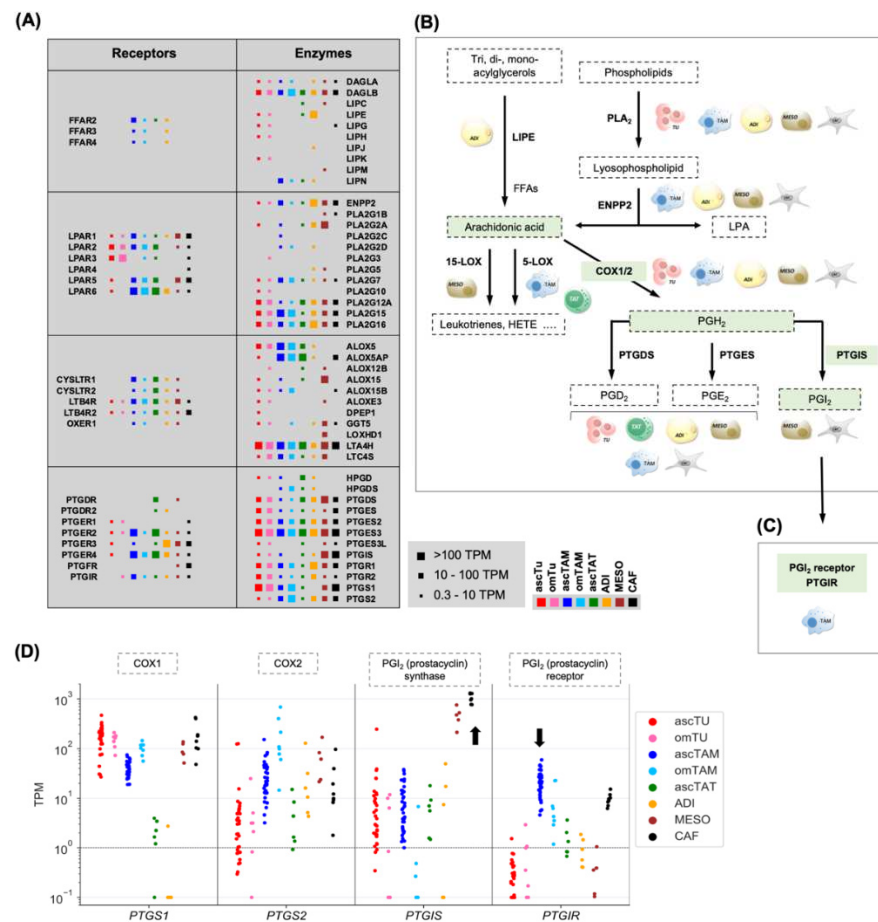


Figure 1. Cell-type-selective biosynthesis of lipid mediators and their targets in the omental TME. (A) Schematic representation of expression patterns of genes coding for key enzymes involved in lipid mediator synthesis or encoding lipid receptors in 8 different cell types as indicated (red: ascTU; pink: omTU; blue: ascTAM; cyan: omTAM; green: ascTAT; yellow: adipocytes; brown: mesothelial cells; black: CAFs after short-term culture in the presence of ascites). The sizes of the filled squares indicate the level of expression determined by RNA-Seq (high: median TPM > 100; intermediate: median TPM 10–100; low: median TPM 0.3–10). ENPP: autotaxin; FFAs: free fatty acids; LIPE: lipase E; LPA: lysophosphatidic acid; PLA₂: phospholipase A₂; PTG: prostaglandin; PGI₂: prostacyclin. (B) Schematic summary of cell-type-selective steps in the biosynthesis of lipid mediators. The AA-PGH₂-PGI₂ pathways driven by COX1/2 and PTGIS is highlighted as green (C) PGI₂ receptor (PTGIR). (D) Dot plots showing TPM for COX1, COX2, PGI₂ (prostacyclin) synthase, and PGI₂ (prostacyclin) receptor across cell types. Legend: ascTU (red), omTU (pink), ascTAM (blue), omTAM (cyan), ascTAT (green), ADI (yellow), MESO (brown), CAF (black).

shaded areas. (C) Cell-type-selectivity of PGI₂ receptor gene (*PTGIR*) expression. (D) Expression of genes involved in PGI₂/prostacyclin synthesis (*PTGS1*, *PTGS2*, *PTGIS*) and signaling (*PTGIR*) based on RNA-Seq data. Protein names are shown at the top. The same samples as in Figure 1A were analyzed. The arrows indicate the selective expression of *PTGIS* in CAF and MESO, and the elevated expression of *PTGIR* in ascTAM.

2.17. Statistical Analysis

Statistical evaluation of RNA-Seq data paired on donor was performed with EdgeR [31]. Paired or unpaired Student's *t*-test (two-sided, unequal variance) was used for comparative analysis of all other data and indicated in the figure legends. Results were expressed as follows: * $p < 0.05$; ** $p < 0.01$; *** $p < 0.001$; **** $p < 0.0001$. Box plots were constructed using Matplotlib. Functional annotation of regulated genes identified by RNA-Seq was performed using the online tool of ConsensusPathDB [32], which uses 32 different public repositories for data analysis (<http://consensuspathdb.org>; accessed on 7 November 2022). Progression-free survival data for HGSC patients were obtained from the Kaplan–Meier Plotter meta-analysis database (version 06/2020 with data for 2.190 OC patients) [33]. Associations with overall survival (OS) were derived from the PRECOG database [34].

3. Results

3.1. A Crucial Role for Tumor-Associated Host Cells in Lipid-Mediated Signaling

We first analyzed our previously published RNA-Seq dataset [24] to identify cell types in ascites [ascTAM, T cells (ascTAT), ascTU] or in omental metastasis [omTU, omTAM, adipocytes (ADI), mesothelial cells (MESO), CAF] involved in the generation of lipid mediators, i.e., expressing key enzymes required for their biosynthesis (Supplementary Table S3).

As illustrated by the data in Figure 1A, Supplementary Table S4, and the schematic summary in Figure 1B, some steps of the biosynthetic pathways were clearly cell-type-selective, including the cleavage of acylglycerols by LIPE (lipase E) from ADI, the generation of LPA by ENPP2 (autotaxin) from stromal cells, the synthesis of lipoxygenase products by TAM (ALOX5) and MESO (ALOX15) and the production of PGI₂ by MESO and CAF (*PTGIS*), while other steps are catalyzed by enzymes in several cell types, albeit with some isoform selectivity.

Some lipid mediators also target selective membrane receptors, such as the free fatty acids receptors *FFAR2/3/4* expressed by TAM and ADI, and the PTGI₂ receptor *PTGIR* predominantly by ascTAM (Figure 1A,C; Supplementary Figure S2; Supplementary Table S5). Since *PTGIS* synthesis is also cell-type-selective as alluded to above, the PGI₂—*PTGIR* pathway seems to be of particular interest with respect to intercellular communication. This is documented in detail in Figure 1D, showing a low median expression of *PTGIS* by all cell types except for MESO and CAF, and the highest expression of *PTGIR* in ascTAM followed by CAF. The data also indicate that *PTGS1* is expressed at high levels in MESO and CAF (and to a lower extent *PTGS2*), which is relevant as cyclooxygenases generate the *PTGIS* substrate (PGH₂) from arachidonic acid (AA). Both consecutively acting enzymes, *PTGS1* and *PTGIS*, are highly expressed in MESO and CAF, suggesting an efficient production of PGI₂ by these cell types. The COX/*PTGIS*-driven synthetic pathway AA—PGH₂—PGI₂ is highlighted in Figure 1B (green boxes).

The potential relevance of this signaling pathway is underlined by the association between *PTGIS* expression in tumor tissue and progression-free survival (PFS) of HGSC patients (KM plotter database [33]: logrank $p = 0.00016$, HR = 1.33; Supplementary Figure S3). Furthermore, PRECOG [34] data analysis of overall survival across different cancer entities revealed an association of high *PTGIS* expression with a short survival for HGSC (z-score: 1.99), whereas opposite associations (z-score < 0) were found for other entities (Figure 2A), pointing to a tumor-type-selective adverse effect in HGSC.

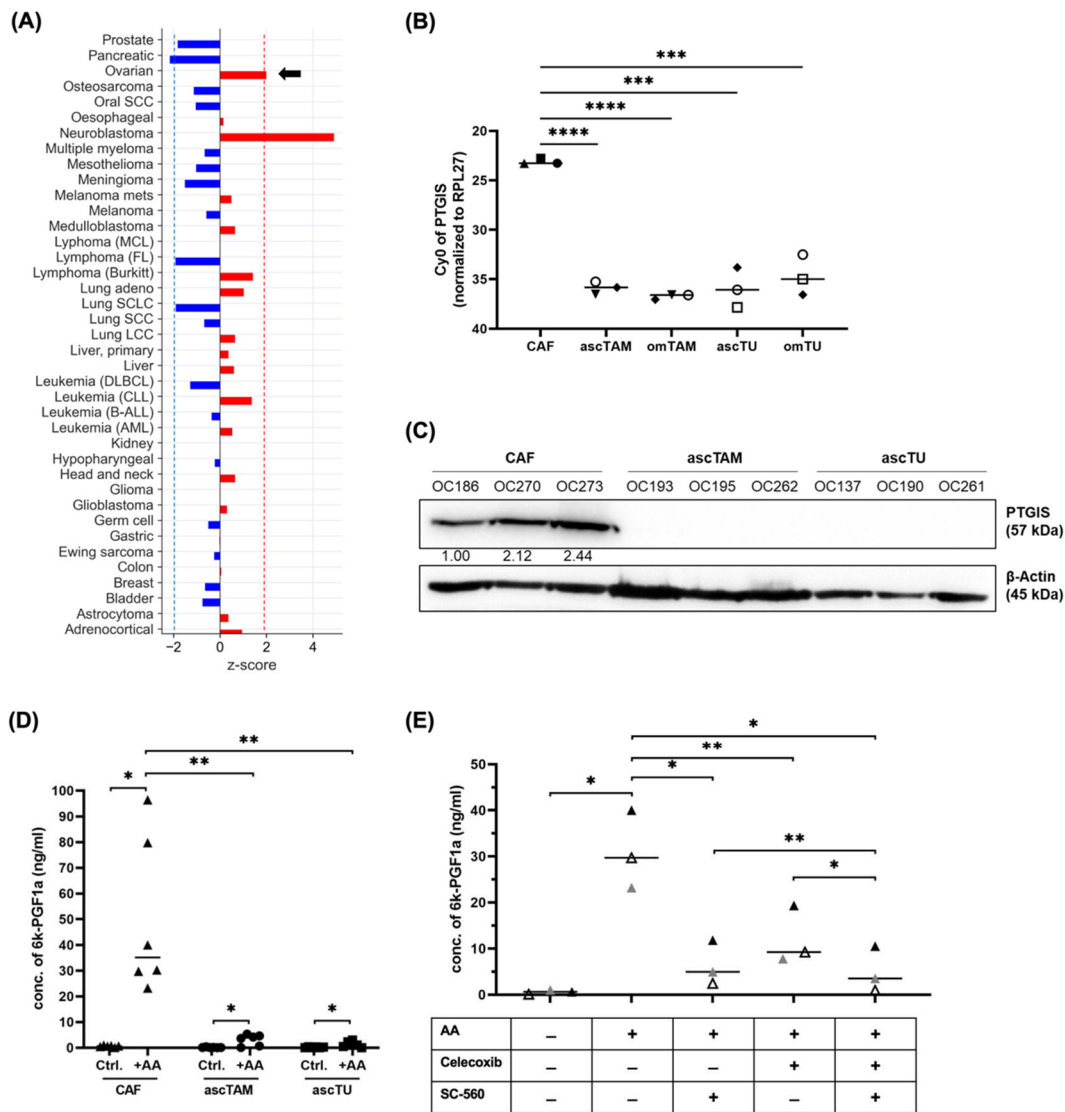


Figure 2. Validation of cell-type-selective PTGIS expression and PGI₂ synthesis. **(A)** Association of PTGIS expression with overall survival (OS) for different cancer entities based on the PRECOG database [34]. Red: positive z-scores (hazard ratio > 1); blue: negative z-scores (hazard ratio < 1). A z-score of |1.96| equals a p value of 0.05. Significance thresholds are indicated by dashed blue and red lines. **(B)** RT-qPCR analysis of PTGIS mRNA expression in CAF, TAM (ascTAM, omTAM) and tumor cells (ascTU, omTU) from n = 3 different patients (patients are distinguished by different symbols). *** p < 0.001; **** p < 0.0001 by unpaired t test. **(C)** Detection of PTGIS protein in CAF, ascTAM and ascTU by immunoblot (n = 3; patient; OC. . . : patient identifiers). β -actin was used as loading control. **(D)** MS-based quantification of 6k-PGF_{1 α} (stable degradation product of PGI₂) in conditioned media (CM) from CAF, ascTAM, and ascTU after serum deprivation in the presence of 50 μ M AA for 24 h. Controls without AA are included for each cell type. * p < 0.05; ** p < 0.01 by unpaired t test (Comparison of different cell types) and paired t test (Ctrl vs. AA-treated cells). **(E)** Effect of COX1/2 inhibitors on PGI₂ biosynthesis by CAF. Concentrations of 6k-PGF_{1 α} were measured by MS in CM of CAF under serum-free conditions in the presence of 50 μ M AA and either 1 μ M COX1 inhibitor SC-560 and/or 10 μ M COX2 inhibitor celecoxib for 24 h. * p < 0.05; ** p < 0.01 by paired t test. Horizontal bars show the mean.

3.2. Validation of PGI₂ Synthesis by Cells of the HGSC TME

In view of the data discussed above, we focused our study on the PGI₂-mediated crosstalk of PTGIS-expressing CAF with PTGIR-positive ascTAM and its potential role in

HGSC progression. We therefore sought to confirm the RNA-Seq data by antibody-based methods and mass spectrometry (MS). The RT-qPCR analysis in Figure 2B confirmed a high expression of *PTGIS* in CAF, whereas TAM and tumor cells from both TME compartments (ascites and omentum) expressed *PTGIS* at low levels. Furthermore, in agreement with the RNA-Seq data, *PTGIS* protein was strongly expressed in CAF, but undetectable in ascTAM and ascTU (Figure 2C). *PTGIS* RNA expression was low, and *PTGIS* protein undetectable, in macrophages independent of their polarization state, i.e., MDM differentiated in either ascites to assume a TAM-like phenotype (asc-MDM) or classically activated by IFN γ /LPS (m1-MDM) (Supplementary Figure S4).

To determine whether *PTGIS* expression in CAF resulted in higher PGI $_2$ synthesis rates, we quantified the stable degradation product of PGI $_2$, 6k-PGF $_{1\alpha}$ released into the culture supernatant. LC-MS/MS-analysis clearly confirmed a strong PGI $_2$ production selectively by CAF compared to ascTAM and ascTU (Figure 2D). Moreover, PGI $_2$ synthesis by CAF could be efficiently blocked by the COX1 inhibitor SC-560 alone or in combination with the COX2 inhibitor celecoxib. Celecoxib alone was less effective (Figure 2E), which is likely due to the lower *PTGS2* expression level in CAF relative to *PTGS1* (Figure 1D). For comparison, we also analyzed PGE $_2$, which was produced mainly by CAF and ascTU (Supplementary Figure S5), consistent with the expression pattern of *PTGES* (Figure 1A). Therefore, we conclude that in contrast to other prostanoids, PGI $_2$ released into the TME of HGSC mainly originates from CAF (and probably MESO as suggested by Figure 1).

3.3. *PTGIR* Expression by Cells of the HGSC TME

To define PGI $_2$ -responsive cell types in the TME, we followed up on the *PTGIR* expression pattern identified by the RNA-Seq analysis in Figure 1D. RT-qPCR confirmed low *PTGIR* expression in all cell types, with the highest levels observed in ascTAM and CAF (Figure 3A), consistent with the RNA-Seq data (Figure 1D). To validate surface expression of *PTGIR* protein, we performed flow cytometric analysis. The specificity of *PTGIR* staining was confirmed in siRNA-treated macrophages (Supplementary Figure S6). In agreement with the RNA expression data, ascTAM exhibited a clear, but variable surface expression of *PTGIR* that was significantly higher compared to ascTU (Figure 3B,C). *PTGIR* protein was not detectable on CAF (Figure 3B,C), which cannot be fully explained by a lower mRNA expression (Figures 1D and 3A), suggesting additional regulatory mechanisms. In line with this hypothesis, *PTGIR* surface expression was comparable in asc-MDM and m1-MDMs in spite of differences in *PTGIR* mRNA expression (Supplementary Figure S7).

3.4. Intracellular cAMP Accumulation by PGI $_2$ Receptor Signaling in ascTAM

We next investigated whether binding of PGI $_2$ to its G $_s$ -coupled receptor *PTGIR* activates adenylate cyclase to mediate intracellular cAMP-accumulation in macrophages. Using the *PTGIR*-specific PGI $_2$ analog MRE-269 [26,35], we observed strong cAMP accumulation in ascTAM, and to a lesser extent in ascTU and CAF samples (Figure 3D), in accordance with their lower *PTGIR* surface expression. Levels of cAMP were highly variable among patients (Figure 3D), presumably reflecting the inter-patient variability of *PTGIR* expression (Figure 3B). A similar increase in cAMP levels were also observed in MRE-269-treated asc-MDM (Figure 3E). These results were confirmed for the PGI $_2$ analogs iloprost and trepostinil [26,35] (Supplementary Figure S8). Addition of the *PTGIR* antagonist CAY10449 reduced the MRE-269-mediated cAMP accumulation in 4 of 6 samples (Figure 3E), but did not reach statistical significance due to high donor-specific variability. Based on these findings we conclude that ascTAM represent a major target for PGI $_2$ derived from CAF (and MESO) in the TME.

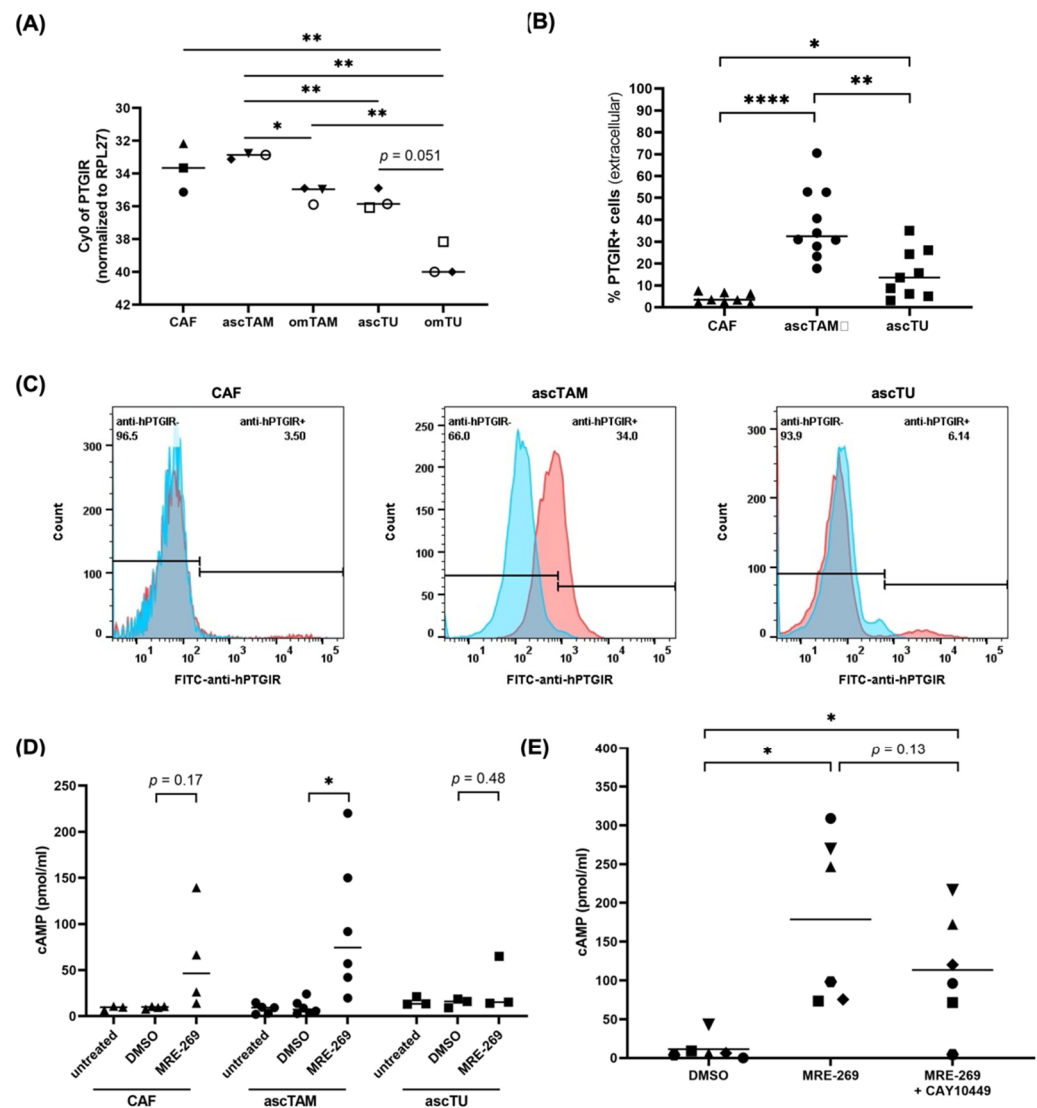


Figure 3. PTGIR expression and signaling in cell types of the HGSC TME. **(A)** RT-qPCR analysis of *PTGIS* mRNA expression in CAF, TAM (ascTAM, omTAM) and tumor cells (ascTU, omTU) from $n = 3$ different patients (patients are distinguished by different symbols). * $p < 0.05$; ** $p < 0.01$ by unpaired t test (Comparison of different cell types) and paired t test (matched pairs of omental and ascites-derived cells). **(B)** Detection of surface expression of PTGIR by flow cytometry in CAF, ascTAM and ascTU. Percentage of positive cells are indicated. Symbols represent different patients ($n = 8$ for CAF; $n = 10$ for ascTAM; $n = 9$ for ascTU). * $p < 0.05$; ** $p < 0.01$, **** $p < 0.0001$ by unpaired t test. **(C)** Exemplary histograms of PTGIR staining. **(D)** Analysis of intracellular cAMP accumulation upon stimulation of CAF, ascTAM and ascTU with 100 nM MRE-269 for 15 min under serum-free conditions. Untreated cells and solvent-treated cells (DMSO) were included as controls. Symbols represent different patients ($n = 4$ for CAF; $n = 6$ for ascTAM; $n = 3$ for ascTU). * $p < 0.05$ by paired t test. **(E)** Repression of cAMP accumulation in asc-MDM pretreated with 1 μ M PTGIR antagonist CAY10449 (1 h) before stimulation with MRE-269. Symbols represent different patients ($n = 6$). * $p < 0.05$ by paired t test. Horizontal bars show the mean.

3.5. PGI₂ Analogs Shift the Differentiation, Transcriptional Profile and Secretome of Macrophages towards a Pro-Tumorigenic Phenotype

To elucidate the functional impact of PGI₂ on ascTAM we determined alterations in the global gene expression profile in response to highly selective PGI₂ analog MRE-269. EdgeR paired test [31] of RNA-Seq data identified $n = 1495$ significantly upregulated genes, and 1801 downregulated genes (FDR < 0.05); Figure 4A; Supplementary Table S6). Of

these, $n = 669$ were upregulated with a fold change (FC) > 2 (Supplementary Table S7) and $n = 588$ were downregulated (Supplementary Table S8). Both M1 and M2 marker genes were affected by MRE-269, but without direction of polarization (Figure 4B). Thus, both M1 (*CCR7*, *CD86*, *ITGAX*) and M2 (*VEGFA*) marker genes were increased by MRE-269, and, conversely, expression of both M1 (*CD80*, *FCGRs*, *TNF*) and M2 (*CD163*, *MRC1/CD206*, *MSR*) genes were inhibited. This pattern is consistent with our previous work showing that ascTAM are characterized by a mixed-polarization phenotype [19].

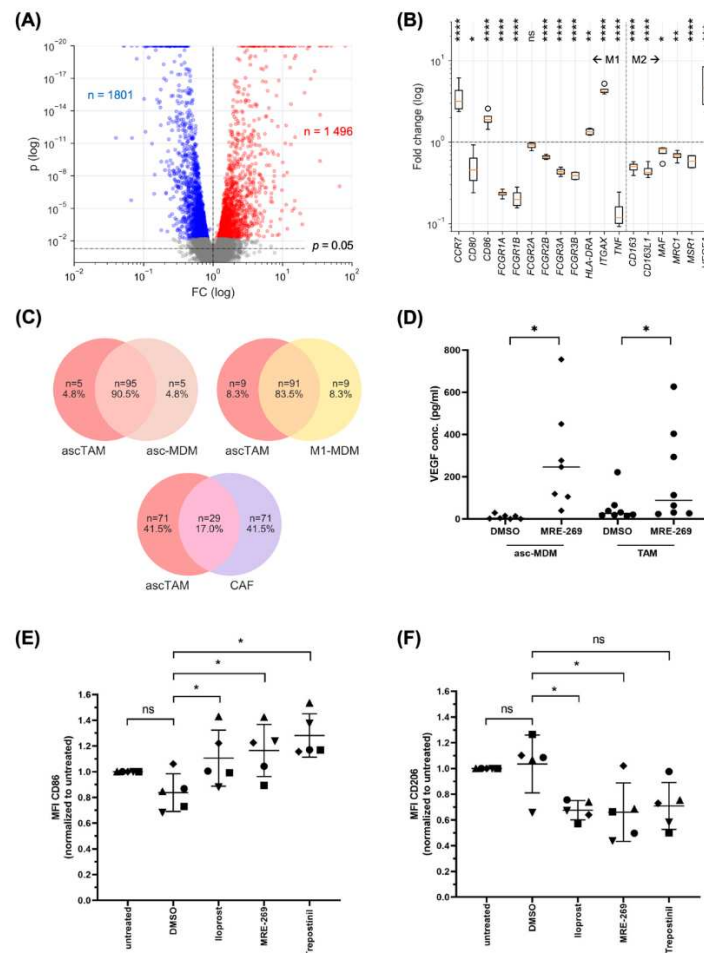


Figure 4. Regulation of the transcriptome and polarization state of macrophages by PGI₂ analogs. (A) Volcano plot depicts genes regulated by MRE-269. ascTAM were treated with 1 μM MRE-269 or solvent control (DMSO) for 5 h and analyzed by RNA-Seq. Red: sites upregulated by MRE-269 relative to solvent control (FC > 1 and FDR < 0.05). Blue: downregulated sites (FC < 1 and FDR < 0.05). Grey: FDR ≥ 0.05. (B) Expression of M1 and M2 marker genes, expressed as the fold change of MRE-269-treated cells relative to solvent control (RNA-Seq data; $n = 4$ biological replicates). Boxplots show the median (line), upper and lower quartiles (box), range (whiskers) and outliers (circles). * FDR < 0.05; ** FDR < 0.01; *** FDR < 0.001; **** FDR < 0.0001; ns, not significant by EdgeR paired test. (C) Venn diagrams illustrating the overlaps of gene sets upregulated by MRE-269 in ascTAM, TAM-like MDM differentiated in the presence of ascites (asc-MDM) and M1-polarized MDM (top 100 genes by FDR in each case). (D) Secretion of VEGF by ascTAM and asc-MDM after stimulation with 100 nM MRE-269 under serum-free conditions measured by ELISA. DMSO: solvent control. Horizontal bars indicate the mean. * $p < 0.05$ by paired t test. (E,F) Flow cytometry analysis CD86 (E) and CD206/MRC1 (F) on asc-MDM treated with 100 nM of the PGI₂ analogs MRE-269, iloprost or trepostinil for 24 h. MFI was expressed relative to untreated controls. Horizontal bars show the mean. * $p < 0.05$; ns: non-significant by paired t test.

To investigate the effects of PGI₂ on macrophages in more detail, we used TAM-like asc-MDM, which show low expression of PTGIS (see Section 3.2) and high expression of PTGIR (see Section 3.3) comparable to ascTAM. The Venn diagram in Figure 4C (top left) demonstrates a strong overlap of 90.5% for the top MRE-269-upregulated genes in TAM and asc-MDM, which was slightly less for MRE-269-upregulated genes in TAM versus M1-polarized MDM with 83.5% (Figure 4C, top right), but low in TAM versus CAF with 11.7% (Figure 4C, bottom). These observations indicate clear cell-type-selective differences in the action of PGI₂, and validate asc-MDM as a suitable model emulating ascTAM. Consistent with this conclusion and the RNA-Seq data, we found a significant induction of VEGFA secretion by MRE-269 in both asc-MDM and ascTAM (Figure 4D). Likewise, flow cytometry confirmed the upregulation of CD86 (Figure 4E) and the downregulation of CD206 (Figure 4F) in ascTAM by MRE-269 as well as two other PGI₂ analogs, Iloprost and Trepstinil.

Functional annotation analysis of the MRE-269-regulated genes by ConsensusPathDB [32] yielded over-represented terms mainly falling into 4 groups (Figure 5A; Supplementary Table S9): (i) GPCR signaling, which is consistent with PTGIR being a GPCR; (ii) Rac/Rho GTPase signaling, which impacts actomyosin-controlled processes; (iii) phagocytosis, which is dependent on Rho GTPases and actomyosin contraction [36]; and (iv) immune cell regulation, including chemokine signaling. Rac/Rho signaling plays a key role in tumor cell adhesion, motility and invasion [37], pointing to a role for PGI₂ in metastasis-associated processes. Consistent with this notion, we found 34 MRE-269-upregulated cytokine genes associated with the term “metastasis” in the genecards.org database, including ANGPTL4, AREG, BMP6, CXCL2, CXCL3, CXC6, EREG, TGFB3, VEGFA, WNT1, WNT5B and WNT7B (Figure 5B; Supplementary Table S7). Furthermore, MRE-269 induced multiple genes coding for extracellular matrix (ECM) proteins and proteases involved in metastasis-associated ECM remodeling (Figure 5C; Supplementary Table S7). Intriguingly, MRE-269 significantly inhibited the expression of 22 cytokine genes, among these CXCL10 and IL12A with pivotal functions in T/NK cell recruitment and activation [38,39] (Figure 5D; Supplementary Table S8). Immune suppression and tumor angiogenesis may also be supported by PGE₂, [40] as the genes involved in its synthesis (PGES, PTGS2/COX2) were also induced by MRE-269 (Figure 5E; Supplementary Table S7).

Since PGI₂-mediated signaling can not only be mediated via PTGIR, but also by binding to nuclear PPARβ/δ, we analyzed potential effects on known PPARβ/δ target genes. As can be seen in Supplementary Table S6, expression of the well-known PPARβ/δ target gene *PDK4* was not upregulated by MRE-269, arguing against a role for PPARβ/δ in mediating the MRE-269 effects observed above. As reported previously [41], ascites contains a high level of endogenous PPARβ/δ ligands blunting the effect of synthetic agonists, consistent with the observed high basal expression of *PDK4* in untreated asc-MDM and ascTAM (Supplementary Table S6).

Taken together, our findings indicate that PGI₂ triggers a shift to a mixed-polarization, immunosuppressed TAM phenotype with angiogenesis- and invasion-promoting features, which is mediated by its membrane receptor PTGIR without contribution by PPARβ/δ.

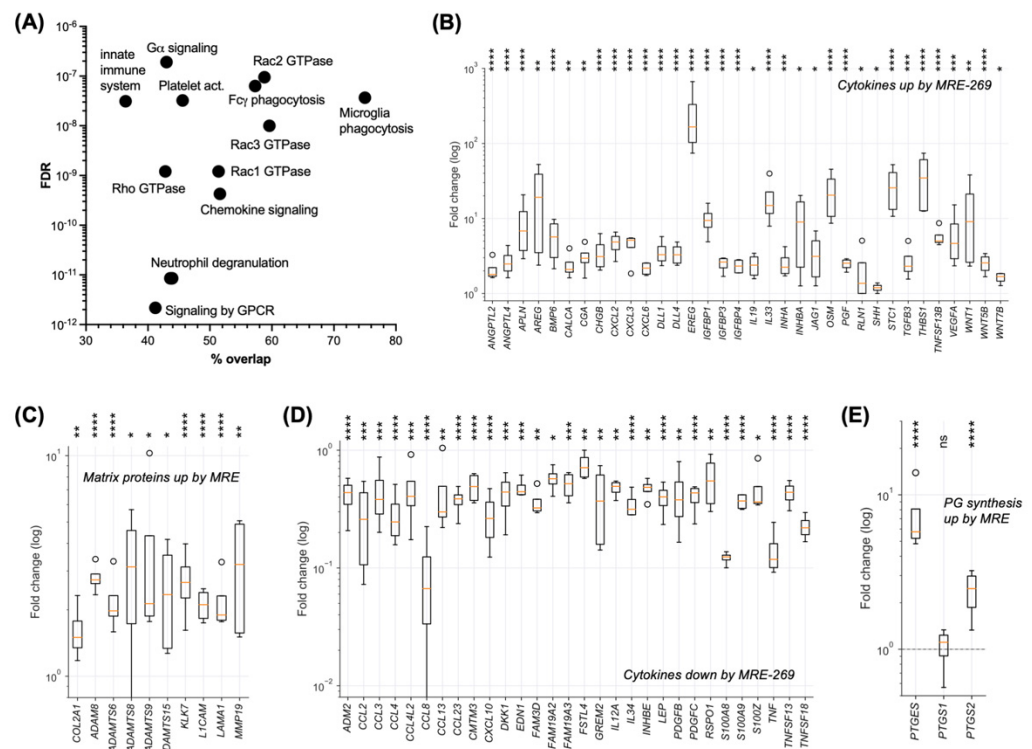


Figure 5. Functions of genes regulated by the PGI₂ analog MRE-269. **(A)** Functional annotation of MRE-269-regulated genes (as in Figure 4A) using the over-representation tool of Consensus-PathDB [32]. The plot depicts the top 12 (by FDR) specific terms. Overlap: percentage of genes in the query set compared to the set representing the respective term. **(B)** Cytokine genes associated with the term “metastasis” in the genecards.org database and upregulated by MRE-269 (FDR < 0.05). **(C)** Metastasis-associated genes coding for ECM components and proteases of the TME significantly upregulated by MRE-269. **(D)** Cytokine genes significantly downregulated by MRE-269. **(E)** Genes involved in prostaglandin synthesis significantly upregulated by MRE-269. Boxplots show the median (line), upper and lower quartiles (box), range (whiskers) and outliers (circles). * FDR < 0.05; ** FDR < 0.01; *** FDR < 0.001; **** FDR < 0.0001; ns, not significant by EdgeR paired test.

3.6. PGI₂ Decreases the Phagocytic Capability of Macrophage

In view of the functional annotation of genes regulated by MRE-269, we sought to investigate its effect on the phagocytic capability of macrophages. Toward this goal, asc-MDM were treated with PGI₂ analogs, and macropinocytosis was quantified by FITC dextran uptake. Compared to m1-MDM, asc-MDM displayed a strong macropinocytotic activity (Supplementary Figure S9A,B), which was significantly diminished by all three PGI₂ analogs (Figure 6A). Furthermore, two different PTGIR antagonists (CAY10449 and CAY10441) could partially reverse the effect of MRE-269 (significant with CAY10441; Figure 6B), indicating a role for PTGIR signaling. A potential contribution of PPARβ/δ activation by PGI₂ analogs in TAM could be ruled out, since macropinocytosis by asc-MDM were not affected by the synthetic PPARβ/δ agonist L165041 (Figure 6B). In contrast, L165041 suppressed the macropinocytotic potential of M0-differentiated MDM (Supplementary Figure S9C). As these cells were not exposed to ascites, they do not accumulate endogenous PPARβ/δ ligands and thus remain responsive to synthetic PPARβ/δ ligands. Our findings therefore support the previously observed inhibition of macropinocytosis by L165041 [42], which does not appear to be relevant for macrophages exposed to HGSC microenvironment.

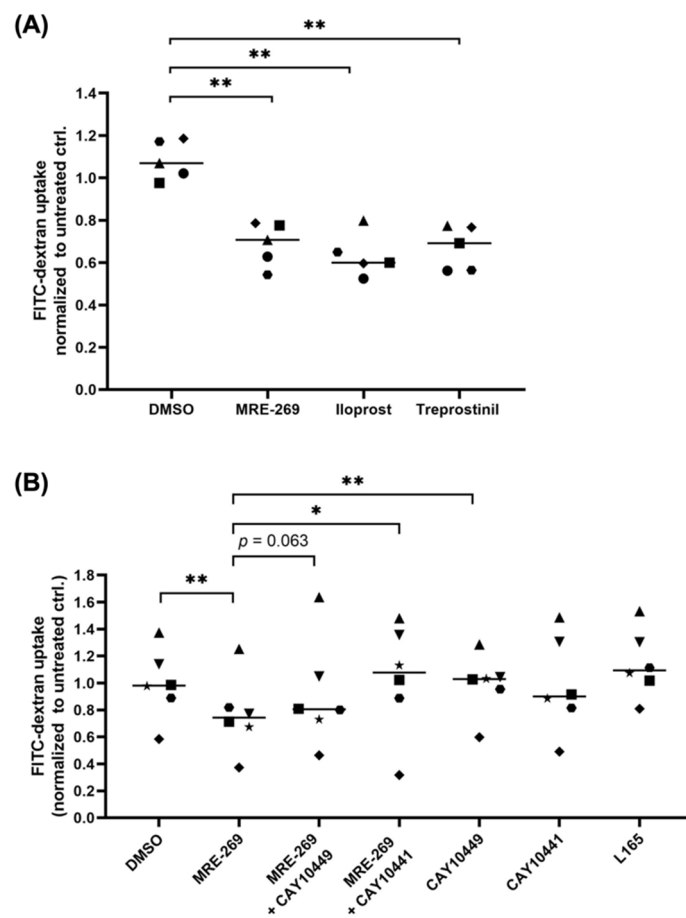


Figure 6. Influence of PGI₂ analogs on macropinocytotic activity of asc-MDM. (A) Macropinocytosis was determined by FITC-dextran uptake by asc-MDM after stimulation with 100 nM MRE-269, iloprost or trepostinil or DMSO (solvent control) for 30 min (n = 5; donors are distinguished by different symbols). Results were normalized to untreated controls. (B) Macropinocytosis of asc-MDM treated with 1 μM PTGIR antagonist (CAY10449 or CAY10441) prior to stimulation with MRE-269 or DMSO. To test for a role of PPARβ/δ in inhibiting macropinocytosis, asc-MDM were stimulated with 1 μM L165041. * $p < 0.05$, ** $p < 0.01$ by paired t test. Horizontal bars show the mean.

We next asked whether CAF could alter the phagocytic potential of macrophages by releasing PGI₂ in a similar way as synthetic PGI₂ analogs. Because of the very short half-life of PGI₂ (<10 min at physiological pH [43]) we used a transwell co-culture system as illustrated in Supplementary Figure S10A. In this experimental setup, asc-MDM and CAF were co-cultured in the presence of exogenous AA as substrate for PGI₂ synthesis, thereby mimicking the situation in HGSC ascites [41]. asc-MDM co-cultured with CAF showed a significant reduction of macropinocytotic activity compared to asc-MDM alone (Supplementary Figure S10B), which was observed with CAF from different HGSC patients. Inclusion of the COX1/2 inhibitors SC-560 and celecoxib to block CAF-derived PGI₂ supply resulted in partial restoration of the macropinocytotic capacity in the presence of CAF (Supplementary Figure S10B). Thus, we conclude that PGI₂ released by CAF can affect the phagocytic potential of TAM via PTGIR signaling.

3.7. Triggering Tumor Migration and Adhesion by Factors Secreted by PGI₂-Treated TAM

Since transcriptomic profiling of ascTAM indicated alterations in the expression of metastasis-associated cytokines and proteins involved in ECM remodeling (Figure 5B,C, Supplementary Table S7), we asked if factors secreted by ascTAM in response to PGI₂ could impact tumor cell migration. We chose primary tumor cells (ascTU) for this purpose, which express very low levels of PTGIS and PTGIR (Figures 2 and 3), so that autocrine effects are

negligible. Tumor migration was studied in a transwell setting, where ascTU from different patients were pre-incubated with conditioned media (CM) from MRE-269-treated ascTAM. As illustrated in Figure 7A,B, the migration of primary tumor cells was significantly enhanced by the conditioned medium from MRE-269-treated compared to untreated TAM, which was partially blocked by the PTGIR antagonist CAY10449, suggesting an involvement of PTGIR signaling. By contrast, CM from ascTAM stimulated with the PPAR β/δ agonist L165041 did not affect tumor cell migration (Figure 7A,B).

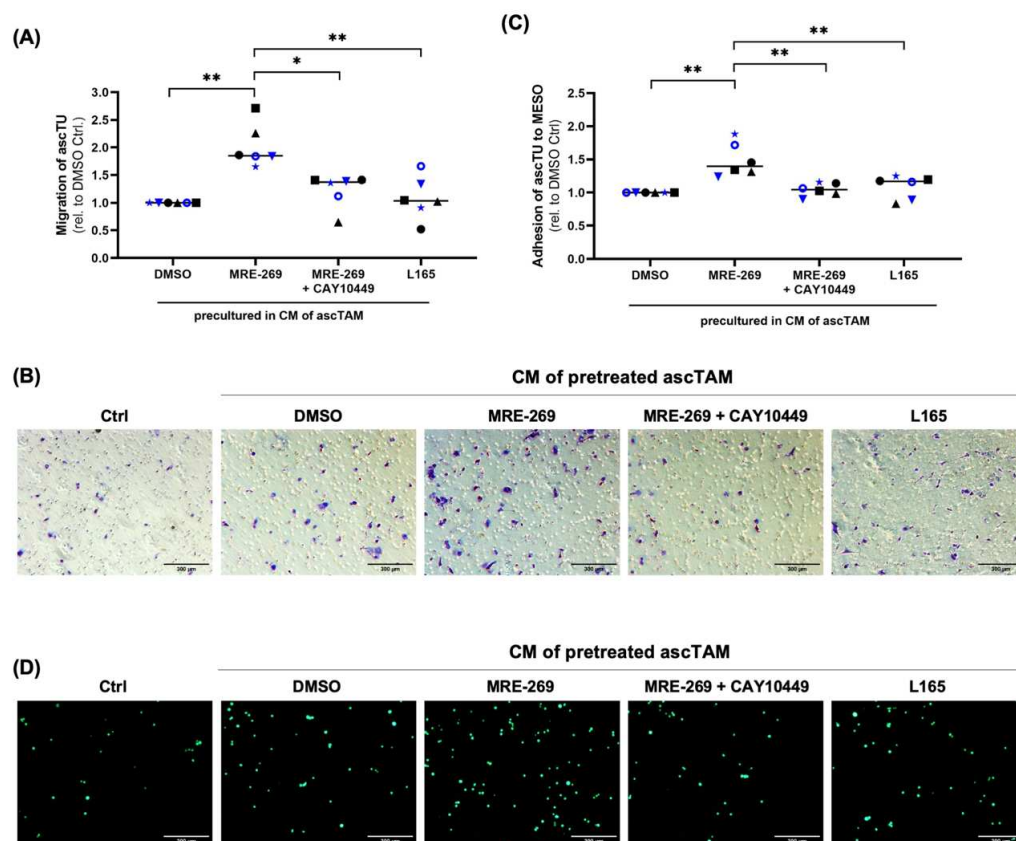


Figure 7. Pro-tumorigenic functions of PGI₂-induced TAM secretomes. **(A)** Migration of primary ascTU pretreated for 24 h with conditioned media (CM) from ascTAM stimulated with MRE-269 (100 nM), MRE-269 (100 nM) + CAY10449 (1 μ M) or PPAR β/δ agonist L165041 (1 μ M). CM from ascTAM treated with DMSO was included as control. Migration was assessed in a Transwell format with 10% FCS as chemoattractant after 24 h and quantified relative to CM from DMSO control with primary ascTU from $n = 2$ patients (different colors) and TAM-conditioned medium from $n = 6$ patients (different symbols). **(B)** Representative microscopic pictures of migrated tumor cells after 24 h exposure to CM from ascTAM. **(C)** Adhesion of primary ascTU cells to a confluent monolayer of peritoneal mesothelial cells (MESO). ascTU (from $n = 2$ patients, indicated by different colors) were preincubated with CM from ascTAM (from $n = 6$ patients) stimulated as described above and labeled with CellTracker Green. Adhesion of ascTU to the MESO layer was evaluated in comparison to CM from ascTAM stimulated with DMSO as solvent control after 2 h of co-culture. **(D)** Representative microscopic pictures of tumor cell adhesion to MESO monolayer after 2 h exposure. Tumor cells were pretreated with CM from ascTAM pretreated with different ligands as indicated. Intactness of the MESO monolayer was verified by staining for the tight junctions scaffolding protein zonula occludens 1 (ZO1) (Supplementary Figure S1). One of the samples analyzed was a low-grade mucinous carcinoma (black triangles in A and C), which was not known at the time of the analysis (OC233 in Table S1). All other samples were isolated from HGSC patients. The data suggest that the effect of MRE-269 is not limited to HGSC. * $p < 0.05$, ** $p < 0.01$, by paired t test. Horizontal bars show the mean.

Finally, we investigated whether PGI₂-induced mediators in the TAM secretome impact tumor cell adhesion to MESO as an early step of tumor invasion. As shown in Figure 7C,D, ascTU pretreated with CM from MRE-269-stimulated ascTAM showed a higher adhesive potential to MESO compared to ascTU incubated with CM from untreated ascTAM. The secretion of adhesion-promoting mediators by ascTAM in response to PGI₂ was dependent on binding to PTGIR as suggested by the inhibitory effect of the PTGIR antagonist CAY10449. Participation of PPAR β/δ was excluded, as the PPAR β/δ agonist L165041 had no effect (Figure 7C,D). In view of these results, we postulate that PGI₂ in the TME promotes tumor migration and invasion by stimulating TAM to secrete pro-migratory and pro-adhesive factors.

4. Discussion

Bioinformatic analysis of global transcriptome for different cell types in malignant ascites and omental metastases of HGSC patients was conducted to define the lipid-mediated intercellular crosstalk as a basis for functional analyses in the context of tumor progression and metastasis. In this network, COX1, COX2, PTGES and PTGIS, which convert AA to bioactive prostanoids, play a pivotal role. In contrast to most other malignancies, COX1 has been reported to be expressed at higher levels than COX2 in HGSC [44], which is consistent with our data for ascTU, omTU and CAF from omental metastases (Figure 1D). Both, COX1 and COX2 overexpression have been strongly implicated in the progression of numerous tumors, including ovarian cancer [45], but the clinical utility of available COX2 inhibitors is limited due to their cardiotoxicity. There is accumulating evidence that the intake of nonsteroidal anti-inflammatory drugs (NSAIDs), in particular acetylsalicylic acid, may be associated with a reduced incidence of ovarian cancer among other tumors, probably via irreversible COX1 inactivation [46–50]. However, data regarding the influence of acetylsalicylic acid on the mortality of ovarian cancer are inconsistent, making further clinical evaluation necessary to be able to draw definitive conclusions [51,52].

Our study provides strong evidence for CAF as an essential producer of PGI₂ in the HGSC TME due to selective upregulation of PTGIS expression (Figure 2). A similar observation was reported for pancreatic ductal adenocarcinoma based on single-cell RNA-Seq data [53]. Physiologically, PGI₂ is synthesized by fibroblasts and is enhanced during wound healing [54]. This is of particular interest, since activated fibroblasts in healing wounds and CAF share many features, which strengthens the evolving concept of cancer as a wound that does not heal [55]. According to our RNA-Seq data (Figure 1), MESO are the only cell population expressing PTGIS at a level similar to CAF which could be explained by the high degree of similarity between these cell types. Due to their plasticity, MESO can acquire a CAF-like state upon stimulation by cytokines present in ascites that have the potential to induce a mesothelial-mesenchymal transition (e.g., TGF β , IL-1 β) [56]. It is therefore likely that MESO also significantly contribute to PGI₂-driven signaling in the HGSC TME.

Even though anti-tumorigenic functions [57] and a favorable clinical outcome have been linked to PGI₂ in several cancers, increased intra-tumoral PTGIS expression derived from stroma cells is associated with poor clinical outcome in HGSC (Figure 2A) suggesting an entity-specific role for PTGIS and its product PGI₂. We have identified TAM in HGSC ascites as an essential target for CAF-derived PGI₂. ascTAM show the highest expression of the PGI₂ receptor PTGIR among cells in the TME, consistent with a strong activation by PGI₂ analogs (Figure 3). CAF also respond to PGI₂ analogs by cAMP accumulation, albeit to a far lesser extent compared to ascTAM, which we attribute to the considerably lower level of PTGIR expression on CAF (Figure 3B,C). Nevertheless, the observed stimulation of cAMP in CAF is in agreement with published data on PGI₂-mediated alterations of fibroblast functions via activation of the cAMP-PKA pathway [58].

Transcriptional profiling and functional analyses suggest that TAM adopt an immunosuppressed phenotype both M1- and M2-like features upon stimulation with the PGI₂ analog MRE-269. For example, MRE-269 treatment inhibited the expression of the

pro-inflammatory *TNF* gene and M1 surface marker genes (*FCGRs*), while increasing the surface expression of the M1-related markers CD86 and secretion of M2-associated VEGF (Figure 4). Furthermore, *CXCL10* and *IL12A*, which play essential roles in the recruitment and activation of T and NK cells [38,39] were repressed by MRE-269 (Figure 5D; Supplementary Table S8). Consistent with these observations, inhibition of pro-inflammatory genes by forced PTGIS expression in macrophages has also been described in a recent study and linked to altered JAK/STAT signaling [22]. Furthermore, CREB target genes (*CEBPB*, *SOCS3*) have been associated with macrophage polarization [59,60], and cAMP was found to exert anti-inflammatory activity by suppressing macrophage functions [61,62]. Consistent with these findings, we observed an upregulation of *KLF4* and the CREB target gene *SOCS3* in the transcriptome of MRE-269-treated TAM, indicative of an involvement of the cAMP-triggered CREB pathway (Supplementary Table S6). PGE₂ has also been reported to promote M2 polarization through activation of the cAMP pathway via cyclic AMP responsive element binding (CREB)-mediated induction of *KLF4* [63].

As of yet, our knowledge regarding the control of macrophage functions by PGI₂—especially in the context of cancer—is limited. Nonetheless, published data showing that PGI₂ analogs inhibit phagocytosis, bacterial killing and secretion of inflammatory cytokines by rat macrophages, point to a role of PGI₂ in immune regulation similar to that of PGE₂ [23]. These authors observed different efficacies of PGI₂ analogs in peritoneal and resident alveolar macrophages, which correlated with their PTGIR expression profile. Our own observations in human TAM fully agree with these data on rodent macrophages. First, we determined a difference in PTGIR expression in TAM subpopulations dependent on their anatomic site, as ascTAM display higher PTGIR expression compared to omTAM (Figure 3A). Second, the phagocytic capacity of asc-MDM was suppressed by PGI₂ analogs, accompanied by downregulation of the phagocytosis-related marker CD206 by MRE-269 and iloprost (Figure 4B,F and Figure 6A). Our data further suggest a direct implication of PTGIR signaling in this process, as the phagocytic potential was partially restored by PTGIR antagonists (Figure 6B). At least for the most specific analog MRE-269, signaling via PGE₂ receptors (PTGER1–4) can be neglected due to a lack of binding affinity [26]. Likewise, signaling via nuclear PPAR receptors has not been reported for MRE-269 in contrast to PGI₂ and some of its analogs such as iloprost and trepostinil which bind directly to PPAR α and β/δ [64,65]. Importantly, even the use of the potent synthetic PPAR β/δ agonist L165041 could not alter the phagocytic capability of asc-MDM, although it was effective in M0 MDM (Figure 6B, Supplementary Figure S9C), which, however, have a low relevance, if any, in the TME. This unresponsiveness of ascTAM is in line with our previous findings showing that PPAR β/δ target genes in ascTAM are upregulated in comparison to M0-MDM due to high levels of fatty acid ligands in HGSC ascites, and therefore are refractory to synthetic PPAR agonists [41]. Based on these data we assume that PGI₂ suppresses phagocytosis by macrophages in the ascites milieu without direct participation of PPARs.

Our results further support a previously unknown link between PGI₂ activation of TAM and the secretion of factors that enhance tumor migration as well as adhesion of primary tumor cells to MESO as a first step of tumor cell invasion (Figure 7). Our data indicate that the secretion of adhesion- and migration-promoting factors by ascTAM is mediated by activation of PTGIR signaling pathways (Figures 6 and 7). This conclusion is in line with the observed upregulation of several genes involved in differentiation, motility and tissue development in MRE-269-stimulated TAM (Figure 5). Macrophages are known to promote tumor cell migration through the secretion of proteins, such as EGF, CHI3L1, IGF1, FN1, TNC and TGFBI [25,66–68]. TGFBI was also found among the upregulated genes by MRE-269 in TAM (Supplementary Table S6). We have previously shown that TAM promote HGSC cell migration by secreting TGFBI [25], linking the PGI₂-triggered signaling in TAM to altered tumor cell properties. Our observations also suggest that PGI₂-activated TAM contribute to tumor angiogenesis by upregulating VEGF (Figure 4D) and PGE₂ synthesis (Figure 5E). This is in line with data from a murine breast cancer model

demonstrating that upstream inhibition of COX2 in macrophage leads to downregulation of VEGFA, VEGFC and MMP9 associated with reduced metastasis [69].

CAF express high levels of PTGIS resulting in elevated PGI₂ synthesis. PGI₂ released into the TME binds to its surface receptor PTGIR on ascTAM to trigger signaling transduction, including cAMP accumulation. PTGIR activation skews TAM to an immunosuppressed and pro-tumorigenic TAM phenotype, characterized by reduced phagocytic capacity, decreased secretion of immune-stimulatory cytokines and enhanced release of molecules (cytokines and growth factors, ECM components and proteases, PGE₂) promoting pro-metastatic processes, like cell migration, adhesion and angiogenesis.

5. Conclusions

As illustrated by the schematic summary in Figure 8, our results provide strong evidence (i) that CAF are main producers of PGI₂ due to high PTGIS expression, (ii) that PGI₂ predominantly targets PTGIR-positive ascTAM to trigger signaling via the PTGIR-cAMP axis and (iii) that PGI₂ triggers a switch towards a pro-tumorigenic and immunosuppressed TAM phenotype with both M1 and M2-like features. These reeducated TAM exhibit low phagocytic capability and reduced expression of immune-stimulatory cytokine genes as well as enhanced secretion of pro-metastatic mediators impacting tumor cell adhesion, migration and angiogenesis. In view of the association of PTGIS with a poor clinical outcome of ovarian cancer, targeting PGI₂ synthesis either directly, or indirectly via COX inhibition, may be a promising option to improve the treatment of HGSC patients.

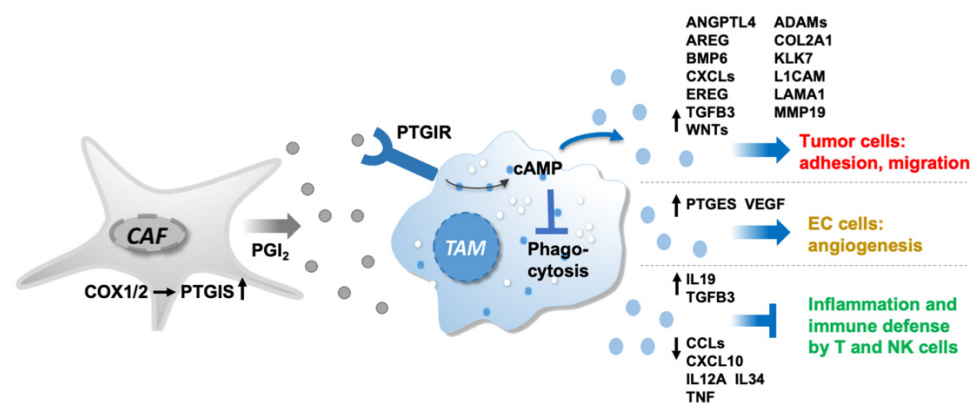


Figure 8. Schematic summary of the PGI₂-mediated crosstalk in the OC microenvironment.

Supplementary Materials: The following supporting information can be downloaded at: <https://www.mdpi.com/article/10.3390/cancers14246154/s1>: Figure S1: Evaluation of the integrity of MESO monolayer for tumor cell adhesion assay; Figure S2: Cell-type-selectivity of genes coding for receptors of lipid mediators; Figure S3: Inverse association of PTGIS expression with relapse-free survival in HGSC patients; Figure S4: PTGIS expression in differently polarized macrophages; Figure S5: PGE₂ synthesis in different cell types of the HGSC TME; Figure S6: Validation of PTGIR staining in macrophages; Figure S7: PTGIR expression in differently polarized macrophages; Figure S8: Induction of PTGIR signaling by different PGI₂ analogs; Figure S9: Impact of PGI₂ analogs on macropinocytosis in differently polarized macrophages; Figure S10: Influence of CAF on macropinocytotic activity of TAM; Figure S11: Original immunoblots (full blots). Original images of immunoblots; Table S1: Ovarian HGSC patient data and samples; Table S2: RT-qPCR primers; Table S3: List of enzymes involved in the synthesis lipid ligands and cognate receptors; Table S4: Expression of genes coding for enzymes involved in the synthesis lipid ligands; Table S5: Expression of genes coding for receptors of lipid ligands; Table S6: Genes regulated in TAM by MRE-296 versus solvent control; Table S7: Genes upregulated in TAM by MRE-296 versus solvent control; Table S8: Genes downregulated in TAM by MRE-296 versus solvent control; Table S9: Pathways annotation (ConsensusPathDB) of MRE-regulated genes in Table S6 (top hits by FDR) in Reactome, KEGG and Wikipathways databases; Table S10: Genes upregulated in asc-MDM.

Author Contributions: Conceptualization, R.M., S.R. and S.M.-B.; Methodology, L.S., I.K., J.P., W.A.N., A.N. and T.S.; Validation, L.S. and F.F.; Formal analysis, L.S., I.K. and J.P.; Investigation: L.S. and I.K.; Resources, J.M.J. and U.W.; Data curation, L.S. and F.F.; Writing—original draft preparation, review and editing, S.R. and R.M.; Visualization, L.S., S.R. and R.M.; Supervision, R.M. and S.R.; Project administration, S.R. and R.M.; Funding acquisition, S.R. and R.M. All authors have read and agreed to the published version of the manuscript.

Funding: This research was funded by the Deutsche Forschungsgemeinschaft (DFG), grant number MU601/22-1 to RM, and by the German Cancer Aid (Deutsche Krebshilfe), grant number 70113255 to RM and SR.

Institutional Review Board Statement: The study was conducted in accordance with the Declaration of Helsinki, and approved by the Ethics Committee of the Philipps University Marburg (reference number 205/10; date of approval: 21 December 2010).

Informed Consent Statement: Informed consent was obtained from all subjects involved in the study.

Data Availability Statement: RNA Seq data were deposited at EBI ArrayExpress (accession numbers MTAB-3167, E-MTAB-4162, E-MTAB-10611, E-MTAB-12437 and E-MTAB-12441. All other data generated or analyzed in this study are included in the supporting information files.

Acknowledgments: We are grateful to T. Plaum-Allmeroth, A. Allmeroth and B. Watzer for excellent technical assistance.

Conflicts of Interest: The authors declare no conflict of interest.

Abbreviations

ADI	adipocytes
asc	ascites
AA	arachidonic acid
CAF	cancer-associated fibroblasts
CM	conditioned medium
COX1/2	cyclooxygenase-1/-2
CREB	cyclic AMP responsive element binding
Ctrl	control
ECM	extracellular matrix
FC	fold change
IBMX	phosphodiesterase (PDE) inhibitor isobutylmethylxanthine
HGSC	high-grade ovarian carcinoma
LPA	lysophosphatidic acids
MDM	monocyte-derived macrophages
MESO	mesothelial cells
MFI	mean fluorescence intensities
MS	mass spectrometry
NSAID	nonsteroidal anti-inflammatory drug
om	omentum
OS	overall survival
PFS	progression-free survival
PGE ₂	prostaglandin E ₂
PGH ₂	prostaglandin H ₂
PGI ₂	prostaglandin E ₂ (prostacyclin)
PPAR β/δ	peroxisome-proliferator-activated receptor β/δ
PTGER	PGE ₂ receptor
PTGIR	prostacyclin receptor
PTGIS	prostacyclin synthase
RNA-Seq	RNA sequencing
TAM	tumor-associated macrophages
TAT	tumor-associated T cells
TME	tumor microenvironment
ZO1	zonula occludens 1

References

1. Reinartz, S.; Lieber, S.; Pesek, J.; Brandt, D.T.; Asafova, A.; Finkernagel, F.; Watzer, B.; Nockher, W.A.; Nist, A.; Stiewe, T.; et al. Cell type-selective pathways and clinical associations of lysophosphatidic acid biosynthesis and signaling in the ovarian cancer microenvironment. *Mol. Oncol.* **2019**, *13*, 185–201. [[CrossRef](#)] [[PubMed](#)]
2. Reinartz, S.; Finkernagel, F.; Adhikary, T.; Rohnalter, V.; Schumann, T.; Schober, Y.; Nockher, W.A.; Nist, A.; Stiewe, T.; Jansen, J.M.; et al. A transcriptome-based global map of signaling pathways in the ovarian cancer microenvironment associated with clinical outcome. *Genome Biol.* **2016**, *17*, 108. [[CrossRef](#)] [[PubMed](#)]
3. Dietze, R.; Hammoud, M.K.; Gómez-Serrano, M.; Unger, A.; Bieringer, T.; Finkernagel, F.; Sokol, A.M.; Nist, A.; Stiewe, T.; Reinartz, S.; et al. Phosphoproteomics identify arachidonic-acid-regulated signal transduction pathways modulating macrophage functions with implications for ovarian cancer. *Theranostics* **2021**, *11*, 1377–1395. [[CrossRef](#)] [[PubMed](#)]
4. Hammoud, M.K.; Dietze, R.; Pesek, J.; Finkernagel, F.; Unger, A.; Bieringer, T.; Nist, A.; Stiewe, T.; Bhagwat, A.M.; Nockher, W.A.; et al. Arachidonic acid, a clinically adverse mediator in the ovarian cancer microenvironment, impairs JAK-STAT signaling in macrophages by perturbing lipid raft structures. *Mol. Oncol.* **2022**, *16*, 3146–3166. [[CrossRef](#)]
5. Kobayashi, K.; Omori, K.; Murata, T. Role of prostaglandins in tumor microenvironment. *Cancer Metastasis Rev.* **2018**, *37*, 347–354. [[CrossRef](#)]
6. Kalinski, P. Regulation of immune responses by prostaglandin E2. *J. Immunol.* **2012**, *188*, 21–28. [[CrossRef](#)]
7. Gupta, R.A.; Tan, J.; Krause, W.F.; Geraci, M.W.; Willson, T.M.; Dey, S.K.; DuBois, R.N. Prostacyclin-mediated activation of peroxisome proliferator-activated receptor delta in colorectal cancer. *Proc. Natl. Acad. Sci. USA* **2000**, *97*, 13275–13280. [[CrossRef](#)]
8. Midgett, C.; Stitham, J.; Martin, K.A.; Hwa, J. Prostacyclin receptor regulation—from transcription to trafficking. *Curr. Mol. Med.* **2011**, *11*, 517–528. [[CrossRef](#)]
9. Shaul, P.W.; Kinane, B.; Farrar, M.A.; Buja, L.M.; Magness, R.R. Prostacyclin production and mediation of adenylate cyclase activity in the pulmonary artery. Alterations after prolonged hypoxia in the rat. *J. Clin. Investig.* **1991**, *88*, 447–455. [[CrossRef](#)]
10. Schwaner, I.; Offermanns, S.; Spicher, K.; Seifert, R.; Schultz, G. Differential activation of Gi and GS proteins by E- and I-type prostaglandins in membranes from the human erythroleukaemia cell line, HEL. *Biochim. Et Biophys. Acta (BBA)—Mol. Cell Res.* **1995**, *1265*, 8–14. [[CrossRef](#)]
11. Moncada, S.; Gryglewski, R.; Bunting, S.; Vane, J.R. An enzyme isolated from arteries transforms prostaglandin endoperoxides to an unstable substance that inhibits platelet aggregation. *Nature* **1976**, *263*, 663–665. [[CrossRef](#)] [[PubMed](#)]
12. Stitham, J.; Midgett, C.; Martin, K.A.; Hwa, J. Prostacyclin: An inflammatory paradox. *Front. Pharmacol.* **2011**, *2*, 24. [[CrossRef](#)] [[PubMed](#)]
13. Li, H.Y.; McSharry, M.; Walker, D.; Johnson, A.; Kwak, J.; Bullock, B.; Neuwelt, A.; Poczobutt, J.M.; Sippel, T.R.; Keith, R.L.; et al. Targeted overexpression of prostacyclin synthase inhibits lung tumor progression by recruiting CD4+ T lymphocytes in tumors that express MHC class II. *Oncoimmunology* **2018**, *7*, e1423182. [[CrossRef](#)] [[PubMed](#)]
14. Keith, R.L.; Geraci, M.W. Prostacyclin in Lung Cancer. *J. Thorac. Oncol.* **2006**, *1*, 503–505. [[CrossRef](#)]
15. Ahn, J.-H.; Lee, K.-T.; Choi, Y.S.; Choi, J.-H. Iloprost, a prostacyclin analog, inhibits the invasion of ovarian cancer cells by downregulating matrix metalloproteinase-2 (MMP-2) through the IP-dependent pathway. *Prostaglandins Other Lipid Mediat.* **2018**, *134*, 47–56. [[CrossRef](#)]
16. Klein, T.; Benders, J.; Roth, F.; Baudler, M.; Siegle, I.; Kömhoff, M. Expression of Prostacyclin-Synthase in Human Breast Cancer: Negative Prognostic Factor and Protection against Cell Death In Vitro. *Mediat. Inflamm.* **2015**, *2015*, 864136. [[CrossRef](#)]
17. Condeelis, J.; Pollard, J.W. Macrophages: Obligate partners for tumor cell migration, invasion, and metastasis. *Cell* **2006**, *124*, 263–266. [[CrossRef](#)]
18. Kawamura, K.; Komohara, Y.; Takaishi, K.; Katabuchi, H.; Takeya, M. Detection of M2 macrophages and colony-stimulating factor 1 expression in serous and mucinous ovarian epithelial tumors. *Pathol. Int.* **2009**, *59*, 300–305. [[CrossRef](#)]
19. Reinartz, S.; Schumann, T.; Finkernagel, F.; Wortmann, A.; Jansen, J.M.; Meissner, W.; Krause, M.; Schwörer, A.-M.; Wagner, U.; Müller-Brüsselbach, S.; et al. Mixed-polarization phenotype of ascites-associated macrophages in human ovarian carcinoma: Correlation of CD163 expression, cytokine levels and early relapse. *Int. J. Cancer* **2014**, *134*, 32–42. [[CrossRef](#)]
20. Worzfeld, T.; Finkernagel, F.; Reinartz, S.; Konzer, A.; Adhikary, T.; Nist, A.; Stiewe, T.; Wagner, U.; Looso, M.; Graumann, J.; et al. Proteotranscriptomics Reveal Signaling Networks in the Ovarian Cancer Microenvironment. *Mol. Cell Proteom.* **2018**, *17*, 270–289. [[CrossRef](#)]
21. Adhikary, T.; Wortmann, A.; Finkernagel, F.; Lieber, S.; Nist, A.; Stiewe, T.; Wagner, U.; Müller-Brüsselbach, S.; Reinartz, S.; Müller, R. Interferon signaling in ascites-associated macrophages is linked to a favorable clinical outcome in a subgroup of ovarian carcinoma patients. *BMC Genom.* **2017**, *18*, 243. [[CrossRef](#)] [[PubMed](#)]
22. Pan, X.-Y.; Wang, L.; You, H.-M.; Cheng, M.; Yang, Y.; Huang, C.; Li, J. Alternative activation of macrophages by prostacyclin synthase ameliorates alcohol induced liver injury. *Lab. Investig.* **2021**, *101*, 1210–1224. [[CrossRef](#)] [[PubMed](#)]
23. Aronoff, D.M.; Peres, C.M.; Serezani, C.H.; Ballinger, M.N.; Carstens, J.K.; Coleman, N.; Moore, B.B.; Peebles, R.S.; Faccioli, L.H.; Peters-Golden, M. Synthetic prostacyclin analogs differentially regulate macrophage function via distinct analog-receptor binding specificities. *J. Immunol.* **2007**, *178*, 1628–1634. [[CrossRef](#)] [[PubMed](#)]
24. Sommerfeld, L.; Finkernagel, F.; Jansen, J.M.; Wagner, U.; Nist, A.; Stiewe, T.; Müller-Brüsselbach, S.; Sokol, A.M.; Graumann, J.; Reinartz, S.; et al. The multicellular signalling network of ovarian cancer metastases. *Clin. Transl. Med.* **2021**, *11*, e633. [[CrossRef](#)] [[PubMed](#)]

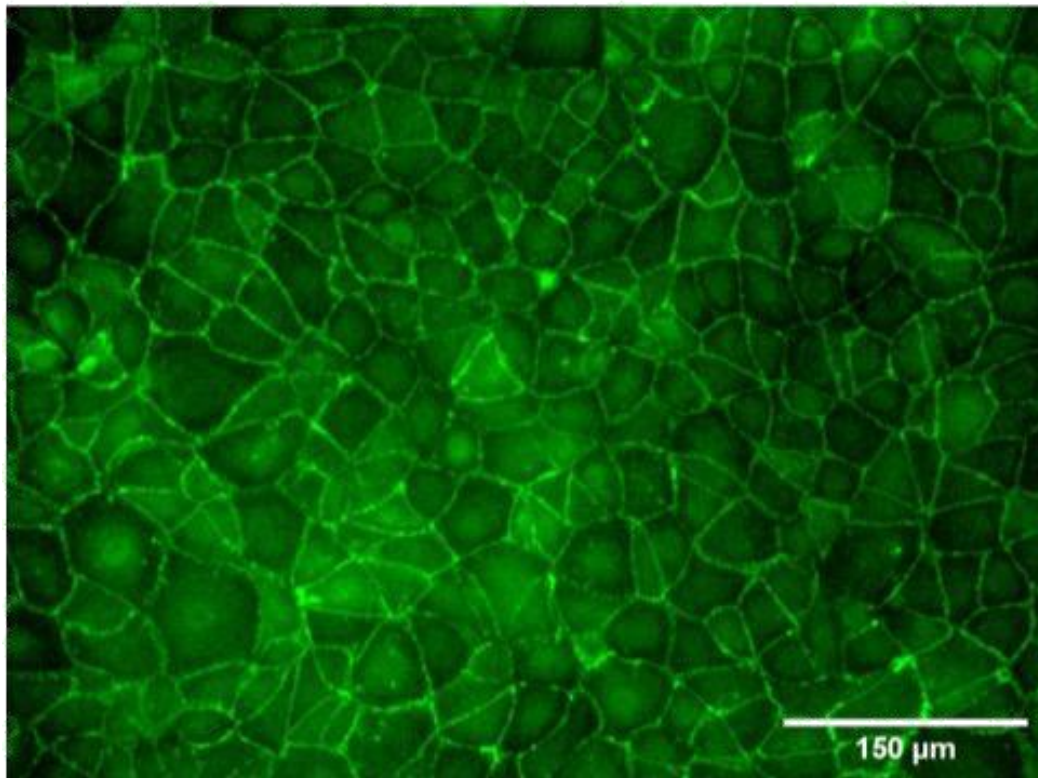
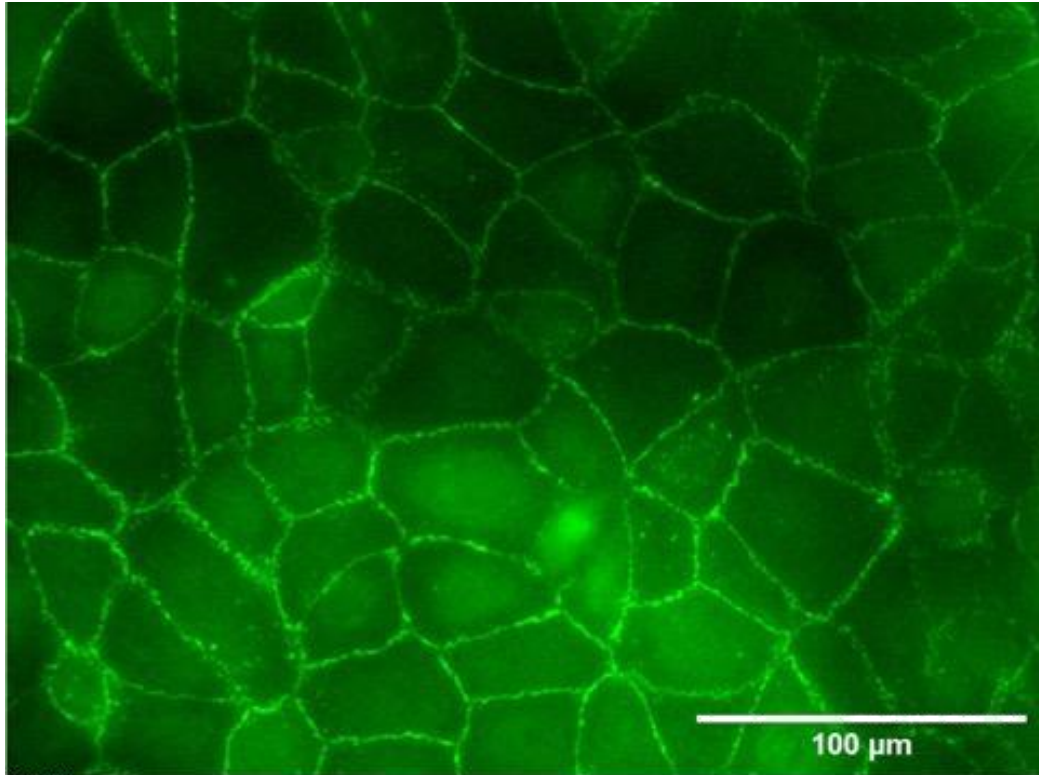
25. Steitz, A.M.; Steffes, A.; Finkernagel, F.; Unger, A.; Sommerfeld, L.; Jansen, J.M.; Wagner, U.; Graumann, J.; Müller, R.; Reinartz, S. Tumor-associated macrophages promote ovarian cancer cell migration by secreting transforming growth factor beta induced (TGFB1) and tenascin C. *Cell Death Dis.* **2020**, *11*, 249. [[CrossRef](#)]
26. Pluchart, H.; Khouri, C.; Blaise, S.; Roustit, M.; Cracowski, J.-L. Targeting the Prostacyclin Pathway: Beyond Pulmonary Arterial Hypertension. *Trends Pharmacol. Sci.* **2017**, *38*, 512–523. [[CrossRef](#)]
27. Banhos Danneskiold-Samsøe, N.; Sonne, S.B.; Larsen, J.M.; Hansen, A.N.; Fjære, E.; Isidor, M.S.; Petersen, S.; Henningsen, J.; Severi, I.; Sartini, L.; et al. Overexpression of cyclooxygenase-2 in adipocytes reduces fat accumulation in inguinal white adipose tissue and hepatic steatosis in high-fat fed mice. *Sci. Rep.* **2019**, *9*, 8979. [[CrossRef](#)]
28. Rohalter, V.; Roth, K.; Finkernagel, F.; Adhikary, T.; Obert, J.; Dorzweiler, K.; Bensberg, M.; Müller-Brüsselbach, S.; Müller, R. A multi-stage process including transient polyploidization and EMT precedes the emergence of chemoresistant ovarian carcinoma cells with a dedifferentiated and pro-inflammatory secretory phenotype. *Oncotarget* **2015**, *6*, 40005–40025. [[CrossRef](#)]
29. Guescini, M.; Sisti, D.; Rocchi, M.B.L.; Stocchi, L.; Stocchi, V. A new real-time PCR method to overcome significant quantitative inaccuracy due to slight amplification inhibition. *BMC Bioinform.* **2008**, *9*, 326. [[CrossRef](#)]
30. Yates, A.D.; Achuthan, P.; Akanni, W.; Allen, J.; Allen, J.; Alvarez-Jarreta, J.; Amode, M.R.; Armean, I.M.; Azov, A.G.; Bennett, R.; et al. Ensembl 2020. *Nucleic Acids Res.* **2020**, *48*, D682–D688. [[CrossRef](#)]
31. Robinson, M.D.; McCarthy, D.J.; Smyth, G.K. edgeR: A Bioconductor package for differential expression analysis of digital gene expression data. *Bioinformatics* **2010**, *26*, 139–140. [[CrossRef](#)] [[PubMed](#)]
32. Herwig, R.; Hardt, C.; Lienhard, M.; Kamburov, A. Analyzing and interpreting genome data at the network level with Consensus-PathDB. *Nat. Protoc.* **2016**, *11*, 1889–1907. [[CrossRef](#)]
33. Gyorffy, B.; Lánckzy, A.; Szállási, Z. Implementing an online tool for genome-wide validation of survival-associated biomarkers in ovarian-cancer using microarray data from 1287 patients. *Endocr. Relat. Cancer* **2012**, *19*, 197–208. [[CrossRef](#)] [[PubMed](#)]
34. Gentles, A.J.; Newman, A.M.; Liu, C.L.; Bratman, S.V.; Feng, W.; Kim, D.; Nair, V.S.; Xu, Y.; Khuong, A.; Hoang, C.D.; et al. The prognostic landscape of genes and infiltrating immune cells across human cancers. *Nat. Med.* **2015**, *21*, 938–945. [[CrossRef](#)] [[PubMed](#)]
35. Clapp, L.H.; Abu-Hanna, J.H.J.; Patel, J.A. Diverse Pharmacology of Prostacyclin Mimetics: Implications for Pulmonary Hypertension. In *Molecular Mechanism of Congenital Heart Disease and Pulmonary Hypertension*; Nakanishi, T., Baldwin, H.S., Fineman, J.R., Yamagishi, H., Eds.; Springer: Singapore, 2020; pp. 31–61. ISBN 978-981-15-1184-4.
36. Mao, Y.; Finnemann, S.C. Regulation of phagocytosis by Rho GTPases. *Small GTPases* **2015**, *6*, 89–99. [[CrossRef](#)]
37. Clayton, N.S.; Ridley, A.J. Targeting Rho GTPase Signaling Networks in Cancer. *Front. Cell Dev. Biol.* **2020**, *8*, 222. [[CrossRef](#)]
38. Liu, M.; Guo, S.; Stiles, J.K. The emerging role of CXCL10 in cancer (Review). *Oncol. Lett.* **2011**, *2*, 583–589. [[CrossRef](#)]
39. Tait Wojno, E.D.; Hunter, C.A.; Stumhofer, J.S. The Immunobiology of the Interleukin-12 Family: Room for Discovery. *Immunity* **2019**, *50*, 851–870. [[CrossRef](#)]
40. Finetti, F.; Travelli, C.; Ercoli, J.; Colombo, G.; Buoso, E.; Trabalzini, L. Prostaglandin E2 and Cancer: Insight into Tumor Progression and Immunity. *Biology* **2020**, *9*, 434. [[CrossRef](#)]
41. Schumann, T.; Adhikary, T.; Wortmann, A.; Finkernagel, F.; Lieber, S.; Schnitzer, E.; Legrand, N.; Schober, Y.; Nockher, W.A.; Toth, P.M.; et al. Deregulation of PPAR β/δ target genes in tumor-associated macrophages by fatty acid ligands in the ovarian cancer microenvironment. *Oncotarget* **2015**, *6*, 13416–13433. [[CrossRef](#)]
42. Adhikary, T.; Wortmann, A.; Schumann, T.; Finkernagel, F.; Lieber, S.; Roth, K.; Toth, P.M.; Diederich, W.E.; Nist, A.; Stiewe, T.; et al. The transcriptional PPAR β/δ network in human macrophages defines a unique agonist-induced activation state. *Nucleic Acids Res.* **2015**, *43*, 5033–5051. [[CrossRef](#)] [[PubMed](#)]
43. Lucas, F.V.; Skrinska, V.A.; Chisolm, G.M.; Hesse, B.L. Stability of prostacyclin in human and rabbit whole blood and plasma. *Thromb. Res.* **1986**, *43*, 379–387. [[CrossRef](#)] [[PubMed](#)]
44. Daikoku, T.; Wang, D.; Tranguch, S.; Morrow, J.D.; Orsulic, S.; DuBois, R.N.; Dey, S.K. Cyclooxygenase-1 is a potential target for prevention and treatment of ovarian epithelial cancer. *Cancer Res.* **2005**, *65*, 3735–3744. [[CrossRef](#)] [[PubMed](#)]
45. Beeghly-Fadiel, A.; Wilson, A.J.; Keene, S.; El Ramahi, M.; Xu, S.; Marnett, L.J.; Fadare, O.; Crispens, M.A.; Khabele, D. Differential cyclooxygenase expression levels and survival associations in type I and type II ovarian tumors. *J. Ovarian Res.* **2018**, *11*, 17. [[CrossRef](#)]
46. Hua, H.; Zhang, H.; Kong, Q.; Wang, J.; Jiang, Y. Complex roles of the old drug aspirin in cancer chemoprevention and therapy. *Med. Res. Rev.* **2019**, *39*, 114–145. [[CrossRef](#)]
47. Zhang, D.; Bai, B.; Xi, Y.; Wang, T.; Zhao, Y. Is aspirin use associated with a decreased risk of ovarian cancer? A systematic review and meta-analysis of observational studies with dose-response analysis. *Gynecol. Oncol.* **2016**, *142*, 368–377. [[CrossRef](#)]
48. Ammundsen, H.B.; Faber, M.T.; Jensen, A.; Høgdall, E.; Blaakaer, J.; Høgdall, C.; Kjaer, S.K. Use of analgesic drugs and risk of ovarian cancer: Results from a Danish case-control study. *Acta Obstet. Gynecol. Scand.* **2012**, *91*, 1094–1102. [[CrossRef](#)]
49. Trabert, B.; Ness, R.B.; Lo-Ciganic, W.-H.; Murphy, M.A.; Goode, E.L.; Poole, E.M.; Brinton, L.A.; Webb, P.M.; Nagle, C.M.; Jordan, S.J.; et al. Aspirin, nonaspirin nonsteroidal anti-inflammatory drug, and acetaminophen use and risk of invasive epithelial ovarian cancer: A pooled analysis in the Ovarian Cancer Association Consortium. *J. Natl. Cancer Inst.* **2014**, *106*, djt431. [[CrossRef](#)]
50. Barnard, M.E.; Poole, E.M.; Curhan, G.C.; Eliassen, A.H.; Rosner, B.A.; Terry, K.L.; Tworoger, S.S. Association of Analgesic Use with Risk of Ovarian Cancer in the Nurses' Health Studies. *JAMA Oncol.* **2018**, *4*, 1675–1682. [[CrossRef](#)]

51. Merritt, M.A.; Rice, M.S.; Barnard, M.E.; Hankinson, S.E.; Matulonis, U.A.; Poole, E.M.; Tworoger, S.S. Pre-diagnosis and post-diagnosis use of common analgesics and ovarian cancer prognosis (NHS/NHSII): A cohort study. *Lancet Oncol.* **2018**, *19*, 1107–1116. [[CrossRef](#)]
52. Wield, A.M.; Walsh, C.S.; Rimel, B.J.; Cass, I.; Karlan, B.Y.; Li, A.J. Aspirin use correlates with survival in women with clear cell ovarian cancer. *Gynecol. Oncol. Rep.* **2018**, *25*, 78–81. [[CrossRef](#)] [[PubMed](#)]
53. Gubbala, V.B.; Jytosana, N.; Trinh, V.Q.; Maurer, H.C.; Naeem, R.F.; Lytle, N.K.; Ma, Z.; Zhao, S.; Lin, W.; Han, H.; et al. Eicosanoids in the pancreatic tumor microenvironment—A multicellular, multifaceted progression. *Gastro Hep Adv.* **2022**, *1*, 682–697. [[CrossRef](#)] [[PubMed](#)]
54. Stratton, R.; Shiwen, X. Role of prostaglandins in fibroblast activation and fibrosis. *J. Cell Commun. Signal.* **2010**, *4*, 75–77. [[CrossRef](#)] [[PubMed](#)]
55. Foster, D.S.; Jones, R.E.; Ransom, R.C.; Longaker, M.T.; Norton, J.A. The evolving relationship of wound healing and tumor stroma. *JCI Insight* **2018**, *3*, e99911. [[CrossRef](#)] [[PubMed](#)]
56. Rynne-Vidal, A.; Au-Yeung, C.L.; Jiménez-Heffernan, J.A.; Pérez-Lozano, M.L.; Cremades-Jimeno, L.; Bárcena, C.; Cristóbal-García, I.; Fernández-Chacón, C.; Yeung, T.L.; Mok, S.C.; et al. Mesothelial-to-mesenchymal transition as a possible therapeutic target in peritoneal metastasis of ovarian cancer. *J. Pathol.* **2017**, *242*, 140–151. [[CrossRef](#)] [[PubMed](#)]
57. Cathcart, M.-C.; Reynolds, J.V.; O’Byrne, K.J.; Pidgeon, G.P. The role of prostacyclin synthase and thromboxane synthase signaling in the development and progression of cancer. *Biochim. Biophys. Acta* **2010**, *1805*, 153–166. [[CrossRef](#)] [[PubMed](#)]
58. Kamio, K.; Liu, X.; Sugiura, H.; Togo, S.; Kobayashi, T.; Kawasaki, S.; Wang, X.; Mao, L.; Ahn, Y.; Hogaboam, C.; et al. Prostacyclin analogs inhibit fibroblast contraction of collagen gels through the cAMP-PKA pathway. *Am. J. Respir. Cell Mol. Biol.* **2007**, *37*, 113–120. [[CrossRef](#)] [[PubMed](#)]
59. Ruffell, D.; Mourkioti, F.; Gambardella, A.; Kirstetter, P.; Lopez, R.G.; Rosenthal, N.; Nerlov, C. A CREB-C/EBPbeta cascade induces M2 macrophage-specific gene expression and promotes muscle injury repair. *Proc. Natl. Acad. Sci. USA* **2009**, *106*, 17475–17480. [[CrossRef](#)]
60. Qin, H.; Holdbrooks, A.T.; Liu, Y.; Reynolds, S.L.; Yanagisawa, L.L.; Benveniste, E.N. SOCS3 deficiency promotes M1 macrophage polarization and inflammation. *J. Immunol.* **2012**, *189*, 3439–3448. [[CrossRef](#)]
61. Clark, K.; MacKenzie, K.F.; Petkevicius, K.; Kristariyanto, Y.; Zhang, J.; Choi, H.G.; Pegg, M.; Plater, L.; Pedrioli, P.G.A.; McIver, E.; et al. Phosphorylation of CRT3 by the salt-inducible kinases controls the interconversion of classically activated and regulatory macrophages. *Proc. Natl. Acad. Sci. USA* **2012**, *109*, 16986–16991. [[CrossRef](#)]
62. Avni, D.; Ernst, O.; Philosoph, A.; Zor, T. Role of CREB in modulation of TNFalpha and IL-10 expression in LPS-stimulated RAW264.7 macrophages. *Mol. Immunol.* **2010**, *47*, 1396–1403. [[CrossRef](#)] [[PubMed](#)]
63. Luan, B.; Yoon, Y.-S.; Le Lay, J.; Kaestner, K.H.; Hedrick, S.; Montminy, M. CREB pathway links PGE2 signaling with macrophage polarization. *Proc. Natl. Acad. Sci. USA* **2015**, *112*, 15642–15647. [[CrossRef](#)] [[PubMed](#)]
64. Chu, L.; Liou, J.-Y.; Wu, K.K. Prostacyclin protects vascular integrity via PPAR/14-3-3 pathway. *Prostaglandins Other Lipid Mediat.* **2015**, *118–119*, 19–27. [[CrossRef](#)] [[PubMed](#)]
65. Hertz, R.; Berman, I.; Keppler, D.; Bar-Tana, J. Activation of gene transcription by prostacyclin analogues is mediated by the peroxisome-proliferators-activated receptor (PPAR). *Eur. J. Biochem.* **1996**, *235*, 242–247. [[CrossRef](#)] [[PubMed](#)]
66. Chen, Y.; Zhang, S.; Wang, Q.; Zhang, X. Tumor-recruited M2 macrophages promote gastric and breast cancer metastasis via M2 macrophage-secreted CHI3L1 protein. *J. Hematol. Oncol.* **2017**, *10*, 36. [[CrossRef](#)] [[PubMed](#)]
67. Liu, L.; Wang, X.; Li, X.; Wu, X.; Tang, M.; Wang, X. Upregulation of IGF1 by tumor-associated macrophages promotes the proliferation and migration of epithelial ovarian cancer cells. *Oncol. Rep.* **2018**, *39*, 818–826. [[CrossRef](#)]
68. Zeng, X.-Y.; Xie, H.; Yuan, J.; Jiang, X.-Y.; Yong, J.-H.; Zeng, D.; Dou, Y.-Y.; Xiao, S.-S. M2-like tumor-associated macrophages-secreted EGF promotes epithelial ovarian cancer metastasis via activating EGFR-ERK signaling and suppressing lncRNA LIMT expression. *Cancer Biol. Ther.* **2019**, *20*, 956–966. [[CrossRef](#)]
69. Na, Y.-R.; Yoon, Y.-N.; Son, D.-I.; Seok, S.-H. Cyclooxygenase-2 inhibition blocks M2 macrophage differentiation and suppresses metastasis in murine breast cancer model. *PLoS ONE* **2013**, *8*, e63451. [[CrossRef](#)]

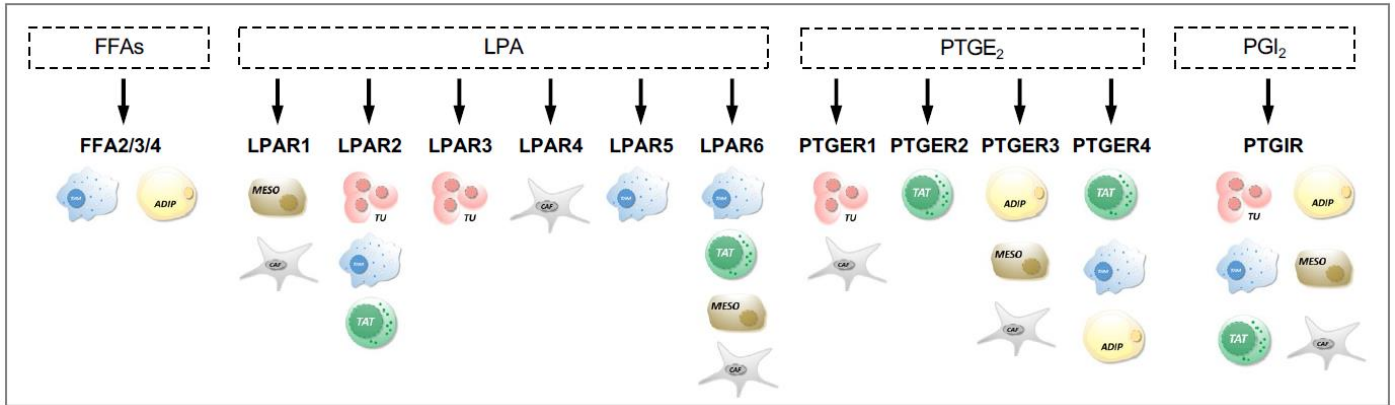
Supplementary Figures S1-S11

Prostacyclin released by cancer-associated fibroblasts promotes immunosuppressive and pro-metastatic macrophage polarization in the ovarian cancer microenvironment

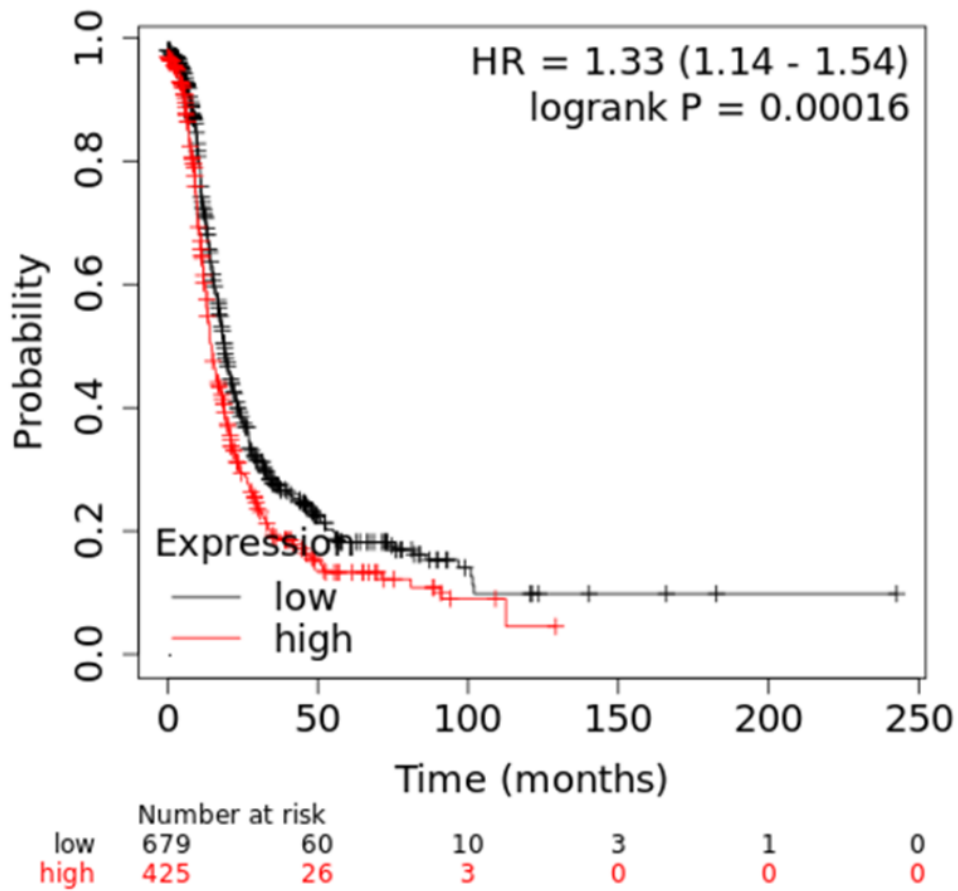
Leah Sommerfeld, Isabel Knuth, Florian Finkernagel, Jelena Pesek, Wolfgang A. Nockher, Julia M. Jansen, Uwe Wagner, Andrea Nist, Thorsten Stiewe, Sabine Müller-Brüsselbach, Rolf Müller and Silke Reinartz



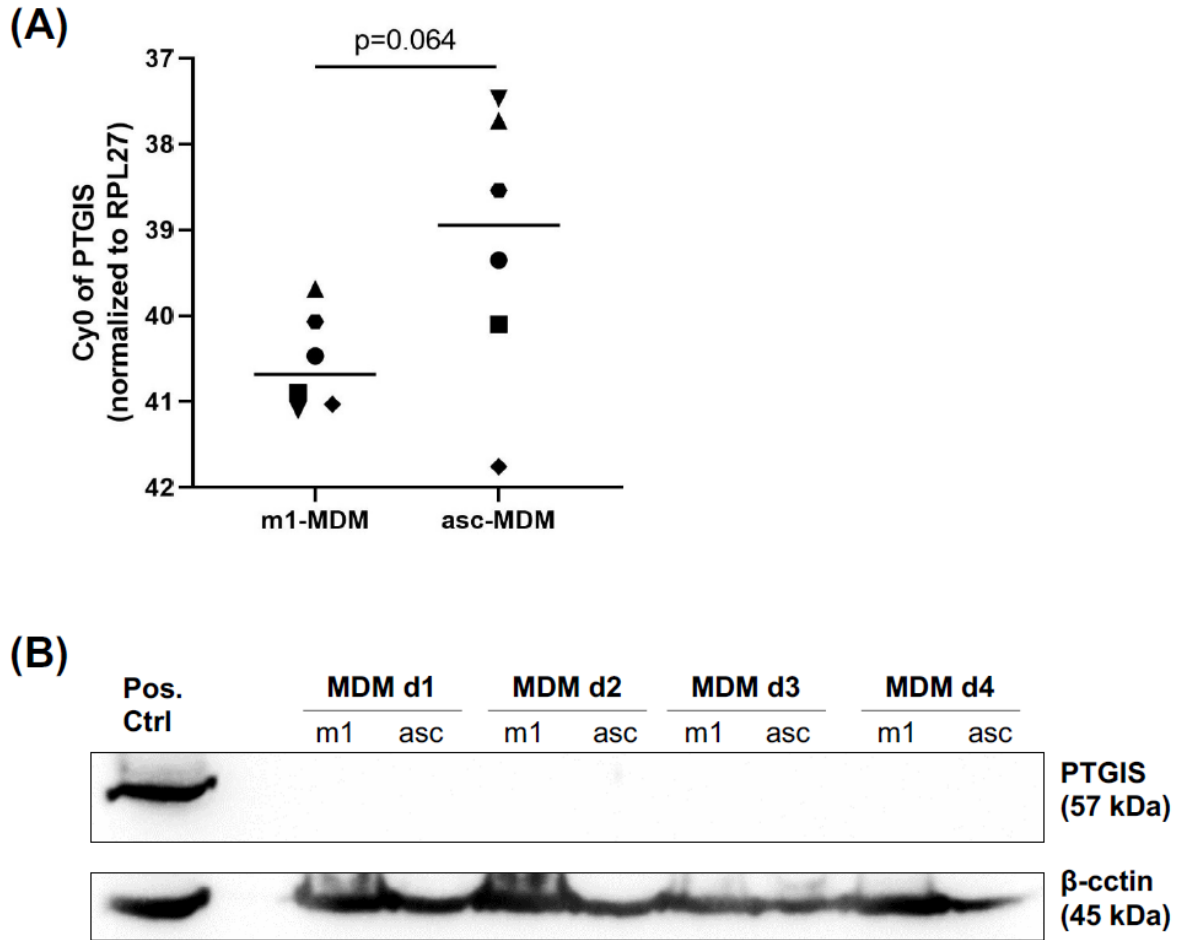
Supplementary Figure S1. Evaluation of the integrity of MESO monolayers for tumor cell adhesion assay. Microscopic evaluation (wells of 96-well plate) showing the integrity of ME-SO monolayers after staining for the tight junctions scaffolding protein zonula occludens 1 (ZO1).



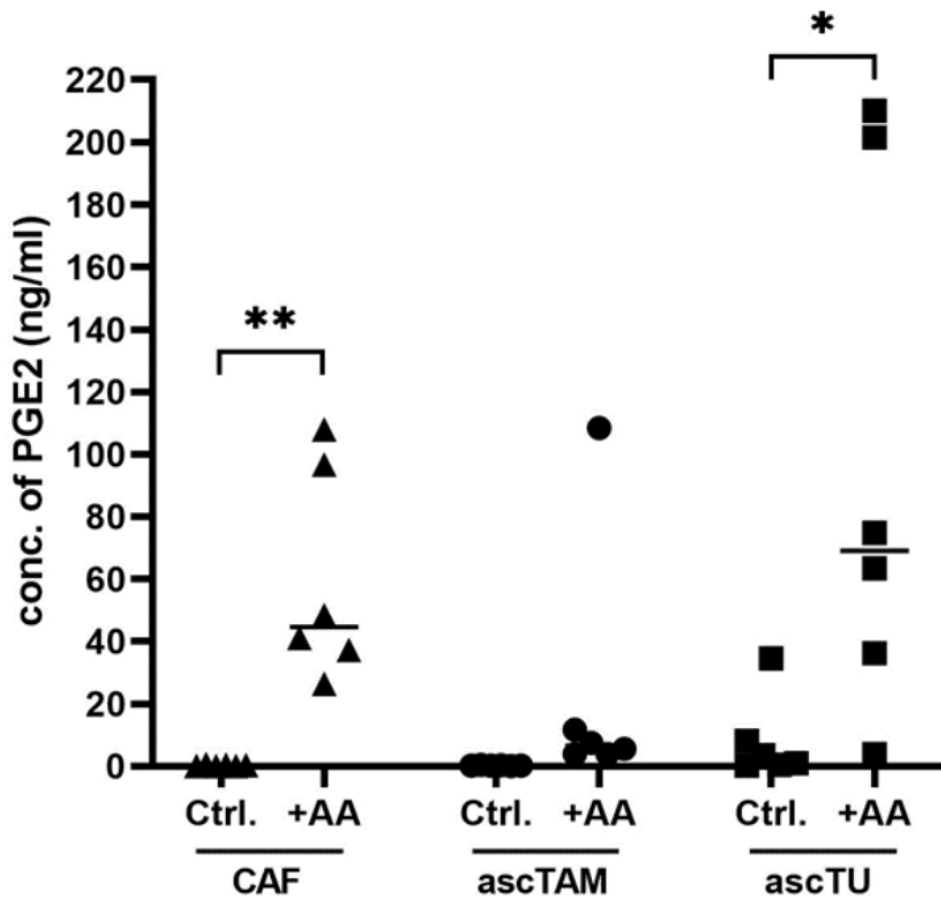
Supplementary Figure S2. Cell-type-selectivity of genes coding for receptors of lipid mediators. The figure is based on the data in Figure 1A and shows the cell types with the highest level of receptor expression.



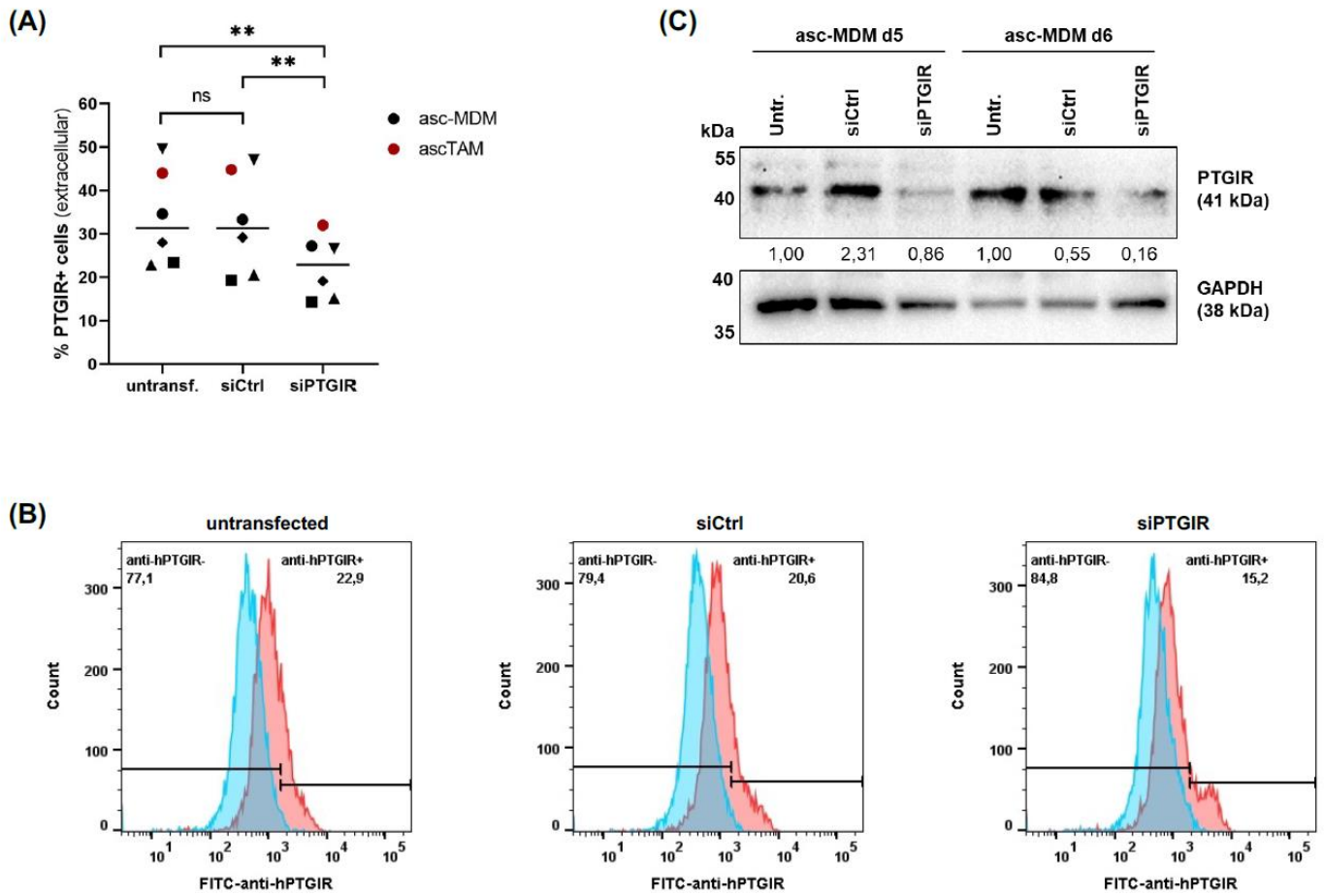
Supplementary Figure S3. Inverse association of PTGIS expression with relapse-free survival in HGSC patients. Kaplan-Meier plot showing the association between relapse-free survival (RFS) and PTGIS expression in tumor tissue (KM plotter: logrank P = 0.00016, HR = 1.33). The plot was generated by KM Plotter [33].



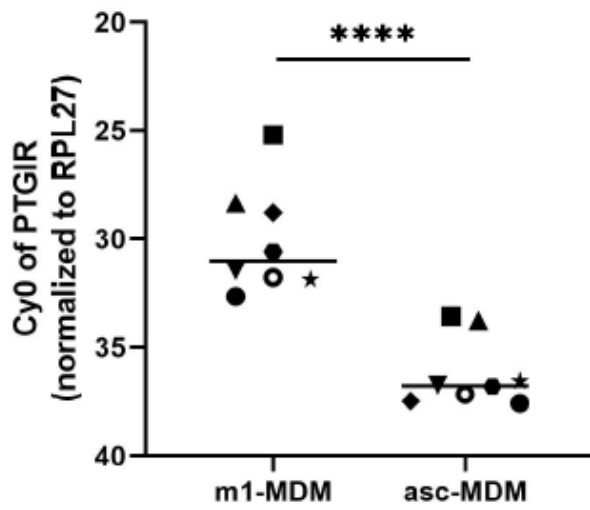
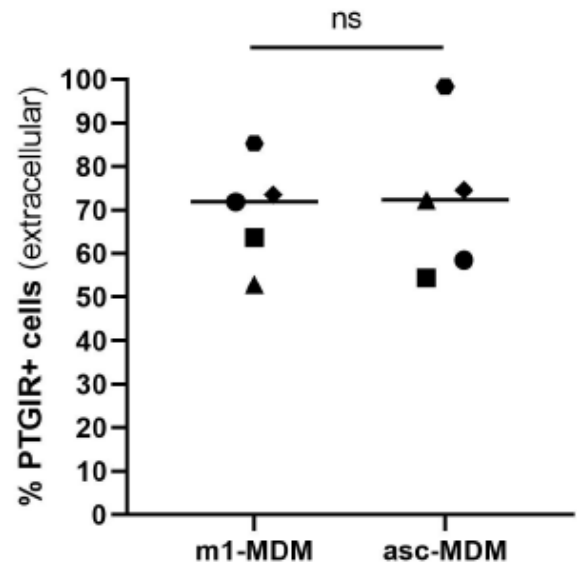
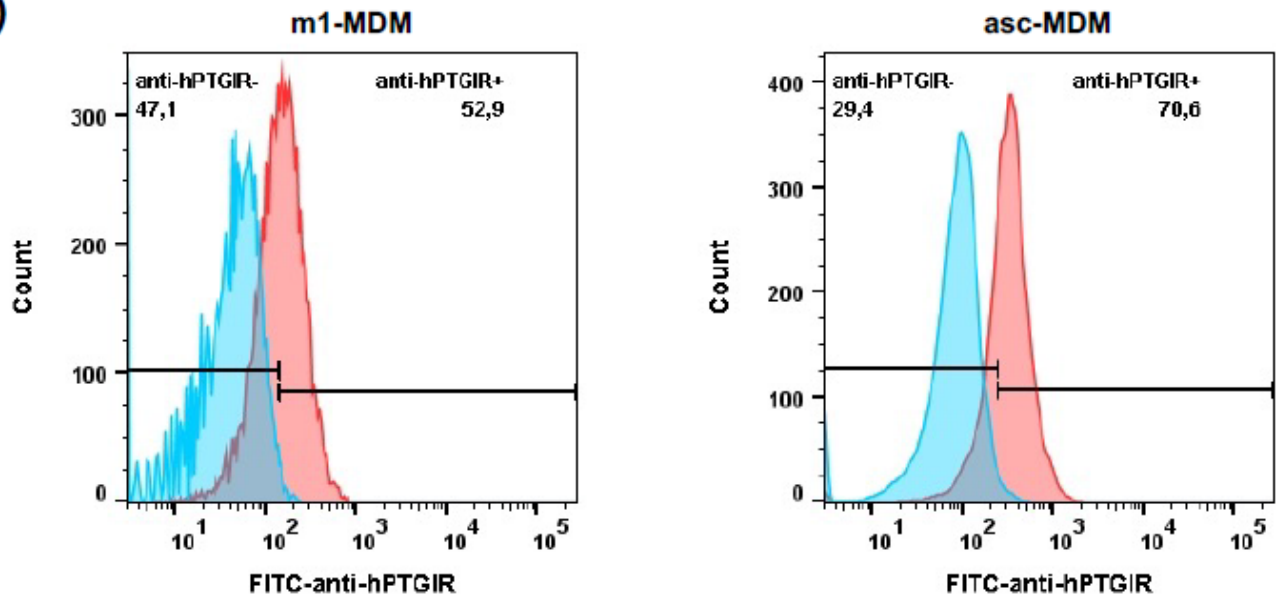
Supplementary Figure S4. PTGIS expression in differently polarized macrophages. **(A)** Expression of PTGIS mRNA in m1-MDM and asc-MDM analyzed by RT-qPCR in $n = 6$ matched pairs of different donors (donors are distinguished by different symbols). p values were determined by paired t test. Horizontal bars show the mean. **(B)** Detection of PTGIS protein in m1-MDM and asc-MDM by immunoblotting ($n = 4$; donor d1-d4). β -actin was used as loading control. A representative blot is shown.



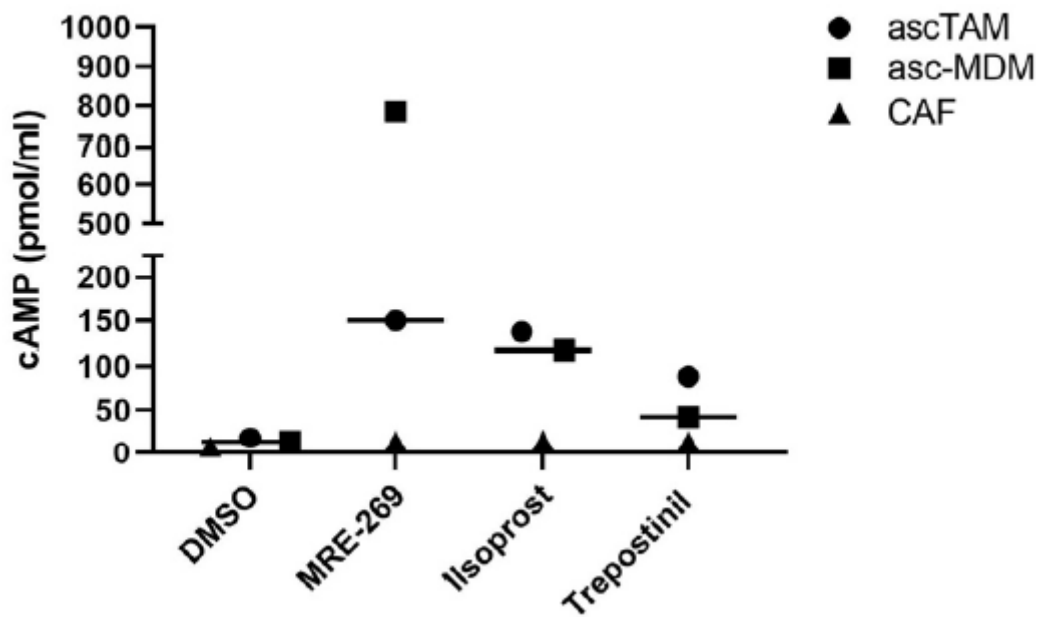
Supplementary Figure S5. PGE2 synthesis in different cell types of the HGSC TME. MS-based quantification of PGE2 in conditioned media (CM) from ascTAM, ascTU and CAF after serum deprivation in the presence of 50 μ M AA for 24 hours. Controls without AA are included for each cell type. * $p < 0.05$; ** $p < 0.01$ by paired t test (Ctrl vs. AA-treated cells). Horizontal bars show the mean.



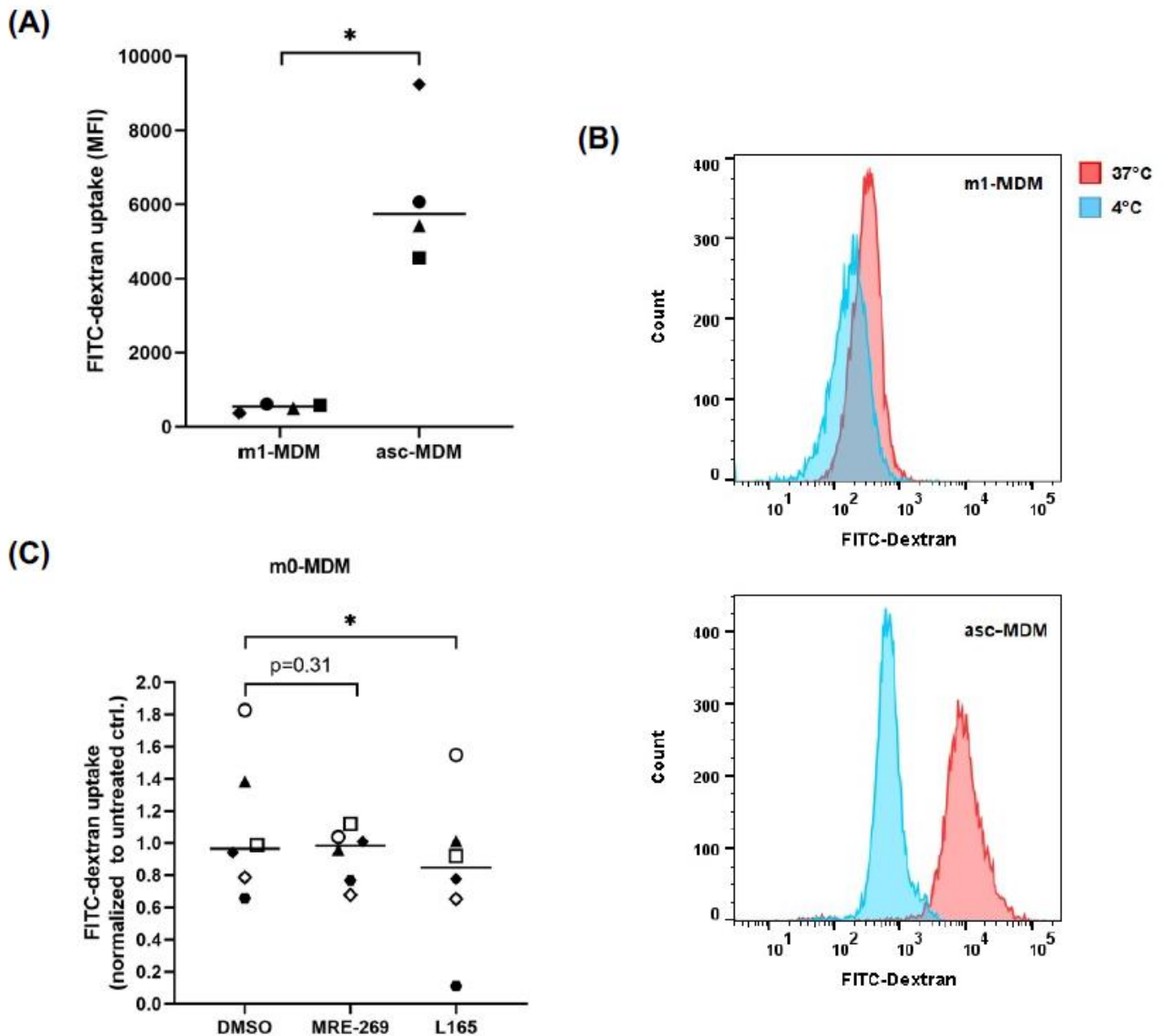
Supplementary Figure S6. Validation of PTGIR staining in macrophages. **(A)** Surface expression of PTGIR in asc-MDM and ascTAM analyzed by flow cytometry after transient transfection with siPTGIR or control siRNA (siCtrl). Untreated macrophages were included as controls ($n = 6$ each). $** p < 0.01$ by paired t test. Horizontal bars show the mean. **(B)** Representative histograms of PTGIR staining for untransfected, siPTGIR- and siCtrl-transfected asc-MDM. **(C)** Immunoblot for PTGIR detection in untransfected, siPTGIR- and siCtrl-transfected asc-MDM of two donors (day 5 and day 6). GAPDH was used as loading control. Quantifications of PTGIR expression relative to GAPDH are indicated.

(A)**(B)****(C)**

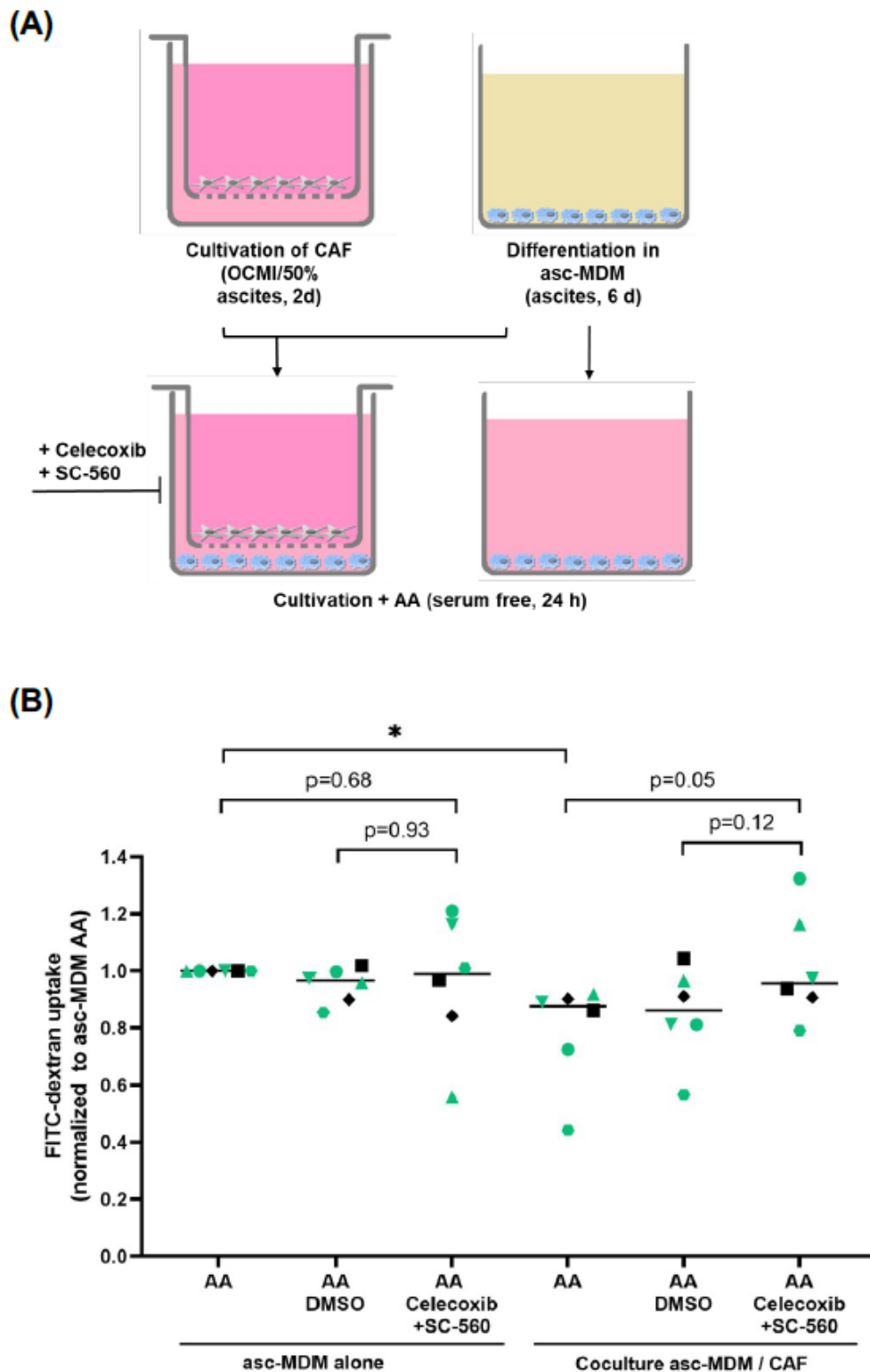
Supplementary Figure S7. PTGIR expression in differently polarized macrophages. **(A)** Expression of PTGIR mRNA in m1-MDM and asc-MDM analyzed by RT-qPCR in $n = 7$ matched pairs of different donors (donors are distinguished by different symbols). **** $p < 0.0001$ by paired t test. **(B)** Detection of PTGIR expression in m1-MDM and asc-MDM by flow cytometry ($n = 5$). p values were determined by paired t test. Horizontal bars show the mean. **(C)** Repe-representative histograms of PTGIR staining in asc-MDM and m1-MDM. Blue: Isotype control; red: PTGIR.



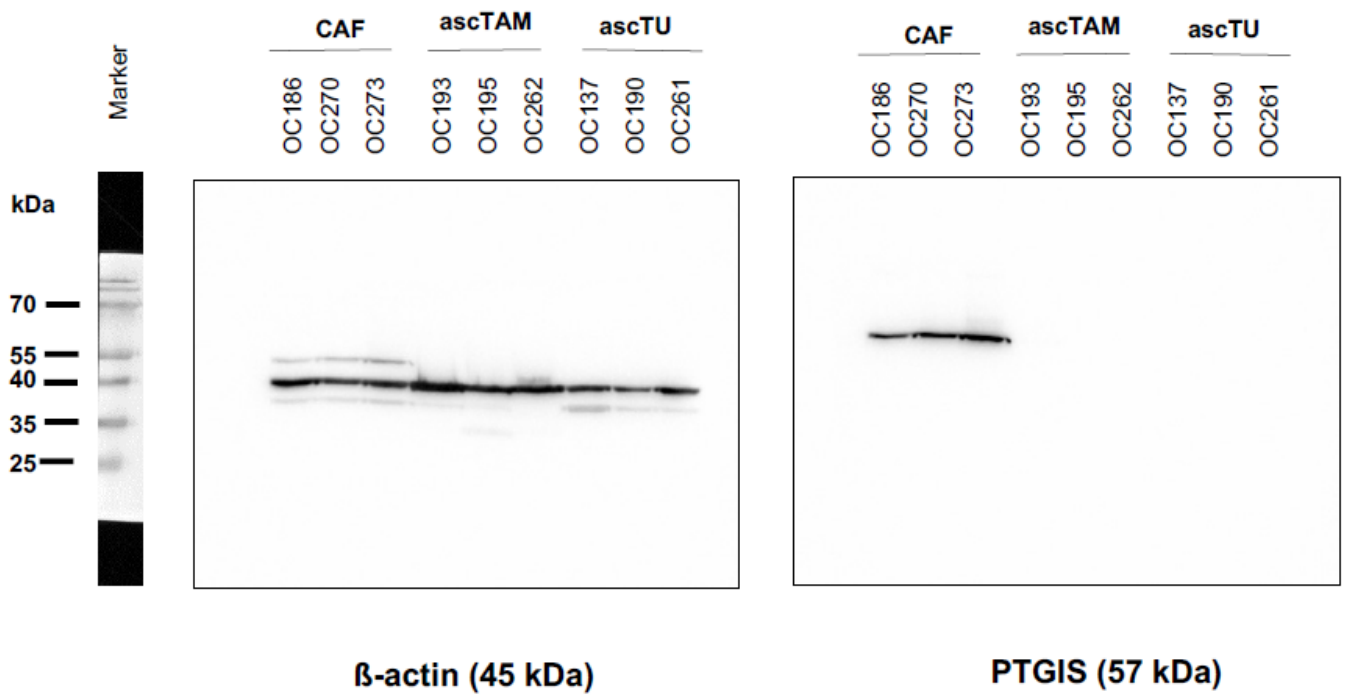
Supplementary Figure S8. Induction of PTGIR signaling by different PGI₂ analogs. Comparative analysis of intracellular cAMP accumulation in asc-MDM, asc-TAM and CAF up-on stimulation with 100 nM MRE-269, iloprost or trepostinil for 15 min under serum-free conditions. Solvent-treated cells (DMSO) were included as controls. Horizontal bars show the mean.



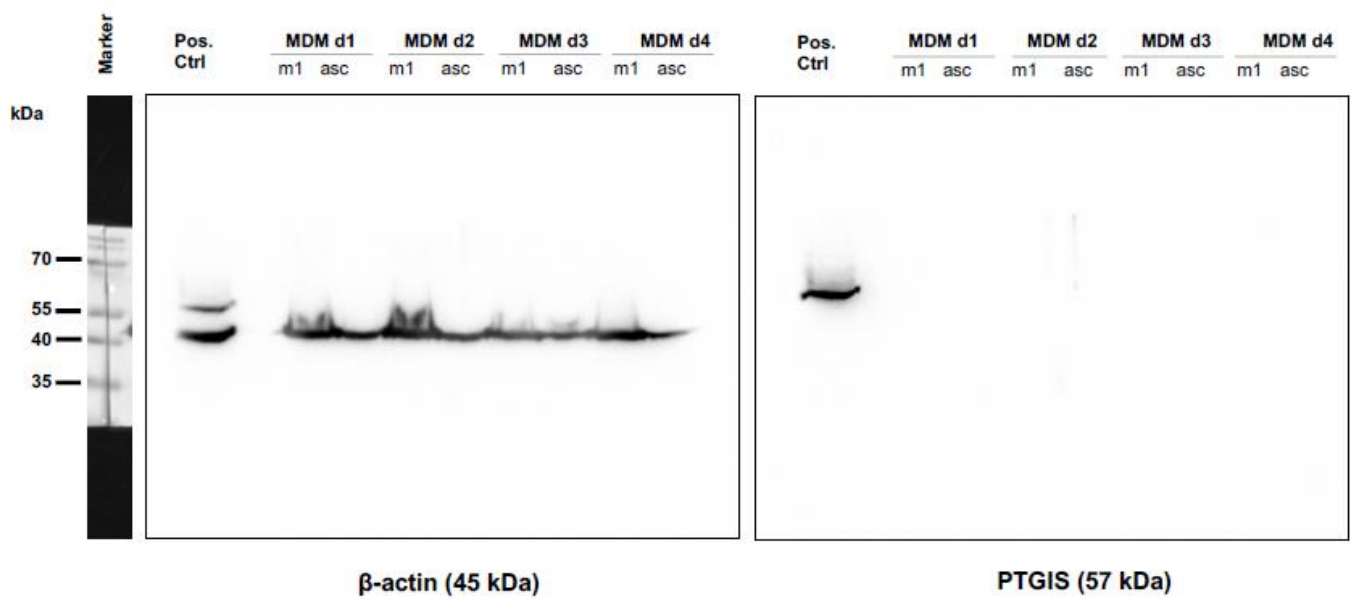
Supplementary Figure S9. Impact of PGI₂ analogs on macropinocytosis in differently polarized macrophages. (A) Macropinocytosis was determined by FITC-dextran uptake of untreated asc-MDM and compared to m1-MDM ($n = 4$ matched donors). * $p < 0.05$ by paired t test. (B) Representative histograms of FITC-dextran uptake in asc-MDM versus m1-MDM. Red: FITC internalization (37 °C); blue FITC binding control (4 °C). (C) Macropinocytosis of M0 MDM ($n = 6$) stimulated with MRE-269 (100 nM) or PPAR β /d agonist L165 (1 μ M). DMSO treated M0 MDM were included as controls. * $p < 0.05$ by paired t test. Horizontal bars show the mean.



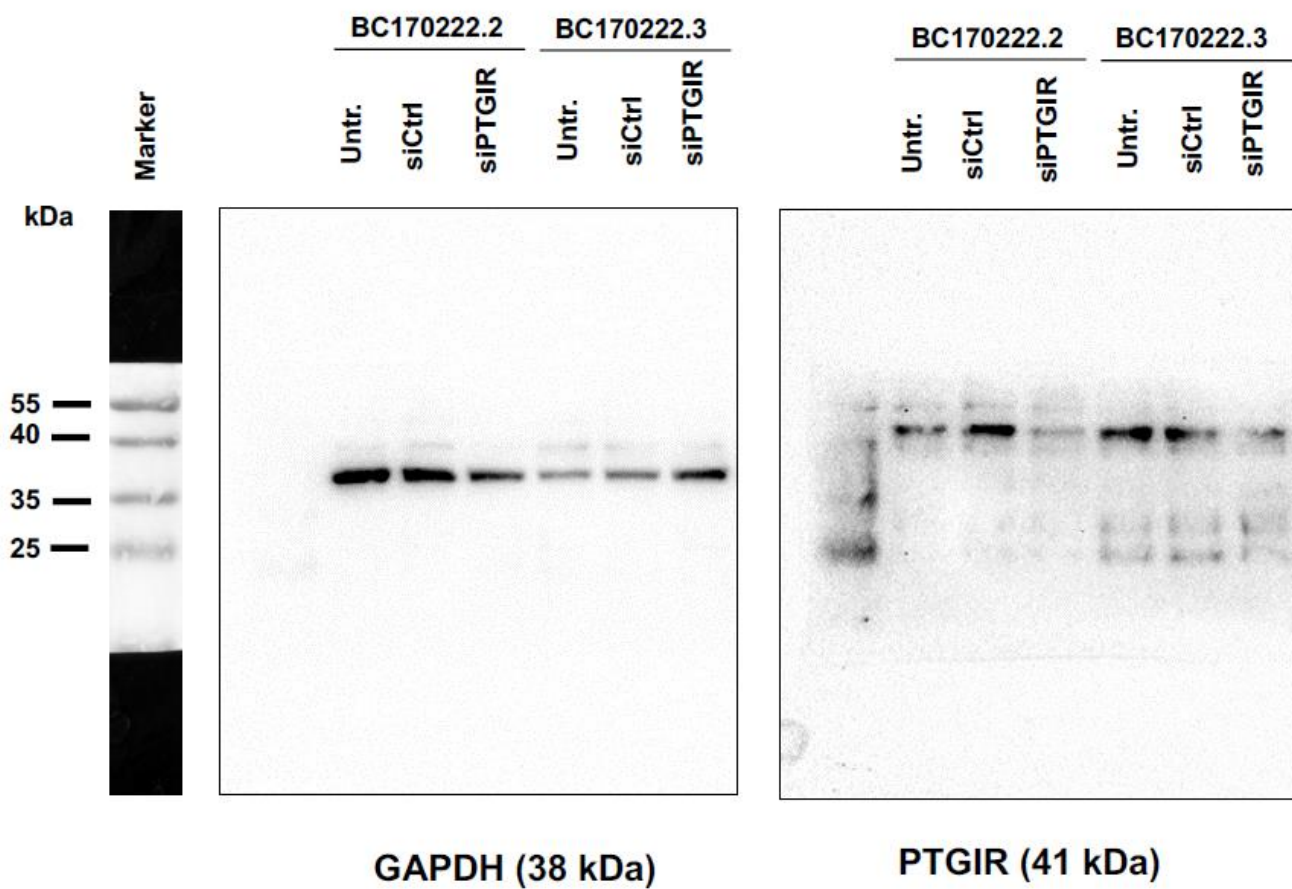
Supplementary Figure S10. Influence of CAF on macrophagocytotic activity of TAM. **(A)** Schematic overview of the experimental setup of CAF / asc-MEM co-culture for evaluation of macrophagocytosis. **(B)** Macrophagocytosis of asc-MDM after co-culture with CAF. Continuous PGI₂ production by CAF in serum-free co-culture was maintained by adding exogenous AA (50 μ M) as a substrate for PGI₂ biosynthesis. For COX1/2 blockade, 1 μ M SC-560 and 10 μ M celecoxib were added to co-cultures for 24 hours. Solvent controls (DMSO) were included. asc-MDM in the absence of CAFs were equally treated. Green dots represent donors responding to COX1/2 inhibitors in co-cultures. * $p < 0.05$ by paired t test. Horizontal bars show the mean.



Supplementary Figure S11. A. Original image (full immunoblot) of Figure 2C.



Supplementary Figure S11. B. Original image (full immunoblot) of Figure S4B.



Supplementary Figure S11. C. Original image (full immunoblot) of Figure S6C.

7. Appendicies

7.1 All publications of the author

Sivakumar, S., Lieber, S., Librizzi, D., Keber, C., **Sommerfeld, L.**, Finkernagel, F., Roth, K., Reinartz, S., Bartsch, J. W., Graumann, J., Müller-Brüsselbach, S., Müller, R. (2023). Basal cell adhesion molecule promotes metastasis-associated processes in ovarian cancer. *Clin Transl Med.* 2023; 13:e1176. <https://doi.org/10.1002/ctm2.1176>

Sommerfeld, L., Knuth, I., Finkernagel, F., Pesek, J., Nockher, W. A., Jansen, J. M., Wagner, U., Nist, A., Stiewe, T., Müller-Brüsselbach, S., Müller, R., & Reinartz, S. (2022). Prostacyclin Released by Cancer-Associated Fibroblasts Promotes Immunosuppressive and Pro-Metastatic Macrophage Polarization in the Ovarian Cancer Microenvironment. *Cancers*, 14(24), 6154. <https://doi.org/10.3390/cancers14246154>

Sommerfeld, L., Finkernagel, F., Jansen, J. M., Wagner, U., Nist, A., Stiewe, T., Müller-Brüsselbach, S., Sokol, A. M., Graumann, J., Reinartz, S., & Müller, R. (2021). The multicellular signalling network of ovarian cancer metastases. *Clinical and Translational Medicine*, 11(11), e633. <https://doi.org/10.1002/ctm2.633>

Steitz, A. M., Steffes, A., Finkernagel, F., Unger, A., **Sommerfeld, L.**, Jansen, J. M., Wagner, U., Graumann, J., Müller, R., & Reinartz, S. (2020). Tumor-associated macrophages promote ovarian cancer cell migration by secreting transforming growth factor beta induced (TGFB1) and tenascin C. *Cell Death & Disease*, 11(4), 249. <https://doi.org/10.1038/s41419-020-2438-8>

7.2 Curriculum vitae

7.3 Directory of academic teachers

My academic teachers in Marburg were:

Adamkiewicz, Adhikary, J. W. Bartsch, U.-M. Bauer, S. Bauer, Becker, Brandt, Brehm, Brendel, Buchholz, Burchert, Conrad, Czubayko, Daut, Decher, Elsässer, Feuser, Frech, Fritz, Greene, Huber, Jacob, Lauth, Lill, Lohoff, Maisner, Mandic, Mühlenhoff, Müller-Brüsselbach, Müller, Neubauer, Oberwinkler, Oliver, Plant, Pogge von Strandmann, Reinartz, Stehling, Steinhoff, Stiewe, Suske, Timmesfeld, Wanzel, Westermann, Worzfeld, Wrocklage.

7.4 Ehrenwörtliche Erklärung

Acknowledgments – Danksagung

An dieser Stelle möchte ich mich bei allen Personen bedanken, die mich in der Zeit meiner Doktorarbeit unterstützt haben und ohne die diese Dissertation nicht möglich gewesen wäre.

Zuallererst möchte ich mich bei Prof. Dr. Rolf Müller und bei Dr. Silke Reinartz für die Aufnahme als Doktorandin und die Bereitstellung dieses interessanten Themas bedanken. Ich möchte mich bei beiden für ihre Betreuung, ihre vielen Ratschläge und Anregungen bedanken. Vielen Dank Silke, dass du als Ansprechpartnerin bei der Entwicklung neuer Versuchsabläufe und bei Problemen immer zur Verfügung stands und mich mit Rat und Tat unterstützt hast. Ich danke der gesamten AG Reinartz, AG Müller, AG Pogge von Strandmann, AG Lauth, Bernhard Wilke und PD Dr. Till Adhikary für die Hilfsbereitschaft und die gute Arbeitsatmosphäre. Ich möchte mich insbesondere bei Anna, Traute und Achim für die vielen hilfreichen Tipps und ermunternden Gespräche und die Zusammenarbeit in vielen Projekten bedanken. Danke Traute, dass du mir bei neuen Zellkultur-Techniken und in der Zellkultur im Allgemeinen geholfen hast. Danke Achim, für deine Unterstützung bei FACS-Färbungen, ELISA und Western Blots. Danke Traute und Achim euch beiden, für die vielen Vor- und Nacharbeiten in der Zellkultur und im Labor und dass ihr bei Problemen bei praktischen Arbeiten immer mit helfenden Händen da ward. Auch bei Anna bedanke ich mich, für die gute Zusammenarbeit, für alle Hilfestellungen und die guten Gespräche. Der ganzen AG Reinartz danke ich für diese gute Zeit als Team mit gegenseitigem Vertrauen und Freundschaft. Bei Prof. Dr. med. Uwe Wagner und bei Dr. Julia Malin Jansen bedanke ich mich für die zur Vergütungstellung des Patientenmaterials bedanken. Zudem bedanke ich mich bei Dr. Florian Finkernagel für die gesamte informatische Auswertung meiner Transkriptions- und Sekretomsdaten. Bei Dr. María Gómez-Serrano bedanke ich mich für die vielen ideenvollen Gespräche und Anregungen. Bei Dr. Andrea Nist und der gesamten Genomics Core Facility bedanke ich mich für die schnell und unkomplizierte Durchführung der RNA-Sequenzierung. Auch bei Dr. Jelena Pesek möchte ich mich bedanken für die massenspektrometische Analyse der Lipid-Mediatoren und bei Dr. Johannes Graumann für die Sekretomanalysen. Abschließend bedanke ich mich bei meiner Familie und meinen Freunden für die viele Unterstützung, die aufmunternden Worte und Ablenkung während meiner Doktorarbeit. Insbesondere möchte ich mich bei meinem Sohn, bei meinen Eltern und Schwestern für ihre Liebe bedanken.